

NO-A106 007

VAN DER WAALS CLUSTERS OF AROMATIC MOLECULES STUDIED
USING SUPERSONIC MOL. (U) AIR FORCE INST OF TECH
WRIGHT-PATTERSON AFB OH J A MENAPACE 1987

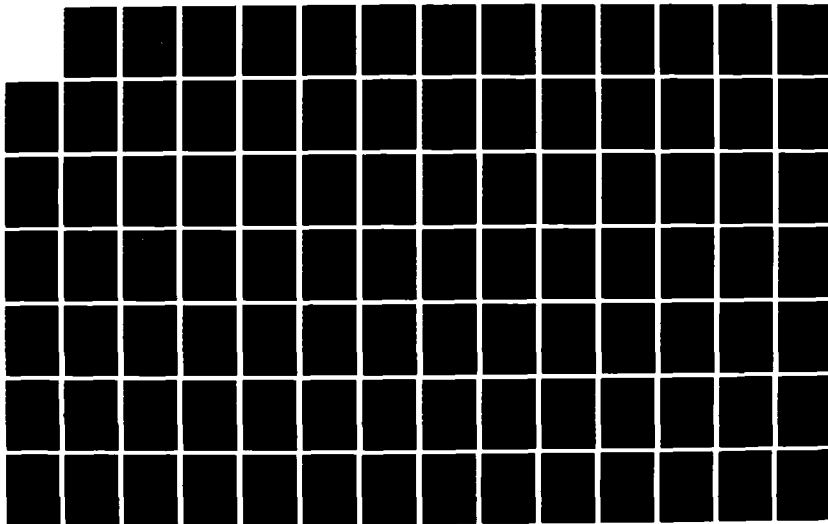
1/4

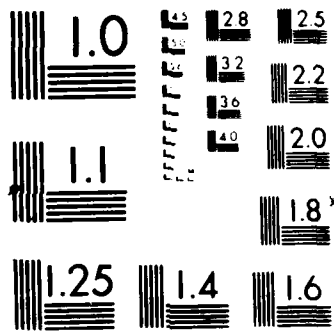
UNCLASSIFIED

AFIT/CI/NR-87-130D

F/G 7/3

ML





AD-A186 087

REPORT DOCUMENTATION PAGE		READ INSTRUCTIONS BEFORE COMPLETING FORM
1. REPORT NUMBER AFIT/CI/NR 87-1300	2. GOVT ACCESSION NO.	3. RECIPIENT'S CATALOG NUMBER DTIC FILE COPY ①
4. TITLE (and Subtitle) Van Der Waals Clusters of Aromatic Molecules Studied Using Supersonic Molecular Jet Spectroscopy		5. TYPE OF REPORT & PERIOD COVERED /M/MS/DISSERTATION
		6. PERFORMING ORG. REPORT NUMBER
7. AUTHOR(s) Joseph Arthur Menapace		8. CONTRACT OR GRANT NUMBER(s)
9. PERFORMING ORGANIZATION NAME AND ADDRESS AFIT STUDENT AT: Colorado State University		10. PROGRAM ELEMENT, PROJECT, TASK AREA & WORK UNIT NUMBERS
11. CONTROLLING OFFICE NAME AND ADDRESS AFIT/NR WPAFB OH 45433-6583		12. REPORT DATE 1987
		13. NUMBER OF PAGES 339
14. MONITORING AGENCY NAME & ADDRESS (if different from Controlling Office)		15. SECURITY CLASS. (of this report) UNCLASSIFIED
		15a. DECLASSIFICATION/DOWNGRADING SCHEDULE
16. DISTRIBUTION STATEMENT (of this Report) APPROVED FOR PUBLIC RELEASE; DISTRIBUTION UNLIMITED		
17. DISTRIBUTION STATEMENT (of the abstract entered in Block 20, if different from Report)		
18. SUPPLEMENTARY NOTES APPROVED FOR PUBLIC RELEASE: IAW AFR 190-1		S DTIC ELECTE D NOV 23 1987 Lynn E. Wolaver Dean for Research and Professional Development AFIT/NR
19. KEY WORDS (Continue on reverse side if necessary and identify by block number)		
20. ABSTRACT (Continue on reverse side if necessary and identify by block number) ATTACHED		

87 11 10 098

13

ABSTRACT OF DISSERTATION

VAN DER WAALS CLUSTERS OF

AROMATIC MOLECULES STUDIED USING

SUPERSONIC MOLECULAR JET SPECTROSCOPY



van der Waals (vdW) clusters of aromatic solutes with various solvents are studied in the gas phase using supersonic molecular jet spectroscopy. Calculations involving ground state cluster binding energy, geometry, and intermolecular vibrational structure are also presented to complement the experiments. The analyses include: spectroscopic studies and theoretical modeling of the intermolecular vibronic structure of benzene solvated by argon, methane, water, and ammonia; spectroscopic studies and theoretical modeling of the intermolecular vibronic torsional structure in benzene solvated by methane, deuteromethane, and carbon tetrafluoride; solvation of pyrazine and pyrimidine by both small hydrocarbon and hydrogen bonding solvents; the study of pyrazine and pyrimidine dimers; and the solvation of macrocycles such as free base phthalocyanine (H_2Pc) and magnesium phthalocyanine ($MgPc$) by small hydrocarbon solvents, hydrogen bonding solvents, and carbon dioxide. ←

The benzene/solvent studies lead to the elucidation of the detailed nature of the intermolecular vibrational structures and the geometries/symmetries present in the clusters. These studies reveal that the majority of the intermolecular vibronic transitions observed involve vdW bending and torsional motion parallel to the solute π cloud. Furthermore, the clusters behave rigidly with regard to internal rotation of the cluster subunits and the clusters possess unique equilibrium geometries.

87 11 10 098

The pyrazine and pyrimidine/solvent and dimer studies demonstrate the detailed effects of the solute ring nitrogens on cluster geometry and on the role of hydrogen bonding in the clusters.

The H_2Pc and $MgPc$ /solvent cluster experiments and models suggest that stable solute solvation sites are located over the phthalocyano core and not over peripheral ring centers. Forbidden low frequency cluster chromophore out-of-plane vibronic transitions are also induced by solvation in both the H_2Pc and $MgPc$ clusters.

Primary References:

1. J. A. Menapace and E. R. Bernstein, Journal of Physical Chemistry, 1987, 91, 2843.
2. J. A. Menapace and E. R. Bernstein, Journal of Physical Chemistry, 1987, 91, 2533.
3. J. A. Menapace and E. R. Bernstein, Journal of Chemical Physics, 1987, 86, 0000.
4. J. Wanna, J. A. Menapace, and E. R. Bernstein, Journal of Chemical Physics, 1986, 85, 777.
5. J. Wanna, J. A. Menapace, and E. R. Bernstein, Journal of Chemical Physics, 1986, 85, 1795.

Secondary References:

1. M. Schauer and E. R. Bernstein, Journal of Chemical Physics, 1985, 82, 726.
2. K. S. Law, M. Schauer, and E. R. Bernstein, Journal of Chemical Physics, 1984, 81, 4871.
3. J. Wanna and E. R. Bernstein, Journal of Chemical Physics, 1986, 84, 927.

Joseph Arthur Menapace, Capt, USAF
Doctor of Philosophy
Department of Chemistry
Colorado State University
Fort Collins, CO 80523
Summer 1987
Dissertation: 339 Pages

DISSERTATION

VAN DER WAALS CLUSTERS OF
AROMATIC MOLECULES STUDIED USING
SUPERSONIC MOLECULAR JET SPECTROSCOPY

Submitted by
Joseph Arthur Menapace
Department of Chemistry

In partial fulfillment of the requirements
for the Degree of Doctor of Philosophy
Colorado State University
Fort Collins, Colorado
Summer 1987



Accession For

DTIS GRAFI	<input checked="" type="checkbox"/>
DTIC TAB	<input type="checkbox"/>
Unannounced	<input type="checkbox"/>
Justification	

A-1

COLORADO STATE UNIVERSITY

16 JUNE 1987

WE HEREBY RECOMMEND THAT THE THESIS PREPARED UNDER OUR
SUPERVISION BY JOSEPH ARTHUR MENAPACE ENTITLED VAN DER WAALS
CLUSTERS OF AROMATIC MOLECULES STUDIED USING SUPERSONIC
MOLECULAR JET SPECTROSCOPY BE ACCEPTED AS FULFILLING IN PART
THE REQUIREMENTS FOR THE DEGREE OF DOCTOR OF PHILOSOPHY.

Committee on Graduate Work

Advisor

Department Head

ABSTRACT OF DISSERTATION

VAN DER WAALS CLUSTERS OF

AROMATIC MOLECULES STUDIED USING

SUPERSONIC MOLECULAR JET SPECTROSCOPY

van der Waals (vdW) clusters of aromatic solutes with various solvents are studied in the gas phase using supersonic molecular jet spectroscopy. Calculations involving ground state cluster binding energy, geometry, and intermolecular vibrational structure are also presented to complement the experiments. The analyses include: spectroscopic studies and theoretical modeling of the intermolecular vibronic structure of benzene solvated by argon, methane, water, and ammonia; spectroscopic studies and theoretical modeling of the intermolecular vibronic torsional structure in benzene solvated by methane, deuteromethane, and carbon tetrafluoride; solvation of pyrazine and pyrimidine by both small hydrocarbon and hydrogen bonding solvents; the study of pyrazine and pyrimidine dimers; and the solvation of macrocycles such as free base phthalocyanine (H_2Pc) and magnesium phthalocyanine ($MgPc$) by small hydrocarbon solvents, hydrogen bonding solvents, and carbon dioxide.

The benzene/solvent studies lead to the elucidation of the detailed nature of the intermolecular vibrational structures and the geometries/symmetries present in the clusters. These studies reveal that the majority of the intermolecular vibronic transitions observed

involve vdW bending and torsional motion parallel to the solute π cloud. Furthermore, the clusters behave rigidly with regard to internal rotation of the cluster subunits and the clusters possess unique equilibrium geometries.

The pyrazine and pyrimidine/solvent and dimer studies demonstrate the detailed effects of the solute ring nitrogens on cluster geometry and on the role of hydrogen bonding in the clusters.

The H_2Pc and $MgPc$ /solvent cluster experiments and models suggest that stable solute solvation sites are located over the phthalocyanine core and not over peripheral ring centers. The H_2Pc /hydrocarbon cluster results parallel those obtained for the benzene and N-heterocycle/hydrocarbon clusters. The H_2Pc and $MgPc$ /alcohol cluster spectra and calculated geometries suggest that the solvent OH groups are intimately involved in the intermolecular interactions. Forbidden low frequency cluster chromophore out-of-plane vibronic transitions are also induced by clustering. This low frequency motion is characterized using an out-of-plane normal coordinate analysis on the H_2Pc moiety.

Joseph Arthur Menapace
Department of Chemistry
Colorado State University
Fort Collins, CO 80523
Summer 1987

ACKNOWLEDGMENTS

I would like to extend my thanks to a number of people whose assistance and support have proved invaluable in making graduate school a worthwhile experience for me. Uppermost of those who have spurred by interest in the details of molecular spectroscopy is Elliot R. Bernstein. I am deeply indebted to Elliot for his constant encouragement and generous advice in my research. His clear insight and helpful discussions were often the only reasons why explanations for several of the effects discussed in this manuscript were pursued.

I am grateful to the members of my Graduate Advisory Committee for taking the time to participate in my research endeavors.

I would like to thank Dr. Joseph Wanna and Dr. Mark Schauer for teaching me the "tricks of the trade". Without them this dissertation would not be nearly as impressive.

I am extremely grateful to Lt. Col. Chester Dymek, the staff at Frank J. Seiler Research Laboratory, and the people behind the United States Air Force Academy Faculty Program for making it possible for me to pursue my education in conjunction with my Air Force career.

Most of all, I would like to thank my lovely wife Lisa, my son Joe Jr., and my daughter Deanna. I am deeply indebted to them for the sacrifices they made and for their encouragement and emotional support during this period of endeavor in my life.

To

Ida M. Menapace,
Janet J. Juranek, and
John E. Juranek Sr.,

With Love... Joe

TABLE OF CONTENTS

CHAPTER ONE	--	Introductory Comments and Overview.....	1
CHAPTER TWO	--	The Vibronic Structure of Solute/Solvent van der Waals Clusters.....	14
CHAPTER THREE	--	The Intermolecular Torsional Structure in Solute/Solvent van der Waals Clusters: Benzene/Methane, /Deuteromethane, and /Carbon Tetrafluoride.....	73
CHAPTER FOUR	--	Hydrogen Bonded and Non-Hydrogen Bonded van der Waals Clusters: Comparison between Clusters of Pyrazine, Pyrimidine, and Benzene with Various Solvents.....	100
CHAPTER FIVE	--	Supersonic Molecular Jet Studies of Pyrazine and Pyrimidine Dimers.....	101
CHAPTER SIX	--	Supersonic Molecular Jet Studies of Phthalocyanines and Their van der Waals Clusters with Small Molecules.....	102
CHAPTER SEVEN	--	Unpublished Results.....	152
CHAPTER EIGHT	--	Future Experiments and Conclusions.....	194
APPENDIX ONE	--	Hydrogen Bonded and Non-Hydrogen Bonded van der Waals Clusters: Comparison between Clusters of Pyrazine, Pyrimidine, and Benzene with Various Solvents.....	206
APPENDIX TWO	--	Supersonic Molecular Jet Studies of Pyrazine and Pyrimidine Dimers.....	218
APPENDIX THREE	--	ECCEMP2.....	227
APPENDIX FOUR	--	VDWNCA.....	272
APPENDIX FIVE	--	H ₂ PCNCA.....	306
APPENDIX SIX	--	3DHRRA.....	331

CHAPTER ONE

INTRODUCTORY COMMENTS AND OVERVIEW

Introduction.

The material contained in this dissertation is largely presented in five publications. In the spirit of completeness and accuracy, these papers are incorporated directly into the dissertation. The first three papers appear as chapters in the body of the manuscript. The remaining two papers appear in reprint form as appendices. The rest of the dissertation entails the introductory comments and overview, unpublished results, future/proposed experiments, conclusions, and the computer programs utilized in this work.

The introductory comments and overview are meant to tie together the body of the dissertation since directly presenting the publications tends to fragment the discussion. They will also provide the reader with the general notions underlying the work presented in detail in each major section or chapter of the dissertation.

The unpublished results contain mostly those data which are not important enough to appear in papers, or data which need additional work to interpret. The data are presented in the dissertation to establish a record of the research conducted in specific areas and to provide future investigators with a basis for further study.

The future/proposed experiments involve both theoretical and experimental studies of solute/solvent cluster systems similar to those

presented in this dissertation. The primary motivation in these proposed experiments is to provide for continued research on cluster systems using the models, procedures, and experimental set-ups currently available in the Bernstein group laboratory.

The presentation of the computer programs used in the cluster studies is largely for the convenience of future investigators. The programs serve as easy references for those conducting research in the same or similar areas as well as provide documentation on the "how to's" of the models used in the studies.

Overview.

The five publications incorporated into this dissertation are divided into five chapters. The work covers: 1) the experimental study and theoretical modeling of the intermolecular vibronic structure of benzene solvated by argon, methane, water, and ammonia; 2) the experimental study and theoretical modeling of the intermolecular vibronic torsional structure in benzene solvated by methane, deuteromethane, and carbon tetrafluoride; 3) the detailed study of the solvation of pyrazine and pyrimidine by both small hydrocarbon and hydrogen bonding solvents; 4) the study of pyrazine and pyrimidine dimers; and 5) the solvation of macrocycles such as free base phthalocyanine and magnesium phthalocyanine by small hydrocarbon solvents, hydrogen bonding solvents, and carbon dioxide. This overview is intended to tie together the major results of these studies and to create a sense of unity and purpose for the studies.

The Vibronic Structure of Solute/Solvent van der Waals Clusters

A large body of data has been accumulated in this laboratory for small aromatic molecules such as benzene, pyrazine, and pyrimidine solvated

with small hydrocarbon solvents such as methane, ethane, and propane, and hydrogen bonding solvents such as water and ammonia. These spectroscopic studies yield observables such as spectral shift which can be related to the difference between the cluster binding energy between the ground and electronic excited states and to cluster geometry. In the majority of the cluster spectra, intermolecular vibronic transitions are observed which can be used to elucidate the cluster symmetry/geometry, electronic state mixing, and the intricacies of the intermolecular potential surface.

Modeling of the intermolecular interaction between the cluster constituents also complements the spectroscopic studies. These calculations allow one to elucidate some physical properties of the clusters such as ground state cluster binding energy and geometry. The calculations always yield results consistent with experimental observations in regard to the number of cluster configurations observed, their respective binding energies, and their qualitative geometries. Modeling of the intermolecular vibronic structure in these molecules adds to the understanding of the cluster systems as it allows one to obtain detailed information on cluster geometry/symmetry and to elucidate the intricacies of the potential established between the cluster constituents.

Presently, little information is available, either experimentally or theoretically, on the details of the intermolecular vibrational structure in the solute/solvent cluster systems. Furthermore, the van der Waals (vdW) modes are interesting as they play a key role in dynamical energy transfer processes in the clusters as well as represent precursors to a variety of motions occurring in liquids and solids.

The modeling of the intermolecular vibrational structure in this study is approached by extending the empirical models previously used to

calculate cluster ground state geometry and binding energy to include modeling of the ground state vdW motion. The vdW vibrational structure is modeled using a normal coordinate analysis in which the clusters are treated as "giant molecules" whose motion is governed by a force field describing both the intra- and intermolecular motion. The intermolecular force field is based upon an atom-atom Lennard-Jones potential function including general non-bonding (6-12), hydrogen bonding (10-12), and monopole charge (1) terms.

Using this model, the eigenvalues and eigenvector normal modes for the vdW motion occurring in benzene(Ar)₁, /(CH₄)₁, /(H₂O)₁, and /(NH₃)₁, and s-tetrazine(Ar)₁ are calculated. The results of these calculations are then used to assign the vdW motions observed in vibronic spectra of the aforementioned cluster systems which are obtained using 1- and 2-color time-of-flight mass spectroscopy (TOFMS). Agreement between the calculations and experiments is excellent for cluster binding energies, symmetries, and vdW frequencies. Essentially, the S₁ ← S₀ vibronic transition of the clusters are completely assigned based upon these calculations.

A number of approximate "diatomic molecule" models are also considered in this study to analyze the vdW structure in benzene(Ar)₁. The cluster vdW modes are modeled using three methods: 1) a Taylor series expansion of the intermolecular potential along the vdW stretching and bending coordinates; 2) a Morse potential fit to the intermolecular potential along the vdW stretching and bending coordinates; and 3) a semi-classical energy level fit to the intermolecular potential using the JWKB method. The models essentially treat the clusters as simple two particle systems whose motions are restricted to

the principle axes of a Cartesian coordinate system and can, thereby, be analyzed using a diatomic molecule type approximation. These models are considered to show the consistency of the calculations between each diatomic molecule model and the intermolecular normal coordinate analysis.

The experimental and theoretical studies on the benzene/solvent systems give rise to several interesting notions which involve the detailed nature of the intermolecular interaction. First, the studies reveal that the weak vdW potential between the cluster solute and solvent is, for the most part, the same for the ground and excited electronic states. Second, the majority of the observed vdW vibronic transitions observed in the cluster spectra are those involving vdW bending and torsional motions parallel to the aromatic π system. Third, these modes are quite active in the Herzberg-Teller vibronic coupling mechanism. And fourth, vdW motions for which the cluster solvent penetrates the aromatic π system of the solute have high frequencies and are typically not observed.

The Intermolecular Vibronic Torsional Structure in Solute/Solvent vdW Clusters: Benzene/Methane, /Deuteromethane, and /Carbon Tetrafluoride - The modeling of the intermolecular motion in the vdW clusters discussed above is basically approached using, more or less, a rigid molecule bound energy well approximation. This approach seems quite reasonable for the vdW stretching and bending degrees of freedom which are essentially translations of the cluster constituents relative to one another. The vdW torsional modes, on the other hand, could in principle not be oscillatory. They could be free or hindered rotation of the cluster solvent relative to the cluster solute. In this regard the

intermolecular normal coordinate analysis may not faithfully reproduce the vdW torsional motion present in the clusters.

To study this possibility, we chose to analyze benzene clustered with methane, deuteromethane, and carbon tetrafluoride. The motivation for studying this "isotopic" cluster solvent series centers upon the elucidation of the vdW torsional structure. Two limiting cases can be proposed in regard to the torsional structure in benzene(CH₄)₁, benzene(CD₄)₁, and benzene(CF₄)₁. In one case, the clusters can possess free internal rotation in which the cluster solvent freely rotates in three dimensions against the benzene frame and the system can be considered internally non-rigid. In the other case, the clusters possess torsional oscillations for which the cluster solvent librates against the benzene frame with a residence time long enough to give rise to "vibration like" motion in an internally rigid molecule regime. Understanding the vdW torsional motion is particularly interesting in these systems as the limiting cases pose questions regarding the physics governing the vdW torsional structure: 1) do the clusters possess free/hindered internal rotation or do they possess torsional oscillations; and 2) in either case, what is the dependence of the intermolecular potential upon the relative orientation of the cluster constituents?

In the studies, the clusters are probed spectroscopically using supersonic molecular jet expansion and 2-color TOFMS techniques. The cluster $S_1 \leftarrow S_0$ intermolecular vibronic structures are then characterized by calculational modeling of the vdW motion. The calculations include: 1) an intermolecular normal coordinate analysis which treats all six vdW modes under a harmonic oscillator assumption; and 2) a three-dimensional hindered rigid rotor analysis which treats only the intermolecular torsional motion.

In the experimental and theoretical studies on the benzene(CH₄)₁, benzene(CD₄)₁, and benzene(CF₄)₁ systems, several interesting results are obtained. First, the cluster vibronic spectra show that the clusters are at least semi-rigid systems with regard to internal rotation of the cluster subunits and that the clusters possess unique equilibrium geometries. Second, the spectra demonstrate that the intermolecular motion present in the systems is oscillatory and, through the "isotopic" shifts observed, that the low-lying eigenstates are nearly harmonic. They are not admixtures of vdW bends, stretches, and free internal rotation as would occur if the clusters were internally non-rigid. Third, both the intermolecular normal coordinate analysis and the three-dimensional hindered rigid rotor analysis indicate that the vdW torsional structure is oscillatory and that the motion is constrained by an orientationally dependent intermolecular potential whose barrier height is on the order of the cluster binding energy.

Hydrogen Bonded and Non-Hydrogen Bonded vdW Clusters: Comparison between Clusters of Pyrazine, Pyrimidine, and Benzene with Various Solvents - The study of the solvation of pyrazine, pyrimidine, and benzene by both small hydrocarbon and hydrogen bonding solvents has led to detailed information about the structure and energetics present in the solute/solvent systems. Our chief motivations for studying these clusters center upon the elucidation of the effects of the ring nitrogen atoms in pyrazine and pyrimidine solutes on cluster geometry and on the role of hydrogen bonding in the pyrazine, pyrimidine, and benzene cluster systems. These studies are of interest as hydrogen bonding interactions are known to play an important role in the intra- and intermolecular interactions responsible for secondary and tertiary

structure, molecular dynamics, and ionic and molecular solvation. Assignment of the spectra obtained in these studies is accomplished through the determination of the cluster spectral shifts, ionization energies, relative intensities, molecular forbidden cluster transitions, and intermolecular potential/cluster geometry calculations. Computer modeling of the cluster systems has proven essential to the understanding of the spectroscopic data. Through the interplay of the computer modeling of these clusters and the spectroscopic data, it is possible to assign probable geometries to many of the spectroscopic features. In many cases this allows one to find the spectral shift corresponding to a specific geometry of a cluster. The assignment of a geometry to the spectral shifts leads to some general conclusions about the types of interactions responsible for the spectral shifts.

In these studies we find that the clusters fall into two general categories: 1) a conventional set containing the aromatic solute/hydrocarbon solvent clusters; and 2) benzene, pyrimidine, pyrazine ammonia and benzene water clusters. The aromatic solute/hydrocarbon cluster spectra are quite similar to one another in that they all possess bathochromic shifts with respect to the isolated chromophore transition. The cluster binding energies and calculated geometries are also similar. The presence of the nitrogen atoms in the aromatic ring of the pyrazine and pyrimidine solutes has a relatively small although discernible effect on the overall intermolecular interaction. In particular, the solvent hydrogen atoms preferentially orient towards the solute nitrogen atoms.

The solute/hydrogen bonding solvent cluster systems, on the other hand, possess vibronic spectra which are all unique and surprisingly

erratic. In these clusters the spectral shifts range from -100 to 500 cm^{-1} , the vdW vibronic motion in the systems range from nonexistent to intense, the vdW modes are in some cases highly perturbing to the solute vibronic structure and energy, and the number of unique cluster geometries range from one to three in an apparently random fashion. In spite of these differences the models used to calculate the cluster geometries and binding energies corroborate the experiments as far as the comparison can be made in regard to cluster symmetry, number of configurations observed, and red and blue shifts in regard to hydrogen bonding. The hypsochromic shifts observed in the pyrazine and pyrimidine ammonia clusters suggest that hydrogen bonding between the ring nitrogen and the solvent hydrogens may be contributing to some extent to the total intermolecular interaction responsible for cluster formation/stabilization. The benzene/ammonia and benzene/water spectra seem to suggest that some type of hydrogen bonding may be occurring in the benzene/water system between the aromatic π cloud and the solvent moiety as the benzene(H_2O)₁ spectral shift is hypsochromic whereas the benzene(NH_3)₁ spectral shift is bathochromic.

Supersonic Molecular Jet Studies of the Pyrazine and Pyrimidine Dimers - The understanding of the solute/solute interactions in the pyrazine and pyrimidine dimer systems is of interest for a number of reasons. First, the dimers serve as model systems for condensed phase structure, dynamics, and nucleation and growth of molecular aggregates. Second, the dimers provide insight into the understanding of the secondary and tertiary structures present in more complicated molecules. And third, studying these clusters in the gas phase yields information on the major interactions responsible for dimer formation and what types of

dimer geometries are most probable in an isolated environment free from the extraneous perturbations present in liquid and solid phases.

The pyrazine and pyrimidine dimers are analyzed using supersonic molecular jet expansion and 2-color TOFMS techniques for which the mass selected optical spectra of the first excited singlet $n\pi^*$ transitions of the dimers are observed. On the basis of what we have learned from the study of the simple solute/solvent clusters, we are able to analyze the dimer systems using cluster ionization energy, vibronic structure, spectral shift, and modeling of the intermolecular potential between the cluster subunits. The interplay of the spectroscopic data and the calculations allows us to obtain a consistent set of geometries for the dimers present in the supersonic expansion.

In the pyrazine dimer system, the experiments and calculations suggest that the both parallel hydrogen bonded and perpendicular dimers are present in the supersonic expansion. The calculations also predict a parallel stacked/ 90° rotated dimer which is not observed. This species most likely forms an excimer in the excited state with a short lifetime and a large red shifted and broad spectrum. The major distinction between the two observed dimer species is determined to be the difference in the involvement of the π clouds in the overall dimer interaction as evidenced by differences in the cluster ionization energy between the two cluster species.

In the pyrimidine dimer, the calculations yield four planar hydrogen bonded species and a parallel stacked/displaced species. The observed dimer vibronic spectra are consistent with these calculated geometries. As in the pyrazine dimer, the ionization energy proves to be an important contribution in determining the number of different

dimer geometries responsible for the observed spectra. Additionally, we find that the dimer spectral shifts depend upon the specific cluster geometry. A bathochromic shift is associated with the parallel stacked/displaced dimer and hypsochromic shifts are associated with the planar hydrogen bonded dimers.

To explore further the agreement between the experiments and calculations on the dimer systems, we also conducted calculations on the tetrazine dimer. Three calculated geometries are obtained for the tetrazine dimer: a parallel stacked/ 90° rotated species, a planar hydrogen bonded species, and a perpendicular species. In this study we find that the calculated geometries are in agreement with geometries determined from rotational analysis.

Computer modeling is determined to be an essential component to the study of these dimer systems. The spectroscopic data are needed to validate the computer modeling techniques, and the calculations help to assign spectra which are otherwise quite puzzling. In this way the interplay between spectroscopy and computer modeling leads to a better understanding of the structure and energetics of the solute/solute systems.

Supersonic Molecular Jet Studies of Phthalocyanines and Their vdW Clusters with Small Molecules - In these studies, free base phthalocyanine (H_2Pc) and magnesium phthalocyanine ($MgPc$) clustered with solvents such as small hydrocarbons (C_nH_{2n+2} ($n=1, 2, 3$)), hydrogen bonding solvents (H_2O , $MeOH$, $EtOH$), and CO_2 are analyzed in an isolated ultracold molecular environment. The clusters are generated using a high temperature continuous supersonic molecular jet especially designed for efficient generation and study of the species in the gas phase. The

advantages of the supersonic molecular jet are exploited in these studies as the complicated phthalocyanine spectra are dramatically simplified and the solvent or environmental perturbations present are controlled in a set and reproducible manner.

Our basic motivation for studying these systems centers upon elucidation of the solvation properties of the macrocycles in a controlled and well-defined environment. In this regard, supersonic molecular jet investigations on the H_2Pc and $MgPc$ solute/solvent clusters can contribute to the resolution of a number of important concerns dealing with the behavior of the systems on the microscopic scale. Questions that we considered in these cluster studies are 1) what are the ground and excited state binding energies between the phthalocyanines and various solvents, 2) what are the preferential interaction sites on the phthalocyanine moiety, 3) what are the most favorable cluster geometries, 4) what types of interactions are important in the intermolecular interaction established between the solute and the solvent, and 5) are changes to the chromophore symmetry/geometry induced by clustering.

The H_2Pc and $MgPc$ solute/solvent clusters are characterized by analysis of their gas phase fluorescence excitation spectra and modeling of the intermolecular potential between the cluster solutes and solvents. In these studies, we find that forbidden cluster chromophore out-of-plane motion is induced by clustering and that elucidation of the nature of this out-of-plane motion is essential to the understanding of the cluster spectra and in the identification of the number of different clusters of a specific composition observed. This prompted us to conduct an out-of-plane normal coordinate analysis on H_2Pc to

characterize the motion. The comparison between these calculations and the experiments makes possible the identification of specific species/geometries responsible for the cluster vibronic transitions observed in the spectra.

Several interesting results are obtained from the cluster studies. First, the cluster vibronic spectra and calculations suggest that stable H_2Pc and $MgPc$ solvation sites are located over the phthalocyanine core. Local minima over peripheral ring centers are either nonexistent or too shallow to accommodate minimum energy bound state geometries. Second, the H_2Pc /hydrocarbon cluster experimental and theoretical results parallel those obtained for benzene and the N-heterocycle/hydrocarbon clusters. The spectral shifts observed in these solvent series are all bathochromic and the magnitudes of the spectral shifts increase with increasing solvent size and polarizability. Third, the H_2Pc and $MgPc$ /alcohol cluster spectra and calculated geometries suggest that the solvent OH group is intimately involved in the intermolecular interactions and contributes significantly to the observed spectral shifts. Fourth, $MgPc$ clusters display weak vdW interactions between the cluster solute and solvent. Actual complexation in which the solvent donates electron density to the solute does not occur. Fifth, excited electronic state splitting may occur in the $MgPc$ clusters due to the reduction in system symmetry upon cluster formation. The degenerate Q band in the isolated $MgPc$ spectrum appears to split into its two components, Q_x and Q_y , in the cluster spectra. Finally, forbidden low frequency cluster chromophore out-of-plane motion is induced by clustering in both the H_2Pc and $MgPc$ systems. Intensity of this motion arises from the reduction of the chromophore symmetry in the clusters.

CHAPTER TWO

THE VIBRONIC STRUCTURE OF SOLUTE/SOLVENT VAN DER WAALS CLUSTERS

Introduction.

The combination of laser spectroscopy and supersonic molecular jet expansions has made possible the study of a wide array of weakly bound van der Waals (vdW) molecules in the gas phase. These clusters, formed in the jet expansion, are stable in the post-expansion region and can be studied as isolated molecules. They are interesting both theoretically and experimentally because of their unique characteristics such as low binding energies, large intermolecular equilibrium distances, and low frequency intermolecular vibrational modes. Furthermore, the vdW clusters only slightly perturb the individual properties of their molecular constituents.¹ These characteristics set the vdW cluster apart as a distinct phase of matter to be explored and understood.

The electronic-vibrational spectroscopy of aromatic molecules like benzene²⁻⁴ and s-tetrazine⁵ clustered with various solvents reveals interesting information regarding unique cluster characteristics. Specifically, the studies show detailed information pertaining to the intermolecular energetics and dynamics of cluster interactions, especially in the area of the clusters' low frequency vdW vibrational modes. These modes are of considerable interest since they represent the precursors of a variety of condensed phase eigenstates such as phonons in

liquids and solids. They are also key factors in cluster dynamics as they play a major role in the energy transfer processes of intramolecular vibrational redistribution (IVR) and vibrational predissociation (VP).

Presently, little information is available concerning the detailed intermolecular vibrational structure in molecule-molecule clusters either experimentally or theoretically. The majority of the theoretical work on cluster energetics and dynamics to date is focused upon the intermolecular modes in simple atom-molecule systems. The energetic studies range from quantitative treatment of the vdW stretch and qualitative discussion of the vdW bends^{1,6,7} in the atom-molecule clusters to full quantitative treatment of both the vdW bends and stretch¹⁶ in systems for which the intermolecular potential is easily modeled. In dynamical studies,^{6,7} primary emphasis is placed upon the vdW stretching mode since it is presupposed that this motion is the major contributor to IVR and VP processes. The clusters are thereby treated quantitatively using a "dumbbell" approximation in which the intermolecular motion is restricted to a stretching mode form. Within this approximation, neglecting the quantitative contributions of the bending/torsional vdW modes in the dynamical scheme seriously limits the application of theoretical treatments to IVR and VP phenomena occurring in molecule-molecule clusters. The stretching mode "restriction" dictates that only certain energy transfer processes can be modeled, specifically those which involve the vdW stretch. Experimental evidence of the theory's limitation⁴ is found in the observation of energy transfer from prepared states tangential to the vdW stretching motion. Part of the difficulty of incorporating the vdW bending and/or torsional modes into the theory is that no model has been demonstrated which

describes adequately either their energetics or mode nature in molecule-molecule clusters.

In previous publications,⁸ we have used theoretical calculations to elucidate structure and binding energy in the vdW cluster ground state. Combining these calculations with experimental observables such as binding energies, ionization energies, spectral shifts, relative feature intensities, and the appearance of cluster constituent, symmetry forbidden, transitions has aided considerably in spectral assignment and understanding. The calculations always yield results consistent with experimental observations in regard to the number of cluster configurations observed, their respective binding energies, and their qualitative geometries.

In the majority of the cluster spectra studied, vdW vibronic features are observed and sometimes assigned based upon overtone and combination band analysis. In other cases, however, these vibronic features are numerous and complex, making elucidation of the mode fundamentals difficult and sometimes impossible. The vdW vibronic feature assignments have been made based upon the assumptions that the vdW stretch occurs at higher frequency and with greater intensity than vdW bends and torsions. Assigning spectra using these assumptions is a difficult task without a priori knowledge of vibronic mode nature since one must consider that, in nonlinear polyatomic molecule-molecule clusters, six vdW modes exist of which only one is a stretching mode. (In a non-linear atom-polyatomic molecule cluster, three vdW modes exist).

The studies reported in this publication involve the calculation of a complete set of ground state vdW vibrational modes for

benzene(Ar)₁, s-tetrazine(Ar)₁, benzene(CH₄)₁, benzene(H₂O)₁, and benzene(NH₃)₁. The calculations are performed using a self-consistent pairwise atom-atom intermolecular potential developed by Scheraga, et al.⁹ containing general nonbonding (6-12), general hydrogen bonding (10-12), and monopole charge parameters. The calculated ground state vdW modes are compared with cluster vibronic spectra previously studied in this^{2,3} and other laboratories.⁵ Consequently, a number of spectral reassignments are suggested. Vibronic selection rules governing the vdW cluster S₁ ← S₀ transitions are also derived based upon calculated ground state cluster mode symmetry, cluster geometry, and experimental observation. Within this framework, ramifications of Herzberg-Teller vibronic coupling are discussed as they pertain to experimental observations of Franck-Condon forbidden transitions.

The calculated vdW vibrations are presented for all systems considered as eigenvector normal modes and eigenvalue energies determined via normal coordinate analysis of the entire vdW cluster.¹⁰ In performing the calculations, the high frequency intramolecular vibrations of the cluster constituents are assumed to be completely uncoupled from the low frequency vdW modes.

Simpler models are also considered in studying the vdW transitions of benzene(Ar)₁. The system is studied using four methods: 1) a Taylor series expansion of the intermolecular vdW potential along the three Cartesian axes in which the term coefficients are related to the vibrational frequencies in these directions; 2) a Morse potential fit to the intermolecular vdW potential along each of the three Cartesian axes; 3) a Morse potential fit to the intermolecular vdW potential using $\beta = \frac{6}{R_0} ;^{1,6,7}$ and 4) a semi-classical energy level fit to the

intermolecular vdW potential using the JWKB method. These studies are presented to show the consistency of the calculations and to reveal the advantages and pitfalls of the models. The four models involve treating the vdW clusters as simple two particle systems whose motions are restricted to the principle axes of the Cartesian coordinate system. The intermolecular vdW potential surfaces are thereby reduced to one-dimensional potential functions which can be analyzed in a diatomic molecule approximation.

The above outlined approaches are all based more or less on a rigid molecule, bound potential energy well approximation. This approach would seem quite reasonable for the stretching(s) and bending (b_x and b_y) degrees of freedom which are essentially translations of the components of the vdW molecules with respect to one another. Torsional modes (t_x , t_y , t_z), on the other hand, could in principle be modeled by a free/hindered rotor formalism.^{11,12} A one-dimensional "free rotor" description has been applied to the symmetry axis (z) torsional motion of benzene and toluene ($(CH_4)_1$, $(CD_4)_1$ and $(CF_4)_1$ and compared to the experimental observations. Preliminary results suggest that this approach does not faithfully reproduce the experimentally observed spectra for this "isotopic" series in terms of line shapes, intensities, major features, and the number of observed transitions. A three-dimensional "free rotor" model has also been applied to this problem in order to treat all torsional modes (t_x , t_y , t_z) simultaneously. Similar difficulties are experienced in fitting the experimentally observed spectra. An account of these studies will be submitted for publication in the near future.

The driving motivation in these studies is to answer the following questions: 1) if parametric calculations involving cluster

geometry and binding energy are consistent with experiment, can the same data set be utilized to calculate intermolecular vibrational modes; and 2) what are the advantages and pitfalls of the various models in regard to the complexity of calculation, the approximations made, and the nature of the results obtained?

Experimental Procedures.

Experimental data pertaining to the benzene(Ar)₁ vdW vibronic spectrum are obtained employing the experimental apparatus and procedures similar to those used previously to study vdW clusters.⁸ The benzene(Ar)₁ S₁ - S₀ spectrum is recorded using a pulsed supersonic molecular jet expansion in combination with 1-color time-of-flight mass spectroscopy (TOFMS). A single Nd³⁺/YAG pumped LDS 698 dye laser whose output is frequency doubled and then mixed with the Nd³⁺/YAG 1.064 μm fundamental is used to probe the 6₀¹ region of the benzene(Ar)₁ cluster. A 5% Ar in He mixture is placed inline with liquid benzene in a trap maintained at room temperature. This three component gas mixture is then expanded using a pulsed nozzle maintained at 100 psig backing pressure. Apparatus chamber pressure is maintained at or below 4 x 10⁻⁶ torr during the experiment.

Theoretical Considerations.

The normal coordinate analyses of the vdW clusters are conducted employing the GF methods of Wilson.¹⁰ These methods involve solving the characteristic equation of 3N-6 coupled harmonic oscillators for its 3N-6 non-zero eigenvalues and eigenvectors. The approach is to treat the vdW cluster as a "giant molecule" and treat both the intramolecular vibrational modes and the intermolecular vdW modes simultaneously. The

intermolecular vdW potential field used in the analyses is expressed in an intermolecular coordinate system. In this coordinate system, the intermolecular force field is diagonal in the $3N$ dimensional space.

The cluster constituent intramolecular vibrational frequencies are considerably higher than those of the vdW modes. A reasonable approximation in this context then is to assume that the intramolecular modes are completely uncoupled from the low frequency vdW modes. Thus, the intramolecular modes are taken to be those of the cluster constituents. The constituent force fields are generated using the central force approximation¹¹ including out-of-plane motion terms. Since the vdW modes arise from the restriction of cluster constituent translations and rotations and the central force approximation adequately reproduces these degrees of freedom, the necessary uncoupling of the intramolecular modes and the intermolecular vdW modes is maintained along with providing adequate vdW mode calculational results. Other, more sophisticated force field approximations are tested in the calculations; the central force approximation is determined to be adequate for calculations of the vdW modes. The only restriction which applies is that the intramolecular field yields mode eigenvalues in the proper frequency regions.

Within the central force approximation, the force field contains only diagonal terms in the internuclear coordinate system. This diagonal force field provides a simple and convenient means of using approximate force constants for intramolecular motion in the calculations. The intramolecular force constants chosen are those pertaining to general functional group stretches and bends.¹¹

The most convenient choice for a coordinate system as the working basis for matrix diagonalization is the Cartesian system. This

coordinate system is chosen since it is the system used in the present cluster configuration calculations, and more importantly, it is the coordinate system in which the \underline{G}^{-1} matrix is diagonal and obvious.

In order to combine the intermolecular and intramolecular force fields algebraically, the force fields are transformed into the Cartesian coordinate system. The transformation yields two $3N$ dimensional \underline{F} matrices. The intramolecular \underline{F} matrix is designated as \underline{F}_0 and the intermolecular \underline{F} matrix is designated as \underline{F}' . The \underline{F}_0 matrix consists of two diagonal blocks containing the coordinates of cluster constituent intramolecular motion. The \underline{F}' matrix contains two off-diagonal blocks and diagonal entries corresponding to the "perturbations" yielding the vdW motion. Adding these two matrices results in the "giant molecule" \underline{F} matrix of order $3N$. This matrix is left-multiplied by the \underline{G} matrix and numerically diagonalized with the eigenvalues and eigenvectors being determined in the usual fashion. Upon diagonalization, the eigenvalues and eigenvectors of intramolecular motion are identified along with those corresponding to cluster translation and rotation. These modes are discarded and the remaining modes are the eigenvalues and eigenvectors of the ground state vdW modes.

The intermolecular force constants used in the normal coordinate analysis are generated from the intermolecular vdW potential by making a harmonic oscillator approximation. Within this approximation, the force constant is simply the second derivative of the potential function,⁹

$$U(r_{ij}) = \sum_{i=1}^n \sum_{j=1}^m \left[\left\{ \frac{A^{kl}}{r_{ij}^{12}} - \frac{C^{kl}}{r_{ij}^6} \right\} (1 - \delta_{HB}^{ij}) + \frac{332.0q_i q_j}{Dr_{ij}} + \right. \\ \left. \left\{ \frac{A'^{kl}}{r_{ij}^{12}} - \frac{C'^{kl}}{r_{ij}^{10}} \right\} \delta_{HB}^{ij} \right] = U(r_{ij})_{NB} + U(r_{ij})_{MC} + U(r_{ij})_{HB} \quad 2.1$$

The potential function contains a general nonbonding potential (NB), a monopole charge potential (MC), and a general hydrogen bonding potential (HB) as a general nonbonding potential (NB), a monopole charge potential (MC), and a general hydrogen bonding potential (HB) in a Lennard-Jones (6-12-1-10-12) form. The total intermolecular interaction is taken as a sum of pairwise atom-atom interactions over all the atoms of each cluster constituent. The r_{ij} 's are the atom-atom distances between atom i on constituent k and atom j on constituent l . The r_{ij} 's represent the coordinates in which the intermolecular force field is diagonal. The second derivative of Equation 2.1 with respect to r_{ij} gives the force constant of the atom-atom interaction as,

$$K_{ij}(r_{ij}) = \sum_{i=1}^n \sum_{j=1}^m \left[\left\{ \frac{12 \cdot 13 \cdot A^{kl}}{r_{ij}^{14}} - \frac{6 \cdot 7 \cdot C^{kl}}{r_{ij}^8} \right\} \times \right. \\ \left. (1 - \delta_{HB}^{ij}) + \frac{2 \cdot 332 \cdot 0 q_i q_j}{Dr_{ij}^3} + \left\{ \frac{12 \cdot 13 A'^{kl}}{r_{ij}^{14}} - \frac{10 \cdot 11 \cdot C'^{kl}}{r_{ij}^{12}} \right\} \delta_{HB}^{ij} \right] \quad 2.2$$

in which the K_{ij} 's are elements of the \underline{F} ' matrix expressed in intermolecular coordinates. These terms are evaluated at the equilibrium configuration of the cluster assuming that the cluster constituents are frozen with regard to intramolecular motion. The potential term coefficients used in the configurational and intermolecular vibrational mode calculations (Equations 2.1 and 2.2) on the systems studied are derived from the theory and data set described by Scheraga et al.⁹

Three additional models are employed to study the benzene(Ar)₁ vdW cluster as a test case. In these models, the vdW cluster is assumed to be a "diatomic molecule" in the sense that the system is considered to be composed of two particles, the benzene molecule (solute) and the

argon atom (solvent). The vdW modes are assumed to arise from restricted one-dimensional motion of the benzene molecule relative to the argon atom. Only the atom-molecule benzene(Ar)₁ cluster will be considered using these models since its vdW modes are easily characterized by simple translations along any of the three Cartesian axes. The vdW stretching mode is taken as motion restricted to the one-dimensional translation moving the cluster constituents apart in opposite directions. The vdW bending modes are considered to be motions restricted to one-dimensional translations which move the cluster constituents parallel to one another in opposite directions.

In the first model considered, one-dimensional potential curves are mapped out by translating the solvent atom relative to the solute molecule in one of the three Cartesian directions. The intermolecular vdW potential is assumed to be represented by a Taylor series expansion about the equilibrium intermolecular distance, R_0 in the form,

$$U(R) = U(R_0) + \left(\frac{dU}{dR} \right)_{R=R_0} R + \frac{1}{2} \left(\frac{d^2U}{dR^2} \right)_{R=R_0} R^2 +$$

2.3

$$\frac{1}{6} \left(\frac{d^3U}{dR^3} \right)_{R=R_0} R^3 + \frac{1}{24} \left(\frac{d^4U}{dR^4} \right)_{R=R_0} R^4 + \dots$$

The expansion coefficients are evaluated by a polynomial fit to the potential curves taking the displacement vector R as the independent variable and $U(R)$ as the dependent variable. The second-order polynomial fit coefficient determines the effective harmonic force constant governing the frequency of bound state motion. The energy of this motion is given by¹²

$$\omega_e = \frac{1}{2\pi c} \left(\frac{k_{eff}}{\mu} \right)^{1/2} \quad 2.4$$

with

$$k_{eff} = \left(\frac{d^2 U}{dR^2} \right)_{R=R_0} = 2(\text{second-order coefficient})$$

$$\frac{1}{\mu} = \frac{1}{m_1} + \frac{1}{m_2}$$

m_1 = solute mass m_2 = solvent mass

The third and fourth order polynomial fit coefficients represent an anharmonic correction term to the energy. From perturbation theory, the correction can be written to first order as¹²

$$\omega_e \chi_e = \frac{3h^2}{32\pi^4 \omega_e^2 \mu^2 c^2} \left(\frac{5g^2 h}{8\pi^2 \omega_e^2 \mu c} - j \right)$$

with

$$g = (\text{third-order coefficient}) = \frac{1}{6} \left(\frac{d^3 U}{dR^3} \right)_{R=R_0} \quad 2.5$$

$$j = (\text{fourth-order coefficient}) = \frac{1}{24} \left(\frac{d^4 U}{dR^4} \right)_{R=R_0}$$

Higher order terms are neglected in the anharmonic corrections since $\omega_e \gg \omega_e \chi_e \gg$ other corrections. A polynomial least-squares fit to tenth order in R is determined to be sufficient to faithfully reproduce the one-dimensional potential curves generated via translation. In passing we note that the Taylor series expansion could also be evaluated directly by taking successive derivatives of Equation 2.1. This may be the method of choice if one is only interested in the lowest order terms in evaluating Equation 2.4 or 2.5, or if one is interested in a more "exact" reproduction of the potential curves in the vicinity of the dissociation limit.

The second model considered involves fitting the one-dimensional potential energy curves, derived in the same manner as previously discussed, to a Morse function of the form,¹⁵

$$U(R) = D_e(e^{-2\beta(R-R_0)} - 2e^{-\beta(R-R_0)}). \quad 2.6$$

The energy levels and anharmonic corrections are evaluated using

$$\omega_e = \beta \left(\frac{D_e h}{2\pi^2 c \mu} \right)^{1/2} \quad 2.7$$

$$\omega_e x_e = \frac{\beta^2 h}{8\pi^2 c \mu} \quad 2.8$$

The last model used involves an energy level fit based upon the semi-classical JWKB method.¹³ In this model, the energy levels are determined from the quantization of the action integral according to the Bohr-Sommerfeld restrictions. The governing equation is

$$I = (2\mu)^{-1/2} \oint [E - U_{\text{eff}}(R)]^{1/2} dR = h(v + 1/2) \quad 2.9$$

Energy level determination is accomplished by numerical integration of (2.9) taking $U_{\text{eff}}(R)$ as the one-dimensional intermolecular vdW potential in a tenth order polynomial form. The path of integration is taken over one complete motion cycle with the boundary conditions established by the intermolecular potential at a specific energy E .

The three "diatomic molecule" models are similar to the linear oscillator model described by Leutwyler et al.¹⁶ In all of the approximations, the atom-molecule systems are assumed to be composed of three uncoupled linear oscillators. The potential surface in these degrees of freedom can thereby be modeled by one-dimensional potential functions.

The models presented here differ from that present in ref. 16 in the respect that the linear oscillator model¹⁶ treats the system as strongly anharmonic; the Taylor series expansion, and Morse fit models treat anharmonicity from the perturbational standpoint. In this respect, the JWKB method is probably the most similar to the linear oscillator model since both approximations fit the intermolecular mode energies using the physical boundary conditions established by the intermolecular potential.

Results.

A. Benzene(Ar)₁.

Figure 2.1 and Table 2.1 present the benzene(Ar)₁ vdW cluster ${}^1B_{2u} \leftarrow {}^1A_{1g}$ spectrum recorded in the region between 38561 cm^{-1} and 38710 cm^{-1} using 1-color TOFMS. The cluster 6_0^1 is "red shifted" by 21 cm^{-1} with respect to the benzene 6_0^1 . The bathochromic shift is indicative of the greater binding energy in the cluster S_1 state relative to the cluster S_0 state. Three vibronic features are observed to the blue of the cluster 6_0^1 . No features are observed in the symmetry "forbidden" benzene 0_0^0 region; therefore, the cluster must have at least a three-fold axis of symmetry.

Figure 2.2 and Table 2.2 contain the calculational results of the ground state configuration and vdW modes of benzene(Ar)₁. Configurational calculations yield a single geometry of minimum energy for the cluster possessing C_{6v} symmetry, Figure 2.2. In this geometry, the argon atom lies 3.44 Å above the benzene molecular plane along the z (six-fold) axis. The ground state cluster binding energy is calculated at 287 cm^{-1} which makes the excited state binding energy 308 cm^{-1} . The calculated intermolecular distance of 3.44 Å compares well with that of

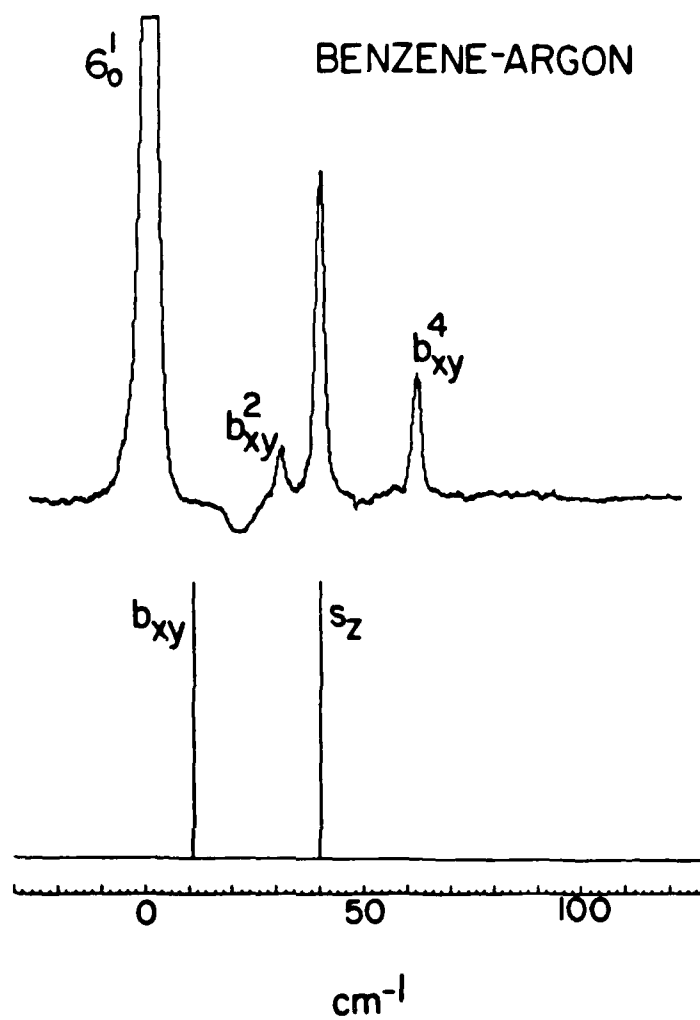


Figure 2.1

Mass selective $S_1 \leftarrow S_0$ spectrum and calculated ground state vdW modes of benzene(Ar)₁. Energy scale is relative to benzene(Ar)₁ 6_0^1 transition (38587.6 cm^{-1}). Nozzle backing conditions: $P_0 = 100 \text{ psig}$, $T_0 = 300 \text{ K}$. Peak positions and assignments as per Table 2.1 and Figure 2.2.

TABLE 2.1

vdW spectral features in benzene(Ar)₁ 6₀¹ region and calculated ground state vdW modes (refer to Figure 2.1).

Energy Relative to Cluster 6 ₀ ¹ (cm ⁻¹)	Calculated Ground ^a State Energy (cm ⁻¹)	Assignment ^a
0 (38587.6)		6 ₀ ¹
	11 (b _{xy})	
30.0		6 ₀ ¹ b _{xy0} ²
39.7	40 (s _z)	6 ₀ ¹ s _{z0} ¹
61.8		6 ₀ ¹ b _{xy0} ⁴

a) vdW mode representations as per Figure 2.2.

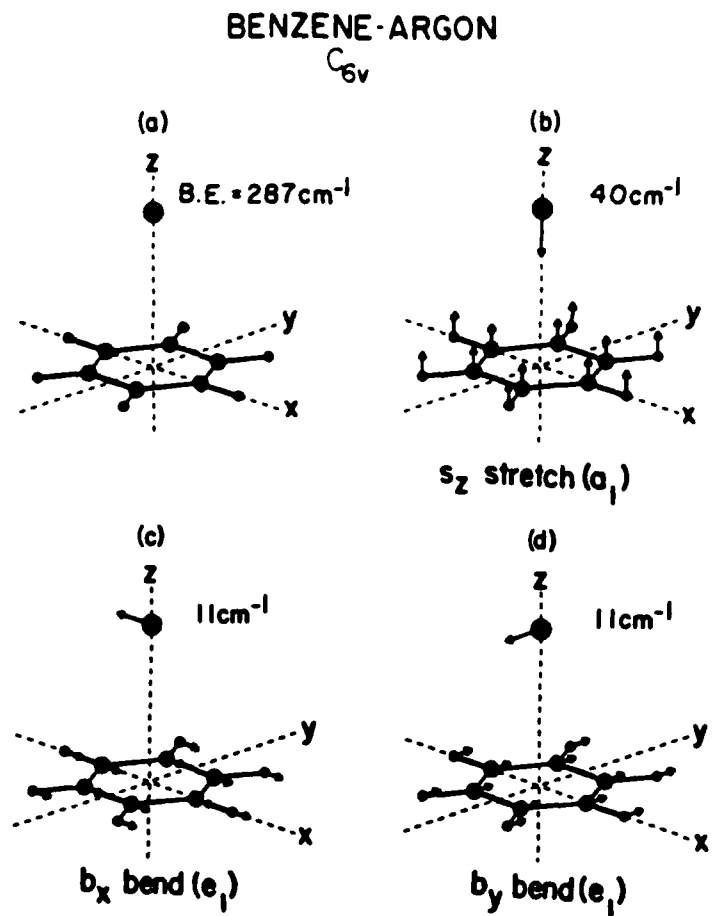


Figure 2.2

Calculated ground state minimum energy configuration (a) and eigenvalue/eigenvector vdW modes (b)-(d) for benzene(Ar)₁. Cluster symmetry is C_{6v} with an equilibrium intermolecular distance of 3.44 Å. Eigenvectors are normalized and displayed at 2x magnification (2 Å total displacement).

TABLE 2.2

Calculated ground state vdW mode energies for benzene(Ar)₁.

Model	$s_z(\text{cm}^{-1})$ ^a	$b_{xy}(\text{cm}^{-1})$ ^a
Taylor Series	40.88 (1.51)	9.80 (.03)
Morse Fit	39.47 (1.36)	10.54 (.10)
JWKB	40.05 (1.43)	9.71 (.02)
Normal Coordinate Analysis	40.0	11.0

- a) Energy presented is for a harmonic oscillator model. Values in parentheses are first order anharmonicity corrections calculated from "diatomic molecule" models. vdW mode representations as per Figure 2.2.

$3.45 \pm .2$ Å obtained from rotational analysis,¹⁵ adding independent proof to the adequacy of the calculations in predicting detailed information on cluster structure.

The eigenvalue energies from the normal coordinate analysis of benzene(Ar)₁ are 40 cm^{-1} and 11 cm^{-1} for the vdW stretch and vdW bends, respectively. The eigenvector normal modes, Figure 2.2, reveal that the vdW stretch entails purely perpendicular motion of the argon atom relative to the benzene molecular plane. Furthermore, the calculations reveal that the two-fold degenerate vdW bending mode involves some combination of motion parallel to the benzene molecular plane. Both of these eigenvector results are consistent with group theoretical arguments as expected.

The "diatomic molecule" model calculations yield three sets of vdW mode energies. The average mode frequencies are 40 cm^{-1} for the vdW stretch, $s_2(a_1)$ and 10 cm^{-1} for the vdW bends $b_{xy}(e_1)$. Figures 2.3 and 2.4 show the details of the one-dimensional potential curve mappings and the results of the model calculations. Note that the z-direction potential curve modeling the vdW stretch looks surprisingly similar in form to that of a typical diatomic molecule. All models yield both adequate potential curve fits and consistent vibrational energy level structures.

B. s-Tetrazine(Ar)₁.

Figure 2.5 presents the results of the ground state configuration and vdW mode analysis of s-tetrazine(Ar)₁. Only the normal coordinate analysis vibrational calculation is presented since this method yields the most informative results for our purposes and the consistency between the eigenvalue/eigenvector results and the "diatomic molecule" results has already been shown for the benzene(Ar)₁ case. Configurational calculations yield a single cluster geometry of minimum

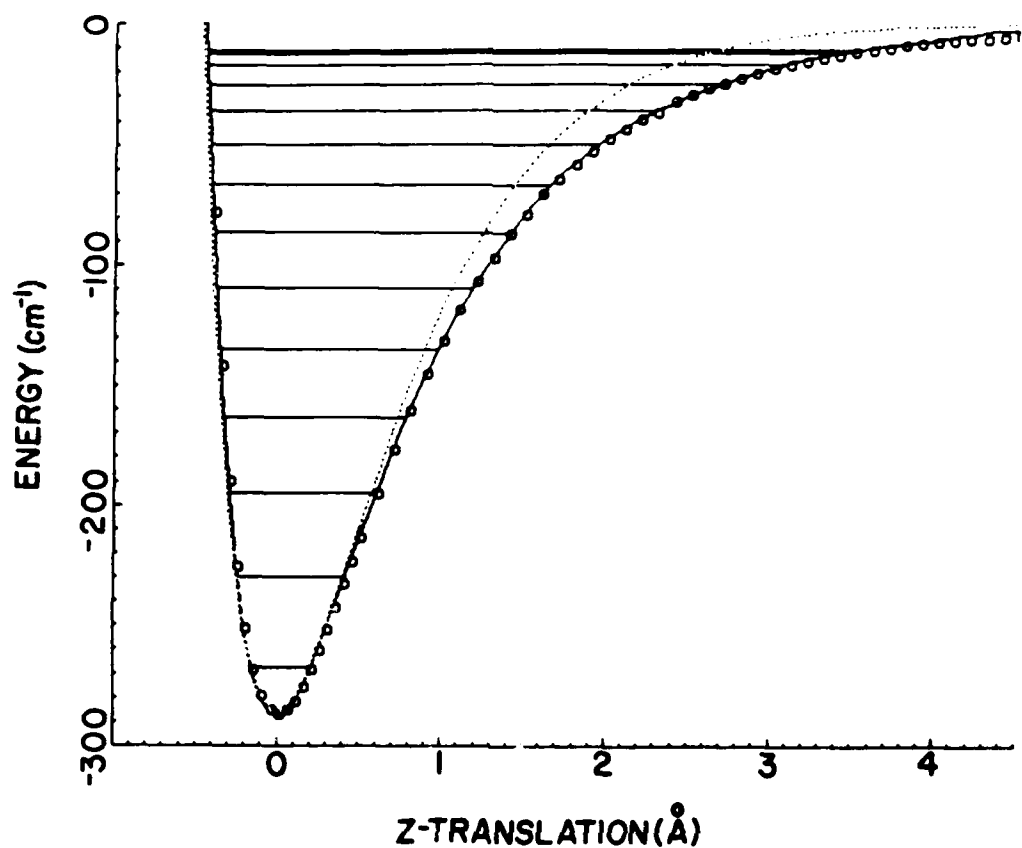


Figure 2.3

z-direction (vdW stretch) potential energy mapping of benzene(Ar)₁. Coordinate system is as shown in Figure 2.2. Translation is along z the axis with x and y coordinates at equilibrium intermolecular distance values. Translation is displayed relative to equilibrium intermolecular distance, 3.44 Å. (6-12) potential energy mapping is represented by o; Taylor series expansion and energy levels are represented by —; Morse fit potential energy curve is represented by ---. Vibrational mode constants as per Table 2.2.

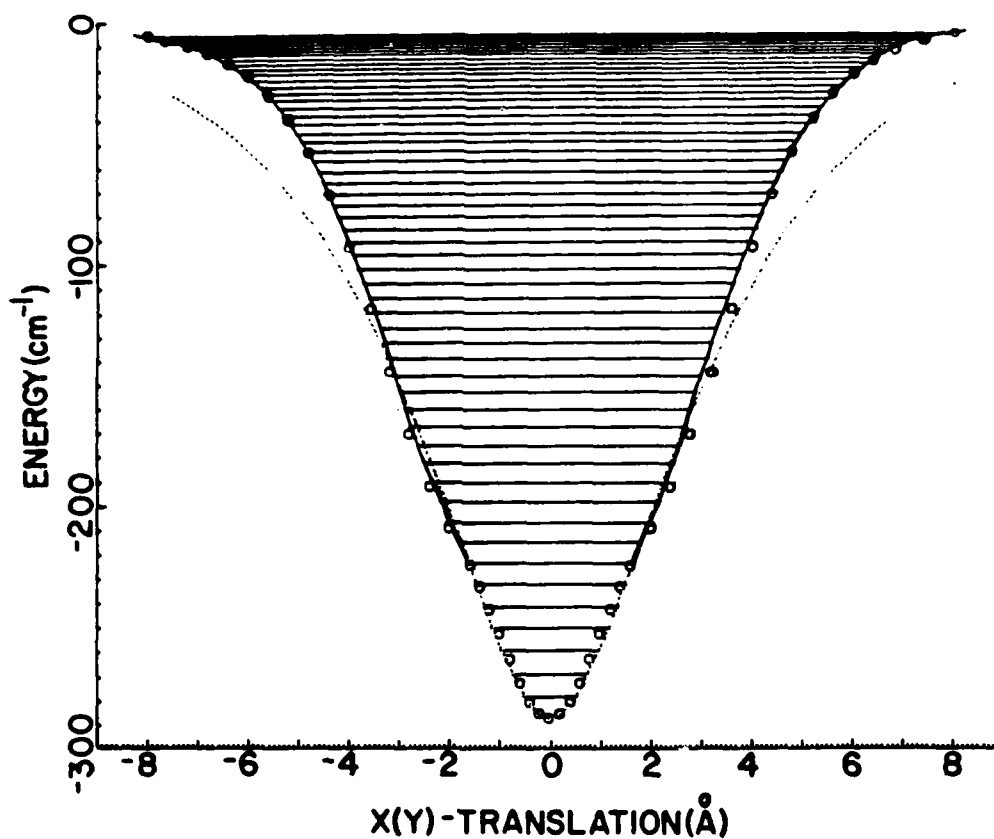


Figure 2.4

x(y)-direction (two-fold degenerate vdW bend) potential energy mapping of benzene(Ar)₁. Coordinate system is as shown in Figure 2.2. Translation is along x(y) axis with z and y(x) coordinates at equilibrium intermolecular distance values. Translation is displayed relative to equilibrium intermolecular distance 3.44 Å. (6-12) potential energy mapping is represented by o; Taylor series expansion and energy levels are represented by —; Morse fit potential energy curve is represented by ---. Vibrational mode constants as per Table 2.2.

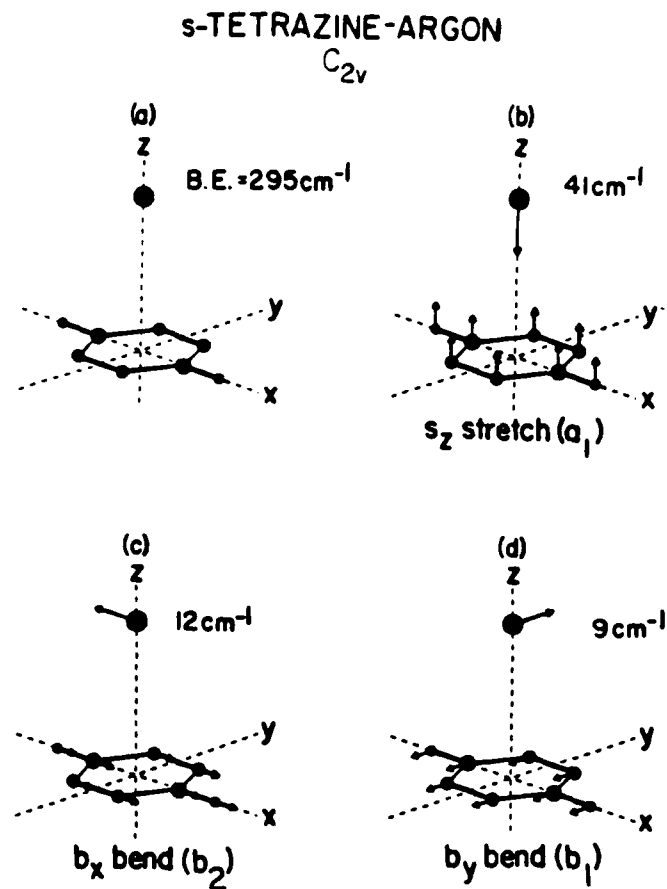


Figure 2.5

Calculated ground state minimum energy configuration (a) and eigenvalue/eigenvector vdW modes (b)-(d) for s-tetrazine(Ar)₁. Cluster symmetry is C_{2v} with an equilibrium intermolecular distance of 3.45 Å. Eigenvectors are normalized and displayed at 2x magnification (2 Å total displacement).

energy possessing C_{2v} symmetry, Figure 2.5. In this geometry, the argon atom lies 3.45 Å above the s-tetrazine molecular plane along the z (two-fold) axis. The calculated ground state cluster binding energy is 295 cm^{-1} . The calculated intermolecular distance of 3.45 Å compares extremely well with the intermolecular distance of 3.45 Å obtained from rotational analysis. The calculated binding energy of 295 cm^{-1} also lies within the experimental limits of $254 < D_0'' < 332 \text{ cm}^{-1}$.⁵ Again, the calculations and experiment are in exact agreement.

The normal coordinate analysis eigenvalues are 41.0 cm^{-1} for the vdW stretching mode $s_z(a_1)$, 9 cm^{-1} for the vdW bending mode $b_y(b_1)$, and 12 cm^{-1} for the vdW bending mode $b_x(b_2)$. The eigenvector normal modes, Figure 2.5 show that the vdW stretch is restricted to motion perpendicular to the s-tetrazine molecular plane while the vdW bends are restricted to motion parallel to the molecular plane. As in the benzene(Ar)₁ analysis, these results are consistent with group theoretical arguments.

C. Benzene(CH₄)₁.

The ground state configuration and vdW eigenvalues/eigenvectors for benzene(CH₄)₁ are shown in Figure 2.6. The results presented for the geometry and binding energy of benzene(CH₄)₁ are in good agreement with previous reports from this laboratory using an exponential-six and Lennard-Jones potential form.² In this geometry, Figure 2.6, the methane center-of-mass lies at 3.47 Å above the benzene molecular plane on the principle z (three-fold) axis. The cluster ground state binding energy is 540 cm^{-1} . The normal coordinate analysis reveals six vdW vibrations, two being two-fold degenerate. The ground state vibrational energies are 82 cm^{-1} for the vdW stretch $s_z(a_1)$.

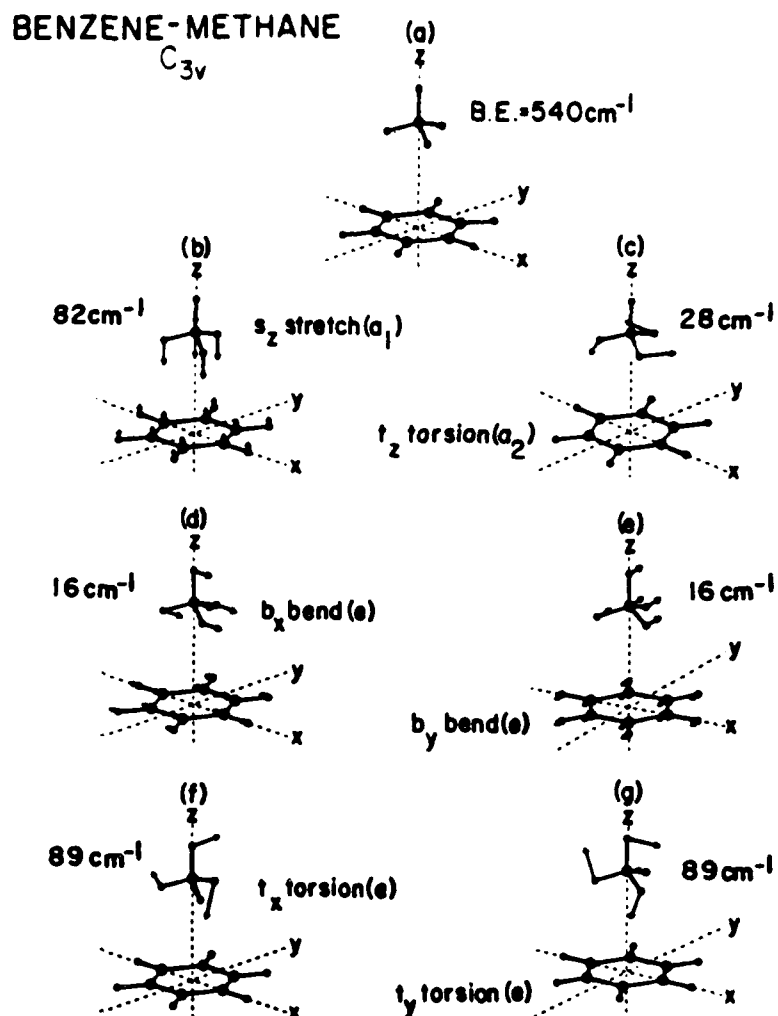


Figure 2.6

Calculated ground state minimum energy configuration (a) and eigenvalue/eigenvector vdW modes (b)-(g) for benzene(CH_4)₁. Cluster symmetry is C_{3v} with an equilibrium intermolecular distance of 3.47 Å. Eigenvectors are normalized and displayed at 2x magnification (2 Å total displacement).

16 cm^{-1} for the vdW bends $b_{xy}(e)$, and 28 cm^{-1} and 89 cm^{-1} for the vdW torsions $t_z(a_2)$ and $t_{xy}(e)$, respectively. The eigenvector normal modes, Figure 2.6, transform as the translational and rotational representations of the C_{3v} point group, as indicated. The vdW stretching mode transforms as the translation of the cluster constituents away from one another along the z (three-fold) axis. The vdW bending modes transform as some combination of cluster constituent translations in opposite directions perpendicular to the three-fold axis in the xy plane. One vdW torsion mode transforms as a rotation of the cluster constituents about the z (three-fold) axis in opposite directions. The remaining two vdW torsions transform as rotations about orthogonal axes perpendicular to the three-fold axis.

D. Benzene(H_2O)₁.

The calculated benzene(H_2O)₁ geometry used in the normal coordinate analysis is similar to that calculated previously.³ Only one minimum energy configuration, which has a binding energy of 504 cm^{-1} , is found. As shown in Figure 2.7, the cluster geometry possesses C_s symmetry with the H_2O center-of-mass located 3.15 Å above the benzene molecular plane.

Six ground state vdW vibrations are calculated for the C_s cluster geometry. Their corresponding eigenvalues and eigenvectors are shown in Figure 2.7. The six vdW modes consist of a vdW stretch at 159 cm^{-1} , two vdW bends at 14 cm^{-1} and 18 cm^{-1} , and three vdW torsions at 40 cm^{-1} , 50 cm^{-1} , and 156 cm^{-1} . The eigenvector normal modes transform as the translational and rotational representations of the C_s point group: the vdW stretch transforms as a z translation; the vdW bends transform as x and y translations; and the vdW torsions transform as R_x , R_y , and R_z rotations.

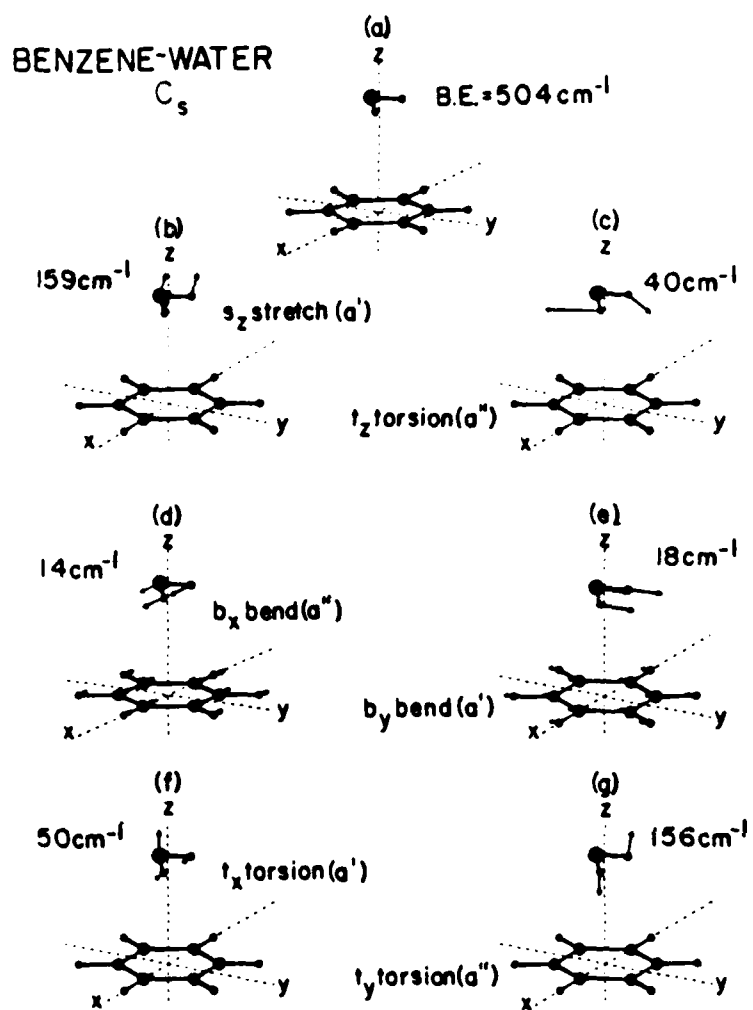


Figure 2.7

Calculated ground state minimum energy configuration (a) and eigenvalue/eigenvector vdW modes (b)-(g) for benzene(H_2O)₁. Cluster symmetry is C_s with an equilibrium intermolecular distance of 3.15 Å. Eigenvectors are normalized and displayed at 2x magnification (2 Å total displacement).

E. Benzene(NH₃)₁.

Configurational calculations on the benzene(NH₃)₁ cluster reveal two minimum energy geometries similar to those obtained previously.³ One cluster geometry possesses C_{3v} symmetry with a binding energy of 711 cm⁻¹ while the other possesses C_s symmetry and a binding energy of 608 cm⁻¹. In the C_{3v} cluster, Figure 2.8, the NH₃ center-of-mass is located 3.23 Å above the benzene molecular plane along the z (three-fold) axis. In the C_s cluster, Figure 2.9, the NH₃ center-of-mass is located 3.29 Å above the benzene molecular plane.

Using the potential surfaces generated from these two configurations, six ground state vdW vibrations are calculated for each geometry. Their corresponding eigenvalues and eigenvectors are shown in Figures 2.8 and 2.9. The C_{3v} cluster ground state normal modes transform in the same manner as those of benzene(CH₄)₁. In the C_s cluster, the ground state normal modes transform similar to those of benzene(H₂O)₁.

Discussion.

To compare the calculated and experimentally observed vdW modes, we assume that the intermolecular potential surface of the cluster is identical in both S₀ and S₁ electronic states. This assumption is justifiable if one considers that cluster fluorescence excitation and dispersed emission spectra are similar for the vdW vibronic transitions.⁴ Furthermore, the small spectral shifts of the chromophore and the weak intensity of the vdW modes signify only small changes in cluster binding energy. This is probably indicative of only slight variations of the potential surface between S₀ and S₁ electronic states.

Comparisons between calculation and experiment are made using group theoretical arguments based on the selection rules governing the

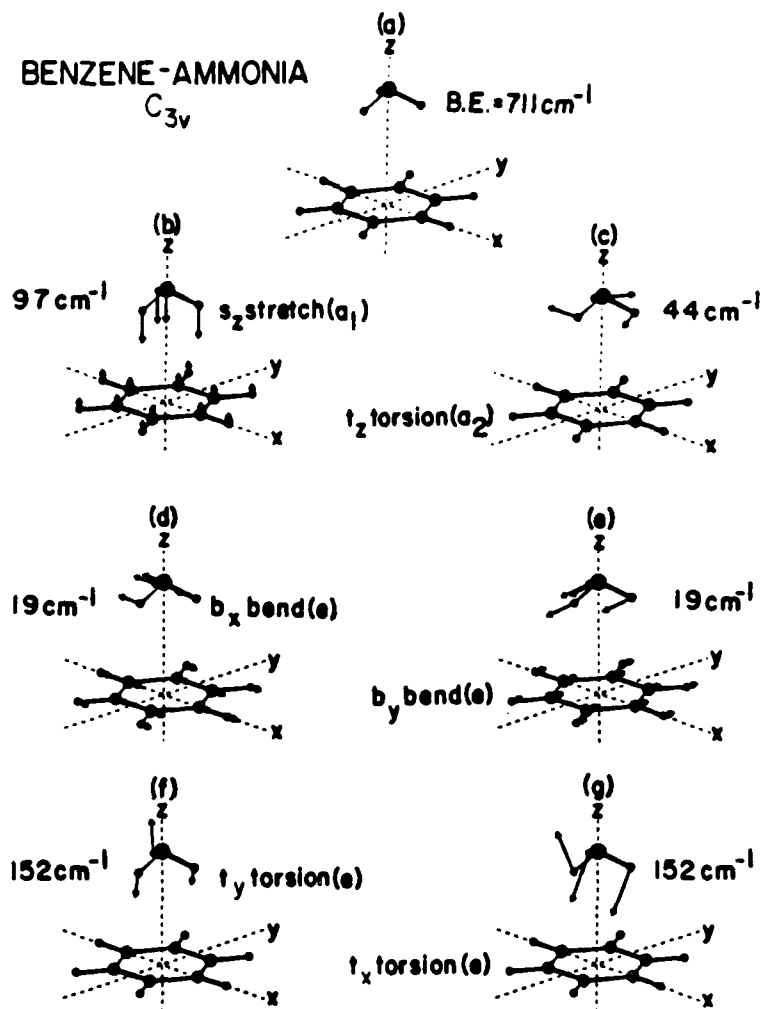


Figure 2.8

Calculated ground state minimum energy configuration (a) and eigenvalue/eigenvector vdW modes (b)-(g) for benzene(NH_3)₁. Cluster symmetry is C_{3v} with an equilibrium intermolecular distance of 3.23 Å. Eigenvectors are normalized and displayed at 2x magnification (2 Å total displacement).

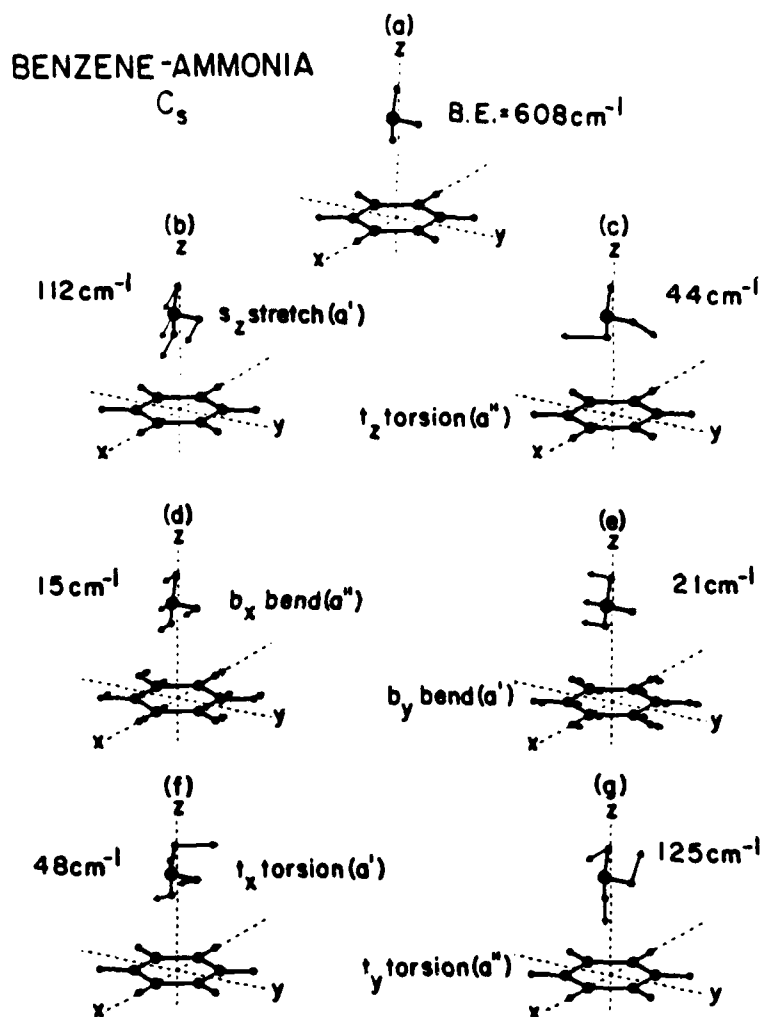


Figure 2.9

Calculated ground state minimum energy configuration (a) and eigenvalue/eigenvector vdW modes (b)-(g) for benzene(NH_3)₁. Cluster symmetry is C_s with an equilibrium intermolecular distance of 3.29 Å. Eigenvectors are normalized and displayed at 2x magnification (2 Å total displacement).

vibronic transitions. Specifically, transition moment matrix elements are qualitatively analyzed using the crude adiabatic approximation for which the vibrational mode dependence on the electronic wave function is explicit. In this case, a standard Herzberg-Teller (HT) expansion and adiabatic wave functions are used¹⁴ with the electronic wave function vibrational mode dependence truncated at second order.

Using this expansion, two unique types of spectra can be generated. First, one could consider that the vdW modes do not participate in the vibronic coupling scheme (Case I) and that they merely enter into the expansion as an additional scalar product (overlap integral). This argument dictates that only totally symmetric Franck-Condon progressions and combination bands are spectroscopically observed. Furthermore, the intensities of these features are solely derived from the cluster chromophore vibronic mode with which they are in combination. Alternatively, one could consider the vdW modes to be capable of vibronic coupling (Case II). In this case, they enter into the HT transition moment equation in the same manner as other vibronically active modes. The operator responsible for these transitions would be of the form

$$\left(\frac{\partial^2 U}{\partial Q_6 \partial q_{vdW}} \right)_{Q_6=Q_6^0, q_{vdW}=q_{vdW}^0} Q_6 q_{vdW} \quad 2.10$$

in which Q_6 is the cluster ν_6 vibrational mode and q_{vdW} is a specific cluster vdW mode. This argument allows the possibility of observing nontotally symmetric vdW fundamentals with "borrowed" intensity due to interelectronic state mixing.

In the individual cluster discussions, the above two cases are considered in order to assign and understand the observed cluster vibronic spectra.

A. Benzene(Ar)₁.

Comparison of the calculated ground state vdW vibrations of benzene(Ar)₁ and the experimental ¹B_{2u} ← ¹A_{1g} vibronic spectrum, Figure 2.1, Table 2.1, and Table 2.2, shows that vibronic assignments can be made based upon calculations for all models analyzed. Considering the transition moment matrix elements for the benzene(Ar)₁ S₁ ← S₀ transition under C_{6v} symmetry, one should expect to observe totally symmetric combination bands of the vdW stretch built upon the cluster 6₀¹. The selection rule for these combination bands is Δv = 0, ±1, ±2, ... Also, one should expect to observe nontotally symmetric vdW bend combinations with the 6₀¹ with the selection rule being Δv = 0, ±2, ±4 ... These selection rules hold for both Case I and Case II type spectra and imply that the vdW modes do not enter into the vibronic intensity borrowing mechanism.

The calculated vdW stretching mode at 40 cm⁻¹ compares quite well with the experimental vibronic feature at 39.7 cm⁻¹ to the blue of the benzene(Ar)₁ 6₀¹. Thus, this feature is assigned to the benzene(Ar)₁ vdW stretch/cluster 6₀¹ combination band 6₀¹ s_z(a₁)₀¹ based upon the Δv = 0, ±1, ±2 ... selection rule.

For vdW bending modes, only odd overtones are expected to be observed as pointed out above. The experimentally observed features at 30.9 cm⁻¹ and 61.8 cm⁻¹ to the blue of the cluster 6₀¹ correspond to overtone features of the vdW bends; using the Δv = 0, ±2, ±4 ... selection rule, the former feature is the first overtone of the vdW bends and the latter is the third. Considering the 30.9 cm⁻¹ feature as the first overtone places the symmetry forbidden bend fundamental at about 15.5 cm⁻¹. This energy lies close to the calculated two-fold

degenerate ground state vdW bend at 11 cm^{-1} . Thus, these two spectral features are assigned to the benzene(Ar)₁ vdW bends first and third overtone/cluster 6_0^1 combination bands, $6_0^1 b_{xy}(e_1)_0^2$ and $6_0^1 b_{xy}(e_1)_0^4$.

Ramifications of Herzberg-Teller vibronic coupling in the benzene(Ar)₁ cluster are obvious. From the derived vibronic selection rules and experimental observation, the benzene(Ar)₁ cluster spectrum is best assigned based upon benzene Herzberg-Teller coupling (i.e., the 6_0^1 feature is allowed) with vdW totally symmetric modes and combinations forming short, weak Franck-Condon progressions built upon the intense benzene transition. In addition, the calculated and observed¹⁵ C_{6v} cluster symmetry is verified by the vdW vibronic structure.

B. s-Tetrazine(Ar)₁.

The selection rules governing the s-tetrazine(Ar)₁ vdW vibronic transitions under C_{2v} symmetry arise from Case I Franck-Condon arguments. The totally symmetric vdW stretch should be observed to the blue of the cluster 0_0^0 following a $\Delta v = 0, \pm 1, \pm 2, \dots$ selection rule. The vdW bends should only be observed in odd overtones ($\Delta v = 0, \pm 2, \pm 4 \dots$) built on the allowed s-tetrazine 0_0^0 transition. As in the benzene(Ar)₁ cluster, no Case II distinction can be made for s-tetrazine(Ar)₁ and thus no vdW Herzberg-Teller vibronic coupling is expected. Unfortunately, a complete experimental spectrum showing the details of the s-tetrazine(Ar)₁ vdW modes is not, as yet, available. The only information in this regard is the identification of the vdW stretching mode at 44 cm^{-1} to the blue of the cluster 0_0^0 by Levy et al.⁵ Other vdW features at 66 cm^{-1} and 108 cm^{-1} to the blue of the cluster 0_0^0 are observed, but they are neither assigned nor are their spectra published.

Figure 2.10 and Table 2.3 compare the calculated ground state vdW mode frequencies with those observed in the s-tetrazine(Ar)₁ $^1B_{3u} \leftarrow ^1A_g$

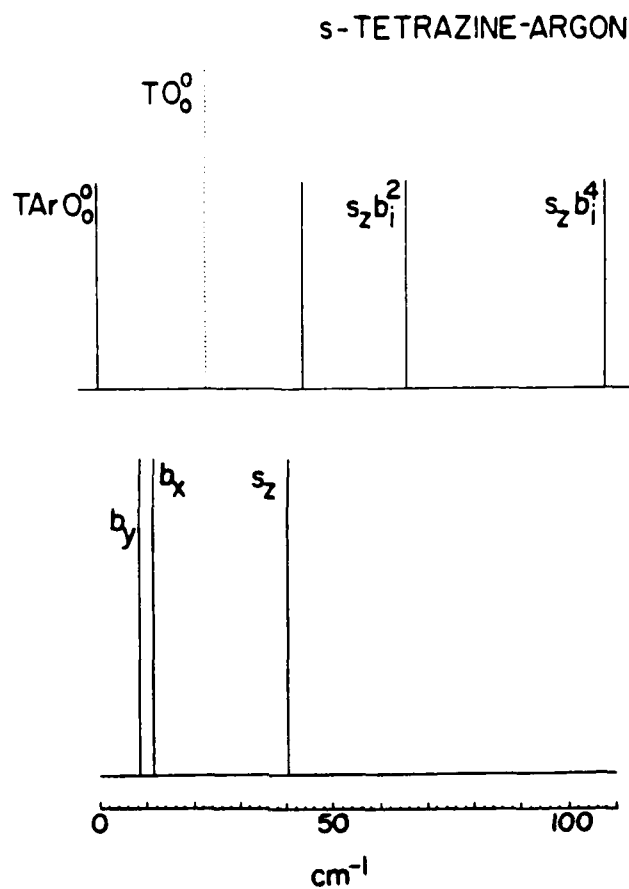


Figure 2.10

Schematic ${}^1B_{3u} \leftarrow {}^1A_g$ spectrum (from ref. 5) and calculated ground state vdW modes of s-tetrazine(Ar)₁. Energy scale is relative to s-tetrazine(Ar)₁ 0_0^0 transition (18104.9 cm^{-1}). Relative feature intensities are not shown. Feature positions and assignments as per Table 2.3 and Figure 2.5. vdW bends are represented by b_i in schematic spectrum (see text for explanation).

TABLE 2.3

vdW spectral features in s-tetrazine(Ar)₁ 0₀⁰ region
(s-tetrazine 1B_{3u} ← 1A_g) and calculated ground state vdW modes (refer to
Figure 2.10).

Energy Relative to Cluster 0 ₀ ⁰ (cm ⁻¹) ^c	Calculated Ground State Energy (cm ⁻¹) ^b	Assignment ^b
0 (18104.9)		0 ₀ ⁰
	9 (b _y)	
	12 (b _x)	
44 ^a	41 (s _z)	s _{z0} ¹
66		s _{z0} ¹ b _{x0} ² or s _{z0} ¹ b _{y0} ²
108		s _{z0} ¹ b _{x0} ⁴ or s _{z0} ¹ b _{y0} ⁴

a) Observed and assigned in Reference 5.

b) vdW mode representations as per Figure 2.5.

c) From Reference 5.

vdW vibronic spectrum. The experimentally assigned vdW stretch at 44 cm^{-1} to the blue of the cluster 0_0^0 corresponds to the 41 cm^{-1} calculated ground state stretch. This motion, like that in the benzene(Ar)₁ cluster, involves perpendicular motion of the argon atom relative to the s-tetrazine molecular plane. Based upon ground state calculations, the feature 66 cm^{-1} to the blue of the cluster 0_0^0 probably corresponds to a vdW stretch/vdW bend overtone combination band, $s_z(a_1)_0^1 b_x(b_2)_0^2$ or $s(a_1)_0^1 b_y(b_1)_0^2$; the feature at 108 cm^{-1} probably corresponds to the next allowed bend overtone/stretch combination band $s(a_1)_0^1 b_x(b_2)_0^4$ or $s(a_1)_0^1 b_y(b_1)_0^4$. No speculation with regard to which band is responsible for the features observed will be made since no spectra of sufficient sensitivity are available for analysis.

C. Benzene(CH₄)₁.

In a previous analysis of the benzene(CH₄)₁ cluster,² three major vdW vibronic features were reported in the cluster 6_0^1 region: these features were assigned to a bend fundamental (27.3 cm^{-1}), a stretch fundamental (32.3 cm^{-1}), and a stretch overtone (51.4 cm^{-1}). The assignments were made based upon the assumptions described in the Introduction.

Considering the HT transition moment matrix elements and assuming a Case I type spectrum, the selection rules for the benzene(CH₄)₁ vdW vibronic transitions are $\Delta v = 0, \pm 1, \pm 2, \dots$ for the vdW stretch and $\Delta v = 0, \pm 2, \pm 4, \dots$ for the vdW bends and torsions when in combination with the cluster 6_0^1 .

The selection rules involved in Case II can be viewed in two ways. The selection rules can be derived using the calculated cluster symmetry of C_{3v} , or they can be derived by considering the cluster

symmetry as C_{6v} . The latter situation arises since the methane center-of-mass is calculated at 3.47 Å above the benzene molecular plane. At this distance, the methane could be viewed as a sphere above the benzene molecular plane and, hence, the use of the C_{6v} point group to represent the vdW mode symmetries could be warranted.

In C_{3v} symmetry Case II, the selection rules for vdW mode combinations with the cluster 6_0^1 are $\Delta v = 0, \pm 1, \pm 2, \dots$ for all six vdW modes. If C_{3v} is the correct cluster physical symmetry and HT vdW coupling exists, all modes can be observed in the cluster 6_0^1 region. In C_{6v} symmetry, Case II, the selection rules for the vdW mode combinations with the cluster 6_0^1 are $\Delta v = 0, \pm 1, \pm 2, \dots$ for the vdW stretch $s_z(a_1)$ and torsion $t_z(a_2)$ and $\Delta v = 0, \pm 2, \pm 4, \dots$ for the two-fold degenerate vdW bends $b_{xy}(e_1)$ and torsions $t_{xy}(e_1)$. In this approximate high symmetry, only the cluster 6^1 and vdW mode t_z are capable of vibronic coupling for the 6_0^1 transition.

Comparison of the experimental 6_0^1 vibronic spectrum of benzene(CH_4)₁ and the calculated ground state vdW vibrations is shown in Figure 2.11 and Table 2.4. The observed feature at 27.3 cm^{-1} to the blue of the cluster 6_0^1 corresponds to the t_z torsion calculated at 28 cm^{-1} . Thus, this feature and its observed overtones at 51.4 cm^{-1} and 73.5 cm^{-1} are reassigned to 6_0^1 vdW torsion combination bands $6_0^1 t_z(a_2)_0^1$, $6_0^1 t_z(a_2)_0^2$, and $6_0^1 t_z(a_2)_0^3$, using the C_{3v} Case II or C_{6v} Case II $\Delta v = 0, \pm 1, \pm 2, \dots$ selection rule. The $\Delta v = 0, \pm 1, \pm 2, \dots$ selection rule suggests that for the benzene(CH_4)₁ system vdW mode Herzberg-Teller vibronic coupling is an important component of the overall intensity mechanism. In the present case, the occurrence of the nontotally symmetric t_z torsion progression implies that the vdW modes are

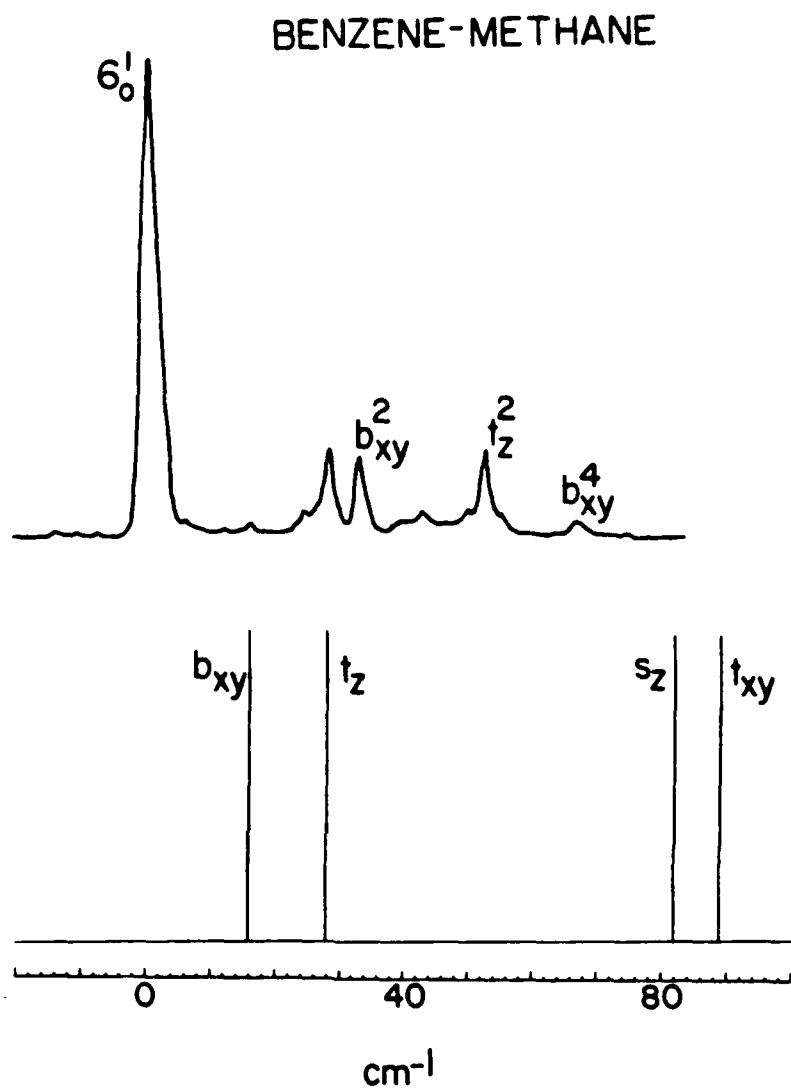


Figure 2.11

Mass selective $S_1 \leftarrow S_0$ spectrum (ref. 2) and calculated ground state vdW modes of benzene(CH_4)₁. Energy scale is relative to benzene(CH_4)₁ 6_0^1 transition (38567.6 cm^{-1}). Feature positions and assignments as per Table 2.4 and Figure 2.6.

TABLE 2.4

vdW spectral features in benzene(CH₄)₁ 6₀¹ region and calculated ground state vdW modes (refer to Figure 2.11).

Energy Relative to Cluster 6 ₀ ¹ (cm ⁻¹) ^a	Calculated Ground State Energy (cm ⁻¹) ^b	Assignment ^b
0 (38567.6)		6 ₀ ¹
16.1	16 (b _{xy})	6 ₀ ¹ h _{xyo} ¹
27.3	28 (t _z)	6 ₀ ¹ t _{zo} ¹
32.3		6 ₀ ¹ b _{xyo} ²
48.4		6 ₀ ¹ b _{xyo} ³
51.4		6 ₀ ¹ t _{zo} ²
64.6		6 ₀ ¹ h _{xyo} ⁴
73.5		6 ₀ ¹ t _{zo} ³
	82 (s _z)	
	89 (t _{xy})	

a) From Reference 2 and unpublished spectra.

b) vdW mode representations as per Figure 2.6.

vibronically active and that assuming them to be nonparticipants in the coupling mechanism oversimplifies the physics necessary to explain the cluster's spectroscopy.

The intense feature at 32.3 cm^{-1} to the blue of the cluster 6_0^1 corresponds to the first overtone of the two-fold degenerate vdW bending mode, $6_0^1 b_{xy}(e)_0^2$, calculated at 16 cm^{-1} . This identification is based upon the observation of a feature at 64.6 cm^{-1} which corresponds to the third overtone of the bends. Furthermore, weak intensity features are observed at about 16.1 cm^{-1} and 48.4 cm^{-1} which could correspond to the vdW bend fundamentals and second overtones. The observation of these features adds proof to the arguments suggesting that the vdW modes are, at least, minor participants in the Herzberg-Teller vibronic coupling scheme. The cluster symmetry and, hence, spectroscopy are thereby also best described using the calculated C_{3v} point group in conjunction with Herzberg-Teller coupling rather than the approximate C_{6v} point group. Based upon this, the features at 32.3 cm^{-1} and 64.6 cm^{-1} are reassigned to vdW bend overtone combinations with the cluster 6_0^1 ; $6_0^1 b_{xy}(e)_0^2$ and $6_0^1 b_{xy}(e)_0^4$ using the C_{3v} selection rule $\Delta v = 0, \pm 1, \pm 2, \dots$. The features are assigned in Table 2.4 and Figure 2.11. The weak features at 16.1 cm^{-1} and 48.4 cm^{-1} are assigned to $6_0^1 b_{xy}(e)_0^1$ and $6_0^1 b_{xy}(e)_0^3$. Based upon the relative intensities displayed in the spectrum, vdW vibronic coupling is an important factor in the intensity of this progression involving the e symmetry bending modes.

Neither the vdW stretch $s_z(a_1)$ nor the two-fold degenerate torsions $t_{xy}(e)$ are observed in the 6_0^1 spectrum. This could be due to poor Franck-Condon factors for these vibronic transitions since they are both calculated to be at relatively high energies (ca. 82 cm^{-1} and

89 cm^{-1} , respectively). Moreover, these modes could be participating in VP since the total energy $6_0^1 s_z(a_1)_0^1$ or $6_0^1 t_{xy}(e)_0^1$ is close to that of, if not above, the cluster's S_1 binding energy. Both the vdW stretch and t_{xy} torsions involve motion perpendicular to the benzene molecular plane: this motion could couple well to the VP process.

D. Benzene(H_2O)₁.

The $S_1 - S_0$ vibronic spectrum of benzene(H_2O)₁ previously observed in this laboratory³ possesses two unique spectral regions located around the cluster 0_0^0 and 6_0^1 containing vdW vibronic features. No vdW vibronic assignments were made in either region and no correlation between the regions was suggested.

Examination of the HT transition moment matrix elements using C_s symmetry and Case I considerations leads to the selection rules $\Delta v = 0, \pm 1, \pm 2, \dots$ for the vdW s_z stretch, b_y bend, and t_x torsion and $\Delta v = 0, \pm 2, \pm 4, \dots$ for the b_x bend, t_y and t_z torsions. Under Case II arguments, the selection rule is $\Delta v = 0, \pm 1, \pm 2, \dots$ for all six vdW modes: all modes are capable of vibronic coupling.

Vibronic spectra of benzene(H_2O)₁ in both cluster 0_0^0 and 6_0^1 regions are reproduced in Figure 2.12 along with the calculated ground state vdW mode energies. The observed feature at 5.2 cm^{-1} (4.8 cm^{-1}) to the blue of the cluster 0_0^0 (6_0^1) transition corresponds to the vdW b_x bend fundamental calculated at 14 cm^{-1} . The observed feature at 16.2 cm^{-1} (15.8 cm^{-1}) to the blue of the cluster 0_0^0 (6_0^1) transition corresponds to the calculated totally symmetric vdW b_y bend at 18 cm^{-1} . Additionally, the observed features at 34.6 cm^{-1} (34.6 cm^{-1}) and 49 cm^{-1} (48.4 cm^{-1}) to the blue of the cluster 0_0^0 (6_0^1) transition are associated with the $t_z(a'')$ and $t_x(a')$ torsion fundamentals calculated at 40 cm^{-1}

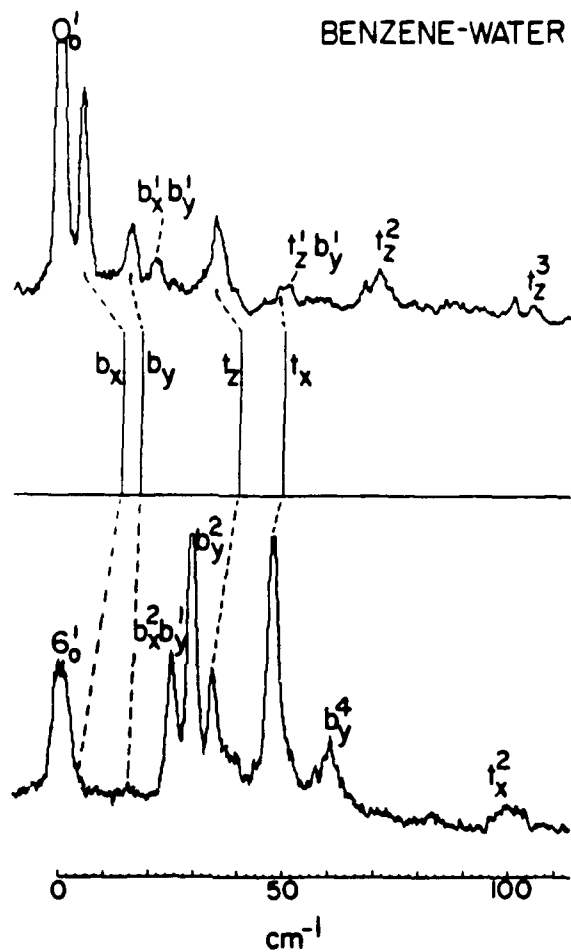


Figure 2.12

Mass selective $S_1 \leftarrow S_0$ spectra (ref. 3) and calculated ground state vdW modes of benzene(H_2O)₁. Energy scale is relative to benzene(H_2O)₁ 0_0^0 and 6_0^1 transitions (38168.6 cm^{-1} and 38655.4 cm^{-1} , respectively). Feature positions and assignments as per Table 2.5 and Figure 2.7. s_z and t_y vdW modes are not shown.

and 50 cm^{-1} , respectively. The occurrence of the nontotally symmetric fundamentals implies that the $\Delta v = 0, \pm 2, \pm 4, \dots$ selection rule for Case I in which the vdW modes are not vibronically coupled is violated. The violation suggests that the vdW modes participate in the vibronic coupling scheme and that the $\Delta v = 0, \pm 1, \pm 2, \dots$ selection rule should apply to all six vdW modes (Case II). Based upon this, the spectra are best assigned, Table 2.5 and Figure 2.12, using both nontotally and totally symmetric vdW progressions.

Assigning the benzene(H_2O)₁ spectra using the C_s point group representations corroborates the calculated cluster geometry. Treating the cluster in approximate high symmetries, such as C_{2v} , leads to selection rules which are clearly violated when applied to spectral observation and assignment. Specifically, the bend and torsion fundamentals are forbidden under these higher symmetry approximations. Furthermore, the spectral assignments using C_s symmetry arguments suggest that the water constituent is likely located above the benzene molecular plane.

Neither the vdW s_z stretch nor the t_y torsion are observed in either spectral region. This as in the benzene(CH_4)₁ case, probably results from poor Franck-Condon factors for these particular modes; they are both calculated to be at relatively high energies (ca. 159 cm^{-1} and 156 cm^{-1} , respectively). Moreover, in the 6_0^1 region, these modes could be participating in VP since the total energy of the system at these levels ($486.8 + 159 \text{ cm}^{-1}$ for the stretch; $486.8 + 156 \text{ cm}^{-1}$ for t_y) is close to, if not above, the cluster binding energy (ca. $= 500 \text{ cm}^{-1}$). The decrease in the hypsochromic shift and the shift of intensity maximum in the vdW manifold in going from the cluster 0_0^0 to the 6_0^1 may also be indicative of the VP process.

TABLE 2.5

vdW spectral features in benzene(H_2O)₁ 0_0^0 and 6_0^1 region and calculated ground state vdW modes (refer to Figure 2.12).

Energy Relative to Cluster 0_0^0 (cm^{-1}) or 6_0^1 (cm^{-1}) ^a	Calculated Ground State Energy (cm^{-1}) ^b	Assignment ^b
0 (38168.6)		0_0^0
5.2	14 (b_x)	b_{x0}^1
16.2	18 (b_y)	b_{y0}^1
21.4		$b_{x0}^1 b_{y0}^1$
25		$b_{x0}^2 b_{y0}^1$
31.9		b_{y0}^2
34.6	40 (t_z)	t_{z0}^1
39.4		$t_{z0}^1 b_{x0}^1$
45.7		b_{y0}^3
49	50 (t_x)	t_{x0}^1
50.8		$t_{z0}^1 b_{y0}^1$
67.4		$t_{x0}^1 b_{y0}^1$
70.3		t_{z0}^2
99.5		t_{x0}^2
103.5		t_{z0}^3
-	156 (t_y)	
-	159 (s_z)	
0 (38655.4)		6_0^1
4.8	14 (b_x)	$6_0^1 b_{x0}^1$
15.8	18 (b_y)	$6_0^1 b_{y0}^1$

TABLE 2.5 (Continued)

25.5		$6_0^1 b_{x_0}^2 b_{y_0}^1$
30.3		$6_0^1 b_{y_0}^2$
34.6	40 (t_z)	$6_0^1 t_{z_0}^1$
39.6		$6_0^1 t_{z_0}^1 b_{x_0}^1$
48.8	50 (t_x)	$6_0^1 t_{x_0}^1$
60.5		$6_0^1 b_{y_0}^4$
97.8		$6_0^1 t_{x_0}^2$
101.0		$6_0^1 t_{z_0}^3$
	156 (t_y)	
	159 (s_z)	

a) From Reference 3.

b) vdW mode representations as per Figure 2.7.

E. Benzene(NH₃)₁.

Benzene(NH₃)₁ clusters recently observed in this laboratory³ yield spectra in both the cluster 0_0^0 and 6_0^1 regions. Two cluster geometries are calculated for the system, one possessing C_s symmetry and the other possessing C_{3v} symmetry. From symmetry arguments the C_s symmetry cluster is the only contributor to the 0_0^0 spectrum while both cluster geometries contribute to the 6_0^1 spectrum. Neither of these spectra were analyzed nor assigned in the initial observation since they are so complicated. They were merely presented as an indication of the notion that cluster vibronic spectra can sometimes be very extensive and congested.

The benzene(NH₃)₁ C_s symmetry cluster follows the same vdW vibronic selection rules as derived for the benzene(H₂O)₁ cluster. In this symmetry, the selection rules for Case I are $\Delta v = 0, \pm 1, \pm 2, \dots$ for the vdW stretch, b_y bend, and t_x torsion and $\Delta v = 0, \pm 2, \pm 4, \dots$ for the b_x bend, t_y and t_z torsions. In Case II the selection rule is $\Delta v = 0, \pm 1, \pm 2, \dots$ for all six vdW modes. Furthermore, the calculated cluster geometries are qualitatively similar. Hence, their 0_0^0 spectra should be qualitatively similar: this is borne out in both experimental results and vibrational mode calculations.

The benzene(NH₃)₁ C_{3v} symmetry cluster follows the same vibronic selection rules as presented for benzene(CH₄)₁. Here the selection rules are either $\Delta v = 0, \pm 1, \pm 2, \dots$ for the vdW stretch and $\Delta v = 0, \pm 2, \pm 4, \dots$ for the vdW bends and torsions (Case I) or $\Delta v = 0, \pm 1, \pm 2, \dots$ for all six vdW modes (Case II).

The calculated ground state vibrational energies and the observed cluster 0_0^0 and 6_0^1 vibronic spectra are compared in Figure 2.13. Due to

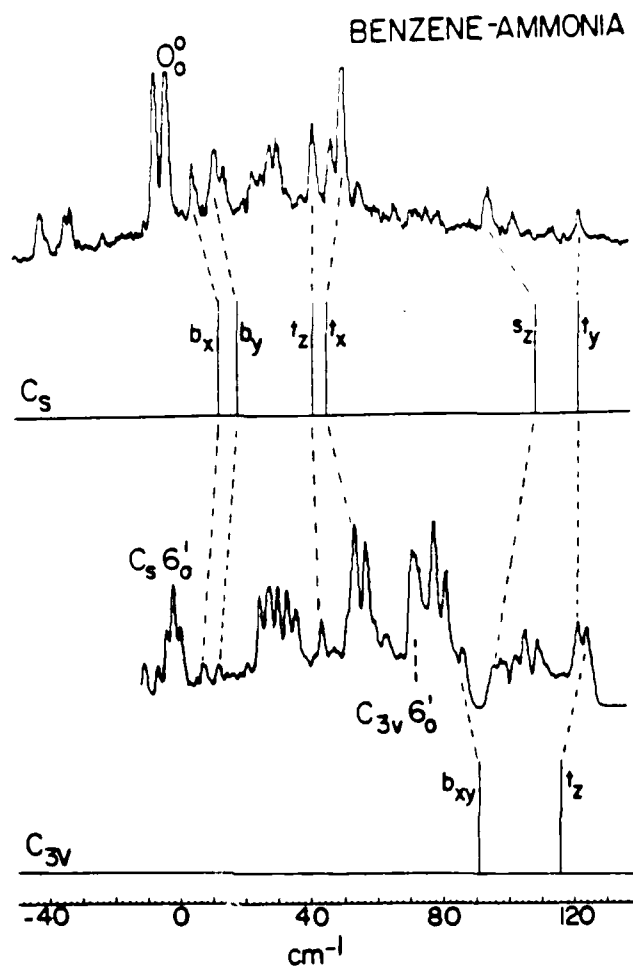


Figure 2.13

Mass selective $S_1 \leftarrow S_0$ spectra (ref. 3) and calculated ground state vdW modes of benzene(NH_3)₁. Energy scale is relative to benzene(NH_3)₁ 0_0^0 and 6_0^1 transitions for C_s cluster (38021.1 cm^{-1} and 38514.7 cm^{-1} , respectively). Feature positions and assignments as per Table 2.6 and Figure 2.8 and 2.9. C_{3v} cluster s_z and t_{xy} modes are not shown.

the complex nature of the spectra which possibly results from hot bands, only tentative assignments of the vdW mode progressions are made. The tentative assignments are based upon both vibrational mode calculations and upon inference from the benzene(H₂O)₁ and benzene(CH₄)₁ cluster spectra.

In the 0₀⁰ spectrum, the most intense low energy feature is assigned to the origin of the cluster's S₁ ← S₀ transition. The smaller intensity features to the red of this feature are thus hot bands which yield the sequence structure in the 0₀⁰ region. The observed feature at 8.8 cm⁻¹ to the blue of the cluster 0₀⁰ corresponds to the nontotally symmetric vdW b_x bend fundamental calculated at 15 cm⁻¹. Additionally, the observed features at 15.0 cm⁻¹, 45.1 cm⁻¹, 54.2 cm⁻¹, 99.6 cm⁻¹, and 127.7 cm⁻¹ correspond to the calculated b_y bend (21 cm⁻¹), t_z torsion (44 cm⁻¹), t_x torsion (48 cm⁻¹), stretch (112 cm⁻¹), and t_y torsion (125 cm⁻¹). The occurrence of the nontotally symmetric fundamentals suggests that the vdW modes participate in vibronic coupling (Case II) and that the Δv = 0, ±1, ±2, ... selection rule should apply to all six vdW modes. Using this selection rule, the spectrum is best assigned, Table 2.6, using both nontotally and totally symmetric vdW progressions.

In the 6₀¹ spectrum, the most intense low energy feature is assigned to the cluster 6₀¹ vibronic origin. This assignment bears a resemblance to the benzene(H₂O)₁ 6₀¹ spectrum in the respect that the 6₀¹ features for both clusters are red shifted relative to that observed at the S₁ ← S₀ origins (ca. 25 cm⁻¹ for benzene(NH₃)₁ and 35 cm⁻¹ for benzene(H₂O)₁).

Table 2.6 presents the C_s symmetry geometry assignments in the 6₀¹ region. The assignments are made using the vdW fundamentals identified

TABLE 2.6

vdW spectral features in benzene(NH₃)₁ 0₀⁰ and 6₀¹ region and calculated ground state vdW modes (refer to Figure 2.13).

Energy Relative to ^a Cluster 0 ₀ ⁰ (cm ⁻¹) or 6 ₀ ¹ (cm ⁻¹)	Calculated Ground State Energy (cm ⁻¹) ^b	Assignment ^{b,c}
-39.2		b _{y2} ⁰
-36.7		
-33.4		b _{x2} ⁰ b _{y1} ⁰
-31.3		b _{y2} ⁰ b _{x0} ¹
-29.6		
-26.7		b _{x1} ⁰ b _{y1} ⁰
-19.2		b _{y1} ⁰
- 6.7		b _{x1} ⁰
- 3.8		
0 (38021.1)		0 ₀ ⁰
8.8	15 (b _x)	b _{x0} ¹
15.0	21 (b _y)	b _{y0} ¹
17.9		b _{x0} ²
24.2		b _{x0} ¹ b _{y0} ¹
26.7		b _{x0} ³
29.0		b _{y0} ²
32.1		b _{x0} ² b _{y0} ¹
34.2		b _{xc} ⁴
37.6		b _{x0} ¹ b _{y0} ²
41.7		
45.1	44 (t _z)	t _{z0} ¹

TABLE 2.6 (Continued)

50.9		
54.2	48 (t_x)	t_{x0}^1
59.7		$t_{z0}^1 h_{y0}^1$
64.7		$t_{x0}^1 b_{x0}^1$
70.4		$t_{x0}^1 h_{y0}^1$
75.5		$t_{x0}^1 b_{x0}^2$
77.2		
80.1		$t_{x0}^1 b_{x0}^1 b_{y0}^1$
83.8		$t_{x0}^1 h_{y0}^2$
99.6	112 (s_z)	s_{z0}^1
101.8		$t_{x0}^1 t_{z0}^1$
107.2		$s_{z0}^1 t_{x0}^1$
111.8		$t_{x0}^1 t_{z0}^1 b_{x0}^1$
114.3		$s_{z0}^1 b_{y0}^1$
119.3		$t_{x0}^1 t_{z0}^1 h_{x0}^2$
122.7		$s_{z0}^1 b_{x0}^1 b_{y0}^1$
127.7	125 (t_y)	t_{y0}^1
- 9.0		$6_0^1 h_{x0}^1$
- 4.9		
- 2.0		
0 (38514.7)		$6_0^1 (C_s)$
2.0		
9.0	15 (b_x)	$6_0^1 b_{x0}^1$
13.1	21 (b_y)	$6_0^1 b_{y0}^1$
22.1		

TABLE 2.6 (Continued)

26.2		$6_0^1 h_{x0}^3$
29.5		$6_0^1 h_{y0}^2$
32.0		$6_0^1 b_{x0}^2 b_{y0}^1$
34.4		$6_0^1 h_{x0}^4$
37.3		$6_0^1 b_{y0}^2 b_{x0}^1$
45.1	44 (t_z)	$6_0^1 t_{z0}^1$
48.7		
53.7		$6_0^1 t_{z0}^1 h_{x0}^1$
55.3	48 (t_x)	$6_0^1 t_{x0}^1$
58.6		$6_0^1 t_{z0}^1 h_{y0}^1$
61.0		$6_0^1 t_{z0}^1 b_{x0}^2$
64.7		$6_0^1 t_{x0}^1 h_{x0}^1$
68.8		$6_0^1 t_{x0}^1 b_{y0}^1$
72.9 [0 (38587.6)]		$6_0^1 (C_{3v})$
74.6		$6_0^1 t_{x0}^1 b_{x0}^2$
79.5		$6_0^1 t_{x0}^1 h_{x0}^1 h_{y0}^1$
83.3		$6_0^1 t_{x0}^1 b_{y0}^2$
87.9	19 (b_{xy})	$6_0^1 h_{xy0}^1 (C_{3v})$
98.7	112 (s_z)	$6_0^1 s_{z0}^1$
100.4		$6_0^1 t_{x0}^1 t_{z0}^1$
103.9		$6_0^1 h_{xy0}^2 (C_{3v})$
107.1		$6_0^1 s_{z0}^1 h_{x0}^1$
111.9		$6_0^1 t_{x0}^1 t_{z0}^1 b_{x0}^1$
114.0		$6_0^1 s_{z0}^1 h_{y0}^1$
123.4		$6_0^1 s_{z0}^1 b_{x0}^1 h_{y0}^1$

TABLE 2.6 (Continued)

125.9	44 (t_z)	$6^1_{z0} t_{z0}^1(C_{3v})$
-	97 (s_z)	-
-	152 (t_{xy})	-

a) From Reference 3.

b) vdW mode representations as per Figure 2.8 and 2.9.

c) C_{3v} cluster 6^1_0 contributions tabulated relative to C_s cluster 6^1_0 origin as in Figure 2.13.

in the 0_0^0 spectrum and $\Delta v = 0, \pm 1, \pm 2, \dots$ selection rule for all six vdW modes (Case II).

The contribution of the C_{3v} symmetry benzene(NH₃)₁ cluster to the 6_0^1 spectrum is observed starting with the feature at 72.9 cm⁻¹ to the blue of the C_s cluster 6_0^1 . Assignment of this feature to the C_{3v} cluster 6_0^1 is based upon the observation that no intense features are seen in either the benzene(NH₃)₁ 0_0^0 or the benzene(H₂O)₁ 6_0^1 spectra at this energy. The observed feature at 15 cm⁻¹ to the blue of the C_{3v} cluster 6_0^1 corresponds to the two-fold degenerate vdW b_{xy} bends at 19 cm⁻¹. The observed feature at 53 cm⁻¹ to the blue of the C_{3v} cluster 6_0^1 is associated with the calculated t_z torsion at 44 cm⁻¹. As in the benzene(CH₄)₁ case, the observation of the b_{xy} and t_z fundamentals implies that the vdW modes participate in the vibronic coupling mechanism (Case II) and that the $\Delta v = 0, \pm 1, \pm 2, \dots$ vibronic selection rule applies for all vdW modes. Based upon this, the best assignments for the C_{3v} cluster vdW vibronics are tabulated in Table 2.6.

F. Morse $\frac{6}{R_0}$ Model.

Calculations of the ground state vdW modes of benzene(Ar)₁ are also conducted using a model described by Jortner et al.^{1,6,7} This model contains a main feature which, at first glance, appears to make it generally applicable in predicting vdW stretching mode frequencies from calculated cluster binding energies and equilibrium intermolecular distances. However, the model turns out to be incorrect in this application. The model employs a simple relationship between the cluster equilibrium intermolecular distance R_0 and the Morse potential parameter β . The relation is derived by equating the second derivative of Equation 2.6 with the second derivative of a single term (6-12)

potential function. This derivation yields the relation $\beta = \frac{6}{R_0}$ which can be used to predict the vdW stretching mode frequency by diatomic Morse fit methods.

Substituting $\beta = \frac{6}{R_0}$ and the calculated ground state cluster binding energy into Equation 2.7 yields a vdW stretching mode energy of 47 cm^{-1} for benzene(Ar)₁ employing Scheraga's potential parameters. Even though the calculated vibrational energy is qualitatively correct, Figures 2.14 and 2.3 show that the $\beta = \frac{6}{R_0}$ relation results in an inadequate reproduction of the potential curve, especially in the critical region near the equilibrium intermolecular distance. At R_0 , the $\beta = \frac{6}{R_0}$ fit overestimates the curvature of the potential by about 33% with respect to the curvature calculated from the one-dimensional potential energy mapping ($1746 \text{ cm}^{-1}/\text{Å}^2$ versus $1312 \text{ cm}^{-1}/\text{Å}^2$) and, therefore, overestimates the stretching mode energy. Additional calculations using the potential data described in ref. 1 and the above approximate model also result in an inadequate potential curve reproduction, Figure 2.15. The potential curvature at R_0 using the $\beta = \frac{6}{R_0}$ fit is overestimated by about 37% with respect to the corresponding curvature calculated via potential energy mapping ($2322 \text{ cm}^{-1}/\text{Å}^2$ versus $1695 \text{ cm}^{-1}/\text{Å}^2$). In this case, the vdW stretching mode is calculated at 55 cm^{-1} .

The failure of the model under both data sets suggests that the model itself is inadequate in this application. The model fails in this application since the $\beta = \frac{6}{R_0}$ relation holds exactly only in systems in which the molecule-atom Lennard Jones parameters have been determined directly. Applying this approximate model to a case in which the potential function is represented by pairwise atom-atom potentials does not take into account the differing contributions of each interaction to the

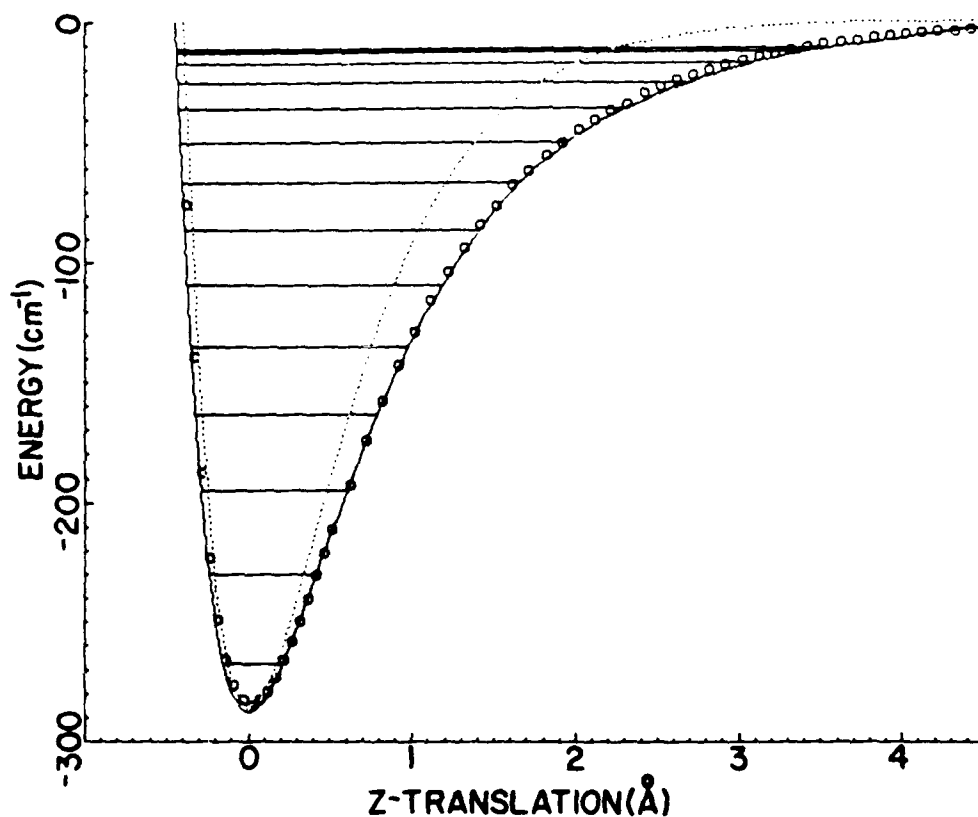


Figure 2.14

z-direction (vdW stretch) potential energy mapping of benzene(Ar)₁ and $\beta = \frac{6}{R_0}$ Morse fit. Translation is relative to equilibrium intermolecular distance, 3.44 Å. (6-12) potential energy mapping using data set from ref. 9 is represented by o; Taylor series expansion and energy levels are represented by —; $\beta = \frac{6}{R_0}$ Morse fit potential energy curve is represent by ---. Taylor series vibrational mode constant as per Table 2.2. $\beta = \frac{6}{R_0}$ Morse fit vibrational constants are $\omega_e = 47.22 \text{ cm}^{-1}$, $\omega_e \chi_e = 1.94 \text{ cm}^{-1}$.

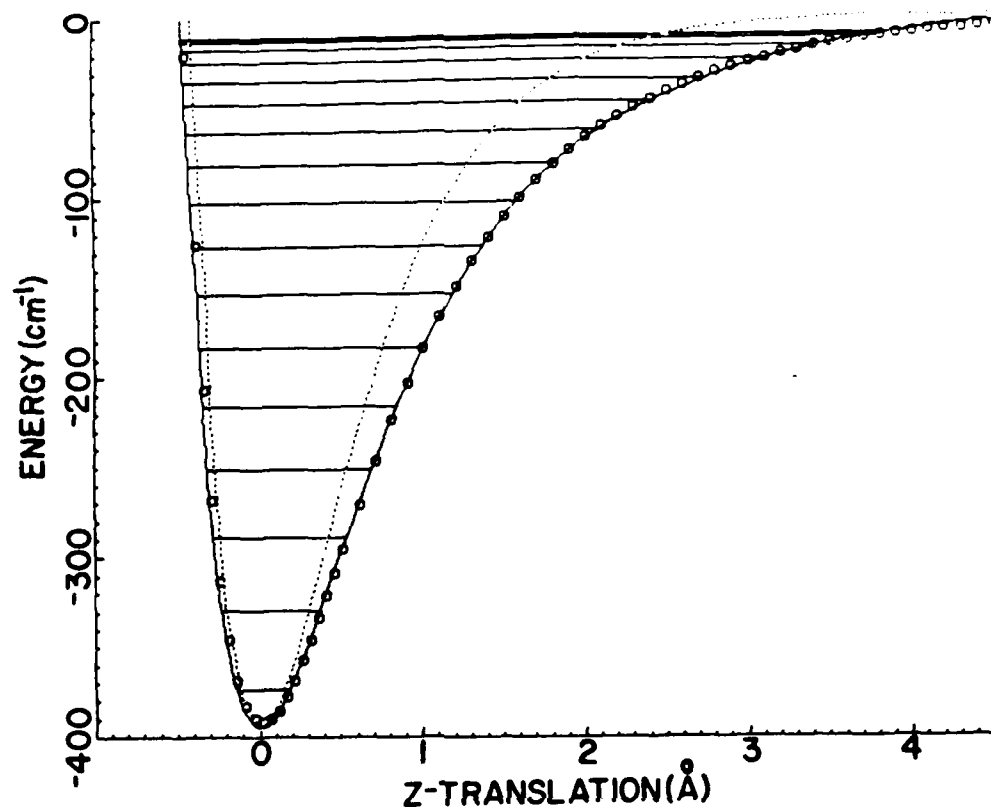


Figure 2.15

z-direction (vdW stretch) potential energy mapping of benzene(Ar)₁ and $\beta = \frac{6}{R_0}$ Morse fit. Translation is relative to equilibrium intermolecular distance, 3.5 Å. (6-12) potential energy mapping using data set from ref. 1 is represented by o; Taylor series expansion and energy levels are represented by — with $\omega_e = 46.68 \text{ cm}^{-1}$ and $\omega_e \chi_e = 1.81 \text{ cm}^{-1}$; $\beta = \frac{6}{R_0}$ Morse fit potential energy curve is represented by ---. $\beta = \frac{6}{R_0}$ Morse fit vibrational mode constants are $\omega_e = 54.84 \text{ cm}^{-1}$ and $\omega_e \chi_e = 1.90 \text{ cm}^{-1}$

potential energy and the equilibrium intermolecular distance. In this more complicated situation, no analytic relationship between β and R_0 exists.

Comparing the vdW stretching mode energies calculated using Jortner's and Scheraga's data sets suggests that a significant difference exists between the two data sets. Benzene(Ar)₁ configurational calculations using Jortner's data set yield a single cluster geometry of C_{6v} symmetry with the argon atom located 3.5 Å above the benzene molecular plane. In this case, the ground state cluster binding energy is 395 cm⁻¹. This binding energy is 108 cm⁻¹ greater than that calculated using Scheraga's data set. The binding energy of 287 cm⁻¹ calculated using Scheraga's data set is probably more accurate since the benzene(Ar)₁ ground state binding energy should be very similar to that calculated for s-tetrazine(Ar)₁. In the latter case, the calculated ground state binding energy of 295 cm⁻¹ compares well with that observed experimentally, 254 < D₀^{''} < 332 cm⁻¹.⁵ Furthermore, generating Lennard-Jones parameters using the data set of ref. 1 yields a binding energy of 359 cm⁻¹ for s-tetrazine(Ar)₁ which is clearly not as accurate as the binding energy reported in this work. The difficulty is due to the consolidation of atom-atom parameters from different data sets. In this respect, great caution must be taken when consolidating parameters since each parameter set is, in general, only self-consistent and may have no meaning when combined with parameters from other sets.

Conclusions

TOFMS studies have been employed to determine the general geometry and symmetry of vdW clusters in the gas phase. Through computer modeling, a correlation between the details of the cluster geometry and

spectral features has been demonstrated. Specifically, the parametric calculations yield useful information regarding cluster geometry, binding energy, and the vdW vibrations. These calculated results are consistent with experiment and serve as predictive and analytic tools which can be used to elucidate and understand the details of vdW cluster energetics.

Of the several models considered in studying the intermolecular vdW modes, simple diatomic approximations yield adequate results when applied to atom-molecule clusters. On the other hand, for molecule-molecule clusters a normal coordinate analysis is essential. The normal coordinate analysis is especially useful for analyzing systems which have little or no symmetry since no a priori knowledge of vdW mode nature is necessary to generate potential energy surface mappings.

Reassignments of and assignments to cluster vdW modes have been made based upon the knowledge gained from calculation. From comparison of calculation and experiment, several conclusions result. First, the actual excited state normal mode vdW frequencies are well fit by the calculated ground state cluster potential. This conclusion, though not surprising, gives independent proof of the invariance of the weak vdW potential between ground and excited electronic states as well as providing a means of using ground state vdW vibrational structure to predict vdW vibronic structure. Second, in the majority of the clusters analyzed, the observed vdW vibrations are those involving bending and torsional motions parallel to the aromatic π system. Furthermore, these modes are, in general, quite active in the Herzberg-Teller vibronic coupling mechanism and significant interelectronic state mixing results. Third, vdW motions which penetrate the aromatic π system have high

frequencies and are only observed in systems in which the Franck-Condon factors and binding energies are favorable. Finally, the observed vibronic structure supports the calculated cluster geometry in all cases.

Acknowledgment

We wish to thank Professor W. Klemperer for a number of helpful, informative, and stimulating discussions concerning van der Waals molecules and the nature of their vibrational spectra.

REFERENCES

1. M.J. Ondrechen, Z. Berkovitch-Yellin, and J. Jortner, *J. Amer. Chem. Soc.* 103, 6586 (1981).
2. M. Schauer and E.R. Bernstein, *J. Chem. Phys.* 82, 726 (1985).
3. J. Wanna, J.A. Menapace and E.R. Bernstein, *J. Chem. Phys.*, 85, 1795 (1986).
4. T.A. Stephenson and S.A. Rice, *J. Chem. Phys.* 81, 1083 (1984).
5. D.V. Brumbaugh, J.E. Kenny, and D.H. Levy, *J. Chem. Phys.* 78, 3415 72(1983).
6. M.L. Sage and J. Jortner, *J. Chem. Phys.* 82 5437 (1985).
7. J.A. Beswick and J. Jortner, *J. Chem. Phys.* 68, 2277 (1978); 69, 512 (1978); 74, 6725 (1981); 71 4737 (1979).
8. J. Wanna and E.R. Bernstein, *J. Chem. Phys.* 84, 927 (1986), and ref. 2 and 3, for example.
9. F.A. Momany, L.M. Carruthers, R.F. McGuire, and H.A. Scheraga, *J. Phys. Chem.* 78, 1595 (1974); G. Nemethy, M.S. Pottle, and H.A. Scheraga, *J. Phys. Chem.* 87, 1883 (1983).
10. E.B. Wilson Jr., J.C. Decius, and P.C. Cross, "Molecular Vibrations, Theory of Infrared and Raman Vibrational Spectra," (McGraw-Hill Book Co., Inc., 1955).
11. G. Herzberg, "Molecular Spectra and Molecular Structure: II Infrared and Raman Spectra of Polyatomic Molecules," (Van Nostrand Reinhold Co., 1945).
12. G. Herzberg, "Molecular Spectra and Molecular Structure: I Spectra of Diatomic Molecules," (Van Nostrand Reinhold Co., 1950).
13. J.L. Steinfield, "Molecules and Radiation: An Introduction to Modern Molecular Spectroscopy," (MIT Press, 1978).
14. G. Fischer, "Vibronic Coupling: The Interaction Between Electronic and Nuclear Motions," (Academic Press, 1984).
15. K.H. Fung, H.L. Selzle and F.W. Schlag, *Z. Naturforsch* 36A, 1778 (1981).

16. S. Leutwyler and A. Schmeizer, *J. Chem. Phys.* 79, 4385 (1983); J. Boesiger and S. Leutwyler, *Chem. Phys.* 126, 283 (1986)

CHAPTER THREE

THE INTERMOLECULAR VIBRONIC TORSIONAL STRUCTURE IN SOLUTE/SOLVENT VAN DER WAALS CLUSTERS: BENZENE/METHANE, /DEUTEROMETHANE, AND /CARBON TETRAFLUORIDE

Introduction.

van der Waals (vdW) complexes of aromatic molecules with hydrocarbon solvents form a class of supramolecular systems whose intermolecular bonding has several interesting features. First, the intermolecular interaction is small and is dominated by long-range dispersive attractions and short-range exchange repulsions. These two features allow the interaction to be modeled using an intermolecular potential of known functional form. For example, the interaction can be modeled by additive atom-atom potentials set in a Lennard-Jones or an Exponential Six format.¹ Second, the interaction potential surface only changes slightly, if at all, upon electronic excitation of the cluster chromophore. Thus, small spectral shifts of the chromophore electronic transition and weak intensity intermolecular vdW mode vibronic transitions are observed.^{2,3} Third, the interaction results in the formation of specific minimum energy cluster configurations. These geometries are interesting since they give insight into the nucleation processes and solvation geometry occurring in both gas and condensed phase systems.¹ Fourth, the small binding energy of the complex and the low frequency vdW vibrational modes are important since they play an essential role in

intramolecular vibrational redistribution (IVR) and vibrational predissociation (VP) cluster dynamic energy transfer processes.⁴ And fifth, cluster structure, binding energy, vdW modes and dynamics (IVR and VP) are essentially dependent on the actual cluster structure and the intricacies of the intermolecular interaction.^{3,5}

In this paper, we report the spectroscopic results of the benzene/deuterated methane ($\text{ben}(\text{CD}_4)_1$) and benzene/carbon tetrafluoride ($\text{ben}(\text{CF}_4)_1$) clusters together with calculated modeling of selected cluster characteristics. The spectroscopic results include the $\pi^* + \pi$ vibronic spectra of the clusters in their respective benzene constituent 6_0^1 regions.

The calculated results include the geometry, the binding energy, and the full eigenvalue/eigenvector intermolecular vibrational structure for the electronic ground state of each cluster. The intermolecular ground state vibrational structure is modeled by two methods: (1) an intermolecular normal coordinate analysis (NCA) which determines all six intermolecular vdW mode fundamentals under a harmonic oscillator assumption,³ and (2) a three dimensional hindered rigid rotor analysis (HRRR) for which an anisotropic perturbation function is applied to the cluster solvents considered to be a perfect sphere in the intermolecular potential well. The intermolecular force constants for the HRRR analysis are obtained under a hindered rigid rotor approximation.

The calculated ground state vibrational structure of the $\text{ben}(\text{CD}_4)_1$ and $\text{ben}(\text{CF}_4)_1$ clusters is compared to the experimental results for the 6_0^1 vibronic structure of benzene. The calculated vibrational structure of the $\text{ben}(\text{CD}_4)_1$ cluster is compared to the experimental results for the 6_0^1 vibronic structure of benzene. The calculated vibrational structure of the $\text{ben}(\text{CF}_4)_1$ cluster is compared to the experimental results for the 6_0^1 vibronic structure of benzene.

ramifications of Herzberg-Teller (H-T) coupling for the observation of "forbidden" vibronic transitions.

The motivation for studying these systems concerns the elucidation of the vdW torsional structure. Two limiting cases can be proposed in regard to the torsional structure of $\text{ben}(\text{CH}_4)_1$, $\text{ben}(\text{CD}_4)_1$, and $\text{ben}(\text{CF}_4)_1$. In one case, the clusters possess free internal rotation between the cluster solute and solvent. The cluster solvent (CH_4 , CD_4 , or CF_4) rotates freely in three dimensions against the benzene framework and the system is considered nonrigid. In the other case, the clusters possess torsional oscillations for which the cluster solvent librates against the benzene frame with a residence time long enough to give rise to "vibration like" motion in a rigid molecule regime.

Elucidation of the vdW torsions is of particular interest in these systems since the aforementioned limiting cases pose questions regarding the actual physics governing the torsional structure. (1) do the clusters possess free internal rotation between the cluster solute and solvent or do they possess torsional oscillations for which the solvent coordinates behave more or less harmonically, and (2) in either case what is the dependence of the internal energy potential on the torsional angle. The dependence of the internal energy potential on the torsional angle is of particular interest since it is this dependence which determines the torsional structure of the cluster.

mixed with the $\text{Nd}^{+3}/\text{YAG}$ 1.064 μm fundamental is used to probe the clusters' $S_1 \leftarrow S_0$ transition in the isolated benzene 6_0^1 region (${}^1\text{B}_{2u} \leftarrow {}^1\text{A}_{1g}; \pi^* \leftarrow \pi$). Subsequent ionization of the clusters is accomplished using a R590 dye laser whose output is frequency doubled and mixed with the $\text{Nd}^{+3}/\text{YAG}$ 1.064 μm fundamental. The ionization laser output is set at 45112 cm^{-1} . A 5% mixture of deuterated methane or carbon tetrafluoride in helium is placed inline with liquid benzene in a trap at room temperature. The three component mixture is expanded using a pulsed molecular jet nozzle having a 500 micron orifice while maintaining 100 psig backing pressure. Apparatus chamber pressure is maintained at or below 5×10^{-6} torr during the experiments.

Theoretical Considerations.

The NCAs are conducted using the same methods as described in our previous publication on vdW cluster vibronic structure.³ For $\text{ben}(\text{CD}_4)_1$, the calculated cluster ground state geometry, force field, and binding energy are taken as those of $\text{ben}(\text{CH}_4)_1$. Only the masses are changed for the deuterium hydrogen substitutions in the NCA. For $\text{ben}(\text{CF}_4)_1$, the cluster ground state geometry and binding energy are calculated via intermolecular energy minimization employing the methods previously described.³ The NCA is conducted using the cluster geometry and force field corresponding to the ground state geometry and force field of the isolated $\text{ben}(\text{CD}_4)_1$ and $\text{ben}(\text{CF}_4)_1$ clusters.

cluster solvent rotates freely in three dimensions against a fixed cluster solute framework. Application of a specified perturbation field results in the eventual restriction of this free rotation to torsional oscillation as the perturbation field magnitude is increased; that is, rotation ceases and vibrational oscillatory motion begins as the residence times of the solvent in the torsional potential well becomes longer.

In the 3D-HRRA, both cluster constituents are assumed internally rigid, their respective internal geometries remaining constant and at "equilibrium". The cluster solvents are taken as the rotating portions of the clusters since their zero field rotational constants are orders of magnitude greater than those of the cluster solute. The hindered solvent rotations are presupposed to contribute to the spectral features observed along with the intermolecular bending and stretching modes.

The 3D-HRRA involves setting up a molecule fixed coordinate system (x,y,z) and a space fixed coordinate system (ξ, η, ζ) on the cluster solvent as shown in Figure 3.1. Both systems have their origins at the nuclear center of mass of the cluster solvent. The molecule fixed coordinate system is chosen such that its principle axes lie along the C_2 rotational axes of the solvent tetrahedron (C_2 point group symmetry). The space fixed coordinate system is chosen to be at the Euler angles $\theta = 45^\circ$ degrees, $\phi = 0^\circ$ degree, and $\chi = 0^\circ$ degree with respect to the ξ, η, ζ axes. The ξ, η, ζ axes are defined by the C_2 rotational axes of the cluster solute.

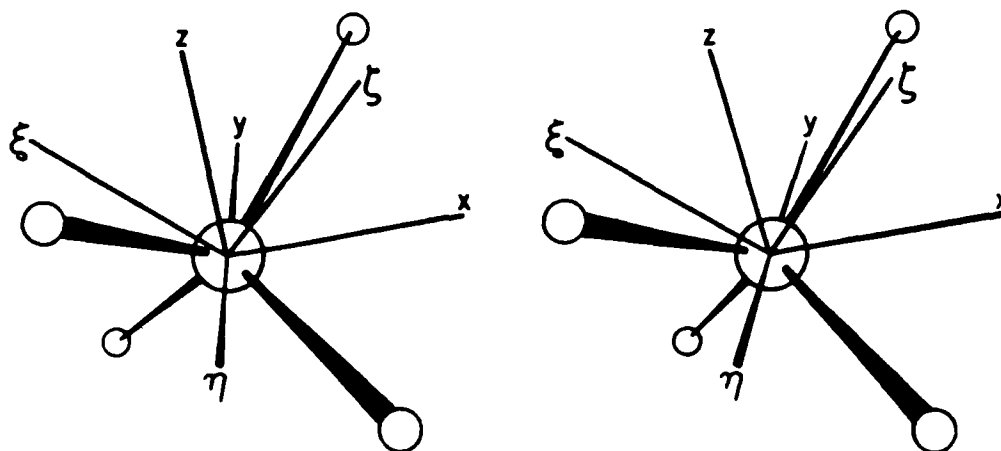


Figure 3.1

Stereoscopic projection of solvent tetrahedron showing relative orientation of the molecule fixed (x, y, z) and space fixed (ξ, η, ζ) coordinate systems used in the dHFFA. The x, y, z coordinate system is located at $\theta = 45^\circ$, $\phi = 0^\circ$ and $\chi = 0^\circ$ in the θ, ϕ, χ coordinate system.

potential magnitude depends upon the relative displacements of all three rotational coordinates as,

$$q = 2\theta + 2\chi + \phi \quad 3.3$$

Inserting Equation 3.3 into Equation 3.2 yields the three dimensional potential function used in the calculations:

$$V(\theta, \phi, \chi) = \frac{V_0}{2} [1 - \cos(2\theta + 2\chi + \phi)] \quad 3.4$$

in which V_0 is the barrier height to internal rotation. The rotational wavefunctions chosen as the basis set for the calculation are the rigid rotor symmetric top wavefunctions which depend on the curvilinear coordinates and on the quantum numbers J , k and m . Under zero field conditions, these wavefunctions are solutions to the spherical top Schrodinger equation,⁸

$$\frac{\hat{H}_0}{\hbar^2} |Jk m\rangle = E_{rot}^J |Jk m\rangle \quad 3.5$$

with eigenvalues corresponding to those of the spherical top. Upon application of the perturbation field, the eigenvalues are obtained by diagonalization of the energy matrix consisting of the elements of the form

$$\begin{array}{rcl}
 |J' - J''| & \leq & 2 & 3.7 \\
 |k' - k''| & = & 2 & 3.8 \\
 |m' - m''| & = & 1. & 3.9
 \end{array}$$

Diagonal matrix elements contain only the zero field spherical top energies and a $V_0/2$ potential term.

The resulting matrix is diagonalized for a selected value of V_0 yielding eigenvalues corresponding to the solvent torsional eigenstates at the specified perturbation. The perturbation is varied until a reasonable fit with the experimental spectrum is obtained. The calculations are performed on a Cyber 205 computer using a basis set consisting of 680 wavefunctions to ensure convergence of the lowest eigenstates at their proper eigenvalues. Only the torsional structures of $\text{ben}(\text{CH}_4)_1$ and $\text{ben}(\text{CD}_4)_1$ are calculated since their respective rotational constants are large enough that the coupling of the rotational levels does not require an extremely large basis set to insure convergence. Matrix elements are determined via numerical integration using a nonadaptive integration routine. The matrix is prediagonalized into a tridiagonal form using orthogonal similarity transformations⁹ and diagonalized using an implicit QL method¹⁰. The rotational constants used for methane and deuterated methane are 5.2 cm^{-1} and 2.6 cm^{-1} respectively.

Results

A. $\text{ben}(\text{CH}_4)_1$

Figures 1 and 2 and Table I present the results of the torsional structure calculations for $\text{ben}(\text{CH}_4)_1$ at $V_0 = 0.0$ and $V_0 = 0.1$ respectively. The torsional energy levels are shown in cm^{-1} and the rotational energy levels are shown in cm^{-1} . The torsional energy levels are shown in cm^{-1} and the rotational energy levels are shown in cm^{-1} .

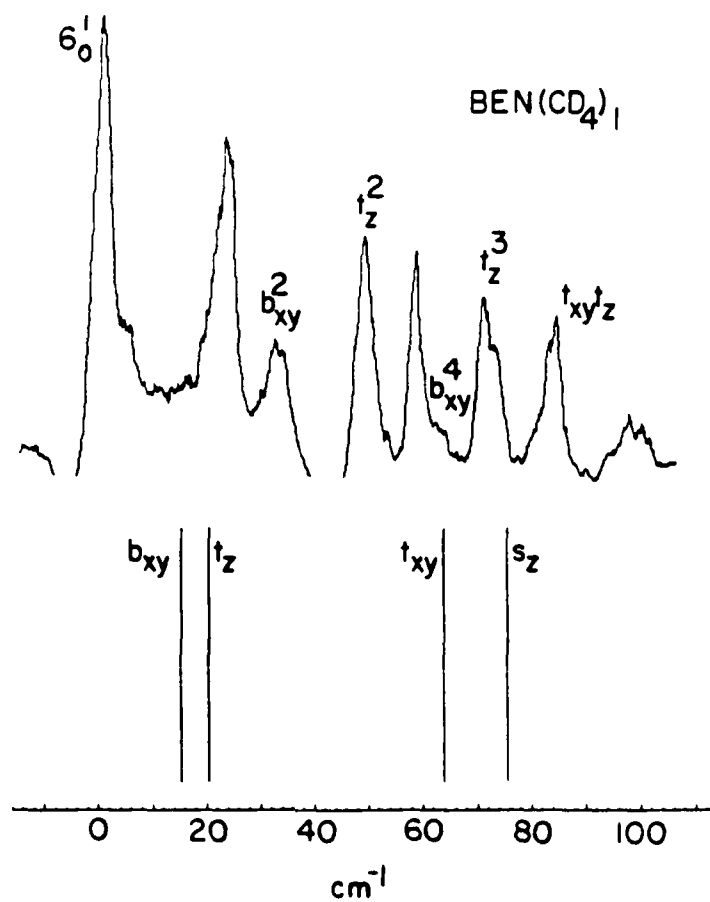


Figure 3.2

Two-color TOFMS $S_1 - S_0$ spectrum and calculated ground state vdW modes (NCA) of $\text{ben}(\text{CD}_4)_1$. Energy scale is relative to $\text{ben}(\text{CD}_4)_1$ 6_0^1 transition (18567.1 cm^{-1}). Feature positions and assignments as per Table 3.1 and Figure 3.1.

TABLE 3.1

vdw spectral features in $\text{ben}(\text{CD}_4)_1$ and $\text{ben}(\text{CH}_4)_1$ 6_0^1 regions
and calculated ground state vdw modes (refer to Figure 3.2).

$\text{ben}(\text{CD}_4)_1$ Energy ^a	3D-HRRA ^c	Assignment ^b	Observed	NCA	3D-HRRA ^c	Assignment ^b
	0(4)	6_0^1	0(38567.6)	0	0(4)	6_0^1
		6_0^1h_{xyo}	16.1	16(b_{xy})		6_0^1b_{xyo}
	21(4)	6_0^1t_{zo}	27.3	28(t_z)	29(4)	6_0^1t_{zo}
		6_0^1b_{xyo}	32.3			6_0^1b_{xyo}
		6_0^1b_{xyo}	48.4			6_0^1b_{xyo}
	47(4)	6_0^1t_{zo}	51.4		54(2)	6_0^1t_{zo}
	68(8)	6_0^1t_{xyo}				
		6_0^1b_{xyo}	64.6			6_0^1b_{xyo}
	75(4)	6_0^1t_{zo}	73.5		73(4)	6_0^1t_{zo}
		6_0^1b_{xyo}		82(e_z)		
	80(12)	6_0^1t_{xyo}		89(t_{xy})	84(8)	

^a Energies reported in cm^{-1} relative to the 6_0^1 cluster origins.

^b Mode representations as per Figure 3.2

^c See "percentages represent structural degeneracy calculated in 3D-HRRA."

^d Reference (end)

difference between S_1 and S_0 for $\text{ben}(\text{CD}_4)_1$ is nearly identical to that of $\text{ben}(\text{CH}_4)_1$. Ten pronounced intermolecular vibronic features are observed to the "blue" of the cluster 6_0^1 . As in the case of the $\text{ben}(\text{CH}_4)_1$ cluster, no features are observed in the symmetry forbidden benzene 0_0^0 region. Thus, the cluster geometry must possess at least a three-fold axis of symmetry.

The calculated $\text{ben}(\text{CD}_4)_1$ geometry (Figure 3.3) is assumed to be the same as that calculated for $\text{ben}(\text{CH}_4)_1$. The geometry possesses C_{3v} point group symmetry. In this geometry, the CD_4 center-of-mass lies 3.47 Å above the benzene molecular plane along the three-fold rotational axis. The ground state binding energy in this configuration is calculated at 540 cm^{-1} . Using the cluster "red shift" of 41.2 cm^{-1} , the excited state binding energy is calculated to be 581 cm^{-1} .

The NCA reveals six vdW vibrations (Figure 3.3 and Table 3.1), two being two-fold degenerate. The ground state vibrational energies are 75 cm^{-1} for the vdW stretch $s_z(a_1)$, 15 cm^{-1} for the bends $b_{xy}(e)$, and 20 cm^{-1} ($t_z(a_2)$) and 64 cm^{-1} ($t_{xy}(e)$) for the vdW torsions. The eigenvector normal modes (Figure 3.3) transform in an identical fashion to those calculated for $\text{ben}(\text{CH}_4)_1$. The vdW stretching mode transforms as the translation of the cluster constituents away from one another along the z (three fold) axis. The vdW bends transform as some combination of cluster constituent translations perpendicular to the z (three fold) axis. The vdW torsions transform as some combination of cluster constituent translations perpendicular to the three fold axis. The $s_z(a_1)$ mode is the symmetric stretch of the cluster constituents along the z axis. The $b_{xy}(e)$ mode is the asymmetric bend of the cluster constituents perpendicular to the z axis. The $t_z(a_2)$ mode is the symmetric torsion of the cluster constituents about the z axis. The $t_{xy}(e)$ mode is the asymmetric torsion of the cluster constituents about the z axis.

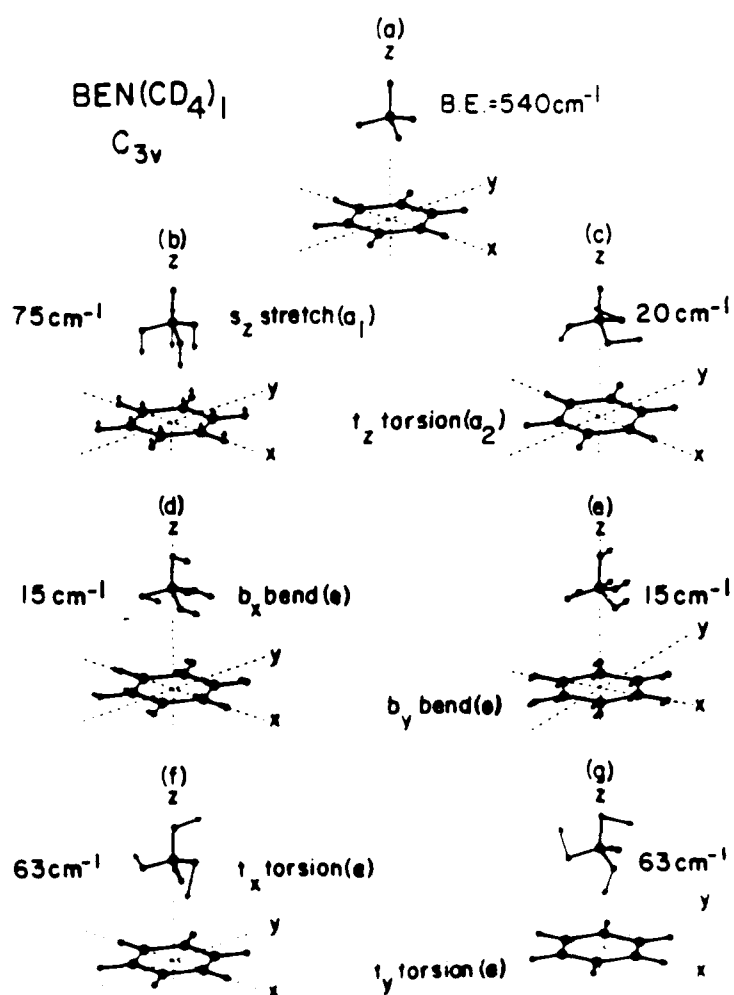


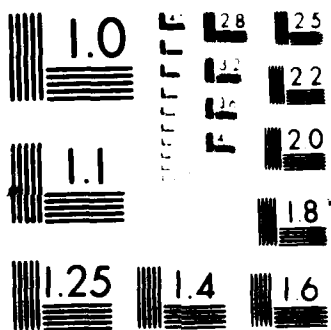
Figure 4.3

calculated ground state minimum energy configuration and N/A energy value eigenvectors for BEN(CD₄)₁. The ground state is shown in (a) and the N/A energy value eigenvectors are shown in (b) through (g). The ground state is shown in (a) and the N/A energy value eigenvectors are shown in (b) through (g). The ground state is shown in (a) and the N/A energy value eigenvectors are shown in (b) through (g).

.....

The 3D HRRA results are also included in Table 3.1 for the lowest eigenstates in the torsional manifold. The torsional mode structure is calculated for $V_0 = 300 \text{ cm}^{-1}$ and $B = 2.6 \text{ cm}^{-1}$. This perturbation results in a reasonable fit for the torsional features observed experimentally. The torsional "zero point energy" is 75 cm^{-1} . Two distinct torsional manifolds result from the calculations: one manifold has eigenvalues grouped quartically (nearly four-fold degenerate located at approximately 21 cm^{-1} , 46 cm^{-1} , and 75 cm^{-1} above the zero point energy) and the other manifold has eigenvalues grouped octally (nearly eight-fold degenerate located at approximately 68 cm^{-1} above the torsional zero point energy).

For comparison, the observed vibronic features for $\text{ben}(\text{CH}_4)_1$ are reproduced in Table 3.1 along with the results of the NCA and the 3D-HRRA. The NCA results for $\text{ben}(\text{CH}_4)_1$ are those reported previously.³ The 3D-HRRA torsional structure is calculated for $V_0 = 300 \text{ cm}^{-1}$ and $B = 5.2 \text{ cm}^{-1}$. This perturbation is chosen since it is assumed that the barrier to internal rotation is nearly identical in the two systems as they only differ by isotopic substitution and have the same electronic structure. Additionally, using the same potential barrier of electronic origin for both CH_4 and CD_4 clusters provides a check on the validity of the model in predicting the torsional mode structure of the clusters. For $\text{ben}(\text{H}_4)_1$ the torsional zero point energy is 96 cm^{-1} . As in the case of the $\text{ben}(\text{CH}_4)_1$ calculations, two distinct torsional manifolds result from the calculations with the eigenvalues grouped quartically at approximately 21 cm^{-1} , 46 cm^{-1} , and 75 cm^{-1} above the zero point energy and the other manifold has eigenvalues grouped octally at approximately 68 cm^{-1} above the zero point energy.



B $\text{Ben}(\text{CF}_4)_1$

Figure 3.4 and Table 3.2 present the $\text{ben}(\text{CF}_4)_1$ cluster spectrum recorded using 2-color TOPMS in the region between 38578.6 cm^{-1} and 38702.6 cm^{-1} . Unlike the $\text{ben}(\text{CD}_4)_1$ and $\text{ben}(\text{CH}_4)_1$ cluster 6_0^1 transitions, the $\text{ben}(\text{CF}_4)_1$ cluster 6_0^1 is blue shifted by 6.1 cm^{-1} with respect to the benzene 6_0^1 . The small hypsochromic shift indicates that the binding energies in the S_0 and S_1 states are nearly identical with the ground state binding energy being slightly greater. The relative displacement between the two potential surfaces is also small since only 5 vdW transitions are observed and their intensities decrease abruptly at about 50 cm^{-1} above the cluster 6_0^1 origin. No cluster spectrum is observed in the forbidden benzene 0_0^0 region indicating that the cluster possesses at least a three-fold rotation axis. This result is not unexpected since the same observation is made for the $\text{ben}(\text{CH}_4)_1$ and $\text{ben}(\text{CD}_4)_1$ systems. The ground state configuration and vdW eigenvalues/eigenvectors are shown in Figure 3.5 and Table 3.2. Only one minimum energy geometry is calculated for the cluster. The geometry has C_{3v} point group symmetry with the CF_4 center-of-mass at 3.43 \AA above the benzene molecular plane along the three-fold axis. The cluster ground state binding energy is 1064 cm^{-1} .

The NCA reveals six vdW vibrations. Their ground state vibrational energies are 69 cm^{-1} for the vdW stretch $s_z(a_1)$, 11 cm^{-1} for the vdW bends $b_{xy}(e)$, and 13 cm^{-1} ($t_z(a_2)$) and 36 cm^{-1} ($t_{xy}(e)$) for the vdW torsions. The eigenvector normal modes transform as the translational and rotational representations of the C_{3v} point group as indicated and in the same manner as those for $\text{ben}(\text{CH}_4)_1$ and $\text{ben}(\text{CD}_4)_1$.

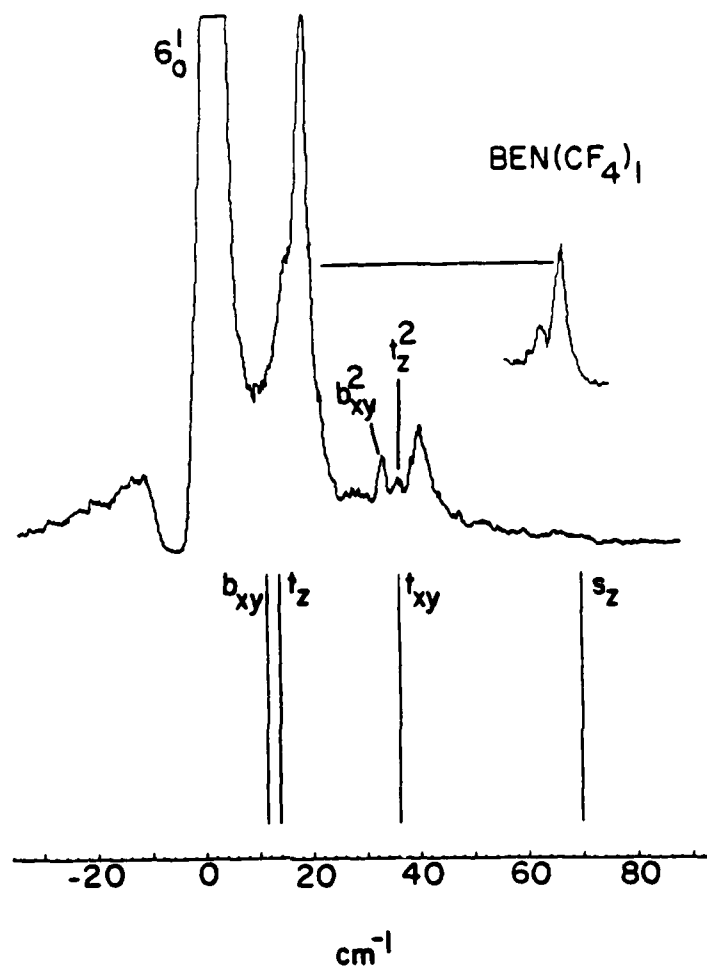


Figure 3.4

Two-color TOFMS $S_1 \leftarrow S_0$ spectrum and calculated ground state vdW modes (NCA) of $\text{ben}(\text{CF}_4)_1$. Energy scale is relative to $\text{ben}(\text{CF}_4)_1$ 6_0^1 transition (38614.7 cm^{-1}). Feature positions and assignments as per Table 3.2 and Figure 3.5.

TABLE 3.2

vdW spectral features in $\text{ben}(\text{CF}_4)_1$ 6_0^1 region and calculated ground state vdW modes (refer to Figure 3.4).

Observed ^a	NCA ^a	Assignment ^b
0(38614.7)	0	6_0^1
15.7	11 (b_{xy})	$6_0^1 b_{xy}^1$
17.4	13 (t_z)	$6_0^1 t_{z0}^1$
32.3		$6_0^1 b_{xy}^2$
35.4		$6_0^1 t_{z0}^2$
39.5	36 (t_{xy})	$6_0^1 t_{xy}^1$
	69 (s_z)	

a) Energies are reported in cm^{-1} relative to the 6_0^1 cluster origin.

b) vdW mode representations as per Figure 3.4.

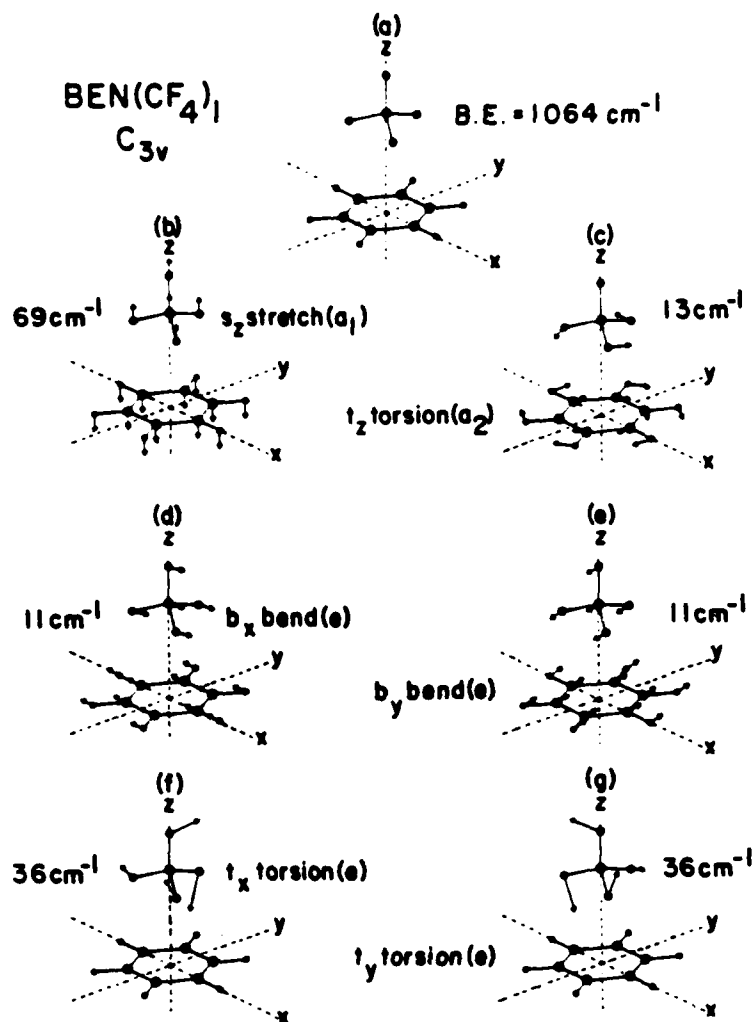


Figure 3.5

Calculated ground state minimum energy configuration (a) and NCA eigenvalue/eigenvector normal modes (b) - (g) for $\text{ben}(\text{CF}_4)_1$. Cluster symmetry is C_{3v} with an equilibrium intermolecular distance of 3.43 Å. Eigenvectors are normalized and displayed at 2x magnification (2 Å total displacement).

Discussion.

In comparing the calculated ground state vdW vibrational structure and experimental vdW vibronic structure, we assume that the intermolecular potential surfaces of the clusters studied are identical in both the S_1 and S_0 electronic states. Additionally, we utilize the group theoretical arguments developed in our previous publication³ on vdW cluster vibronic structure to assign and understand the observed cluster spectra.

A. $\text{Ben}(\text{CD}_4)_1$.

The calculated ground state vdW vibrations (NCA) of $\text{ben}(\text{CD}_4)_1$ and the experimental vibronic spectrum is shown in Figure 3.2 and Table 3.1. As previously, the assignments are made by direct comparison between the calculations and the experimental vibronic spectra. The intense feature at 22.5 cm^{-1} to the blue of the cluster 6_0^1 corresponds to the t_z torsion calculated at 20 cm^{-1} . Thus this feature and its observed overtones at 48.4 cm^{-1} , 70.5 cm^{-1} , and 100 cm^{-1} are assigned to 6_0^1 vdW combination bands $6_0^1 t_z(a_2)_0^1$, $6_0^1 t_z(a_2)_0^2$, $6_0^1 t_z(a_2)_0^3$, and $6_0^1 t_z(a_2)_0^4$. The features at 32 cm^{-1} and 62.7 cm^{-1} to the blue of the cluster 6_0^1 correspond to the first and third overtones of the two-fold degenerate vdW bending modes whose fundamental is calculated at 15 cm^{-1} . They are assigned to the 6_0^1 combination bands $6_0^1 b_{xy}(e)_0^2$, and $6_0^1 b_{xy}(e)_0^4$, respectively. The feature at 58.1 cm^{-1} to the blue of the cluster 6_0^1 is assigned to a two-fold degenerate t_{xy} vdW torsions/cluster 6_0^1 combination band, $6_0^1 t_{xy}(e)_0^1$. The t_{xy} torsion fundamental is calculated at 64 cm^{-1} . With this assignment and that of the t_z torsion, the feature at 84 cm^{-1} is assigned to the $6_0^1 t_{xy}(e)_0^1 t_z(a_2)_0^1$ combination band. The vdW stretch is calculated at 75 cm^{-1} . This mode is identified in the

cluster vibronic spectrum at 72.9 cm^{-1} to the blue of the cluster 6_0^1 origin and is thus assigned as $6_0^1 s_z(a_1)_0^1$. Under this scheme, we assign the features at 93.3 cm^{-1} and 97.5 cm^{-1} as $6_0^1 s_z(a_1)_0^1 b_{xy}(e)_0^1$ and $6_0^1 s_z(a_1)_0^1 t_z(a_2)_0^1$ combination bands.

The torsional structure resulting from the 3D-HRRA for $\text{ben}(\text{CD}_4)_1$ (Table 3.1), confirms the torsional assignments made using the NCA. The quartically grouped torsional levels at 21 cm^{-1} , 46 cm^{-1} and 75 cm^{-1} correspond to those associated with the t_z torsion and its overtones in the cluster spectrum at 22.5 cm^{-1} , 48.4 cm^{-1} and 70.5 cm^{-1} . The octally grouped torsional levels at 68 cm^{-1} correspond to the t_{xy} torsion assigned at 58.1 cm^{-1} .

The correspondence between these levels and those calculated using the NCA can be understood as follows. In the 3D-HRRA, four symmetrically equivalent minima exist in the torsional potential surface. These minima correspond to the four ways of placing the solvent tetrahedron upon the solute with a tetrahedral face toward the solute molecular plane. If the barrier between these minima is infinitely high, penetration of the local wavefunctions through the barrier separating the potential minima does not take place. In this case, each "well" contains eigenstates corresponding to intermolecular torsions which occur with small amplitude about each potential well minimum. Since the four "potential wells" are identical in shape and depth, a four-fold "structural" degeneracy exists in which all four potential wells contain identical torsional structure. Thus, for example, a non degenerate torsional eigenstate actually has a four fold structural degeneracy, etc.

Considering the actual situation in which the potential barrier is finite, tunneling occurs and the "structural" degeneracy is lifted via interaction of the local wavefunctions through the potential barrier. The eigenstate splitting due to this tunneling may, or may not, be observed depending on the experimental resolution and the relative difference between the eigenstate energy and the barrier height. Splitting of the "structural" degeneracy in the lower portion of the potential well is minimal unless the barrier is low. Based on the calculations, energy level splittings of the first few sets of eigenstates should not be observed unless the barrier is below 150 cm^{-1} .

At moderate barriers (about 300 cm^{-1}), the eigenstates in the lower portion of the well are nearly degenerate and behave more or less harmonically. For all practical purposes, we can assume these levels to be degenerate. The torsional level structure can then be determined from the eigenstates in one of the minima. Thus, the 3D-HRRA torsional structure calculation simplifies into the NCA. Physically, the cluster can be considered at least "semi-rigid" in the respect that it has a definable equilibrium configuration. The potential energy barrier separating one minimum from the others in the potential surface is large and may be of the order of the cluster binding energy.

The vibronic structure in both the $\text{ben}(\text{CH}_4)_1$ and $\text{ben}(\text{CD}_4)_1$ spectra suggests that the systems are more or less rigid. None of the observed vibronic state energies follow a free rotor formalism for which the energy level structure is described by Equation 3.2. If the systems behaved nonrigidly, the free rotor eigenstates would lie at approximately $2.6J(J+1) \text{ cm}^{-1}$ and $5.2J(J+1) \text{ cm}^{-1}$ for $\text{ben}(\text{CD}_4)_1$ and $\text{ben}(\text{CH}_4)_1$, respectively, and a $\Delta J = \pm 1$ selection rule would govern the transitions

In the $\text{ben}(\text{CH}_4)_1$ and $\text{ben}(\text{CD}_4)_1$ systems, the t_z torsional mode shifts by 17.6 % upon deuterium substitution of the cluster solvent. Both the NCA and 3D-HRRA models predict a 28.6% frequency shift for t_z , while the free rotor model would predict a 50% frequency shift for t_z upon deuteration. Considering that only one mode is taken into account and the mode couplings may be different in the protonated and deuterated clusters, we conclude that torsional tunneling does not take place in the lower levels of the $\text{ben}(\text{CH}_4)_1$ and $\text{ben}(\text{CD}_4)_1$ cluster potential wells and that the clusters can be considered to be rigid.

The negligible isotopic red shift in the b_{xy} bends also suggests that the cluster is rigid and that the entire observed spectrum is not solely due to internal rotation. The same rationale holds for the vdW stretch: its observation also dispels the notion that only rotor modes occur in the spectrum. No experimental isotopic shift can be determined for the stretching mode, however, since it is not observed in the $\text{ben}(\text{CH}_4)_1$ system. Theoretically, the mode should red shift by 8.5% upon deuteration of the cluster solvent. The $\text{ben}(\text{CH}_4)_1$ stretch should then be at about 80 cm^{-1} in the vibronic spectrum based upon the observed stretch in the $\text{ben}(\text{CD}_4)_1$ system. (The $\text{ben}(\text{CH}_4)_1$ stretch is calculated by the NCA to be at 82 cm^{-1}).

The $\text{ben}(\text{CD}_4)_1$ cluster spectrum is also substantially richer than the $\text{ben}(\text{CH}_4)_1$ spectrum in the respect that both the vdW stretch and t_{xy} torsions are observed along with well developed t_z torsion and bend progressions. This is probably due to more favorable Franck-Condon factors in the $\text{ben}(\text{CD}_4)_1$ case resulting from the isotopic substitution.

As is the case for $\text{ben}(\text{CH}_4)_1$, H-T coupling influences the vibronic intensities (selection rules) in the $\text{ben}(\text{CD}_4)_1$ spectrum. The

nontotally symmetric modes t_z , t_{xy} and b_{xy} all appear in the spectrum with $\Delta v = 0, \pm 1, \pm 2, \pm 3, \dots$ selection rules as can be seen in Figure 3.2 and Table 3.1.

B. $\text{Ben}(\text{CF}_4)_1$.

Comparison of the calculated ground state vdW vibrations (NCA) of $\text{ben}(\text{CF}_4)_1$ and the experimental cluster spectrum is presented in Figure 3.4 and Table 3.2. The intense feature at 17.4 cm^{-1} to the blue of the $\text{ben}(\text{CF}_4)_1$ 6_0^1 corresponds to the t_z torsion calculated at 13 cm^{-1} . Thus, this feature and its first overtone at 35.4 cm^{-1} are assigned to the 6_0^1 vdW combination bands $6_0^1 t_z(a_2)_0^1$ and $6_0^1 t_z(a_2)_0^2$. The shoulder feature at 15.7 cm^{-1} to the blue of the cluster 6_0^1 corresponds to the vdW two-fold degenerate b_{xy} bend fundamental calculated at 11 cm^{-1} . Taking this feature as the combination band $6_0^1 b_{xy}(e)_0^1$ leads to the assignment of the b_{xy} bend first overtone $6_0^1 b_{xy}(e)_0^2$ at 32.3 cm^{-1} . Finally, the spectral feature at 39.5 cm^{-1} in the $\text{ben}(\text{CF}_4)_1$ spectrum corresponds to the t_{xy} torsion calculated at 36 cm^{-1} . Thus, the feature is assigned to the combination band $6_0^1 t_{xy}(e)_0^1$.

The $\text{ben}(\text{CF}_4)_1$ spectrum, like the $\text{ben}(\text{CD}_4)_1$ and $\text{ben}(\text{CH}_4)_1$ spectra, suggests that the system is rigid. Since the rotational constant for CF_4 is small (ca. 0.18 cm^{-1}), the free rotor energy level structure should appear at about $.37 \text{ cm}^{-1}$ intervals. This structure is not observed. Instead, the spectrum possesses oscillatory torsional structure commensurate with the NCA theoretical predictions. These theoretical and experimental results demonstrate the rigidity of the systems.

The $S_1 \leftarrow S_0$ excitation of the $\text{ben}(\text{CF}_4)_1$ cluster involves very little change in cluster geometry. In this spectrum, the progression

intensities decrease dramatically at energies greater than the 6_0^1 cluster origin. In the lowest two vdW mode progressions, the intensities decrease approximately 13% between the mode fundamentals and the first overtones. Furthermore, the high energy vdW stretch calculated at 69 cm^{-1} is not observed. At these high energies, the Franck-Condon factors must be very small.

The observation of the nontotally symmetric vdW b_{xy} bends and the t_z torsion progressions with a $\Delta v = 0, \pm 1, \pm 2 \dots$ selection rule suggests that interelectronic state mixing (H-T coupling) is an important contributor to the mode intensity mechanism. As in the $\text{ben}(\text{CH}_4)_1$ and $\text{ben}(\text{CD}_4)_1$ cases, H-T coupling becomes apparent in the low lying vdW modes of the $\text{ben}(\text{CF}_4)_1$ system. In fact, the interelectronic state mixing is substantial in the $\text{ben}(\text{CF}_4)_1$ system and can be demonstrated by the observation of the well defined bend fundamental at 15.7 cm^{-1} and by the observation of the t_{xy} torsion fundamental (39.5 cm^{-1}). Both of these latter features should not be observed if H-T coupling is not present.

Summary and Conclusions.

Two-color TOFMS and supersonic molecular jet techniques have been employed to study the $S_1 \leftarrow S_0$ vibronic spectra of $\text{ben}(\text{CD}_4)_1$ and $\text{ben}(\text{CF}_4)_1$ vdW clusters. These studies reveal detailed information regarding the geometries, the intermolecular energetics, and the physical nature of the vdW interactions present in the systems. The experimental observations demonstrate that the clusters are at least semi-rigid systems possessing unique equilibrium geometries and that the intermolecular motion present in the systems is oscillatory. Through comparison of these spectra with those of $\text{ben}(\text{CH}_4)_1$ previously studied in this

laboratory, the "isotopic" shifts observed in the intermolecular vibronic structures demonstrate that all the low lying intermolecular eigenstates are nearly harmonic. They are not admixtures of correlated intermolecular bends and stretches and free intermolecular rotation, as would occur if the clusters behaved nonrigidly.

The rigidity of the clusters is further demonstrated by theoretical treatment of the intermolecular motion. Both the NCA and 3D-HRRA models indicate that the intermolecular torsional motion is oscillatory and that the motion is constrained by an orientationally dependent intermolecular potential. Detailed analysis of the intermolecular interaction reveals that the torsional motion is governed by a three dimensional potential possessing torsional barriers on the order of the cluster binding energy. At this barrier magnitude, torsional tunneling in the lower portions of the potential is minimal and the residence time of the cluster constituents in a particular well minimum is substantially longer than the timescale of experimental observation.

The assignment of geometry and identification of the intermolecular modes using the theoretical models has also proven useful in understanding the physics governing the spectroscopic properties of the clusters. The observation of nontotally symmetric intermolecular mode fundamentals and combination bands in the vibronic spectra suggest that interelectronic state mixing (H-T coupling) is an important factor in the overall intensity mechanism governing the transitions. Additionally, the interelectronic state mixing is most important for the low-lying intermolecular bending and torsional modes.

Both the NCA and the 3D-HRRA adequately model the intermolecular modes in the systems studied; however, the NCA is the more useful here

The rigidity of these systems is a function of the geometry of the system and the nature of the solvent rotational dynamics. An example of a bent state for which $\theta = 1$ has a displacement in the θ coordinate of ± 2 and γ displacements may or may not be present depending on the values of the l and m quantum numbers. Given the geometry of the system, then, low barrier one dimensional rotation (solvent rotating around the cluster three fold C-X bond axis) is not possible. Basically the two dimensional hindering in bent(X_4)₂ clusters is insufficient to produce the one dimensional rotation occurring in "attached tops" such as toluene.¹¹

Acknowledgment

We wish to thank Professor W. Klemperer for many helpful discussions and suggestions concerning the rigidity of vdW molecules.

REFERENCES

1. M. Schauer and E.R. Bernstein, *J. Chem. Phys.* 82, 726 (1985); M. Schauer, K.S. Law and E.R. Bernstein, *J. Chem. Phys.* 82, 736 (1985); J. Wanna and E.R. Bernstein, *J. Chem. Phys.* 84, 927 (1986).
2. T.A. Stephenson and S.A. Rice, *J. Chem. Phys.* 81, 1083 (1984).
3. J.A. Menapace and E.R. Bernstein, *J. Phys. Chem.* 90, 000 (1987) and references therein.
4. J.A. Beswick and J. Jortner, *J. Chem. Phys.* 74, 6725 (1981) and references therein; D.F. Kelley and E.R. Bernstein, *J. Phys. Chem.* (to be published).
5. D.F. Kelley and E.R. Bernstein, *J. Phys. Chem.* 90, 5461 (1986).
6. T.M. Miller and B. Bederson, *Adv. At. Mol. Phys.* 13, 1 (1977); "Handbook of Chemistry and Physics" 53rd Ed. (CRC Press, 1973); G. Nemethy, M.S. Pottle and H.A. Scheraga, *J. Phys. Chem.* 87, 1883 (1983) and references therein.
7. B.L. Crawford Jr., *J. Chem. Phys.* 8, 273 (1940); K.S. Pitzer and W.D. Gwinn, *J. Chem. Phys.* 10, 428 (1942); G. Herzberg, "Molecular Spectra and Molecular Structure: II. Infrared Raman Vibrational Spectra", (McGraw-Hill Book Co., Inc. 1955).
8. P.R. Bunker, "Molecular Symmetry and Spectroscopy", (Academic Press, 1979).
9. R.S. Martin, C. Reinsch and J.H. Wilkinson, *Num. Math.* 11, 181 (1968).
10. R.S. Martin and J.H. Wilkinson, *Num. Math.* 12, 377 (1968); A. Dubrille, *Num. Math.* 15, 450 (1970).
11. P.J. Breen, J.A. Warren, E.R. Bernstein and J.I. Seeman, *J. Chem. Phys.* (to be published).

CHAPTER FOUR

HYDROGEN BONDED AND NON-HYDROGEN BONDED VAN DER WAALS
CLUSTERS: COMPARISON BETWEEN CLUSTERS OF PYRAZINE, PYRIMIDINE,
AND BENZENE WITH VARIOUS SOLVENTS
(Reprint contained in Appendix One)

CHAPTER FIVE

SUPERSONIC MOLECULAR JET STUDIES OF THE PYRAZINE AND
PYRIMIDINE DIMERS

(Reprint contained in Appendix Two)

CHAPTER SIX

SUPERSONIC MOLECULAR JET STUDIES OF PHTHALOCYANINES AND THEIR VAN DER WAALS CLUSTERS WITH SMALL MOLECULES

Introduction.

Supersonic molecular jet spectroscopy can be utilized to study weakly bound solute/solvent van der Waals (vdW) clusters in the gas phase.¹ These investigations have increased our understanding of the intra- and intermolecular energetics and dynamics present in the solute/solvent systems as well as the nucleation and growth of small clusters.²⁻¹¹ The vdW clusters studied in our laboratory thus far center around aromatic hydrocarbon and N-heterocycle solutes clustered with small hydrocarbon and hydrogen bonding solvents. We are currently expanding our studies of solute/solvent systems to include clusters of small molecules with macrocycles, such as free-base phthalocyanine (H_2Pc) and magnesium phthalocyanine ($MgPc$).

Considerable interest exists in phthalocyanine (Pc) compounds as coloring agents, photosensitizers, organic semiconductors, and as model systems for biologically important species, such as porphyrins. Pc's have exceptional color, chemical, temperature, and solubility characteristics which make them attractive for use as coloring agents in commercial dyeing and painting processes.¹² The unique electrical properties of Pc's serve as building blocks in a number of important technical applications involving electronic devices. For example, thin film

sandwich photovoltaic cells containing Pc's have been fabricated which possess photocurrent quantum efficiencies of as much as 10%.¹³ Pc films have also been shown to possess both n- and p- type semiconductor properties.¹⁴

Of particular interest are the interactions between Pc's and other molecular species. Pc films have been observed to respond electrically to the presence of vapors such as BF_3 , NO_2 , and NH_3 .¹⁵ Interaction between the film surface and the vapors produces reversible and reproducible film conductivity changes which make the measuring of molecular concentrations of these species at the ppm to ppb levels possible. Pc's and porphyrins have also been studied as photocatalysts for the reduction of water to hydrogen.¹⁶ Photochemical generation of hydrogen from water is a very attractive goal for photochemical storage of solar energy. Since water does not absorb at solar wavelengths present at the earth's surface, the photoreductive reactions must be sensitized by dyes. Pc's are good candidates as dyes in this respect since they absorb in the visible spectrum where peak solar radiation occurs.¹⁷ The elucidation of the trapping and transduction mechanisms of solar energy into useful chemical energy is of particular importance in these systems as it may yield insight into the understanding of the basic process of photosynthesis in biologically active systems such as green plants and bacteria.¹⁸ Studying the interactions between Pc's and small "solvents" may also prove useful in understanding the transport and storage of small molecules and the transfer of electrons in a variety of biologically active species such as hemoglobin, myoglobin, and cytochromes.¹⁹

Supersonic molecular jet investigations can contribute to the resolution of a number of important concerns dealing with the behavior of Pc/solvent systems on the microscopic scale. Questions that can be considered are (1) what are the ground and excited state interaction energies between Pc and various solvents, (2) what are the preferential intermolecular interaction sites on the Pc moiety, (3) what are the most favorable cluster geometries, (4) what types of interactions are important in the intermolecular potential established between the solute and solvent, and (5) are changes in the chromophore symmetry/geometry induced by clustering. The answers to these questions will certainly be helpful to those employing Pc's or related systems in reactions and other chemical processes.

In this paper, we report the spectroscopic results of H_2Pc and $MgPc$ clustered with hydrocarbon solvents (CH_4 , C_2H_6 , and C_3H_8), hydrogen bonding solvents (H_2O , $MeOH$, $EtOH$), and CO_2 along with the calculated modeling of selected cluster characteristics. The spectroscopic results include the $\pi^* \leftarrow \pi$ fluorescence excitation (FE) spectra of the clusters near the Pc 0_0^0 transition. The calculated results include the ground state geometry and the binding energy for each of the cluster systems studied. The H_2Pc cluster spectra and calculated geometries and binding energies are compared with those obtained for the $MgPc$ clusters. Differences and similarities between the $H_2Pc(MgPc)$ clusters and the aromatic hydrocarbon and N-heterocycle clusters are discussed. Specifically, trends in spectral shifts, relative solute/solvent orientations, and binding energies are noted. Finally, the results of an out-of-plane normal coordinate analysis for Pc are discussed and compared to both Pc and cluster spectra within the first few hundred wavenumbers of the origin transition.

Experimental Procedures.

The majority of the apparatus used in these experiments has been previously described;²⁻⁷ therefore, only a description of the equipment and procedures unique to the present studies will be discussed. A high temperature continuous supersonic nozzle fabricated to generate and analyze the H_2Pc and $MgPc$ clusters is shown in figure 6.1. The expansion region is constructed by welding a stainless steel pinhole (Micro Engineering) A onto a 1/4 inch tube connector gland (Cajon VCR) B. The pinhole/gland is attached to the nozzle backing region C using a 1/4 inch tube connector (Cajon VCR) D. Stainless steel gaskets are used to insure proper connector sealing throughout the nozzle operating temperature range. This setup allows different size pinhole assemblies (nozzle throats) to be attached to the nozzle to obtain various peak experimental backing pressure and gas throughput conditions. A 100 micron pinhole is used to perform the expansion in the H_2Pc and $MgPc$ cluster experiments. The nozzle backing region is constructed from 1/2 inch stainless steel tubing. The tubing extends through the vacuum chamber wall E passing through a vacuum quick disconnect (MDC Vacuum) F. Connection of the nozzle to the expansion gas line is accomplished using a stainless steel tube connector (Swagelok) G. Solid samples are placed in the nozzle backing region using a quartz "boat" H which can be inserted into the nozzle through the expansion gas line connection. The "boat" facilitates access to the nozzle backing region while the nozzle is in the vacuum chamber and is heated. It allows for easy inspection of the sample during and after an experiment without nozzle removal or nozzle cooling. The nozzle is heated using two heating coils (ARI Industries) I located around the expansion and backing regions. The

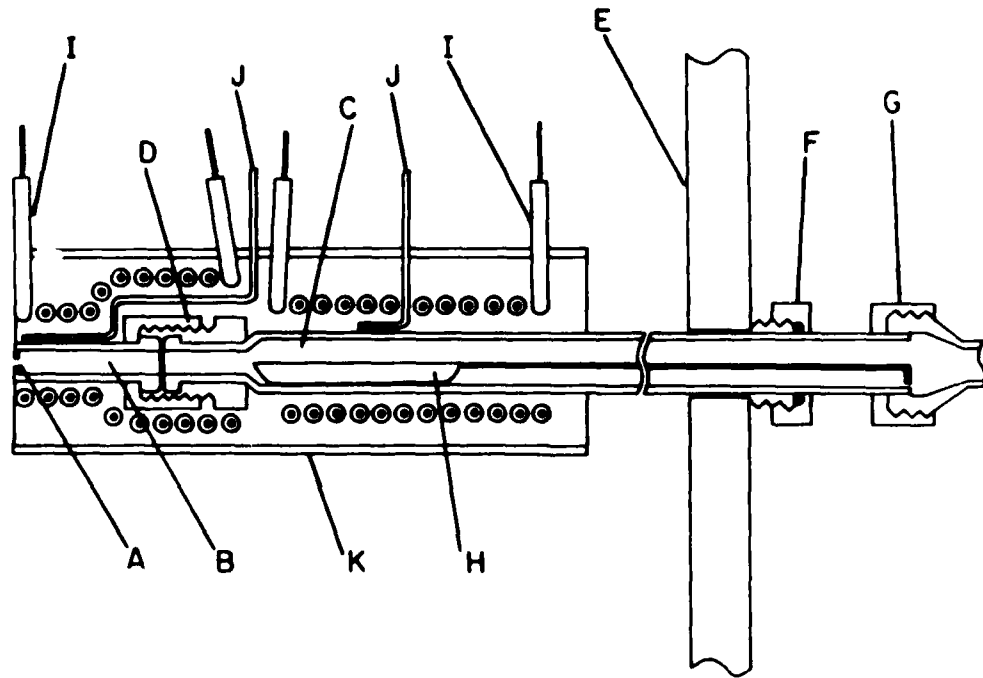


Figure 6.1

High temperature continuous supersonic molecular jet nozzle (see text).

heaters are capable of maintaining the nozzle at temperature up to 650°C. The heaters are independently controlled using two transformer assemblies. Nozzle temperature is monitored using two iron-constantan thermocouples (Omega) J placed around the expansion and backing regions. The nozzle/heater assembly is enclosed in a stainless steel shield K to minimize heat loss and to maintain uniform nozzle heating.

FE spectra of the H_2Pc , $MgPc$, and their respective solvent clusters are obtained using a Nd^{+3}/YAG pumped DCM (Exciton) dye laser. Dye laser output is 46-60 mJ/pulse in the vicinity of the H_2Pc and $MgPc$ 0_0^0 transitions. Total excited state fluorescence is collected using a $f/1.2$ 5 cm lens focused at 5-8 mm in front of the nozzle throat and detected by a water cooled RCA C31034 photomultiplier tube. The photomultiplier tube output is amplified 10x using an Ortec 9301 amplifier. The signal is then sent to a boxcar/computer for averaging and digital storage. Fluorescence wavelength calibration is provided by an optogalvanic cell with iron and neon lines as standards.

H_2Pc (Aldrich) and $MgPc$ (Eastman Kodak) are purified by vacuum sublimation before use. The solid samples are pelletized prior to insertion into the nozzle to minimize consumption. Granular samples placed in the nozzle are consumed at a rate of ca. 45 mg/hr. Pelletization reduces sample consumption by about a factor of thirty without significant loss in fluorescence intensity.

The H_2Pc and $MgPc$ solid samples are heated to 380-640° C to provide sufficient vapor density to perform the spectroscopy. Methane, ethane, propane or carbon dioxide is doped into helium carrier gas at concentrations of up to 1% (partial pressure). The gas is then mixed with the H_2Pc or $MgPc$ in the nozzle backing region and expanded using

pressures ranging from 100-200 psig. Water, methanol, or ethanol is seeded into the helium carrier gas by passing the carrier gas through an inline trap containing the liquid solvent.

Calculations of the ground state cluster binding energies and geometries are conducted using an empirical intermolecular potential generated from additive atom-atom potentials set into a Lennard-Jones format. The potential includes general non-bonding (6-12), monopole charge (1), and hydrogen bonding (10-12) terms.²⁰ The H₂Pc and MgPc structures used in the calculations are obtained from crystal structure data.²¹ The atom-atom potential for magnesium is approximated using experimentally determined polarizabilities²², interatomic distance²³, and the Slater-Kirkwood approximation²⁴. Atomic partial charges employed to model the monopole charge interaction are taken from extended Huckel²⁵ calculations. The hydrocarbon and water structures are those previously used in studying benzene and N-heterocycle clusters.^{2,8-10} The CO₂, MeOH, and EtOH structures are taken from ref. 26, 27, and 28, respectively.

The out-of-plane normal coordinate analysis for H₂Pc is conducted using the FG matrix method of Wilson et. al.²⁹ The details of the analysis will be reported elsewhere.³⁰ Briefly, the nuclear motion is modeled using a set of 82 internal coordinates: 48 C-C(N) bond torsions, 18 C(N)-H bond wags, and 16 C-C(N) bond wags. The valence force field for the \underline{F} matrix consists of the diagonal force constants describing the out-of-plane ground state motions in benzene.³¹ In this gross approximation, all H₂Pc bond torsions force constants are assumed to be the same as the C-C torsions in benzene. All bond wag force constants are assumed to be the same as the benzene C-H wags. The secular equation

describing the nuclear motion is symmetry factored into four species sets (B_{1u} , A_u , B_{2g} , and B_{3g}) under the D_{2h} point group. The factored equations are individually diagonalized to yield 15 B_{1u} , 13 A_u , 13 B_{2g} , and 14 B_{3g} out-of-plane frequency eigenvalues and eigenvector normal modes. (See Table 6.1).

Results.

A. Isolated Ultracold Molecular FE Spectra of H_2Pc and $MgPc$.

Figure 6.2 presents the FE spectrum of the H_2Pc $S_1 \leftarrow S_0$ transition (Q_x band) in the vicinity of the 0_0^0 . The spectrum is taken at 200 psig helium backing pressure (P_0), a nozzle expansion region temperature (T_e) of $570^\circ C$, and a nozzle backing region temperature (T_b) of $460^\circ C$. The general nature of the spectrum has been previously described.³² The purpose of its reproduction in this paper is 1) to present a detailed account of the low frequency vibronic transitions observed in the vicinity of the 0_0^0 which have not been previously reported in the literature Table 6.2, and 2) to provide an isolated chromophore spectrum which can be compared to the cluster spectra, all of which are taken under nearly identical experimental conditions.

The FE spectrum of the $MgPc$ $S_1 \leftarrow S_0$ transition (Q band) in the vicinity of the 0_0^0 is shown in Figure 6.3. The spectrum is taken using $P_0 = 120$ psig helium, $T_e = 630^\circ C$, and $T_b = 397^\circ C$. Table 6.3 lists the energies of the vibronic transitions observed in this portion of the spectrum.

B. Hydrocarbon Clusters: CH_4 , C_2H_6 , and C_3H_8 .

The H_2Pc /hydrocarbon cluster FE spectra observed in the vicinity of the H_2Pc 0_0^0 are presented in Figure 6.4. The energies of

TABLE 6.1

Calculated out-of-plane mode frequencies for H₂Pc.

Calculated Mode Energy (cm ⁻¹)	D _{2h} Symmetry Species	Observed Overtone ^a Energy (cm ⁻¹)	Mode Designation
14.8	B _{1u}	31.2 (15.6)	A
24.5	B _{1u}	51.8 (25.9)	B
84.0	B _{1u}	163.7 (81.9)	C
33.1	A _u	71.4 (35.7)	D
71.7	A _u	141.7 (70.9)	E
38.6	B _{2g}	85.4 (42.7) or 100.6 (50.3)	F
72.1	B _{2g}	176 (88) or 203.1 (101.6)	G
38.2	B _{3g}	85.4 (42.7) or 100.6 (50.3)	H
71.4	B _{3g}	176 (88) or 203.1 (101.6)	J

a) Values in parentheses are forbidden fundamental mode energies inferred from overtone transitions.

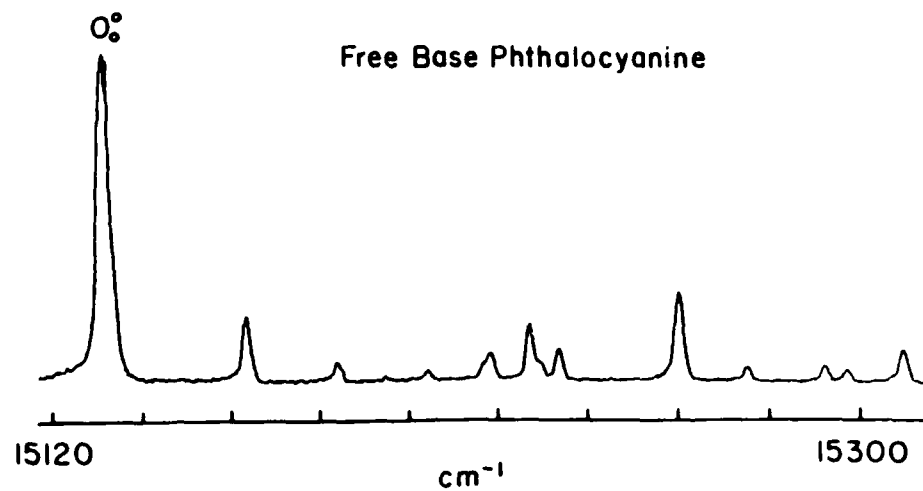


Figure 6.2

FE spectrum of 0₀⁰ region of H₂Pc taken at T_e = 570°C, T_b = 460°C, and P₀ = 200 psig He. Peak assignments are given in Table 6.2.

TABLE 6.2

Observed vibronic transitions in the vicinity of the $H_2Pc\ 0_0^0$.

Energy (vac. cm^{-1})	Wavelength (vac. Å)	Energy Relative to 0_0^0 (cm^{-1})	Assignment ^a
15131.8	6608.6	0	0_0^0
15163.0	6595.0	31.2	A_0^2
15183.6	6586.1	51.8	B_0^2
15193.9	6581.6	62.0	A_0^4
15203.2	6577.6	71.4	D_0^2
15215.6	6572.2	83.8	$A_0^2 + B_0^2$
15217.2	6571.5	85.4	F_0^2 or H_0^2
15225.8	6567.8	93.9	(b)
15228.0	6566.9	96.2	$A_0^1 + C_0^1$
15232.4	6564.9	100.6	F_0^2 or H_0^2
15258.7	6553.6	126.9	(b)
15273.5	6547.3	141.7	E_0^2
15290.5	6540.0	158.7	$126.9 + A_0^2$
15295.5	6537.9	163.7	C_0^2
15307.8	6532.6	176	G_0^2 or J_0^2

a) Assignments based on normal coordinate analysis results
(see Table 6.1).

b) Modes possibly due to in-plane motion.

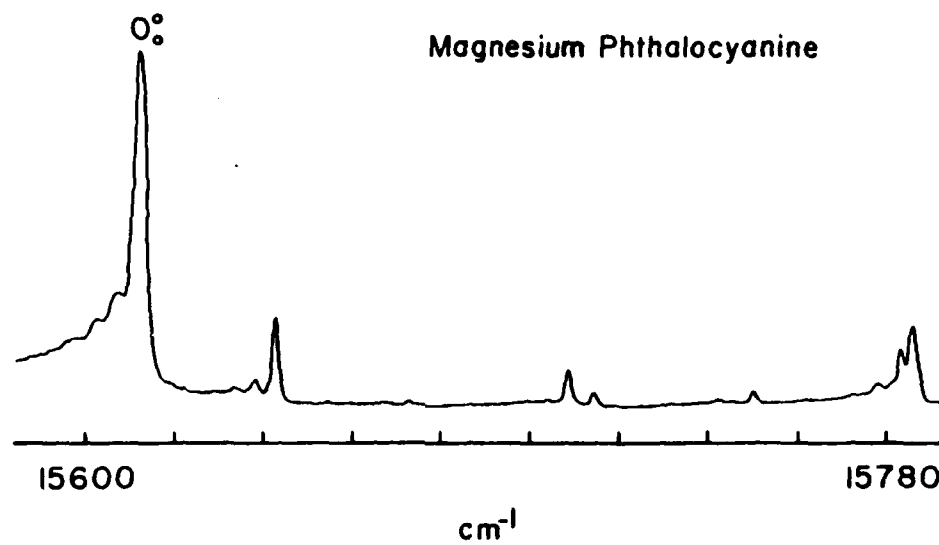


Figure 6.3

FE spectrum of 0_0^0 region of MgPc taken at $T_e = 630^\circ\text{C}$, $T_b = 397^\circ\text{C}$, and $P_0 = 120$ psig He. Peak assignments are given in Table 6.3.

TABLE 6.3

Observed vibronic transitions in the vicinity of the MgPc 0_0^0 .

Energy (vac. cm^{-1})	Wavelength (vac. \AA)	Energy Relative to 0_0^0 (cm^{-1})	Assignment ^a
15612.1	6404.5	0	0_0^0
15643.0	6392.6	30.9	A_0^2
15666.7	6383.0	54.6	B_0^2
15673.2	6380.3	61.1	A_0^4
15704.4	6367.6	92.3	F_0^2 or H_0^2
15709.0	6365.8	96.9	(b)
15714.6	6363.5	102.5	F_0^2 or H_0^2
15742.1	6352.4	130.0	
15750.1	6349.2	138.0	E_0^2
15778.0	6337.9	165.9	
15783.5	6335.7	171.4	
15786.0	6334.7	173.9	(b)

a) Assignments based on normal coordinate analysis results
(see Table 6.1).

b) Modes are due to in-plane motion.

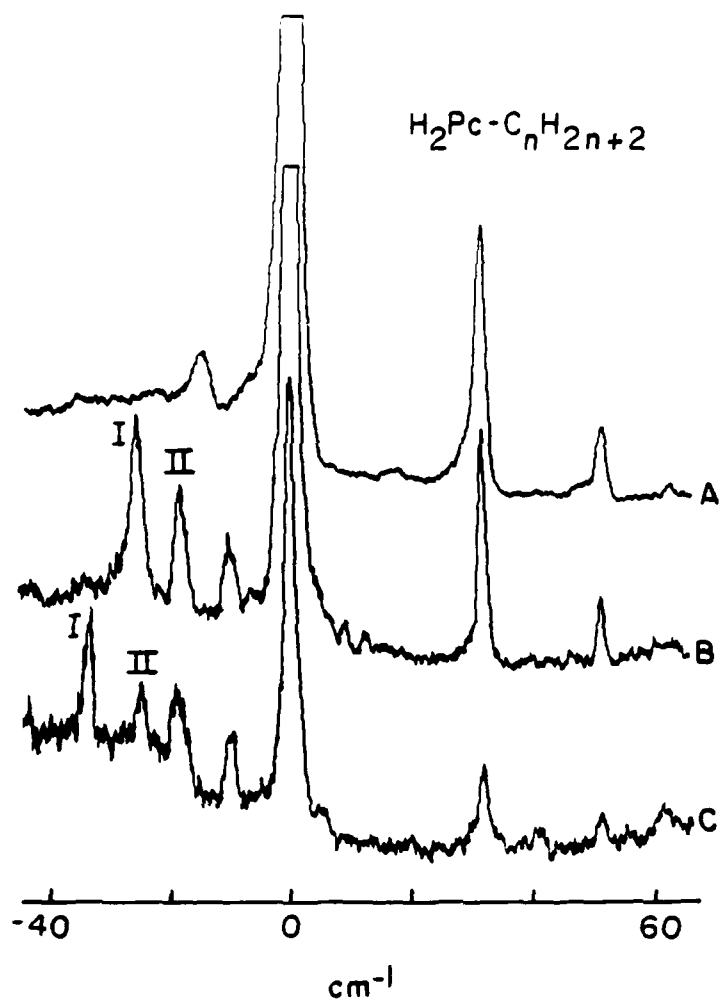


Figure 6.4

PE spectra of $\text{H}_2\text{Pc}/\text{C}_n\text{H}_{2n+2}$ clusters in the vicinity of the $\text{H}_2\text{Pc } 0_0^0$. The $\text{H}_2\text{Pc}(\text{CH}_4)_1$ spectrum (A) is taken at $T_e = 540^\circ\text{C}$, $T_b = 430^\circ\text{C}$, $P_0 = 200$ psig He, and .1% CH_4 . The $\text{H}_2\text{Pc}(\text{C}_2\text{H}_6)_1$ spectrum (B) is taken at $T_e = 540^\circ\text{C}$, $T_b = 430^\circ\text{C}$, $P_0 = 160$ psig He, and .1% C_2H_6 . The $\text{H}_2\text{Pc}(\text{C}_3\text{H}_8)_1$ spectrum (C) is taken at $T_e = 580^\circ\text{C}$, $T_b = 435^\circ\text{C}$, $P_0 = 160$ psig He, and .1% C_3H_8 . Peak assignments are given in Table 6.4.

the observed cluster transitions are listed in Table 6.4. In these experiments, solvent concentration is varied between .07 and 1% and the backing pressure is varied between 0 and 300 psig. Below .07% solvent concentration, no cluster transitions are observed; above about .3%, the cluster spectra appear broad and featureless to the red of the $\text{H}_2\text{Pc } 0_0^0$. Below 50 psig backing pressure, the spectra become broad; at 100 psig to 300 psig, no new cluster transitions emerge in the region probed.

Sharp spectra of MgPc /hydrocarbon clusters could not be generated. Through the range of .06 to 3% solvent concentration, the spectra vary from no observable cluster transitions to broad cluster bands which extend some 60 cm^{-1} to the red of the MgPc origin.

The ground state geometries calculated for the H_2Pc /hydrocarbon clusters are shown in Figure 6.5. The cluster binding energies and solute/solvent center-of-mass coordinates are listed in Table 6.5. For $\text{H}_2\text{Pc}(\text{C}_2\text{H}_6)_1$, a geometry nearly isoenergetic with geometry II is calculated but not shown. The geometry is largely the same as II but has the C_2H_6 long axis rotated by 90° about the H_2Pc symmetry z axis with respect to geometry II. The geometry has a binding energy of 1564 cm^{-1} . For $\text{H}_2\text{Pc}(\text{C}_3\text{H}_8)_1$, two additional cluster geometries are calculated and not shown. Geometry III is similar to geometry II in that the solvent C_2 axis lies perpendicular to the H_2Pc molecular plane; however, the C_3H_8 is inverted in this geometry with respect to geometry I. The cluster binding energy is 1975 cm^{-1} . Geometry IV is nearly isoenergetic with geometry I. The geometry is largely the same as II but has the C_3H_8 rotated by 90° about the H_2Pc symmetry z axis. This geometry has a binding energy of 2202 cm^{-1} .

TABLE 6.4

H₂Pc/Hydrocarbon cluster transitions in the vicinity of H₂Pc 0₀⁰.

Species	Energy (vac. cm ⁻¹)	Cluster 0 ₀ ⁰ Rela- tive to H ₂ Pc 0 ₀ ⁰ (cm ⁻¹)	Energy Relative to Cluster 0 ₀ ⁰ (cm ⁻¹)	Assignment
H ₂ Pc(CH ₄) ₁	15117.2	-14.6	0	0 ₀ ⁰
	15148.5		31.3	A ₀ ²
	15163.5		51.3	B ₀ ²
H ₂ Pc(C ₂ H ₆) ₁	15105.9	-25.9	0	I 0 ₀ ⁰
	15121.5		15.6	A ₀ ¹
	15138.6		32.7	A ₀ ²
	15113.0	-18.8	0	II 0 ₀ ⁰
	15144.3		31.3	A ₀ ²
H ₂ Pc(C ₃ H ₆) ₁	15098.4	-33.4	0	I 0 ₀ ⁰
	15113.2		14.8	A ₀ ¹
	15106.7	-25.1	0	II 0 ₀ ⁰
	15122.4		15.7	A ₀ ¹
	15138.1		31.4	A ₀ ²

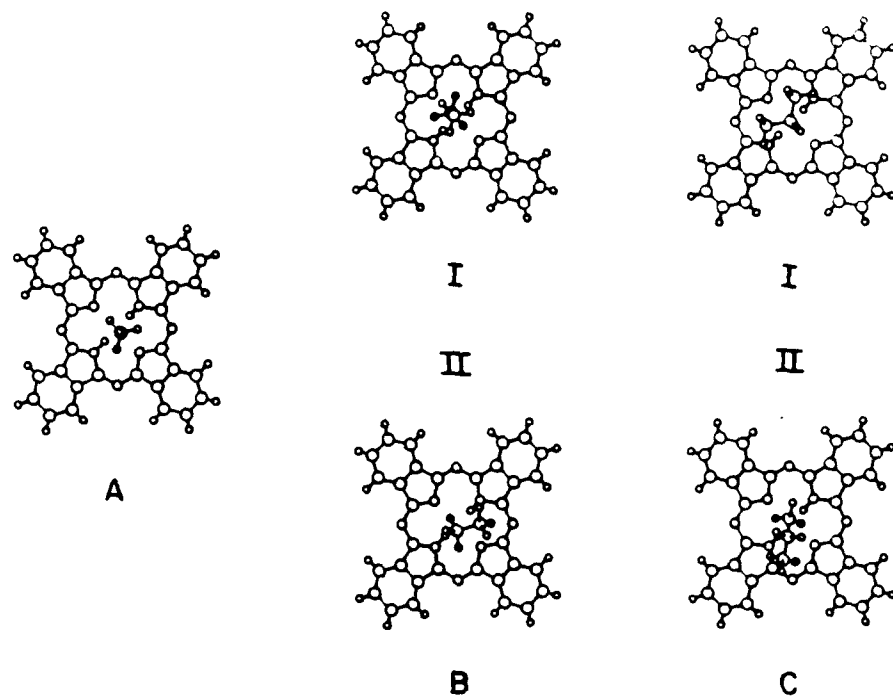


Figure 6.5

Calculated minimum energy geometries for $\text{H}_2\text{Pc}(\text{CH}_4)_1$ (A), $\text{H}_2\text{Pc}(\text{C}_2\text{H}_6)_1$ (B), and $\text{H}_2\text{Pc}(\text{C}_3\text{H}_8)_1$ (C). The cluster binding energies and solute/solvent center-of-mass coordinates are given in Table 6.5.

TABLE 6.5

Calculated cluster binding energies, solvent center-of-mass positions, and solvent orientation specifics.

Cluster	Fig. Ref.	Binding Energy (cm ⁻¹)	Location of Solvent Center-of-Mass ^a (Å)			Solvent Orientation (Remarks)
			x	y	z	
H ₂ Pc(CH ₄) ₁	5	1176	.246	.209	3.005	Three solvent hydrogens point toward solute.
H ₂ Pc(C ₂ H ₆) ₁	5	1360	.133	.383	3.747	(I). Lower solvent CH ₃ is situated as CH ₄ in H ₂ Pc(CH ₄) ₁ .
	5	1574	.672	.022	3.206	(II). Centermost solvent CH ₃ has two hydrogens toward solute.
H ₂ Pc(C ₃ H ₈) ₁	5	2024	.293	-.929	3.456	(II). Terminal CH ₃ groups on solvent point toward solute. Each CH ₃ has two hydrogens pointing down.
	5	2225	.427	.408	3.312	(I).
H ₂ Pc(H ₂ O) ₁	6	1617	.042	-.030	2.550	Solvent hydrogens point toward solute
H ₂ Pc(MeOH) ₁	6	1884	-.101	.260	2.965	Two solvent CH ₃ hydrogens and hydroxyl hydrogens point toward solute.
H ₂ Pc(EtOH) ₁	6	2055	.592	.602	3.143	(I).
	8	2082	-.013	-.005	3.488	(II). Solvent groups closest to solute are situated as MeOH in H ₂ Pc(MeOH) ₁ .
MgPc(H ₂ O) ₁	9	1553	.492	1.478	3.011	Solvent hydrogens point toward solute.
MgPc(MeOH) ₁	9	2013	.447	1.602	3.363	Solvent hydroxyl hydrogen points toward solute.
MgPc(EtOH) ₁	9	2954	-.076	.937	3.351	
H ₂ Pc(CO ₂) ₁	11	1992	.126	.017	2.784	
Mg(CO ₂) ₁	11	2336	.986	1.937	3.142	

a) The solute center of mass is located at x = y = z = 0 for all clusters.

C. H₂O, MeOH, and EtOH Clusters with H₂Pc and MgPc.

Figures 6.6 and 6.7 and Table 6.6 present the H₂O, MeOH, and EtOH, solute/solvent cluster spectra observed in the vicinity of their respective H₂Pc and MgPc 0₀⁰ transitions. The H₂Pc cluster spectra are observed using P₀ = 150 psig helium, T_e = 570°C, and T_b = 435°C. The MgPc cluster spectra are observed using P₀ = 135 psig helium, T_e = 630°C, and T_b = 480°C.

The ground state geometries calculated for the above mentioned cluster series are shown in Figures 6.8 and 6.9. The cluster binding energies and geometry specifics are listed in Table 6.5. For H₂Pc(EtOH)₁, a geometry similar to geometry I is calculated but not shown. The cluster binding energy is 2053 cm⁻¹. This geometry has the EtOH rotated by 90° about the H₂Pc symmetry z axis with respect to I.

D. CO₂ Clusters of H₂Pc and MgPc.

The H₂Pc/CO₂ and MgPc/CO₂ FE spectra observed in the vicinity of the cluster chromophore 0₀⁰ transitions are shown in Figure 6.10. The cluster transition energies are listed in Table 6.7. In these experiments, both backing pressure and CO₂ concentration are varied. As in the H₂Pc/hydrocarbon cluster experiments, no new or additional sharp cluster transitions are observed under these conditions. The ground state cluster geometries for H₂Pc(CO₂)₁ and MgPc(CO₂)₁ are shown in Figure 6.11. The cluster binding energies are listed in Table 6.5.

Discussion.

Before analyzing the individual cluster systems in detail, we will discuss the low frequency out-of-plane vibrational motion of isolated H₂Pc and MgPc. Elucidation of the out-of-plane motion in these molecules is essential to the understanding of the cluster spectra and

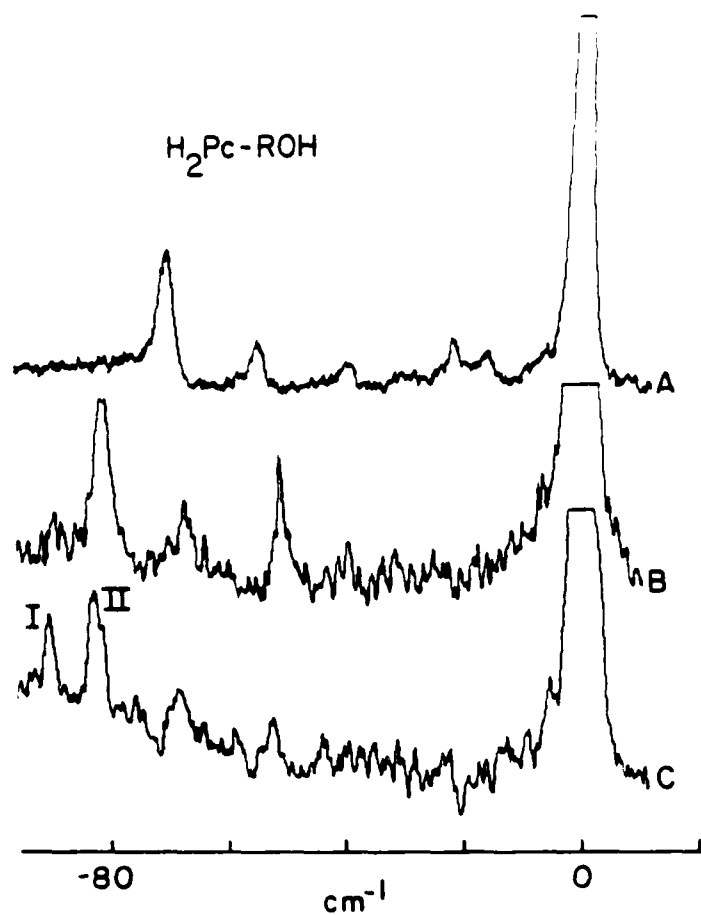


Figure 6.6

FE spectra of $\text{H}_2\text{Pc}/\text{ROH}$ clusters in the vicinity of the $\text{H}_2\text{Pc } 0_0^0$. The spectra are obtained using $T_e = 570^\circ\text{C}$, $T_b = 435^\circ\text{C}$, and $P_0 = 150$ psig He. Traces (A), (B), and (C) correspond to $\text{H}_2\text{Pc}(\text{H}_2\text{O})_1$, $\text{H}_2\text{Pc}(\text{MeOH})_1$, and $\text{H}_2\text{Pc}(\text{EtOH})_1$, respectively. Peak assignments are given in Table 6.6.

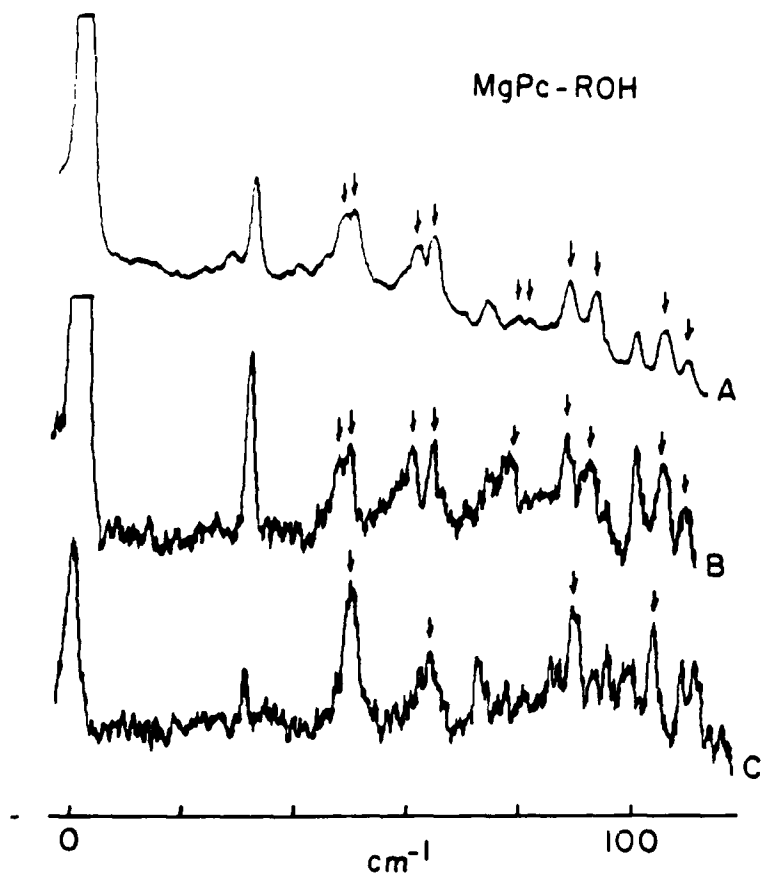


Figure 6.7

FE spectra of MgPc/ROH clusters in the vicinity of the MgPc 0_0^0 . Traces (A), (B), and (C) correspond to MgPc(H_2O)₁, MgPc(MeOH)₁, and MgPc(EtOH)₁, respectively. The spectra are taken at $T_e = 630^\circ\text{C}$, $T_b = 480^\circ\text{C}$, and $P_0 = 135$ psig He. Peak assignments are given in Table 6.6. The arrows indicate cluster transitions.

TABLE 6.6

$H_2Pc(H_2O)_1$, $H_2Pc(MeOH)_1$, $H_2Pc(EtOH)_1$, $MgPc(H_2O)_1$, $MgPc(MeOH)_1$,
and $MgPc(EtOH)_1$ cluster transitions in the vicinities of the
chromophore 0_0^0 .

Species	Energy (vac. cm^{-1})	Cluster 0_0^0 Relative to to $H_2Pc/MgPc$ 0_0^0 (cm^{-1})	Energy Relative to Cluster 0_0^0 (cm^{-1})	Assignment
$H_2Pc(H_2O)_1$	15060.6	-71.2	0	0_0^0
	15076.3		15.7	A_0^1
	15091.8		31.2	A_0^2
	15108.2		47.6	A_0^3
	15115.7		55.1	B_0^2
$H_2Pc(MeOH)_1$	15049.8	-82.0	0	0_0^0
	15066.1		16.3	A_0^1
	15081.2		31.4	A_0^2
$H_2Pc(EtOH)_1$	15040.9	-90.9	0	I 0_0^0
	15035.3 ^a		15.8	A_0^1
	15051.7 ^a		32.2	A_0^2
	15048.5	-83.3	0	II 0_0^0
	15064.6		16.1	A_0^1
	15080.2		31.7	A_0^2
$MgPc(H_2O)_1$	15658.7	46.6	0	0_0^0
	15672.6		13.9	A_0^1
	15683.0			
	15687.8		29.1	A_0^2
	15696.4		37.7	F_0^1 or H_0^1
	15715.8		57.1	B_0^2

TABLE 6.6 (Continued)

Species	Energy (vac. cm^{-1})	Cluster O_0^0 Relative to to $\text{H}_2\text{Pc/MgPc}$ O_0^0 (cm^{-1})	Energy Relative to Cluster O_0^0 (cm^{-1})	Assignment
	15660.4	48.3	0	O_0^0
	15674.6		14.2	A_0^1
	15690.2		29.8	A_0^2
	15701.0		40.6	F_0^1 or H_0^1
	15717.3		56.9	B_0^2
$\text{MgPc}(\text{MeOH})_1$	15658.4	46.3	0	O_0^0
	15672.5		14.1	A_0^1
	15687.9		29.8	A_0^2
	15696.8		38.4	F_0^1 or H_0^1
	15713.7		55.3	B_0^2
	15660.4	48.3	0	O_0^0
	15674.8		14.4	A_0^1
	15690.3		29.9	A_0^2
	15701.2		40.8	F_0^1 or H_0^1
	15717.8		57.4	B_0^2
$\text{MgPc}(\text{EtOH})_1$	15661.7	49.6	0	O_0^0
	15676.3		14.6	A_0^1
	15684.7			
	15700.6		38.9	F_0^1 or H_0^1
	15714.6		52.9	B_0^2

a) Weak features (Figure 6.6) - assignment must be considered tentative

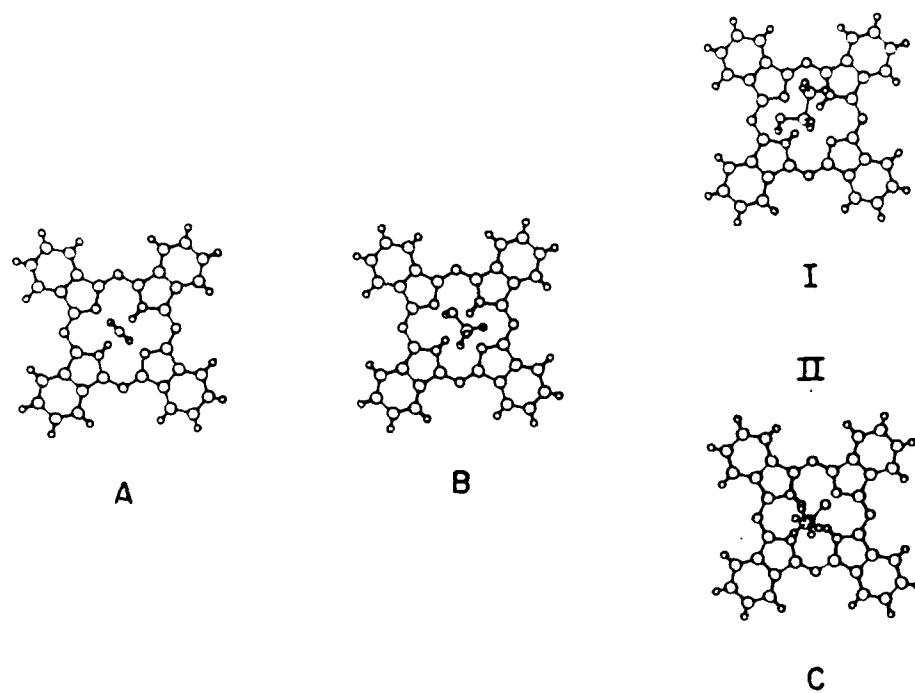
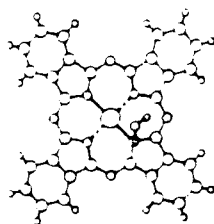
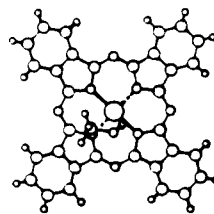


Figure 6.8

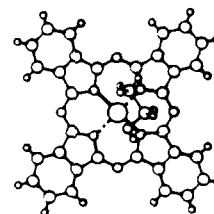
Calculated minimum energy geometries for $\text{H}_2\text{Pc}(\text{H}_2\text{O})_1$ (A), $\text{H}_2\text{Pc}(\text{MeOH})_1$ (B), and $\text{H}_2\text{Pc}(\text{EtOH})_1$ (C). The cluster binding energies and solute/solvent center-of-mass coordinates are given in Table 6.5.



A



B



C

Figure 6.9

Calculated minimum energy for $\text{MgPc}(\text{H}_2\text{O})_1$ (A), $\text{MgPc}(\text{MeOH})_1$ (B), and $\text{MgPc}(\text{EtOH})_1$ (C). The cluster binding energies and solute/solvent center-of-mass coordinates are given in Table 6.5.

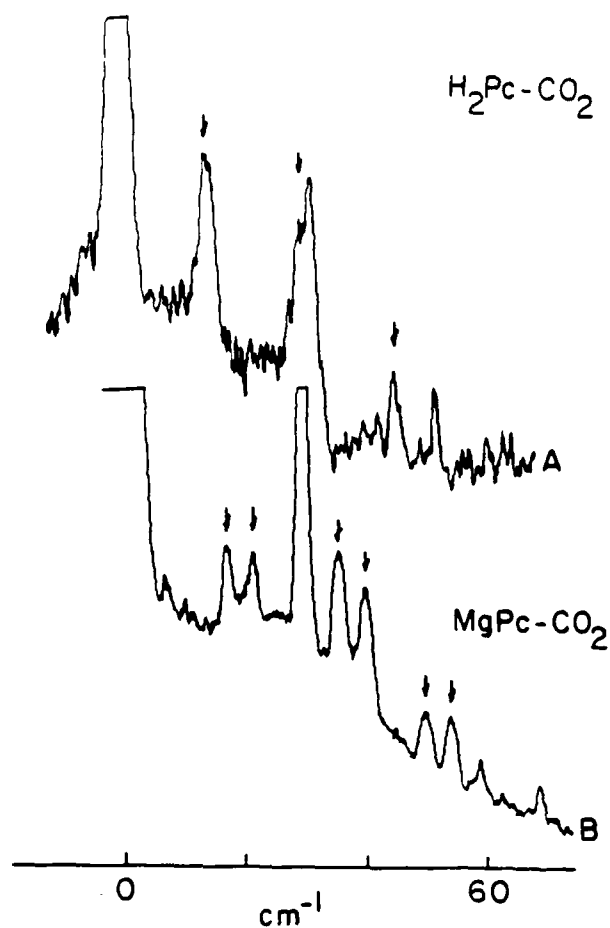


Figure 6.10

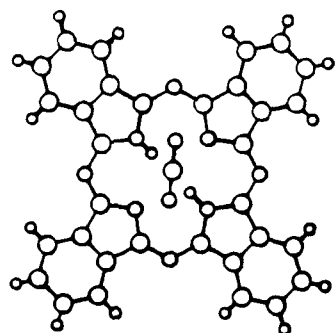
FE spectra of $\text{H}_2\text{Pc}(\text{CO}_2)_1$ and $\text{MgPc}(\text{CO}_2)_1$ in the vicinities of the cluster chromophore 0_0^0 transitions. The $\text{H}_2\text{Pc}(\text{CO}_2)_1$ spectrum (A) is taken at $T_e = 500^\circ\text{C}$, $T_b = 485^\circ\text{C}$, $P_0 = 150$ psig He, and .2% CO_2 . The $\text{MgPc}(\text{CO}_2)_1$ spectrum (B) is taken at $T_e = 443^\circ\text{C}$, $T_b = 412^\circ\text{C}$, $P_0 = 150$ psig He and .2% CO_2 . Peak assignments are given in Table 6.7. The arrows indicate cluster transitions.

TABLE 6.7

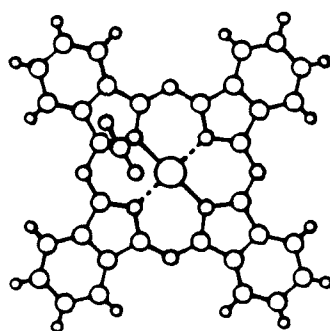
$\text{H}_2\text{Pc}(\text{CO}_2)_1$ and $\text{MgPc}(\text{CO}_2)_1$ cluster transitions in the vicinity of the chromophore 0_0^0 .

Species	Energy (vac. cm^{-1})	Cluster 0_0^0 Relative to to H_2Pc / MgPc 0_0^0 (cm^{-1})	Energy Relative to Cluster to Cluster 0_0^0 (cm^{-1})	Assignment
$\text{H}_2\text{Pc}(\text{CO}_2)_1$	15145.8	14.0	0	0_0^0
	15161.2		15.4	A_0^1
	15176.5		30.7	A_0^2
$\text{MgPc}(\text{CO}_2)_1$	15630.0	17.9 ^a	0	0_0^0
	15649.9		19.9	A_0^1
	15664.6		34.6	A_0^2
	15634.7	22.6 ^a	0	0_0^0
	15655.8		21.1	A_0^1
	15667.0		32.3	A_0^2

a) Transitions correspond to same cluster species (see text)



A



B

Figure 6.11

Calculated minimum energy geometries for H₂Pc(CO₂)₁ (A) and MgPc(CO₂)₁ (B). The cluster binding energies and center-of-mass coordinates are given in Table 6.5.

in the identification of the number of different clusters of a specific composition observed. The nature of molecular motion associated with each spectral feature is determined by using the results of an out-of-plane normal coordinate analysis for isolated H_2Pc . Table 6.1 lists the nine lowest energy out-of-plane modes calculated. Given the qualitative nature of the force field used in the analysis, the calculated vibrational energies compare quite well with the fundamental energies inferred from the observed overtone transitions presented in Figure 6.2 and Table 6.2.

Three B_{1u} fundamentals are calculated at 14.8, 24.5 and 84.0 cm^{-1} . In the isolated H_2Pc spectrum, these vibrations are observed as symmetric overtones at 31.2 (A_0^2), 51.8 (B_0^2), 62.0 (A_0^4), and 163.7 (C_0^2) cm^{-1} . The symmetry forbidden fundamentals are thus located at 15.6, 25.9 and 81.9 cm^{-1} using a harmonic oscillator assumption. Two A_u modes calculated at 33.1 and 71.7 cm^{-1} correspond to the forbidden out-of-plane fundamentals at 35.7 and 70.9 cm^{-1} which are observed as overtones at 71.4 (D_0^2), and 141.7 (E_0^2) cm^{-1} . The two B_{2g} (B_{3g}) modes calculated at 38.6 (38.2) and 72.1 (71.4) cm^{-1} correspond to the fundamentals of the observed overtone transitions at 85.4 and 100.6 (F_0^2 or H_0^2) cm^{-1} and at 176 and 203.1 (G_0^2 or J_0^2) cm^{-1} . The low energy out-of-plane vibronic transitions in the vicinity of the $MgPc$ origin are similarly assigned (Figure 6.3 and Table 6.3).

Five out of the nine lowest energy out-of-plane vibrations are responsible for the vibronic transitions observed in the first 100 cm^{-1} of the H_2Pc S_1 manifold. These five modes involve large amplitude displacements of the four isoindole groups comprising H_2Pc . The qualitative forms of the motion can be described by the two sets of

operations indicated in Figure 6.12: (a) the tilt of the isoindole groups around the line A through the pyrrole α carbons; and (b) the rotation of the isoindole groups around the line B between the inner ring nitrogens and the midpoint between outer benzene carbons. The B_{1u} vibration calculated at 14.8 cm^{-1} corresponds to (a) type motion in which a set of opposite isoindole groups tilts out of the molecular plane in one direction and other set of opposite isoindole groups tilts out of the plane in the opposite direction. The B_{1u} vibration calculated at 24.5 cm^{-1} is similar to the 14.8 cm^{-1} mode; however, all the isoindole groups tilt out of the plane about the A axis (Figure 6.12) in the same direction. The mode form looks similar to the forming of a "bowl" out of the phthalocyano skeleton. The A_u mode (33.1 cm^{-1}) involves type (b) motion of adjacent isoindole groups in one direction and the other two adjacent isoindole groups in the opposite direction. The motion looks like "ruffling" of the molecular skeleton. The B_{2g} mode (38.6 cm^{-1}) corresponds to (a) and (b) type motions of opposite isoindole groups. The vibration form is such that one set of the opposite groups tilts out of the molecular plane about A in different directions. The other set of opposite groups rotates about B in the same direction. Overall, the motion looks similar to the forming of a "chair" out of the phthalocyano moiety. The B_{3g} mode (38.2 cm^{-1}) form is similar to that associated with the B_{2g} mode. The motion is the same in both cases; however, the (a) and (b) motion is exchanged between the two opposite groups in the B_{3g} mode with respect to the motion in the B_{2g} mode.

Chromophore out-of-plane fundamental and/or overtone transitions are observed in the vicinity of the cluster origins (vide infra) for all of the H_2Pc and $MgPc$ systems discussed below. The observation of the

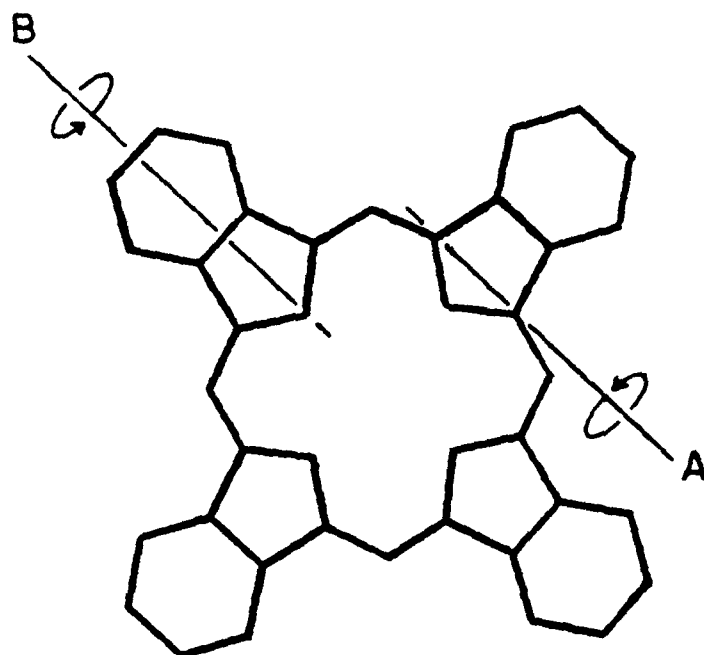


Figure 6.12

Operations showing qualitative out-of-plane vibrational motion in $H_2Pc/MgPc$.

cluster chromophore out-of plane fundamentals in the cluster spectra can be rationalized using the results of the above normal coordinate analysis and group theoretical arguments: clusters have reduced symmetry with respect to the isolated chromophore H_2Pc or $MgPc$ but nearly identical chromophore molecular vibrations. For example, in the $H_2Pc(H_2O)_1$, the symmetry is reduced from D_{2h} to, at most, C_{2v} (see Figure 6.8). Under this reduced symmetry, the forbidden B_{1u} fundamental vibrations in isolated H_2Pc correlate to A_1 vibrations in C_{2v} . The modes are therefore fully allowed by symmetry and should, in principle, be observed if Frank-Condon factors are favorable.

vdW vibrational mode eigenvectors and eigenvalues have been calculated for a number of different solute/solvent systems, including benzene, pyrazine, etc. with many of the same solvents employed in this work.^{10,11} Based on these previous studies, we can estimate that the lowest energy vdW modes for the H_2Pc and $MgPc$ /solvent systems are ca. 50 cm^{-1} . Thus, features between cluster origins and ca. $+50\text{ cm}^{-1}$ are most likely not vdW vibronic modes of the clusters. Moreover, these same studies demonstrate that high energy vdW modes ($> 50\text{ cm}^{-1}$) do not have large intensity due to poor Franck-Condon factors. A fuller discussion of these issues is presented below.

On the basis of the above notions, the cluster spectra are analyzed using four premises. First, the cluster transitions are identified as those features not associated with the isolated H_2Pc or $MgPc$ moiety. Second, the cluster origins are assigned to be the lowest energy cluster transitions observed. Third, the cluster vibronic manifolds associated with each of the origins should, and do, exhibit chromophore out-of plane fundamental and overtone transitions

commensurate with those observed and/or calculated for isolated H_2Pc or $MgPc$. And fourth, due to the similarity between the vdW potential surfaces for the chromophore S_0 and S_1 states and the relatively large energies (see below) of the vdW modes in these systems, little if any vdW vibronic mode intensity should be observed.

A. Hydrocarbon Clusters of H_2Pc and $MgPc$.

The H_2Pc /methane spectrum, Figure 6.4a and Table 6.4, exhibits a cluster transition at 14.6 cm^{-1} to the red of the H_2Pc 0_0^0 . This transition is assigned to the 0_0^0 of a single H_2Pc /methane species. As discussed above, features 31.3 and 51.3 cm^{-1} to the blue of the cluster 0_0^0 correspond to cluster chromophore out-of-plane symmetric overtones, A_0^2 and B_0^2 . Both transitions are shifted by -14.6 cm^{-1} with respect to their corresponding transitions in the isolated H_2Pc spectrum. The A_0^1 transition is not observed as it may be weak and/or within the linewidth of the H_2Pc isolated molecule 0_0^0 .

The cluster transitions are most likely due to $H_2Pc(CH_4)_1$ since no new additional sharp transitions are observed when either the CH_4 concentration or the backing pressure is increased. Increasing the CH_4 concentration and/or backing pressure should yield higher order clusters. From prior experience with other solute/solvent cluster systems,²⁻⁹ higher order clusters typically yield more than one set of cluster transitions. Additive shifts are also observed in most cases resulting from inhomogeneous nucleation processes in which solvent molecules bind symmetrically to opposite sides of the chromophore molecular plane.

The predominance of 1:1 solute/solvent clusters in the expansion may be rationalized on the basis of large solute/solvent binding energy

versus small solvent dimer binding energy. In the systems presently studied, the solute/solvent binding energies are sufficiently large that when a solvent dimer collides with a solute molecule, the dimer dissipates some of the cluster binding energy via vibrational predissociation. This interactive collision leaves one solvent molecule bound to the solute while the other solvent carries off enough of the cluster energy to stabilize the vdW bond until further collisional cooling can take place. These notions would lead one to conclude that 1:1 solute/solvent clustering predominates in the other clusters systems analyzed as well.

The existence of a single $H_2Pc(CH_4)_1$ geometry responsible for the cluster origin in the spectrum is further corroborated by the ground state configuration calculation depicted in Figure 6.5a. In this geometry, the CH_4 cluster subunit is situated above the H_2Pc plane and is coordinated to the π -cloud of the aromatic ring. The cluster geometry is interesting in the respect that the cluster solvent uniquely lies nearly over the H_2Pc core: none of the several potential cluster sites located over each of the H_2Pc closed ring subunits is apparently a true local minimum. One can envision three distinct cluster sites on the H_2Pc moiety: 1) above the H_2Pc core (most stable); 2) above one of its four five-membered rings; or 3) above one of its four six-membered rings (least stable). If all three of these sites were physically accessible, three different cluster spectral shifts should be observed corresponding to the three distinct sites. Since the single cluster origin in the spectrum suggests that only one geometry is stable, two out of the three speculated minima are either nonexistent or not sufficiently deep to accommodate bound state geometries. The observed

cluster origin at -14.6 cm^{-1} from the $\text{H}_2\text{Pc } 0_0^0$ probably corresponds to a geometry very similar to the calculated one (Figure 6.5a).

H_2Pc clustered with ethane, Figure 6.4b and Table 6.4, reveals two cluster origins at 25.9 and 18.8 cm^{-1} to the red of the $\text{H}_2\text{Pc } 0_0^0$. Two weak transitions to the blue of the $\text{H}_2\text{Pc } 0_0^0$ correspond to cluster chromophore out-of-plane vibrations A_0^2 built upon the two cluster origins. The transition at -10.3 corresponds to the fundamental of the out-of-plane cluster chromophore vibration A_0^1 (15.6 cm^{-1}) built upon the origin at -25.9 cm^{-1} . The cluster chromophore fundamental built upon the cluster origin at -18.8 cm^{-1} is not observed as it may be weak and/or within the linewidth of the $\text{H}_2\text{Pc } 0_0^0$.

These cluster manifolds most likely correspond to $\text{H}_2\text{Pc}(\text{C}_2\text{H}_6)_1$ clusters since, as in the $\text{H}_2\text{Pc}(\text{CH}_4)_1$ case, as both concentration and backing pressure are varied, the spectrum does not yield any additional sharp transitions. Furthermore, no additive spectral shifts are observed indicative of higher order clusters with ethane subunits situated above and below the H_2Pc plane. The same arguments used to rationalize the predominance of 1:1 clusters in the $\text{H}_2\text{Pc}(\text{CH}_4)_1$ case are applicable to this system as well.

The two $\text{H}_2\text{Pc}(\text{C}_2\text{H}_6)_1$ cluster geometries shown in Figure 6.5b support the assignment of two cluster geometries. Both geometries have the C_2H_6 situated over the center of the H_2Pc core as found for $\text{H}_2\text{Pc}(\text{CH}_4)_1$. Geometry I should yield a larger spectral shift than geometry II based upon polarizability arguments previously discussed for single ring cluster systems.^{2,8} Briefly, the species with the larger spectral shift is associated with the solute/solvent relative orientation for which the direction of the large solvent polarizability is

perpendicular to the solute molecular plane. Using this argument, a geometry similar to I would be associated with the cluster origin 25.9 cm^{-1} to the red of the $\text{H}_2\text{Pc } 0_0^0$. As mentioned in the Results Section, two specific solvent orientations are consistent with the qualitative solute/solvent geometry of calculated $\text{H}_2\text{Pc}(\text{C}_2\text{H}_6)_1$ configuration II (see fig 6.5b). One would not expect a spectroscopic difference between the two geometries as they differ by a 90° rotation about the symmetry z axis of H_2Pc . These two directions as far as the H_2Pc moiety is concerned should be roughly equivalent in terms of polarizabilities and π -cloud overlap.

The H_2Pc /propane clusters, Figure 6.4c and Table 6.4, are assigned on the basis of similar arguments presented for the other two hydrocarbon clusters studied. In the spectrum, two $\text{H}_2\text{Pc}(\text{C}_3\text{H}_8)_1$ cluster origins appear at 33.4 and 25.1 cm^{-1} to the red of the $\text{H}_2\text{Pc } 0_0^0$. Two cluster vibronic manifolds to the blue of each origin are assigned to cluster chromophore vibronic fundamentals and first overtones. For the cluster manifold beginning at -33.4 cm^{-1} , the A_0^1 occurs at 14.8 cm^{-1} to the blue of the cluster 0_0^0 . For the cluster manifold beginning at -25.1 cm^{-1} , the A_0^1 and A_0^2 occur at 15.7 and 31.4 cm^{-1} to the blue of the cluster 0_0^0 .

Geometries similar to those shown in Figure 6.5c could be associated with the two observed cluster manifolds. Different spectral shifts for the two geometries most likely result from difference in π -cloud solvation. The propane solvent interacts less with the H_2Pc π -cloud in geometry II than in geometry I since the C_2 axis of the cluster solvent (direction of small polarizability) is perpendicular to the H_2Pc molecular plane in geometry II but parallel to the plane in

geometry I. A geometry similar to I could thus be responsible for the cluster manifold beginning at -33.4 cm^{-1} and a geometry similar to II could be associated with the manifold beginning at -25.1 cm^{-1} .

The $\text{H}_2\text{Pc}(\text{C}_2\text{H}_6)_1$ and the $\text{H}_2\text{Pc}(\text{C}_3\text{H}_8)_1$ spectra exhibit A_0^1 transitions which are forbidden in isolated H_2Pc . A similar change in selection rules upon clustering has been reported for the benzene/solvent systems.^{2,9-11} In the latter systems, the observations suggest that the presence of the cluster solvent over the solute molecular plane is sufficient to induce the forbidden benzene 0_0^0 transition if the three-fold rotation axis of the solute is destroyed. Furthermore, the selection rules governing the intermolecular vdW motion follow the reduced symmetry of the cluster systems. This minimum perturbation may also be the driving force which induces the vibronic transitions in the H_2Pc /hydrocarbon clusters. The perturbation in the present instance may even be large enough to cause the cluster chromophore to adjust its geometry in an attempt to wrap itself around the cluster solvents to establish optimal π -cloud overlap. The observation of the B_{1u} fundamental at 15 cm^{-1} serves as evidence supporting this notion as molecular displacement along this coordinate appears to yield favorable Franck-Condon factors. The A_0^1 transition is also observed in all the other H_2Pc and MgPc clusters studied as well. These observations would lead one to conclude that the clusters are not planar in the excited electronic state.

In general the H_2Pc /hydrocarbon cluster series is similar to the benzene and N-heterocycle/hydrocarbon cluster series previously studied.^{2,8,10,11} The H_2Pc /hydrocarbon clusters $S_1 \rightarrow S_0$ transitions all exhibit bathochromic shifts with respect to the cluster chromophore

transition. The direction of the shifts is the same as that observed in the single ring cluster systems. These shifts indicate that the binding energies of the clusters become larger in the electronic excited state than in the ground state. Upon excitation, the cluster chromophore π -cloud expands and becomes more diffuse. The π -cloud can thus participate more effectively in intermolecular bonding. The net result is stabilization of the vdW bond and a larger binding energy in the cluster S_1 state relative to the S_0 state.

As in the single ring cluster systems, the H_2Pc /hydrocarbon cluster spectral shifts and calculated binding energies increase with increasing solvent size and π -cloud overlap. The shifts also depend upon the relative orientation of the cluster solute and solvent. The spectral shifts for the H_2Pc /hydrocarbon series are about a factor of two smaller than those observed in the single ring aromatic/hydrocarbon systems. The difference in the spectral shift magnitudes can be attributed to smaller changes in the intermolecular interaction resulting from smaller overall π -cloud overlap between the solute and the solvents at the H_2Pc core site. The conjugated π -electron path in H_2Pc circles around the core yielding a π -cloud "void" at the central core of the molecule. Thus, cluster solvents situated over the core do not overlap with the solute π -cloud as much as they do in single ring systems. The large size and extensive delocalization of the solute π -cloud may also be contributing factors since they minimize electron density changes at the binding site when an electron is promoted from a π - and a π^* -orbital.

The cluster geometries calculated for the H_2Pc /hydrocarbon series compare well with the geometries calculated, and in some cases

experimentally verified, for the single ring cluster series as far as the cluster solvent orientations are concerned. The geometries, however, are unique in the respect that both the spectra and the calculations suggest that the favorable binding site is the H_2Pc core and is not at peripheral ring centers.

The one major difference between the H_2Pc /hydrocarbon cluster spectra and the benzene/hydrocarbon cluster spectra is the absence of observable intermolecular vdW mode intensity in the H_2Pc cluster spectra. The lowest energy vdW motion (bending) is expected to be observed at about 50 cm^{-1} to the blue of the cluster origins based upon calculational modeling of intermolecular mode energetics.^{10,11} The vdW stretch is expected to occur at about 100 cm^{-1} above the cluster origin. The absence of $\Delta v = \pm 1$ vdW mode transitions in the H_2Pc clusters may be due to poor Franck-Condon factors. The large size and extensive delocalization of the H_2Pc π -cloud yields little change in the electron density at the cluster site when a single electron is promoted from a π - to a π^* -orbital. Thus, one might expect that the intermolecular potential surfaces of the two states are nearly superimposable even though the binding energy of the excited state is slightly different (ca. 1%) than that of the ground state. The net result is the observation of vdW sequence structure ($\Delta v = 0$) giving rise to cluster origins and cluster chromophore vibrations only. These arguments probably hold for all the cluster systems investigated in this study as well.

B. H_2O , MeOH, and EtOH Clusters of H_2Pc and MgPc.

H_2Pc clustered with H_2O , Figure 6.6a and Table 6.6, yields a spectrum exhibiting a single cluster vibronic manifold with an origin 71.2 cm^{-1} to the red of the H_2Pc 0_0^0 . The single cluster (chromophore)

vibronic manifold suggests that one $\text{H}_2\text{Pc}/\text{H}_2\text{O}$ species is responsible for the observed spectrum. The spectrum is assigned to $\text{H}_2\text{Pc}(\text{H}_2\text{O})_1$ based upon the same arguments developed for the $\text{H}_2\text{Pc}/\text{hydrocarbon}$ clusters. The assignment is supported by the ground state configuration calculations for which a single geometry is obtained, Figure 8a. In this geometry, the H_2O is situated over the H_2Pc core. The transitions at 15.7, 31.2, and 47.6 cm^{-1} to the blue of the cluster 0_0^0 correspond H_2Pc out-of-plane vibrations A_0^1 , A_0^2 and A_0^3 . The feature at 55.1 cm^{-1} to the blue of the cluster 0_0^0 corresponds to the B_0^2 cluster chromophore transition.

Clustering H_2Pc with MeOH yields a cluster spectrum, Figure 6.6b and Table 6.6, associated with $\text{H}_2\text{Pc}(\text{MeOH})_1$ which has an origin 82.0 cm^{-1} to the red of the H_2Pc 0_0^0 . The cluster chromophore out-of-plane vibrations A_0^1 and A_0^2 are observed at 16.3 and 31.4 cm^{-1} to the blue of the cluster 0_0^0 . The assignment of a single cluster manifold is supported by the single calculated ground state geometry obtained (Figure 6.8b).

H_2Pc cluster with EtOH, Figure 6.6c and Table 6.6, yields a spectrum exhibiting two cluster (chromophore) vibronic manifolds which can be assigned as due to two $\text{H}_2\text{Pc}(\text{EtOH})_1$ species. The first cluster origin is at 90.9 cm^{-1} to the red of the H_2Pc 0_0^0 and the second cluster manifold begins at 83.3 cm^{-1} to the red of the H_2Pc 0_0^0 . The cluster chromophore vibrations A_0^1 and A_0^2 can be identified in these manifolds at 16.1 and 31.7 cm^{-1} .

The two $\text{H}_2\text{Pc}(\text{EtOH})_1$ cluster species responsible for the observed spectrum can be associated with geometries similar to those shown in Figure 6.8c. In geometry I the EtOH solvent interacts more with the H_2Pc π -cloud than in geometry II and, therefore, geometry I should

exhibit a larger spectral shift. Thus a geometry similar to I could be associated with the cluster whose origin is at 90.9 cm^{-1} and a geometry similar to II could be associated with the cluster whose origin is at -83.3 cm^{-1} with respect to the $\text{H}_2\text{Pc } 0_0^0$.

The $\text{H}_2\text{Pc}/\text{H}_2\text{O}$, $\text{H}_2\text{Pc}/\text{MeOH}$, and $\text{H}_2\text{Pc}/\text{EtOH}$ cluster spectra suggest that the solvent OH group is intimately involved in the intermolecular interaction. The red shifts for all three clusters are similar and larger than those observed in the $\text{H}_2\text{Pc}/\text{hydrocarbon}$ systems. The MeOH and EtOH cluster shifts are larger than that observed in the H_2O cluster suggesting that the shifts are dependent upon the combined effects of the OH group and the hydrophobic portions of the cluster solvents. If, on the other hand, the alkyl groups were pointing toward the solute, one would expect the spectral shifts for MeOH/EtOH clusters to be similar to those observed in the hydrocarbon clusters. In these geometries, the alkyl groups would be the major contributors in the intermolecular interaction.

The large spectral shifts, the interaction of the OH group with H_2Pc , and the ground state configuration calculations lead one to postulate that hydrogen bonding may be occurring in these cluster systems. Hydrogen bonding can occur to some extent between the solute inner ring nitrogens and/or pyrrole hydrogens and the solvent OH groups: the H_2Pc inner ring nitrogens have large electron density^{19,33} which can enhance the hydrogen bonding of solvent OH groups. Since the observed chromophore transition is $\pi^* \leftarrow \pi$, a large red shift can be expected.

The $\text{MgPc}(\text{H}_2\text{O})_1$, $\text{MgPc}(\text{MeOH})_1$, $\text{MgPc}(\text{EtOH})_1$ cluster spectra, Figure 6.7 and Table 6.6, are very similar to one another. The $\text{MgPc}(\text{H}_2\text{O})_1$ spectrum can be assigned as arising from two different cluster manifolds with origin

at 46.6 and 48.3 cm^{-1} to the blue of the $\text{MgPc } 0_0^0$. Cluster chromophore out of plane vibrations are observed for both manifolds. The A_0^1 and the A_0^2 are observed at 13.9 (14.2) cm^{-1} and 29.1 (29.8) cm^{-1} to the blue of the origins. B_0^2 transitions are observed at 57.1 (56.9) cm^{-1} . The $\text{MgPc}(\text{MeOH})_1$ and $\text{MgPc}(\text{EtOH})_1$ spectra are similarly assigned.

The $\text{MgPc}(\text{ROH})_1$ series differs from the $\text{H}_2\text{Pc}(\text{ROH})_1$ series in three aspects. First, the $\text{MgPc}(\text{ROH})_1$ spectra exhibit hypsochromic shifts with respect to the isolated MgPc spectrum. The direction of the spectral shifts indicate that the solute and solvents interact more strongly in S_0 than in S_1 . The major difference between the two solute systems studied is the phthalocyano core environment: the pyrrole hydrogens in H_2Pc are replaced by a magnesium in MgPc . The hypsochromic shift suggests that the core is responsible for the larger ground state interaction. The greater stabilization in the ground state can, in principle, be due to interactions ranging from weak nonbonded vdW interactions to actual complexation in which the solvent donates an electron pair to the solute via the central metal atom.¹⁹ On the basis of the size of the spectral shifts observed, the interaction is most likely due to weak vdW interactions. If the solvent were to donate significant electron density to the central Mg atom in MgPc (a coordination bond formation) or if the Mg were to move significantly out of the Pc molecular plane,³⁴ cluster formation would drastically perturb the chromophore electronic environment and yield relatively large spectral shifts. Observation of weak vdW interactions between MgPc and H_2O , EtOH , and phenol in the IR region leads to similar conclusions.³⁵

Second, the spectral shifts in the $\text{MgPc}(\text{ROH})_1$ series are virtually identical. This observation suggests that the OH group is

intimately involved in the interaction and, furthermore, is largely responsible for the observed spectral shifts. The ground state configuration calculations, Figure 6.9, support the notion that the OH group is the major contributor to the interaction. All three calculated geometries depicted in Figure 6.9 have the solvents situated so that the OH groups point towards the MgPc core. Moreover, one would not expect to observe sharp cluster transitions if the hydrophobic portions of the solvents were the major contributors to the interaction.

Third, the $\text{MgPc}(\text{ROH})_1$ spectra show two nearly isoenergetic cluster origins and vibronic manifolds. These cluster features could be due to either two cluster species which are nearly spectroscopically identical or they could be due to the splitting of the two-fold degenerate chromophore S_1 state via vdW cluster formation. The former situation probably does not occur since these doublets are present in all the MgPc clusters observed. One would not typically expect to see this type of coincidence in the different cluster systems especially when two solvent series are considered. In MgPc clusters, clustering reduces the system symmetry (see Figure 6.9 for example) and the four-fold symmetry axis of the MgPc chromophore is destroyed. The degenerate Q band (E_u in D_{4h}) may thus split into Q_x and Q_y bands (B_{2u} and B_{3u} in D_{2h}); the splitting is small, however, due to the small perturbation caused by vdW clustering. Similar removal of degeneracies occurs for benzene clusters,^{2,9,10} and for ground state vibrations of MgPc/ H_2O , /EtOH, and /phenol systems.³⁵

C. CO_2 Clusters of H_2Pc and MgPc.

H_2Pc clustered with CO_2 , Figure 6.10a and Table 6.7, yields a spectrum with a single cluster origin blue shifted by 14 cm^{-1} with

respect to the isolated $\text{H}_2\text{Pc } 0_0^0$. The cluster manifold is assigned to a $\text{H}_2\text{Pc}(\text{CO}_2)_1$ species. Cluster chromophore out-of-plane vibrations A_0^1 (15.4 cm^{-1}) and A_0^2 (30.7 cm^{-1}) built upon the cluster origin are also observed. The calculated ground state geometry, Figure 6.11a, further supports the existence of a single cluster species responsible for the spectrum. In this geometry, the CO_2 moiety is situated over the H_2Pc core.

The $\text{H}_2\text{Pc}(\text{CO}_2)_1$ spectrum is different than the other H_2Pc clusters studied in that it is the only system exhibiting a hypsochromic shift. The exact nature of the interaction responsible for the spectral shift in this system is not known and more work on CO_2 solute/solvent systems is necessary to establish a firm argument. On the basis of the interactions responsible for the spectral shifts in the hydrocarbon and hydrogen bonded solute/solvent systems, the major interaction responsible for the shift appears to involve solvent/solute π -cloud overlap. In the ground state, the solute and solvent most likely interact through π - π interactions. Upon excitation the diffuse nature of the solute π^* state reduces the interaction between the π systems and results in a loss in S_1 binding energy relative to S_0 .

MgPc clustered with CO_2 , Figure 6.10b and Table 6.7, reveals a cluster spectrum with two parallel vibronic progressions. The appearance of the two cluster manifolds is probably due to the same type of electronic state splitting that occurs in the $\text{MgPc}(\text{ROH})_1$ systems. The cluster origins are blue shifted by 17.9 and 22.6 cm^{-1} with respect to the $\text{MgPc } 0_0^0$. As in $\text{H}_2\text{Pc}(\text{CO}_2)_1$, well defined cluster chromophore vibronic transitions are observed. The A_0^1 and A_0^2 transitions built upon the origin at 17.9 cm^{-1} occur at 19.9 and 31.1 cm^{-1} to the blue of this

origin. The A_0^1 and A_0^2 transitions built upon the 22.6 cm^{-1} origin occur at 21.1 and 32.3 cm^{-1} to the blue of the origin. The existence of a single $\text{MgPc}(\text{CO}_2)_1$ species responsible for the cluster transitions is supported by the ground state configuration calculation shown in Figure 6.11b.

The $\text{MgPc}(\text{CO}_2)_1$ cluster spectrum differs from that of the other MgPc clusters studied in that the magnitude of the hypsochromic shift is smaller for $\text{MgPc}(\text{CO}_2)_1$. This difference can possibly be attributed to the difference in the major mode of interaction between the solute and solvent. In $\text{MgPc}(\text{CO}_2)_1$, the major interaction may be due to the same type of π -cloud interaction as suggested for the $\text{H}_2\text{Pc}(\text{CO}_2)_1$ interaction as the spectral shifts are comparable for the two systems. If the solvent oxygen/solute magnesium interaction were the major contributor, one could expect a larger hypsochromic shift comparable to those found for the $\text{MgPc}(\text{ROH})_1$ systems.

Summary and Conclusions.

FE spectroscopy is used to probe the optical spectra of vdW clusters of H_2Pc and MgPc in the vicinity of the cluster 0_0^0 transitions. A continuous supersonic molecular jet capable of operating at temperatures up to 650°C is employed to generate the ultracold molecular beam. Spectroscopic observables, such as spectral shift and forbidden chromophore vibronic transitions, combined with computer modeling of ground state cluster intermolecular interactions, allow for the elucidation of the nature of the intermolecular potential and qualitative geometry of the H_2Pc and MgPc clusters studied. The conclusions drawn from this work are as follows:

1) The cluster vibronic spectra and theoretical calculations suggest that stable H_2Pc and $MgPc$ clusters have solvents situated over the center of the phthalocyano core. Local minima over peripheral solute rings are either nonexistent or too shallow to accommodate minimum energy bound state geometries;

2) H_2Pc /hydrocarbon clusters are similar to the benzene and N-heterocycle/hydrocarbon clusters previously studied. The spectral shifts in these solute/solvent series are all bathochromic. The magnitudes of the spectral shifts increase with increasing solvent size and polarizability. The qualitative cluster geometries responsible for the observed spectra are similar with respect to solute/solvent orientation is concerned;

3) In both H_2Pc and $MgPc$ clusters, the H_2O , $MeOH$, and $EtOH$ moieties are situated over the Pc core in such a manner that the OH groups are intimately involved in the intermolecular interactions and contribute significantly to the spectral shifts;

4) Hydrogen bonding may be occurring to some extent between H_2Pc and solvent ROH moieties;

5) $MgPc$ clusters display weak vdW interactions between the cluster solute and solvent. Actual complexation in which the solvent donates an electron pair to the solute does not occur;

6) Forbidden low frequency cluster chromophore out-of plane vibronic transitions are induced by clustering in both H_2Pc and $MgPc$ systems. Intensity due to this motion arises from the reduction of the chromophore symmetry in the clusters. The perturbation may be large enough to cause the cluster chromophore geometry to change in an attempt to maximize π -cloud overlap with the solvent; and

7) Excited electronic state splitting occurs in the MgPc clusters due to the reduction in system symmetry upon cluster formation. The degenerate Q band appears to split into its two components, Q_x and Q_y .

REFERENCES

1. D.H. Levy, L. Wharton and R.E. Smalley, "Chemical and Biochemical Applications of Lasers," (Academic Press, New York, 1977) Vol. II.
2. M. Schauer and E.R. Bernstein, *J. Chem. Phys.* 2, 726 (1985).
3. M. Schauer, K.S. Law and E.R. Bernstein, *J. Chem. Phys.* 2, 736 (1985).
4. K.S. Law and E.R. Bernstein, *J. Chem. Phys.* 82, 2856 (1985).
5. K.S. Law, M. Schauer, and E.R. Bernstein, *J. Chem. Phys.* 81, 4871 (1984).
6. E.R. Bernstein, K. Law, and M. Schauer, *J. Chem. Phys.* 80, 207 (1984).
7. M. Schauer, K. Law, and E.R. Bernstein, *J. Chem. Phys.* 81, 49 (1984).
8. J. Wanna and E.R. Bernstein, *J. Chem. Phys.* 84, 927 (1986).
9. J. Wanna, J.A. Menapace, and E.R. Bernstein, *J. Chem. Phys.* 85, 1795 (1986).
10. J.A. Menapace and E.R. Bernstein, *J. Phys. Chem.* 91, 0000 (1987).
11. J.A. Menapace and E.R. Bernstein, *J. Phys. Chem.*, to be published (1987).
12. F.H. Moser and A.H. Thomas, "The Phthalocyanines", (CRC Press Boca Raton, 1983) Vol. I and II.
13. R.O. Loutfy, C.K. Hsiao, and R. Ho, *Can. J. Phys.* 61, 1416 (1983); P.C. Rieke and N.R. Armstrong, *J. Phys. Chem.* 89, 1121 (1985); T.J. Klofta, P.C. Riecke, C.A. Linkous, W.J. Buttner, A. Nanthakumar, T.D. Mewborn and N.R. Armstrong, *J. Electrochem. Soc.*, 132, 2134 (1985); M. Shimura and A. Toyoda, *Jpn. J. App. Phys. Part 1* 23, 1462 (1984).
14. M. Maitrot, G. Guillaud, B. Bondjema, J.-J. Andre, H. Strzelecka, J. Simon and R. Even, *Chem. Phys. Lett.* 133, 59 (1987).

15. H. Wohltjen, W.R. Barger, A.W. Snow and N.L. Jarvis, *IEEE Transactions on Electron Devices*, 32, 1170 (1985); S. Baker, G.G. Roberts and M.C. Petty, *IEEE Proc. Part I, Solid State Electron Devices* 130, 260 (1983); R.L. van Ewyk, A.V. Chadwick and J.D. Wright, *J. Chem. Soc. Far. I*, 76, 2194 (1980).
16. J.R. Darwent, *Chem. Commun.*, 805 (1980); T. Tanno, D. Wohrle, M. Kaneko, and A. Yamada, *Ber. Bunsen. Physik. Chem.* 84, 1032 (1980); G. Melendon and D.S. Miller, *Chem. Commun.*, 533 (1980); I. Okura, M. Takeuchi and N. Kimthuan, *Chem. Lett.* 765 (1980).
17. J.R. Bolton, *Solar Energy*, 20, 181 (1978).
18. J. Barber, "Primary Processes of Photosynthesis", (Elsevier, New York, 1977).
19. D. Dolphin, "The Porphyrins" (Academic Press, New York, 1979), Vols. III, V, and VII; J.E. Falk, "Porphyrins and Metalloporphyrins", (Elsevier, New York, 1964).
20. F.A. Momany, L.M. Carruthers, R.F. McGuire and H.A. Scheraga, *J. Phys. Chem.* 78, 1595 (1974); G. Nemethy, M.S. Pottle, and H.A. Scheraga, *J. Phys. Chem.* 87, 1883 (1983).
21. B.F. Hoskins and S.A. Mason, *Chem. Commun.*, 554 (1969); The phthalocyano skeleton in MgPc is assumed to be the same as H₂Pc in the calculations. The H₂Pc imino hydrogens are replaced by a magnesium atom at the center-most position to model the MgPc structure.
22. T.M. Miller and B. Bederson, *Adv. At. Mol. Phys.* 13, 1 (1977).
23. A. Bondi, *J. Phys. Chem.* 68, 441 (1964).
24. R.A. Scott and H.A. Scheraga, *J. Chem. Phys.* 45, 2091 (1965).
25. A. Henriksson and M. Sundbom, *Theor. Chim. Acta. (Berl.)* 27, 213 (1972); A.M. Schaffer, M. Gouterman, and E.R. Davidson, *Theor. Chim. Acta. (Berl.)* 30, 9 (1973).
26. G. Herzberg, "Molecular Spectra and Molecular Structure III. Electronic Spectra and Electronic Structure of Polyatomic Molecules" (van Nostrand, New York, 1966).
27. R.F. McGuire, F.A. Momany, and H.A. Scheraga, *J. Phys. Chem.* 76, 375 (1972).
28. P. Jonsson, *Acta. Cryst.* B32, 232 (1976).
29. E.B. Wilson Jr., J.C. Decius, and P.C. Cross, "Molecular Vibrations: Theory of Infrared and Raman Vibrational Spectra" (McGraw-Hill Book Co., Inc., 1955).
30. J.A. Menapace, Ph.D. Thesis, Colorado State University, 1987.

31. P.C. Painter and J.L. Koenig, *Spectrochim. Acta.* 33A, 1019 (1977).
32. P.S.H. Fitch, C.A. Haynam, and D.H. Levy, *J. Chem. Phys.* 73, 1064 (1980).
33. H.C. Longuet-Higgins, C.W. Rector and J.R. Platt, *J. Chem. Phys.* 18, 1174 (1950).
34. M.S. Fischer, D.H. Templeton, A. Zalkin and M. Calvin, *J. Am. Chem. Soc.* 93, 2622 (1971).
35. B. Stymne, F.X. Sauvage and G. Wettermark, *Spectrochim. Acta.* 35A, 1195 (1979).

CHAPTER SEVEN

UNPUBLISHED RESULTS

This chapter discusses the results of an out-of-plane normal coordinate analysis on H_2Pc and the results of the 2-color TOPMS experiments on H_2Pc and $MgPc$. These results are presented to establish an up-to-date record of our work in these areas and to outline the basic approaches used in the analyses.

Out-of-Plane Normal Coordinate Analysis on Isolated H_2Pc .

Out-of-plane fundamental and/or overtone vibronic transitions are observed in the vicinity of the O_n^0 transitions in the H_2Pc and $MgPc$ spectra as well as in all the H_2Pc and $MgPc$ solute/solvent van der Waals clusters presented in Chapter 6. Elucidation of the out-of-plane motion in these molecules has proven useful in the understanding of the cluster spectra and in the identification of the number of different clusters of a specific composition observed. In this section, we report the details of the out-of-plane normal coordinate analysis on isolated H_2Pc . This normal coordinate analysis is used to determine the nature of the molecular motion occurring in both the $H_2Pc(MgPc)$ molecule and $H_2Pc(MgPc)$ cluster spectra.

The out-of-plane normal coordinate analysis on H_2Pc is conducted using the PG matrix methods described by Wilson et al.¹ These methods essentially involve expressing the secular equation of $N-3$ coupled harmonic oscillators describing the out-of-plane motion in matrix form

and solving for its $N-3$ non-zero eigenvalues and eigenvectors. To simplify the calculations, the molecular symmetry of H_2Pc is utilized to symmetry (block) factor the potential energy (\underline{F}) and kinetic energy (\underline{G}) matrices to yield "submatrices" each of which describes a particular species of vibrational motion dictated by the vibrational symmetry. The analysis is set up by 1) determining the symmetry of the vibrational motion, 2) selecting a complete set of internal coordinates to describe the motion, 3) obtaining the elements of the \underline{F} and \underline{G} matrices in this coordinate scheme, 4) constructing normalized symmetry coordinates using the complete internal coordinate set as a basis, and 5) symmetry factoring the \underline{F} and \underline{G} matrices using the symmetry coordinates.

The H_2Pc molecule is depicted in Figure 7.1a. This planar molecule contains 18 hydrogen atoms, 32 carbon atoms, and 8 nitrogen atoms, and has 55 out-of-plane normal vibrations that are distributed among the following irreducible representations under the D_{2h} point group:

$$\Gamma_{\text{vib}} = 15 B_{1u} + 13 A_u + 13 B_{2g} + 14 B_{3g}$$

Two types of internal coordinates are used to describe the H_2Pc out-of-plane vibrational motion, bond torsion and out-of-plane bond wagging. The bond torsion coordinate, Figure 7.1b, is defined in the situation when the atoms (2 and 3) at each end of a bond are also bonded to additional atoms (1 and 4) by bonds not colinear with the bond connecting atoms 2 and 3. The terminal bonds taken together with the connecting bond define two planes. Nuclear deformation may thus be expressed by the angle τ defined as the dihedral angle between the two

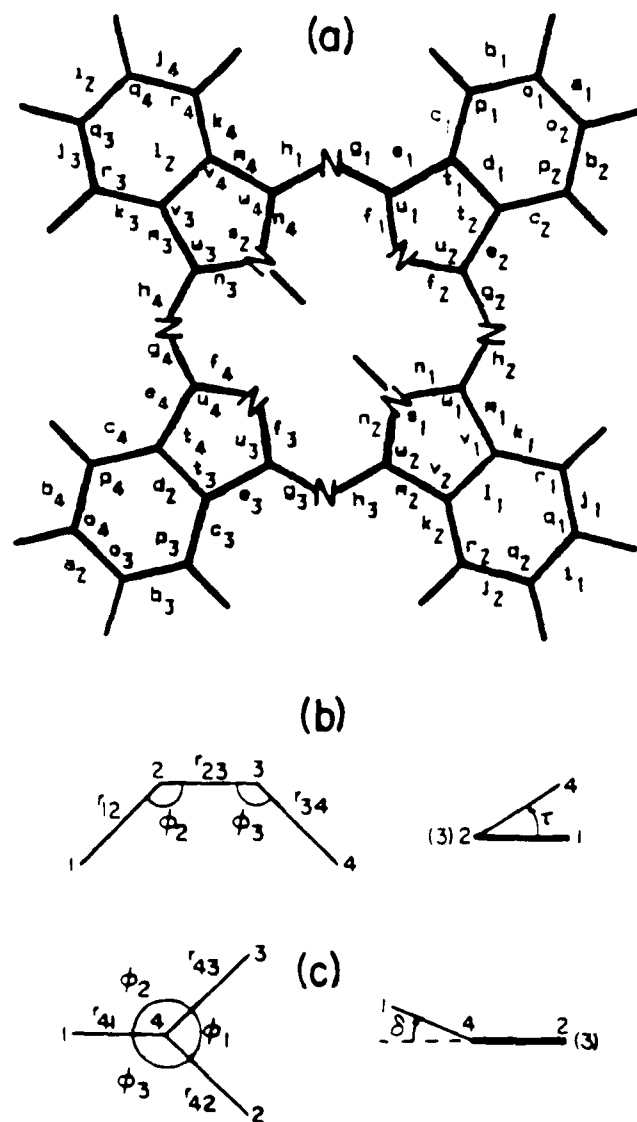


Figure 7.1

a) Out-of-plane internal coordinates used in H_2Pc NCA. Coordinates a-n are bond torsions and coordinates o-w are bond wags. b) Definition of bond torsion τ in terms of bond lengths and bond angles. c) Definition of bond wag γ in terms of bond lengths and bond angles.

planes. The displacement of the atoms in this internal coordinate for atoms 1-4 bonded in sequence is expressed by the following \bar{s} vectors:¹

$$7.1a \quad \bar{s}_{\tau_1} = \frac{-\hat{e}_{12} \times \hat{e}_{23}}{r_{12} \sin^2 \phi_2}$$

$$7.1b \quad \bar{s}_{\tau_2} = \frac{r_{23} - r_{12} \cos \phi_2}{r_{23} r_{12} \sin \phi_2} \frac{\hat{e}_{12} \times \hat{e}_{23}}{\sin \phi_2} - \frac{\cos \phi_3}{r_{23} \sin \phi_3} \frac{\hat{e}_{13} \times \hat{e}_{32}}{\sin \phi_3}$$

$$7.1c \quad \bar{s}_{\tau_3} = [(14)(23)] \bar{s}_{\tau_2}$$

$$7.1d \quad \bar{s}_{\tau_4} = [(14)(23)] \bar{s}_{\tau_1}$$

for which the terms in square brackets are permutation operators. Equations 7.1c and 7.1d thereby state that the \bar{s}_{τ_3} and \bar{s}_{τ_4} vectors can be obtained by permutation of atoms 1 and 4, and 2 and 3 in the expressions for \bar{s}_{τ_1} and \bar{s}_{τ_2} .

The out-of-plane wagging coordinate, Figure 7.1c, is defined at an atom for which three coplanar bonds are coincident. The deformation angle γ is formed by atoms 2, 3, and 4. The s vectors describing the atomic displacements in this internal coordinate are:¹

$$7.2a \quad \bar{s}_{\gamma_2} = \frac{1}{r_{41}}$$

$$7.2b \quad \bar{s}_{\gamma_2} = \frac{\sin \phi_2}{r_{42} \sin \phi_1}$$

$$7-2c \quad s_{\gamma_3} = \frac{\sin \phi_2}{r_{13} \sin \phi_1}$$

$$7-2d \quad s_{\gamma_4} = \frac{1}{r_{11}} \frac{\sin \phi_2}{r_{12} \sin \phi_1} \frac{\sin \phi_1}{r_{13} \sin \phi_1}$$

In order to obtain a kinematically complete set of internal vibrational coordinates, bond torsions are chosen at each non-terminal bond, and out of plane wagging coordinates are chosen at each atom for which three coplanar bonds meet.² This prescription yields 18 bond torsion coordinates and 11 out of plane wagging coordinates which completely describe the out of plane motion in the H_2P_2 moiety. Twenty seven redundancies are distributed among the vibrational symmetries $B_{1g}(11)$, $A_g(9)$, $B_{2g}(7)$, and $B_{3g}(7)$ in this internal coordinate scheme. These redundancies are carried through the calculations so that symmetry coordinates can be used to block factor the secular equation into the four symmetry species sets.

The 18 bond torsion coordinates are located in 11 symmetry equivalent sets designated as γ_i in Figure 7-1a. The atoms in each coordinate are numbered using a clockwise numbering scheme to define vectors with atom 1 moving in the z direction and atom 2 moving in the xz direction (Figure 7-1b). Positive γ_i is the measured angle in the counterclockwise direction when looking down the bond between atoms 2 and 3 with atom 2 nearer to the observer. When two or more angles in the molecule contain the bond torsion coordinate, the coordinate is oriented so that its terminal atoms point towards the H_2P_2 center and its terminal bonds are situated in a syn conformation.

The 34 out-of-plane wagging coordinates are located in 9 symmetry equivalent sets designated as o – w in Figure 7.1a. The atoms in each coordinate are numbered using a counterclockwise convention (Figure 7.1c). Positive displacement in γ is measured by out-of-plane motion of atom 1 in the $-z$ direction. Coordinates containing hydrogen (o–s) are numbered so that the hydrogen atom is designated as atom 1. Coordinates t and v are oriented such that atom 1 corresponds to the benzene C–H carbon atom. Coordinates u and w are numbered so that the bridge nitrogen atom is designated as atom 1.

The elements of the G matrix are obtained using the internal coordinate s vectors (Equations 7.1 and 7.2) and

$$G_{ij} = \sum_a \frac{1}{m_a} (\alpha_i^a \alpha_j^a + \beta_i^a \beta_j^a) \quad (7.1.3)$$

for which $\frac{1}{m_a}$ is the reciprocal of the mass of atom a . The non-zero terms in the summation are those corresponding to atoms common to the two internal coordinates i and j in question. The geometric parameters used to determine the internal coordinate s vectors are based upon the results of a neutron diffraction analysis of R_2Pc .¹ These parameters are slightly modified, however, to reduce the total number of different G matrix elements that need to be calculated. In this approximation all the porphole subunits comprising R_2Pc are assumed to contain identical interatomic distances and bond angles. The interatomic distances and bond angles are thus taken as average values of the parameters determined from the crystallographic data. The geometric parameters used in the calculations are presented in Figure 7.2. The G matrix elements calculated from Equations 7.1.3 are given in Table 7.1.

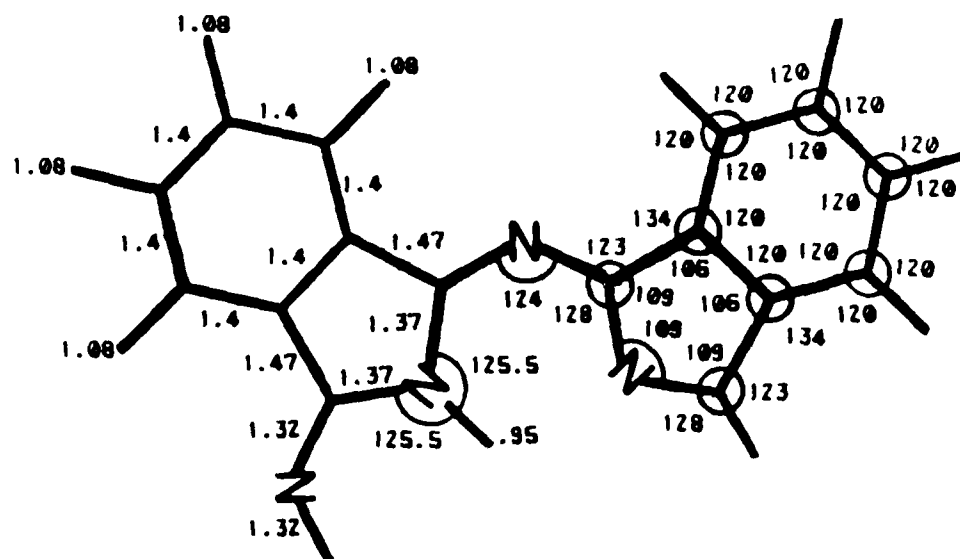


Figure 7.2

Geometric parameters used in H₂Pc NCA. Bond lengths are expressed in angstroms and bond angles are in degrees. The parameters are averaged to D_{4h} symmetry to simplify the calculations.

TABLE 7.1

Kinetic Energy (G) Matrix Elements for H₂Pc Out-of-Plane Motion ^a

Matrix Element (A-g/mol) ⁻¹	Matrix Element (A-g/mol) ⁻¹	Matrix Element (A-g/mol) ⁻¹	
G(a1a1)	.56689	G(c1c1)	.56689
G(a1b1)	-.45351	G(c1c2)	.22676
G(a1b2)	-.45351	G(c1d1)	-.45351
G(a1c1)	.22676	G(c1e1)	-.21223
G(a1c2)	.22676	G(c1e2)	-.18273
G(a1d1)	-.11338	G(c1f1)	.09890
G(a1o1)	.47094	G(c1f2)	.04945
G(a1o2)	-.47094	G(c1o1)	.26002
G(a1p1)	-.26002	G(c1o2)	-.04909
G(a1p2)	.26002	G(c1p1)	-.47094
G(a1t1)	.04909	G(c1p2)	.04909
G(a1t2)	-.04909	G(c1t1)	.39084
		G(c1t2)	-.20143
		G(c1u1)	-.07794
		G(c1u2)	.03897
G(d1d1)	.56689	G(e1e1)	.32338
G(d1e1)	.26331	G(e1e2)	.10262
G(d1e2)	.26331	G(e1f1)	-.26292
G(d1f1)	-.09890	G(e1f2)	.10302
G(d1f2)	-.09890	G(e1g1)	-.25421
G(d1o1)	-.04909	G(e1g2)	.05108
G(d1o2)	.04909	G(e1h1)	.09148
G(d1p1)	.26002	G(e1p1)	.06978
G(d1p2)	-.26002	G(e1p2)	-.04423
G(d1t1)	-.37849	G(e1t1)	-.27633
G(d1t2)	.37849	G(e1t2)	.16750
G(d1u1)	.07794	G(e1u1)	.28850
G(d1u2)	-.07794	G(e1u2)	.00059
G(g1g1)	.76450	G(h1h1)	.76450
G(g1g2)	-.06129	G(h1h4)	-.06129
G(g1h1)	-.59954	G(h1h3)	.05108
G(g1h4)	.09148	G(h1h4)	-.25421
G(g1n3)	.05879	G(h1n3)	-.21488
G(g1n4)	-.09307	G(h1n4)	.29100
G(g1s2)	.04786	G(h1s2)	-.25909
G(g1t1)	.10364	G(h1t1)	-.04667
G(g1u1)	-.48542	G(h1u1)	.25929
G(g1u2)	-.04284	G(h1v4)	-.10364
G(g1v4)	.04667	G(h1w3)	.04284
G(g1w4)	-.25929	G(h1w4)	.48542
		G(i1i1)	.56689
		G(i1j1)	-.45351
		G(i1j2)	.45351
		G(i1k1)	.22676
		G(i1k2)	.22676
		G(i1l1)	-.11338
		G(i1q1)	.47094
		G(i1q2)	.47094
		G(i1r1)	-.26002
		G(i1r2)	.26002
		G(i1v1)	.04909
		G(i1v2)	.04909

TABLE 7.1 (Continued)

Matrix Element (A-g/mol) ⁻¹	Matrix Element (A-g/mol) ⁻¹	Matrix Element (A-g/mol) ⁻¹	
G(j1j1)	.56689	G(1111)	.56689
G(j1j2)	.22676	G(11m1)	.26331
G(j1k1)	-.45351	G(11m2)	.26331
G(j1k2)	-.11338	G(11n1)	-.09890
G(j1m1)	.08058	G(11n2)	-.09890
G(j1m2)	.05107	G(11q1)	-.04909
G(j1n1)	-.04945	G(11q2)	.04909
G(j1q1)	-.47094	G(11r1)	.26002
G(j1q2)	.26002	G(11r1)	-.26002
G(j1r1)	.47094	G(11v1)	-.37849
G(j1r2)	-.04909	G(11v2)	.37849
G(j1v1)	-.22615	G(11w1)	.07794
G(j1v2)	.03674	G(11w2)	-.07794
G(j1w1)	.03897		
G(m1m1)	.32338	G(n1n1)	.33332
G(m1m2)	.10262	G(n1n2)	-.27330
G(m1n1)	-.26292	G(n1r1)	-.04283
G(m1n2)	.10302	G(n1s1)	.31472
G(m1r1)	.06978	G(n1v1)	.17404
G(m1r2)	-.04423	G(n1v2)	.00738
G(m1s1)	-.19027	G(n1w1)	-.29377
G(m1v1)	-.27663	G(n1w2)	-.18581
G(m1v2)	.16750		
G(m1w1)	.28650		
G(m1w2)	.00059		
G(p1p1)	1.40434	G(q1q1)	1.40434
G(p1t1)	-.25096	G(q1q2)	-.28030
G(p1t2)	.03182	G(q1r1)	-.28030
G(p1u1)	.03375	G(q1r2)	.04252
		G(q1v1)	.04252
G(s1s1)	1.55488	G(t1t1)	.38645
G(s1v1)	.03210	G(t1t2)	.16585
G(s1s2)	.03210	G(t1u1)	.18867
G(s1w1)	.21009	G(t1u2)	.02525
G(s1w2)	-.21009		
G(v1v1)	.38645	G(w1w1)	.42178
G(v1v2)	.16585	G(w1w2)	.02994
G(v1w1)	.18867		
G(v1w2)	.02525		

a) Only those elements necessary to generate the G matrix in terms of symmetry coordinates are shown

The elements of the \underline{F} matrix in terms of the bond torsion and out-of-plane wagging coordinates, Table 7.2, are simply expressed as valence force constants $F_{tt'}$, for which t and t' correspond to the two internal coordinates in question. For the purpose of this calculation, the \underline{F} matrix elements are taken as the diagonal force constants describing the out of plane motion of benzene.⁴ In this approximation, all H_2Pc bond torsion force constants are assumed to be the same as those corresponding to the $C-C$ torsions in benzene. The out of plane wagging force constants are assumed to be the same as those corresponding to benzene out of plane $C-H$ wags. All off diagonal force constants are taken as zero. This force field scheme, even though not quantitatively accurate, will allow for the elucidation of the general nature of the out of plane motion in H_2Pc , as it will yield characteristic frequencies for the particular molecular segments participating in the various vibrational motions. No attempt is made to refine the force field used in the calculations, since the experimental information on the out of plane vibrations in H_2Pc is limited to those possessing C_2 symmetry, and are not used^{5,6} in the frequency calculations. The number of force constants that would be determined is equal to the number of experimental frequencies available.

The constant problem has to be solved by the use of the \underline{G} matrix, which is factored into the \underline{B} and \underline{D} matrices, $\underline{G} = \underline{B}\underline{D}\underline{B}^T$, where \underline{B} is the product of the \underline{C} matrix and the $\underline{M}^{-1/2}$ matrix, $\underline{B} = \underline{C}\underline{M}^{-1/2}$, and \underline{D} is the inverse of the product of the \underline{C} matrix and the $\underline{M}^{-1/2}$ matrix, $\underline{D} = (\underline{C}\underline{M}^{-1/2})^{-1}$. The \underline{B} matrix is a $3N \times 3N$ matrix, where N is the number of atoms in the molecule. The \underline{D} matrix is a $3N \times 3N$ matrix, where N is the number of atoms in the molecule. The \underline{C} matrix is a $3N \times 3N$ matrix, where N is the number of atoms in the molecule. The $\underline{M}^{-1/2}$ matrix is a $3N \times 3N$ matrix, where N is the number of atoms in the molecule.

The \underline{B} matrix is a $3N \times 3N$ matrix, where N is the number of atoms in the molecule.

The \underline{D} matrix is a $3N \times 3N$ matrix, where N is the number of atoms in the molecule.

TABLE 7.2

Potential Energy (\underline{F}) Matrix Elements for H_2Pc Out-of-Plane Motion ^a

Matrix Element (mdyn-A/rad ²)	Matrix Element (mdyn-A/rad ²)	Matrix Element (mdyn-A/rad ²)
P(a1a1) .1190	P(b1b1) .1190	P(c1c1) .1190
P(d1d1) .1190	P(e1e1) .1190	P(f1f1) .1190
P(g1g1) .1190	P(h1h1) .1190	P(i1i1) .1190
P(j1j1) .1190	P(k1k1) .1190	P(l1l1) .1190
P(m1m1) .1190	P(n1n1) .1190	P(o1o1) .3237
P(p1p1) .3237	P(q1q1) .3237	P(r1r1) .3237
P(s1s1) .3237	P(t1t1) .3237	P(u1u1) .3237
P(v1v1) .3237	P(w1w1) .3237	

a) Only those elements necessary to generate the \underline{F} matrix in terms of symmetry coordinates are shown

TABLE 7.3

Normalized Symmetry Coordinates for $H_2^{16}O$ in Terms of Bond Torsion and Out-of-Plane Wagging Coordinates.

B_{1u} :	$B=1/2(b_1-b_2+b_3-b_4)$	B_{2g} :	$B=1/2(b_1-b_2-b_3+b_4)$
	$C=1/2(c_1-c_2+c_3-c_4)$		$C=1/2(c_1-c_2-c_3+c_4)$
	$E=1/2(e_1-e_2+e_3-e_4)$		$E=1/2(e_1-e_2-e_3+e_4)$
	$F=1/2(f_1-f_2+f_3-f_4)$		$F=1/2(f_1-f_2-f_3+f_4)$
	$G=1/2(g_1-g_2+g_3-g_4)$		$G=1/2(g_1-g_2-g_3+g_4)$
	$H=1/2(h_1-h_2+h_3-h_4)$		$H=1/2(h_1-h_2-h_3+h_4)$
	$J=1/2(j_1-j_2+j_3-j_4)$		$I=1/\sqrt{2}(i_1-i_2)$
	$K=1/2(k_1-k_2+k_3-k_4)$		$J=1/2(j_1+j_2-j_3-j_4)$
	$M=1/2(m_1-m_2+m_3-m_4)$		$K=1/2(k_1+k_2-k_3-k_4)$
	$N=1/2(n_1-n_2+n_3-n_4)$		$L=1/\sqrt{2}(l_1-l_2)$
	$O=1/2(o_1+o_2+o_3+o_4)$		$M=1/2(m_1+m_2-m_3-m_4)$
	$P=1/2(p_1+p_2+p_3+p_4)$		$N=1/2(n_1+n_2-n_3-n_4)$
	$Q=1/2(q_1+q_2+q_3+q_4)$		$O=1/2(o_1+o_2+o_3+o_4)$
	$R=1/2(r_1+r_2+r_3+r_4)$		$P=1/2(p_1+p_2-p_3-p_4)$
	$S=1/\sqrt{2}(s_1+s_2)$		$Q=1/2(q_1-q_2-q_3+q_4)$
	$T=1/2(t_1+t_2+t_3+t_4)$		$R=1/2(r_1-r_2-r_3+r_4)$
	$U=1/2(u_1+u_2+u_3+u_4)$		$T=1/2(t_1+t_2-t_3-t_4)$
	$V=1/2(v_1+v_2+v_3+v_4)$		$U=1/2(u_1+u_2-u_3-u_4)$
	$W=1/2(w_1+w_2+w_3+w_4)$		$V=1/2(v_1-v_2-v_3+v_4)$
			$W=1/2(w_1-w_2-w_3+w_4)$
A_u :	$A=1/\sqrt{2}(a_1+a_2)$	B_{3g} :	$A=1/\sqrt{2}(a_1-a_2)$
	$B=1/2(b_1+b_2+b_3+b_4)$		$B=1/2(b_1+b_2-b_3-b_4)$
	$C=1/2(c_1+c_2+c_3+c_4)$		$C=1/2(c_1+c_2+c_3+c_4)$
	$D=1/2(d_1+d_2)$		$D=1/\sqrt{2}(d_1-d_2)$
	$E=1/2(e_1+e_2+e_3+e_4)$		$E=1/2(e_1+e_2-e_3-e_4)$
	$F=1/2(f_1+f_2+f_3+f_4)$		$F=1/2(f_1+f_2-f_3-f_4)$
	$G=1/2(g_1+g_2+g_3+g_4)$		$G=1/2(g_1+g_2-g_3-g_4)$
	$H=1/2(h_1+h_2+h_3+h_4)$		$H=1/2(h_1+h_2-h_3-h_4)$
	$I=1/\sqrt{2}(i_1+i_2)$		$J=1/2(j_1-j_2-j_3+j_4)$
	$J=1/2(j_1+j_2+j_3+j_4)$		$K=1/2(k_1-k_2-k_3+k_4)$
	$K=1/2(k_1+k_2+k_3+k_4)$		$M=1/2(m_1-m_2-m_3+m_4)$
	$L=1/\sqrt{2}(l_1+l_2)$		$N=1/2(n_1-n_2-n_3+n_4)$
	$M=1/2(m_1+m_2+m_3+m_4)$		$O=1/2(o_1+o_2+o_3+o_4)$
	$N=1/2(n_1+n_2+n_3+n_4)$		$P=1/2(p_1-p_2-p_3+p_4)$
	$O=1/2(o_1+o_2+o_3+o_4)$		$Q=1/2(q_1+q_2+q_3+q_4)$
	$P=1/2(p_1+p_2+p_3+p_4)$		$R=1/2(r_1+r_2+r_3+r_4)$
	$Q=1/2(q_1+q_2+q_3+q_4)$		$S=1/\sqrt{2}(s_1+s_2)$
	$R=1/2(r_1+r_2+r_3+r_4)$		$T=1/2(t_1+t_2+t_3+t_4)$
	$T=1/2(t_1+t_2+t_3+t_4)$		$U=1/2(u_1+u_2+u_3+u_4)$
	$U=1/2(u_1+u_2+u_3+u_4)$		$V=1/2(v_1+v_2+v_3+v_4)$
	$V=1/2(v_1+v_2+v_3+v_4)$		$W=1/2(w_1+w_2+w_3+w_4)$
	$W=1/2(w_1+w_2+w_3+w_4)$		

TABLE 7.4

Observed and calculated frequencies and tentative assignments
of the out-of-plane vibrations in H₂Pc.

Mode	Calc (cm ⁻¹)	Obsd ^a (cm ⁻¹)	Mode	Calc (cm ⁻¹)	Obsd ^a (cm ⁻¹)
B _{1u} 1	14.8	15.6	B _{2g} 29	38.6	42.7/50.3
2	24.5	25.9	30	72.1	88/101.6
3	84.0	81.9/90	31	154.5	
4	145.3	127	32	185.2	
5	158.9	140	33	317.2	
6	230.5	282	34	343.1	
7	333.7	342	35	510.1	
8	362.3	342	36	686.8	
9	608.3		37	737.4	
10	735.3	725	38	791.1	
11	739.6	725	39	889.0	
12	777.5	775	40	968.1	
13	962.7	945	41	1146.3	
14	967.8	945			
15	1014.4				
A _u 16	33.1	35.7	B _{3g} 42	38.2	42.7/50.3
17	71.7	70.9	43	71.4	88/101.6
18	136.4		44	147.2	
19	310.4		45	183.3	
20	321.0		46	315.8	
21	427.6		47	339.5	
22	593.2		48	498.1	
23	690.5		49	648.3	
24	747.9		50	728.4	
25	884.5		51	740.7	
26	891.8		52	887.2	
27	1146.1		53	962.7	
28	1146.6		54	1013.2	
			55	1046.3	

a) From Chapter 6 and References 5-7.

frequencies obtained from the vibronic spectrum discussed in Chapter 6 and from infrared spectra.⁵⁻⁷ The comparison between the experimental vibronic transitions and the calculated mode frequencies is made on the premise that the ground and excited state potential surfaces are nearly superimposable. This notion is demonstrated experimentally by FE and DE spectra of H_2Pc for which the vibrational energies in the S_1 and S_0 states differ by at most 5-10%.⁸ Overall, the calculated frequencies compare quite well with those observed given the qualitative nature of the force field used in the analysis. Based upon this calculation, we propose tentative out-of-plane mode assignments for the experimentally observed out-of-plane modes.

The eigenvectors corresponding to the calculated vibrations are listed in Table 7.5. From the eigenvector normal mode forms, the out-of-plane motion can be qualitatively categorized into 1) macrocycle ring deformation, 2) isoindole ring deformation, and 3) C(N)-H out-of-plane wagging motion types.

The 0-100 cm^{-1} region is dominated by macrocycle ring deformation for which large amplitude out-of-plane motion of the four isoindole subunits occurs. This motion is located principally at the pyrrole α carbon/bridge nitrogen bonds (internal coordinates g and h). Modes 1, 2, 29, and 42 possess potential energy distributions (PED's) ranging from 40-70% in these coordinates.⁹ From the H_2Pc vibronic spectrum presented in Chapter 6, these modes are observed as symmetric overtones at $312(1_0^1)$, $518(2_0^2)$, $854(100_0^6)$ (29_0^2 or 42_0^2), and 1006 cm^{-1} (185.4 cm^{-1}) (42_0^2 or 29_0^2) which places their forbidden fundamental transitions at 156 , 259 , $427(50_0^3)$, and 503 cm^{-1} (42_0^2) respectively. Mode 3 is also observed in the far infrared at about

TABLE 7.5

Out-of-Plane Eigenvector Normal Modes Calculated for H₂Pc.

Mode	Eigenvector in Terms of Symmetry Coordinates ^a						
B _{1u} 1	-.1925	E+.3323	F-.5829	G-.5838	H+.1920	M-.3315	N
2	+.1445	E-.2212	F-.4510	G+.4565	H+.1508	M-.2315	N
	-.1601	T-.4253	U-.1593	V-.4301	W		
3	-.1407	B+.1407	C+.2406	E-.3954	F-.2622	G-.2505	H
	+.1249	J-.1249	K-.2630	M+.4325	N-.1782	T-.3704	U
	+.1546	V+.3658	W				
4	+.2500	B-.2500	C+.1753	E-.2864	F+.4221	J-.4221	K
	+.2154	M-.3503	N+.2378	T+.3941	V		
5	-.4540	B+.4540	C-.1235	E+.1986	F+.3185	G+.2819	H
	+.2686	J-.2686	K-.1022	N-.3632	T+.2143	V	
6	-.2158	B+.2158	C+.2602	E-.4307	F+.3443	G-.3574	H
	-.2686	J+.2686	K+.2611	M-.4326	N		
7	+.4007	B-.4007	C+.1469	F+.1347	G+.2009	H-.4019	J
	+.4019	K-.1001	N-.1467	P+.1469	R-.3105	T+.3080	V
8	+.3543	B-.3543	C-.1204	F+.3123	G-.3064	H+.3398	J
	-.3398	K-.1220	N-.1550	P-.1486	R-.3523	T-.3374	V
9	-.2060	E+.3418	F+.3697	H+.2649	M-.4400	N-.1226	R
	+.3238	S+.1214	T-.2491	U-.1993	V+.4342	W	
10	+.1423	F+.2272	G-.1518	H+.7619	O+.4266	P+.2763	Q
	+.1549	R-.1440	U				
11	+.2943	O+.1455	P-.8353	Q-.4128	R		
12	-.2613	E+.4334	F+.5511	G-.3320	H-.2233	O-.2469	S
	+.1401	T-.4163	U-.1263	W			
13	+.2919	J-.2919	K+.1121	P-.4025	Q+.7437	R+.2462	S
	1314	V					
14	+.3040	B-.3040	C-.4032	O+.7618	P-.1213	R-.1672	S
15	+.1864	G-.3675	H-.2153	M+.3567	N-.1856	R-.7004	
	+.1115	V-.2899	W				

TABLE 7.5 (Continued)

Mode	Eigenvector In Terms of Symmetry Coordinates ^a							
A _u 16	+.1503	C-.1656	D+.3721	E-.1410	F-.3954	G+.3954	H	
	-.1503	K+.1656	L-.3721	M+.1410	N-.3513	U+.3513	W	
17	+.1385	A-.2577	C+.2891	D-.4917	E+.1849	F-.1825	G	
	-.1825	H+.1385	I-.2577	K+.2891	L-.4917	M+.1849	N	
	+.1189	U+.1189	W					
18	+.1640	A-.2530	C+.2932	D-.3954	E+.1482	F-.3436	G	
	+.3436	H-.1640	I+.2530	K-.2932	L+.3954	M-.1482	N	
	-.1435	U+.1435	W					
19	-.4671	A+.4560	B-.1114	D-.4671	I+.4560	J-.1114	L	
	+.1435	O+.1435	Q+.1147	U+.1147	W			
20	+ 4538	A- 4675	B+.1189	C+ 1184	E- 4538	I+ 4674	J	
	-.1189	K- 1184	M- 1480	O+ 1480	Q			
21	1059	A+ 2007	B- 3027	C+ 2501	D- 1274	E+ 2660	G	
	+ 2660	H- 1059	I+ 2007	J- 3027	K+ 2501	L- 1274	M	
	1197	P- 1197	R 4232	U- 4232	W			
22	2790	C+ 2637	D+ 1224	E+ 4457	G 4457	H+ 2790	K	
	2637	L 1224	M- 2217	P+ 2217	R 2228	T 1726	U	
	+ 2228	V+ 1726	W					
23	2202	C+ 2154	D+ 3039	F 1141	F 2202	K+ 2154	L	
	+ 3039	M 1141	N 3936	P 3936	R 2859	T+ 2103	U	
	2859	V+ 2103	W					
24	2115	E+ 4645	G 4645	H+ 2115	M- 1335	N 1217	U	
	1335	Q 3217	R+ 1434	T 2901	U 1434	V+ 2901	W	
25	+ 2260	C- 2463	D- 1918	E+ 2260	K- 1189	L- 1274	M	
	4200	O 2953	P 4200	Q 2953	R+ 2179	T 1726	U	
	+ 2179	V 1726	W					
26	2359	C- 2072	D+ 2072	E- 1993	F 1993	G+ 2359	H	
	2072	I 2072	M+ 1993	N 1993	O 1993	Q 1993	U	
	2494	T+ 1472	U 1472	V 1472	W			
27	2314	A 2922	B+ 1420	C- 1420	D+ 2314	E- 1420	F	
	1420	K 1420	L- 1420	M 1420	N 1420	O 1420	U	
	1343	T+ 1343	U					
28	2115	A 2115	B+ 2115	C- 2115	D+ 2115	E- 2115	F	
	1335	K+ 1335	L- 1335	M 1335	N 1335	O 1335	U	
	1472	T+ 1472	U					

TABLE 7.5 (Continued)

Mode		Eigenvector in Terms of Symmetry Coordinates ^a						
B _{2g}	29	+.1179 -.2328	B-.1179 M+.2209	C+.7966 T+.3514	G+.2358 U+.1308	H-.1072 W	K+.1191	L
	30	+.1944 +.2386	E-.3189 N-.2474	F+.1762 U+.1803	I-.3289 W	K+.3688	L-.6348	M
	31	+.4865 +.4174	B-.4865 T-.1334	C+.2356 U	E-.3831	F-.1991	G-.2474	H
	32	-.2591 -.1695 +.2327	B+.2591 I+.2071 W	C+.2861 K-.2518	E-.4743 L+.2789	F+.3997 M-.1045	G-.3046 N-.1103	H T
	33	+.1522 -.1268	B-.1522 K-.1341	C+.1101 M+.1997	F+.1459 Q+.1220	H-.6255 W	I+.6320	J
	34	+.5224 -.2029	B-.5224 P-.4420	C+.2596 T+.1149	G+.1907 W	I-.2203	J+.1214	K
	35	+.1951 +.3102	E-.3237 L-.1786	F+.1469 R-.1474	G-.5439 T+.1811	H+.1498 U-.1829	J-.3424 V-.4103	K W
	36	+.1769 +.1406	E-.2934 N+.1104	F-.1897 Q+.4846	G+.2833 R+.2496	K-.2768 U+.3592	L-.3744 V-.2422	M W
	37	+.1404	G-.1394	H+.8457	O+.4460	P+.1139	R	
	38	+.2411 2127	E-.3999 R-.1237	F-.5561 T+.3913	G+.4052 U+.1936	H+.1672 W	O-.1267	Q
39	1437 1061	G+.1652 N+.5692	H+.1397 Q+.3794	I+.3067 R+.3486	K+.3357 V+.1822	L+.2825 W	M	
40	+.3071	B+.3071	C+.4067	O+.7691	P+.1705	T		
41	+.1168 +.4584	E+.4128 R+.1910	F+.3424 V	K+.2172	I+.1147	M+.5471		
B _{2g}	42	+.1168 +.4584	E+.4128 R+.1910	F+.3424 V	K+.2172	I+.1147	M+.5471	
	43	+.1168 +.4584	E+.4128 R+.1910	F+.3424 V	K+.2172	I+.1147	M+.5471	
	44	+.1168 +.4584	E+.4128 R+.1910	F+.3424 V	K+.2172	I+.1147	M+.5471	

TABLE 7.5 (Continued)

Mode	Eigenvector in Terms of Symmetry Coordinates ^a							
45	+.1615	A-.2996	C+.2421	D-.2706	E+.1013	F-.2789	G-.2199	
	+.4128	H-.3138	J+.3138	K+.2646	M-.4396	N-.2199		
	-.1479	V						
46	+.6131	A-.6148	B+.1105	C+.1002	D+.1202	E+.1396	G-.1240	
	+.1985	J-.1985	K+.1148	N-.1941	O-.1218	T-.1240	V	
47	+.2509	A-.2843	B+.1431	C+.1198	E-.2690	H-.4985	J	
	+.4985	K+.1890	R+.1240	U+.4040	V			
48	-.1501	B+.3268	C-.2935	D-.4908	G+.2145	M-.3584	N	
	+.1623	P+.1237	S+.1631	T+.4080	U-.2014	V+.2426	W	
49	+.2737	C-.2640	D-.2379	E-.2581	G+.4123	H-.1837	M	
	+.3052	N+.3212	P+.1007	R-.3008	S+.2819	T+.1333	V	
	-.3401							
50	+.1284	C-.1271	D-.2979	E+.1118	F+.4455	G-.3629	H	
	-.1031	N+.1451	O+.4155	P-.2352	Q-.1579	R+.2259	S	
	+.2291	T-.3401	U+.1628	W				
51	+.1861	G-.1684	H+.1407	P+.8176	Q+.3895	R+.1560	S	
	-.1236	U-.1071	V+.1140	W				
52	-.1411	A+.3139	C-.3430	D-.2800	E+.1051	F+.1211	G	
	-.5828	O-.3970	P+.3518	T-.1677	U			
53	-.2953	J+.2953	K+.4070	Q-.7522	R-.2439	S+.1332	V	
54	-.1645	G+.3629	H-.2170	M+.3595	N-.1909	R+.7091	S	
	+.1130	V-.2908	W					
55	+.3167	A-.4127	B+.3424	C-.2172	D-.1148	E+.5470	O	
	-.4583	P+.1911	T					

a) Symmetry coordinates contributing less than 1% to the potential energy distribution are not included.

cm^{-1} . The eigenvector forms for modes 3, 16, 17, 19, and 13 are less characteristic in the g and h internal coordinates as they are dominated by pyrrole α -carbon/bridge nitrogen bond torsions (g and h) coupled with pyrrole skeleton torsion coordinates (e, f, and m). These modes occur in the infrared spectrum at $1037(35^2)$, $714(19^2)$, $1417(17^2)$, $170(20^2)$, $113(9^2)$ or 1375 , and $299(1^2)$, $176(1^2)$, $147(1^2)$ or 195^2 , which place their forbidden fundamental transitions at 819 , 357 , 709 , $281(1.6)$, and $191(1^2)$, $188(1^2)$, respectively.

Isoindole ring deformation occurs mainly in the region between 100 and 700 cm^{-1} . The dominant out of plane motions in this region arise from the coupled deformation of the benzene and pyrrole moieties as can be seen by the large PED contributions from the a, f, and n coordinates in Table 7.5. T. Kobayshi⁵ has assigned far infrared bands at 127 , 140 , 282 , and 342 cm^{-1} to isoindole ring deformations on the basis of comparative analyses of free base and metallophthalocyanines. These bands correspond to the calculated modes 4(145.3 cm^{-1}), 5(158.9 cm^{-1}), 6(230.5 cm^{-1}), 7(333.7 cm^{-1}), and 8(362.3 cm^{-1}) respectively. The far infrared studies also show that the band observed at 282 cm^{-1} contains contributions from both the isoindole ring and bridge nitrogen motions. The eigenvector form for mode 6 corroborates this assignment as it possesses a PED of about 25% in the pyrrole α -carbon/bridge nitrogen torsion coordinates (g and h).

In the region between 700 – 1100 cm^{-1} , C(N)-H out of plane wagging dominates. From the eigenvector normal mode forms, the C-H vibrations are, for the most part, uncoupled from the H_2Pc ring modes as the out-of-plane wagging coordinates o-r account for between 71 and 97% of the PED's responsible for the motions. The infrared spectrum of H_2Pc

possesses bands at 725, 775, and 945 cm^{-1} which can be attributed to B_{1u} type out-of-plane C-H wagging.⁷ The normal coordinate analysis reveals C-H wagging mode frequencies in this vicinity at 735.3 (mode 10), 739.6 (mode 11), 777.5 (mode 12), 962 (mode 13), and 967.8 cm^{-1} (mode 14). The only large discrepancy between the calculated frequencies and the experimental data involves out-of-plane (B_{1u}) wagging motion of the imino hydrogens. This mode is calculated to occur at 1014.4 cm^{-1} (mode 15) with a PED of 49% in the s internal coordinate, but it has been assigned to a band observed in the vicinity of 700 cm^{-1} ,^{6,7} based upon isotopic substitution. Intramolecular hydrogen bonding between the imino hydrogens and adjacent core nitrogen atoms may account for the large difference between the calculated and observed/assigned modes. However, mode 9 calculated at 608.3 cm^{-1} is near the assigned N-H out-of plane wagging frequency and exhibits an 11% PED contribution from the N-H wagging coordinate, s, and 20% from the pyrrole torsion coordinate, m. Performing the normal coordinate analysis using deuterons at the pyrrole nitrogens results in mode 9 red shifting to 536.3 cm^{-1} ($\nu\text{H}/\nu\text{D} = 1.13$) and mode 15 red shifting to 916 cm^{-1} ($\nu\text{H}/\nu\text{D} = 1.11$). These results suggest that the mode responsible for the band observed at 711 cm^{-1} could be due to highly coupled motion between the N-H group and the pyrrole ring and not to characteristic N-H motion which should occur in the 900-1000 cm^{-1} region.

SUMMARY AND CONCLUSIONS:

An out-of-plane normal coordinate analysis is conducted on H_2Pc to characterize the large amplitude low frequency motion present in both the isolated H_2Pc and MgPc moieties as well as their respective vdW clusters with small solvents (see Chapter 6). The out-of-plane normal

coordinate analysis is conducted using the FG matrix method. The nuclear motion is modeled by a set of 82 internal coordinates; 48 C-C(N) bond torsions, 18 C(N)-H bond wags, and 16 C-C(N) bond wags. The force field used in the model consists of the diagonal force constants describing the out-of-plane motion in benzene. The resulting eigenvalues and eigenvector normal modes are compared with experiment and tentative assignments are proposed based upon the calculations. In the comparison, observed vibronic symmetric overtone transitions and infrared active B_{1u} vibrational transitions are utilized. Overall, agreement between the observed and calculated frequencies is excellent given the qualitative nature of the force field used in the analysis and the fact that the force field is not refined/fit to the experiments.

H₂Pc AND MgPc 2-Color TOFMS Experiments:

Ultracold 2-color TOFMS spectra of H₂Pc and MgPc could not be observed with the current experimental apparatus configuration available in the laboratory. In initial attempts to obtain 2-color TOFMS spectra of the macrocycles, spectra were observed which were not tunable when the pump laser frequency was varied. Both helium and argon carrier gases were employed to expand the molecules into the vacuum apparatus; however, the spectra were significantly broadened. These results are somewhat surprising since ultracold 2-color TOFMS spectra of small aromatic molecules such as benzene, pyrazine, and aniline have been observed in the existing apparatus.¹⁰⁻¹² One possible explanation for the nontunability is that the molecules are vibrationally/rotationally hot when they reach the section of the apparatus where the spectra are taken. In this case, molecular heating may occur in the section of the apparatus between the supersonic nozzle and the TOFMS flight tube.

In the existing apparatus,¹² Figure 7.3, the supersonic expansion is sampled using a compound angle conical skimmer.¹³ The sampled portion of the supersonic expansion then travels about 50 cm to the TOFMS ionization area where it is optically probed. Based upon the aforementioned experimental observations, the expansion could be disturbed to some extent by the presence of the skimmer in the supersonic flow path. In order to understand the interferences in the supersonic flow which result in molecular heating, it is instructive to look at the physical properties of the supersonic expansion before, at, and after the skimmer.

Assuming that the expansion proceeds in an adiabatic and isentropic manner and that the expanding gases can be considered ideal, the centerline translational temperature T_1 , the centerline static pressure P_1 , and the centerline static density ρ_1 of the expansion before the skimmer can be described by¹⁴

$$7.4a \quad T_1 = \left(1 + \frac{\gamma-1}{2} M_1^2\right)^{-1} T_0$$

$$7.4b \quad P_1 = \left(1 + \frac{\gamma-1}{2} M_1^2\right)^{\frac{-\gamma}{\gamma-1}} P_0$$

$$7.4c \quad \rho_1 = \left(1 + \frac{\gamma-1}{2} M_1^2\right)^{\frac{-1}{\gamma-1}} \rho_0$$

as a function of centerline Mach number M_1 , nozzle backing region stagnation temperature T_0 , stagnation pressure P_0 , stagnation density ρ_0 , and $\gamma = C_p/C_v = 5/3$ for monatomic carrier gases. The centerline Mach

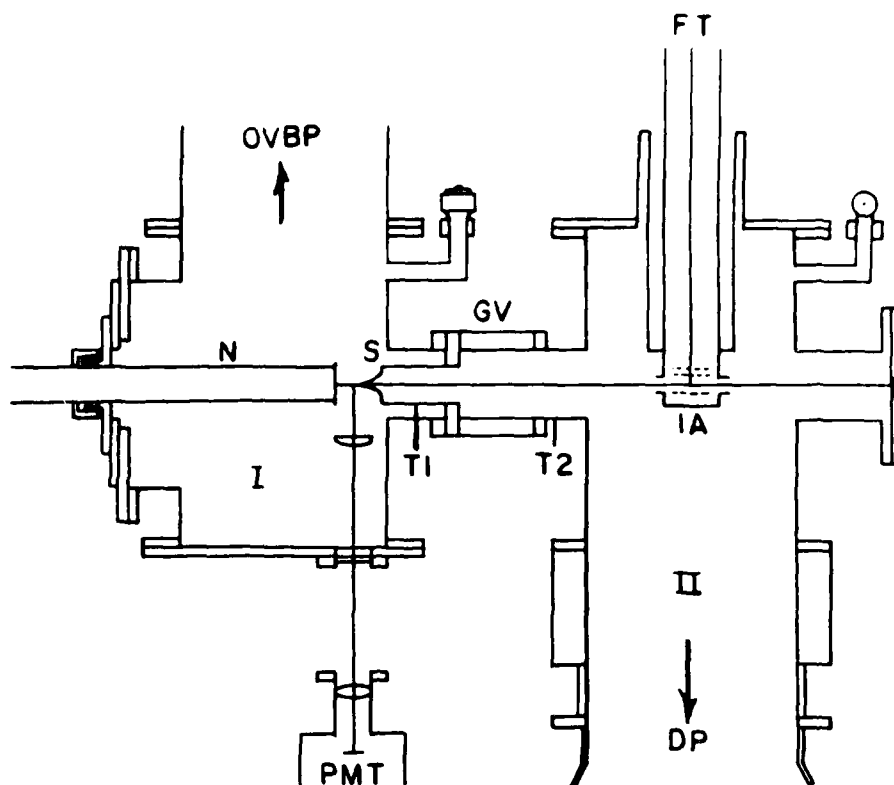


Figure 7.3

Supersonic molecular jet apparatus. I - PE chamber. OVBP - oil vapor booster pump. N - nozzle. S - skimmer. PMT - photomultiplier tube. T1 - 2 inch tubing. T2 - 3 1/2 inch tubing. GV - 3 inch gate valve. II - TOFMS chamber. FT - flight tube. IA - ionization area. DP - diffusion pump.

number is a function of downstream distance from the nozzle throat and can be expressed as¹⁵

$$7.5 \quad M_1 = 3.26 \left(\frac{x - 0.75D}{D} \right)^{\gamma-1} \frac{1}{2} \left(\frac{\gamma+1}{\gamma-1} \right) / 3.26 \left(\frac{x - 0.75D}{D} \right)^{\gamma-1}$$

for which x is the centerline downstream distance and D is the supersonic nozzle throat diameter. Since the vacuum chamber pressure is finite, acceleration of the expansion will cease at a terminal Mach number which can be determined using Equation 7.4a and¹⁴

$$7.6 \quad \frac{T_1}{T_0} = \left(\frac{P_1}{P_0} \right)^{\frac{\gamma-1}{\gamma}}$$

for which P_1 is the vacuum chamber static pressure. For the continuous supersonic nozzle used in the experiments, typical nozzle backing pressures are around 150 psig. The static pressure in the vacuum chamber at this backing pressure is about 2×10^{-3} torr. The nozzle throat diameter is typically 100 microns. Using Equations 7.4a, 7.5 and 7.6, the centerline terminal Mach number for the expansion is calculated to be at $M_t = 36$ and is reached at about 4 mm downstream of the nozzle throat.

The supersonic flow properties are described by Equations 7.4-6 until the flow encounters the skimmer or until the flow passes through the Mach disk which is located at a downstream position determined by¹⁵

$$7.7 \quad X_{MD} = .67 D \left(\frac{P_0}{P_1} \right)^{1/2}$$

At the two-point isentropic processes, the gas must cool which heats the flow and can return it to subsonic speed. In the experiment conducted, the supersonic flow is sampled at nozzle-skimmer distances between 20 and 40 mm which is considerably less than the position of the Mach disk calculated to lie at 132 mm downstream using Equation 7.7.

Figure 7.4 presents the centerline temperature profiles for supersonic expansions beginning at $T_0 = 773$ K and $T_0 = 298$ K as a function of downstream distance x calculated using Equations 7.4 and 7.5 with the centerline terminal Mach number taken at 36. On the basis of the calculations, the temperature profiles for supersonic expansions beginning at elevated temperatures ($T_0 = 773$ K) are largely the same as those beginning at room temperature ($T_0 = 298$ K). Thus, H_2Pc and $MgPc$ should, therefore, be nearly as internally cold before the skimmer as other species observed in the supersonic molecular jet generated by using room temperature expansions assuming that rotational and vibrational temperatures equilibrate near the translational temperature.^{15,16} These notions are corroborated experimentally in FE for which ultracold spectra of H_2Pc , $MgPc$, and their respective solute/solvent clusters are observed. (The FE spectra are taken between 4 and 8 mm from the nozzle throat, well upstream of the Mach disk.)

Large deviation from isentropic flow may occur at the skimmer which can result in molecular heating. The interferences from the skimmer can be attributed to shock waves forming in the expansion as the flow passes through the skimmer. The physical properties of the supersonic flow after passing through the shock waves can be expressed as a function of upstream conditions and the angle of the shock waves with

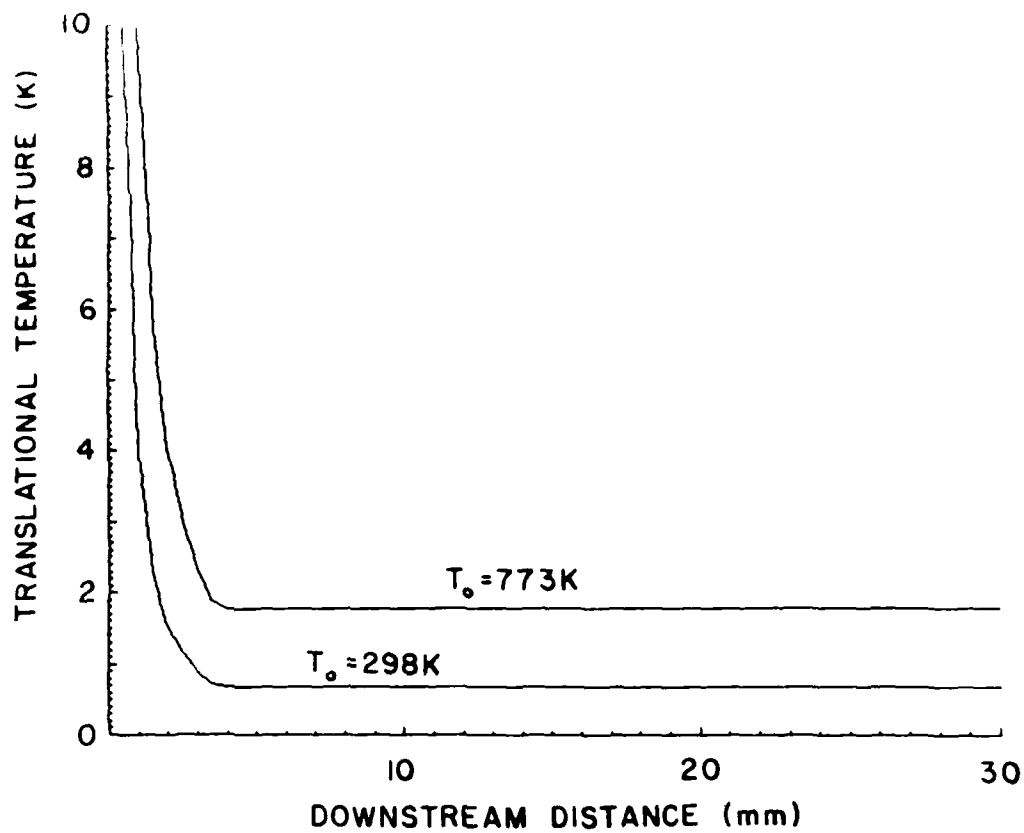


Figure 7.4

Downstream distance versus centerline translational temperature for supersonic expansions beginning at 773 K and 298 K.

respect to the flow direction. The centerline downstream translational temperature T_2 , static pressure P_2 , and static density ρ_2 are¹⁴

$$7.8a \quad T_2 = \left(\frac{2\gamma}{\gamma+1} M_1^2 \sin^2 \epsilon - \frac{\gamma-1}{\gamma+1} \right) \left(\frac{\gamma-1}{\gamma+1} + \frac{2}{(\gamma+1)M_1^2 \sin^2 \epsilon} \right) T_1$$

$$7.8b \quad P_2 = \left(\frac{2\gamma}{\gamma+1} M_1^2 \sin^2 \epsilon - \frac{\gamma-1}{\gamma+1} \right) P_1$$

$$7.8c \quad \rho_2 = \left(\frac{(\gamma+1) M_1^2 \sin^2 \epsilon}{2 + (\gamma-1) M_1^2 \sin^2 \epsilon} \right) \rho_1$$

for which M_1 is the Mach number just upstream of the shock wave and ϵ is the flow deflection angle between the shock wave and the flow direction. Downstream/upstream translational temperature ratio versus flow deflection angle for an upstream Mach number of 36 is plotted in Figure 7.5. The plot demonstrates the severe heating effects that can occur in the flow as it passes through the shock wave. The most severe case is at $\epsilon = 90^\circ$ which corresponds to a normal shock wave. Here, the downstream temperature is about 405 times the upstream temperature. Even at smaller flow deflection angles (oblique shock waves), the heating is significant. For example at $\epsilon = 10^\circ$, the downstream temperature is a factor of 13 greater than the upstream temperature.

Bier and Hagena have shown, by Schlieren photographs, the types of possible skimmer interferences present in the expansion.¹⁷ At large nozzle/skimmer distances, the shock wave system in the expanding jet gas is similar to that depicted in Figure 7.6a, for which the supersonic flow is contained in oblique and normal shock (Mach disk) waves. In

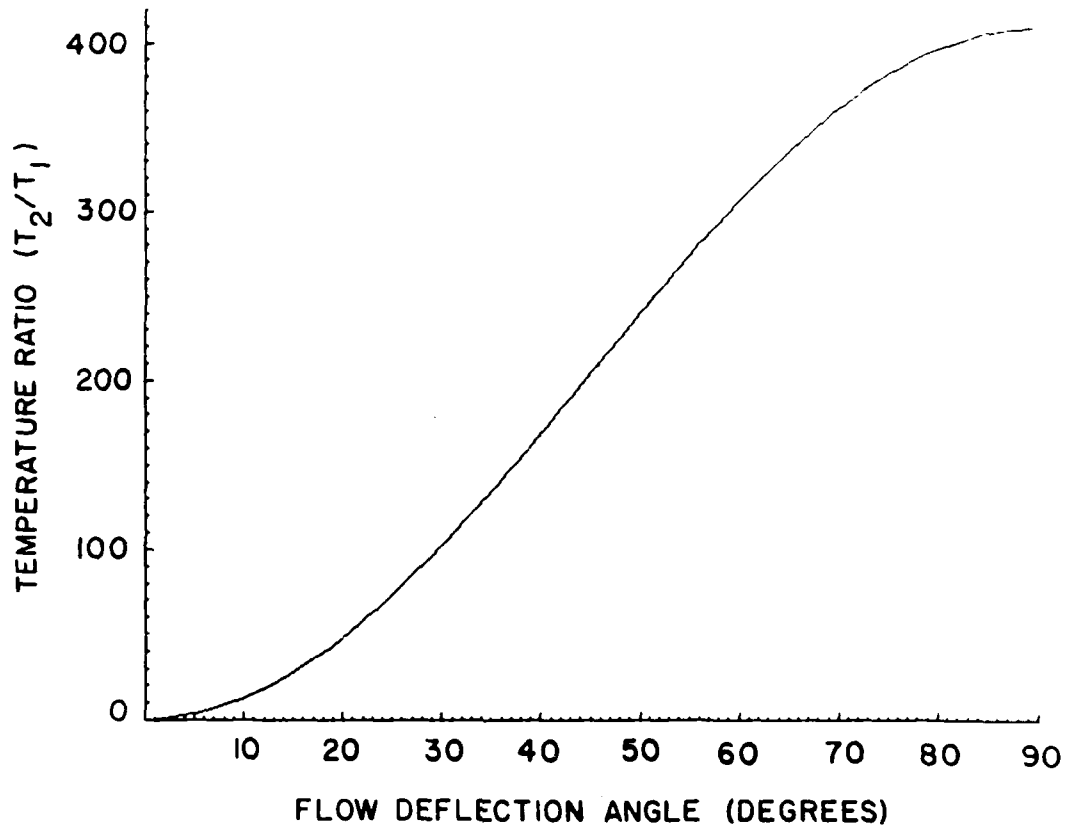


Figure 7.5

Flow deflection angle versus downstream/upstream centerline translational temperature ratio for flow across a shock wave at an upstream Mach number of 36.

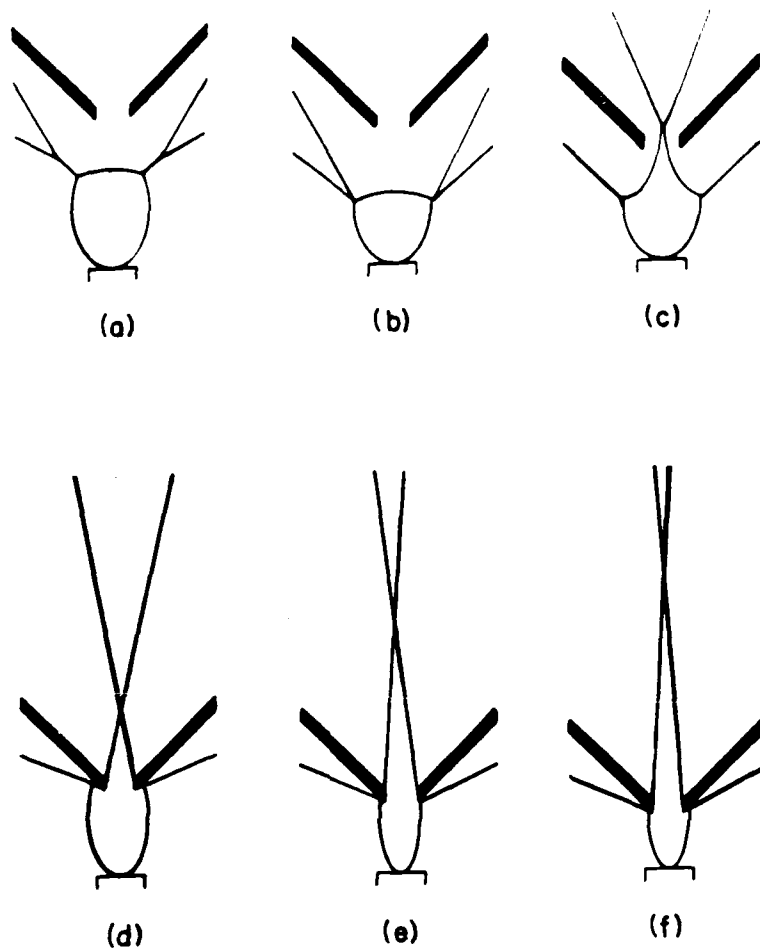


Figure 7.6

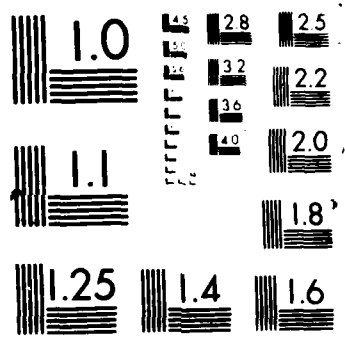
Shock wave system in a supersonic molecular jet expansion in the presence of a skimmer downstream of the nozzle throat.

In this case, the skimmer orifice lies in the subsonic flow downstream of the normal shock wave. The normal shock wave heats the flow and the molecules penetrate the shock wave boundaries. This interference is the most severe source of nozzle beam heating since all molecules entering the skimmer are in subsonic flow and internally hot. As the nozzle is moved towards the skimmer, the shock system in the jet stream is deformed, and the shock waves move towards the nozzle. Figures 7.6b-7.6c. Here, the normal shock wave is still detached from the skimmer orifice and results in "shock beam" formation. On further approach of the nozzle to the skimmer, the normal shock wave attaches to the skimmer orifice, Figures 7.6d-7.6f. The normal shock wave becomes oblique shock waves on both the upstream and downstream sides of the skimmer. The oblique shock wave upstream of the skimmer should not affect the supersonic flow at this nozzle/skimmer distance unless the skimmer mount or chamber walls are in close proximity of the skimmer orifice. Molecules entering the skimmer are in supersonic flow and may be subsequently heated upon traversing the oblique shock waves downstream of the skimmer. The amount of heating which occurs in the downstream oblique shock system depends upon the static pressure behind the skimmer and upon the flow deflection angle.

Molecular heating which occurs in the shock waves can be thought of as a sequence of collisional energy transfer processes up the molecular vibrational and rotational manifolds. Each elementary step involves the deposition of a small amount of vibrational and rotational energy at the expense of translational energy. Since single ring systems yield ultracold 2-color TOFMS spectra and the macrocycles do not, differences must exist between the collisional energy transfer

processes present in the shock waves at or near the skimmer for the molecular systems considered. Two major distinctions can be cited between the single ring systems and H_2Pc / $MgPc$ which may play a significant role in accounting for the difference in molecular heating by the shock system. First, the macrocycles are about 3 times larger in diameter than the single ring systems. Approximating the molecules as hard spheres, one finds that H_2Pc / $MgPc$ will undergo between 6 and 9 times more collisions in the shock system than the single ring molecules depending upon whether they collide with carrier gas molecules or with other macrocycles. Second, H_2Pc and $MgPc$ possess a large number of vibrational modes compared to the single ring systems (168 for H_2Pc versus 30 for benzene); in particular, many of these modes are of low frequency. H_2Pc has nine ground state vibrational modes with energies below 100 cm^{-1} . These low-lying vibrational levels may facilitate heating of the macrocycles. As the large molecules pass through the shock system, the interconversion of small amounts of translational energy into vibrational energy should be more efficient than in the single ring systems for which the lowest ground state vibrational levels lie at about 400 cm^{-1} . Either or both of these two factors may contribute to the molecular heating of the macrocycles.

Since the skimmer used in the initial experiments did not perform satisfactorily in maintaining internally cold H_2Pc / $MgPc$ beams, a new skimmer was designed to minimize the shock wave effects on the supersonic flow. Particular attention was focused upon the length of the skimmer, the diameter of the skimmer orifice, and the interior and exterior skimming angles.



The length of the skimmer is important since the skimmer must be sufficiently long so that the oblique shock wave system does not cause flow perturbations about the skimmer orifice due to skimmer mount or vacuum chamber wall interactions. These interactions tend to degrade supersonic beam skimming by creating a boundary layer at the skimmer mount or chamber walls which rotates the attached shock wave towards a critical angle (more normal to the supersonic flow) which could yield shock wave detachment and the formation of a bow shock wave similar to that shown in Figure 7.6b-7.6c.^{17,18}

The diameter of the skimmer orifice dictates the gas throughput of the skimmer.¹⁹ Too large a skimmer diameter will cause TOFMS chamber pumping problems as well as an increase in the intensity of the oblique shock wave system downstream of the skimmer orifice.

The internal skimming angle must be as large as possible to insure that molecules entering the skimmer orifice and striking the skimmer walls can be pumped away fast enough to minimize scattering/heating of the beam molecules.^{19,20} Too small an internal skimming angle will cause skimmer choking and boundary layer formation which results in an increase in the oblique shock wave intensity downstream of the skimmer orifice, similar to that occurring if the skimmer orifice diameter is too large.

The exterior skimming angle determines the upstream flow deflection caused by the skimmer. The angle must be kept small enough so that the oblique shock wave will not detach from the skimmer orifice and destroy the supersonic flow before the molecules pass through the skimmer. The maximum flow deflection angle ϵ_{\max} which can be negotiated by a supersonic flow without shock wave detachment is given by¹⁴

$$7.9 \quad \sin^2 \epsilon_{\max} = \frac{1}{\gamma M_1^2} \left(\frac{\gamma+1}{4} M_1^2 - 1 + \left[(\gamma+1) \left(1 + \frac{\gamma-1}{2} M_1^2 + \frac{\gamma+1}{16} M_1^4 \right) \right]^{1/2} \right)$$

as a function of Mach number M_1 at the skimmer orifice. The maximum flow deflection angle is related to the maximum exterior skimming angle δ_{\max} and skimmer Mach number by¹⁴

$$7.10 \quad \frac{1}{\tan \delta_{\max}} = \left(\frac{9(\gamma+1)}{20} \frac{M_1^2}{M_1^2 \sin^2 \epsilon_{\max} - 1} - 1 \right) \tan \epsilon_{\max}$$

The maximum flow deflection angle and the maximum exterior skimming angle are plotted versus Mach number in Figure 7.7.

From Figure 7.7, the maximum flow deflection angle and the maximum exterior skimming angle approach limiting values at Mach numbers above 6. The high Mach number of the supersonic flow used in the experiments thus makes it possible to use a skimmer with exterior skimming angles of up to 46° . 41° was selected for the exterior skimming angle used in the new skimmer to provide a safety factor to avoid the occurrence of a normal detached shock upstream of the skimmer orifice. A 35° interior skimming angle was selected for the new skimmer as it was the largest feasible angle with respect to the exterior skimming angle that the skimmer could be ground without causing structural problems. The skimmer shape was chosen as conical. The length of the skimmer was selected at 47 mm using the exterior skimming angle and a skimmer base diameter of 35 mm. This length is about a factor of 2 larger than that of the skimmer utilized in the initial TOFMS experiments. This larger skimmer should minimize possible upstream boundary layer and chamber wall effects.^{14,19,20} The maximum diameter of the skimmer orifice was selected at 2 mm to avoid TOFMS chamber pumping

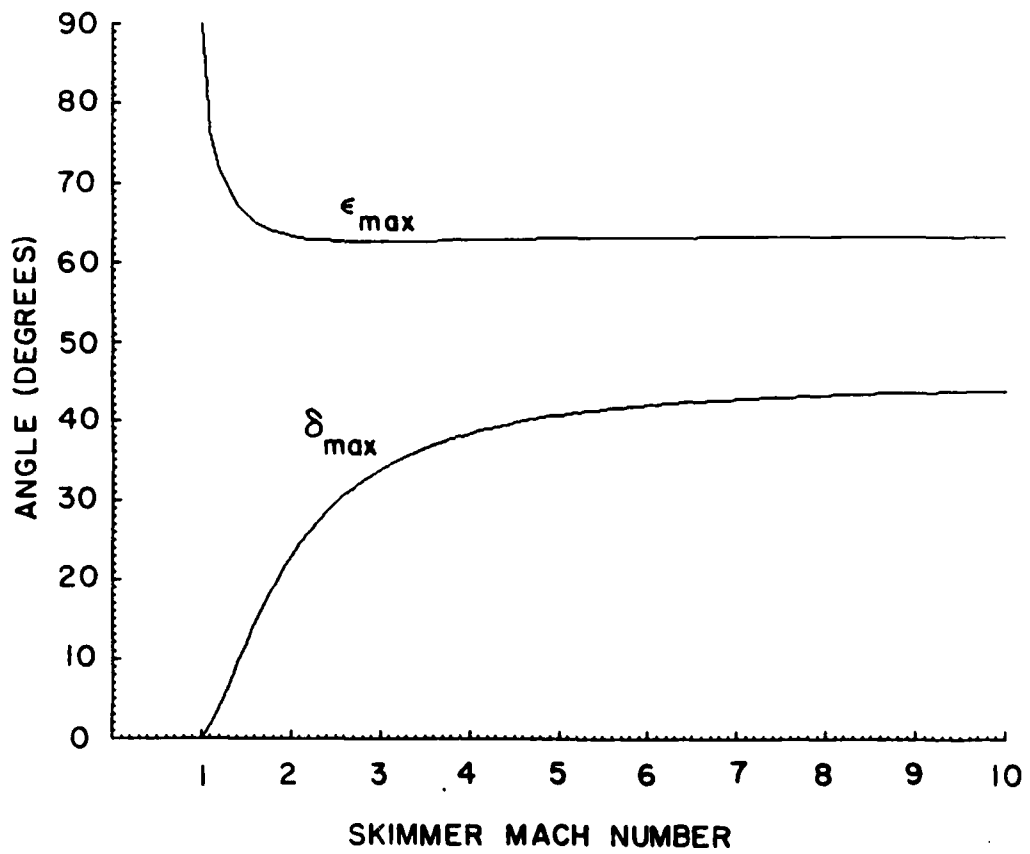


Figure 7.7

Maximum flow deflection angle (ϵ_{max}) maximum skimming angle (δ_{max}) versus skimmer Mach number.

problems. Three skimmers were fabricated possessing the above length, skimming angles, and orifice diameters of .5, 1, and 2 mm in order to determine the optimal skimmer configuration since no theoretical relationship exists between skimmer orifice diameter and supersonic flow characteristics. These skimmers should give an indication of the interference caused by the oblique shock system downstream of the skimmer. The intensities of the shock waves should decrease with decreasing skimmer orifice diameter on the basis of skimmer throughput, boundary layer, and skimmer choking arguments.

2-color TOFMS spectra of H_2Pc taken using the three skimmers are shown in Figure 7.8. The spectra are taken using 428°C nozzle backing region temperature, 560°C nozzle tip temperature, 25 mm nozzle/skimmer distance, and 2.5 psig argon nozzle backing pressure. On decreasing the skimmer orifice from 2 to .5 mm, the spectra evolve from being broad and featureless (trace A) to being "quasi" cold (trace C). In both traces B and C, the H_2Pc O_0^0 and A_0^2 are observed; however, the spectra are smeared out by rotational broadening and vibrational sequence congestion. The sequence structure in trace C is about 40 cm^{-1} wide and peaks at about 16 cm^{-1} to the red of the H_2Pc O_0^0 . Similar sequence structure is also observed to the red of the A_0^2 . Assuming a 10% decrease in vibrational frequency between the ground and excited states for H_2Pc , a vibrational temperature of about 150 K can be estimated from the observed sequence structure.

These experiments identify the skimmer as being the major source of interference in the supersonic expansion. In particular, the observations suggest that the downstream oblique shock system is responsible for the molecular heating since the interference decreases with

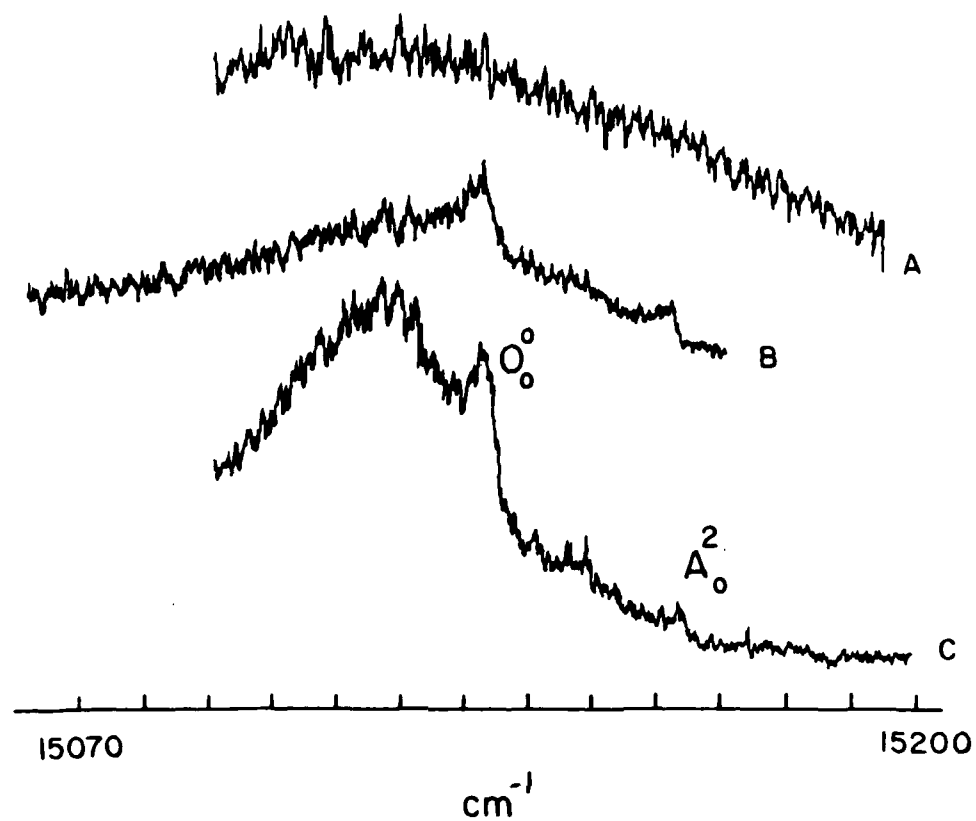


Figure 7.8

2-color TOFMS of H_2Pc in the vicinity of the Q_x band 0_0^0 . Trace A taken using a 2 mm skimmer orifice. Trace B taken using a 1 mm skimmer orifice. Trace C taken using a .5 mm skimmer orifice.

decreasing skimmer orifice diameter. The maintenance of at least some degree of cold internal temperatures in the spectrum taken using the .5 mm orifice skimmer (trace C) demonstrates that the downstream shock wave intensity is still large enough to cause observable skimmer interference in the supersonic flow. This notion is corroborated by experiments using higher backing pressures of argon carrier gas (up to 50 psig) which yield broad spectra that can be attributed to an increase in the downstream skimmer interferences similar to those observed using the 2 mm orifice skimmer.

As mentioned above, the intensity of the downstream oblique shock wave depends upon the static pressure in the vacuum chamber directly downstream of the skimmer. In order to minimize the interference caused by the downstream shock system, the static pressure in this area should be kept lower than the upstream static pressure so that skimmer choking and boundary layer formation does not occur.^{14,19,20} In the existing apparatus (Figure 7.3), the region between the skimmer and the TOFMS chamber is constructed using two lengths of 2 inch diameter (4 1/3 inches long) and 3 1/2 inch diameter (4 1/3 inches long) tubing and a 3 inch gate valve assembly (4 1/3 inches long). The region directly downstream of the skimmer is displaced by about 70 cm from the TOFMS chamber diffusion pump. The tubing between the two vacuum chambers essentially forms a "dead end" region with a leak provided by the skimmer which may not be adequately evacuated by the TOFMS chamber pumping system. A pressure gradient may thus be present in this region which may give rise to the shock system interference observed.

Other vacuum systems²¹ which utilize skimmers to sample the supersonic expansion differ in design from our existing apparatus.

These systems possess two key design features that minimize the effects of the downstream shock waves. First, the vacuum systems are designed for the efficient removal of gas molecules from the post-skimmer region by pumping directly downstream of the skimmer with pumps capable of sustaining static pressures of about 10^{-6} torr. Second, the systems allow for minimization of chamber wall/boundary layer effects in the post-skimmer region by making the chambers large and divergent with respect to the skimmer base. Neither of these features is incorporated in the existing apparatus design.

A proposed modification to the existing apparatus which incorporates the aforementioned design features is shown in Figure 7.9. The modification involves replacing the 3 inch gate valve, the interchamber tubing, and the 6 inch chamber connecting ports with 12 inch connecting ports and a 16 inch port flange with a divergent hole bored in its center. The 12 inch connecting ports will provide for more than adequate divergence downstream of the skimmer as well as provide for more efficient pumping of the region by the existing TOPMS pumping system. The 16 inch flange serves as both a chamber divider and as a skimmer mounting surface. The skimmer can be mounted in the chamber by clamping its base over the hole in the 16 inch flange with a small flange assembly. For FE experiments, the skimmer can be removed and a sealing plate can be placed over the flange hole to isolate the FE chamber from the TOPMS chamber. The connecting ports can be constructed with different lengths so that the 16 inch flange/skimmer assembly can be located closer to the TOPMS flight tube. This will allow for an overall shorter nozzle/TOPMS ionization area distance which should increase the molecular density at the ionization area by a factor of $2500/X_2$ for which X is the nozzle/TOPMS ionization area distance in cm.

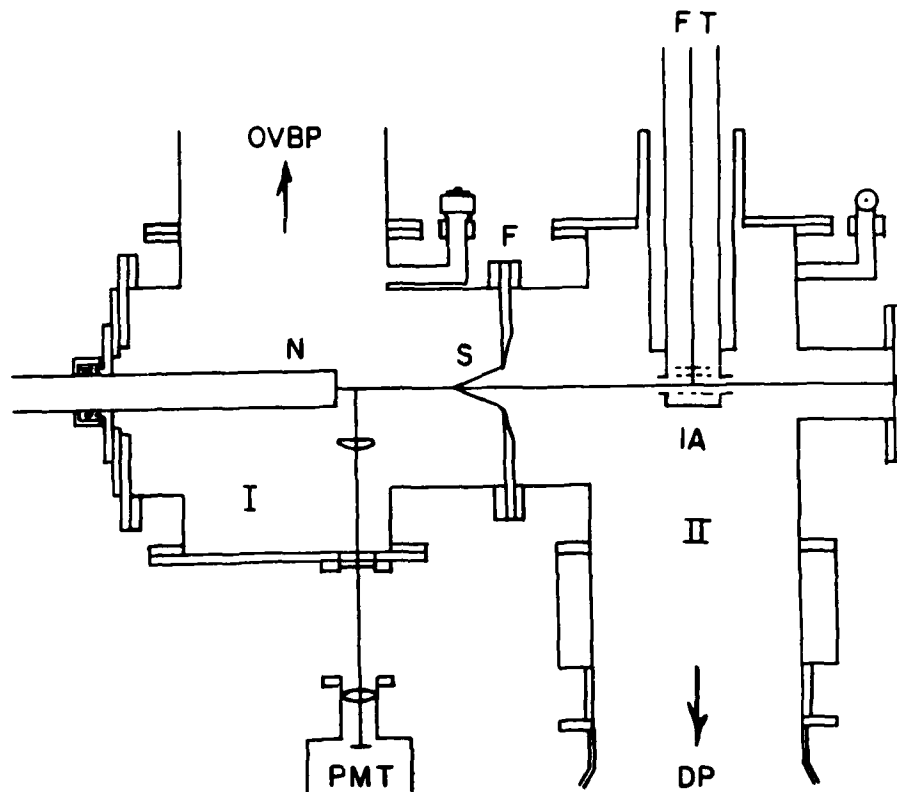


Figure 7.9

Proposed supersonic molecular jet apparatus. I - PE chamber. OVBP - oil vapor booster pump. N - nozzle. S - skimmer. PMT - photomultiplier tube. F - 16 inch Flange. II - TOFMS chamber. FT - flight tube. IA - ionization area. DP - diffusion pump.

SUMMARY AND CONCLUSIONS:

Initial attempts to obtain ultracold 2-color TOFMS spectra of H_2Pc and $MgPc$ yielded negative results. Both helium and argon carrier gases were employed to expand the macrocycles into the vacuum apparatus; however the spectra were significantly broadened. The nontunability of the spectra with varying pump laser frequency was attributed to molecular heating of the H_2Pc and $MgPc$ moieties by shock waves in the vicinity of the skimmer used to sample the supersonic expansion. New skimmers were designed to minimize the shock wave effects on the supersonic flow. "Quasi" cold 2-color TOFMS spectra of H_2Pc were obtained using these skimmers. Experiments identified the skimmer as being the major source of interference in the molecular expansion. In particular, the observations suggest that a downstream (Chamber II) oblique shock system is responsible for the molecular heating. Through identification of key apparatus design factors which should minimize the downstream shock wave effects, proposed modifications to the existing laboratory apparatus are suggested. The proposed modifications involve enlarging the region downstream of the skimmer to allow for more effective pumping and to minimize skimmer choking and boundary layer effects in the post-skimmer region.

REFERENCES

1. E.B. Wilson Jr., J.C. Decius, and P.C. Cross, "Molecular Vibrations, Theory of Infrared and Raman Vibrational Spectra," (McGraw-Hill Book Co., Inc., 1955).
2. J.C. Decius, *J. Chem. Phys.* 17, 1315 (1949).
3. B.F. Hoskins and S.A. Mason, *Chem. Comm.*, 554 (1969).
4. P.C. Painter and J.L. Koenig, *Spectrochimica Acta.* 33A, 1019 (1977).
5. T. Kobayashi, *Spectrochimica Acta.* 26A, 1313 (1970).
6. T. Kobayashi, F. Kurokawa, N. Uyeda, and E. Suito, *Spectrochimica Acta.* 26A, 1305 (1970).
7. B. Stymne, F.X. Sauvage, and G. Wettermark, *Spectrochimica Acta.* 35A, 1195 (1979).
8. P.S.H. Fitch, C.A. Hayman, and D.H. Levy, *J. Chem. Phys.* 73 1064 (1980).
9. The PED's are calculated by using $\% \text{ PED} = 100 \times |C_i|^2$ for which C_i is the eigenvector coefficient for symmetry coordinate i in the eigenvector normal modes.
10. J. Wanna and E.R. Bernstein, *J. Chem. Phys.* 85, 1795 (1986); J. Wanna, J.A. Menapace and E.R. Bernstein, *J. Chem. Phys.* 85, 1795 (1986).
11. E.R. Bernstein, K. Law and M. Schauer, *J. Chem. Phys.* 80, 634 (1984); M. Schauer and E.R. Bernstein, *J. Chem. Phys.* 82, 726 (1985).
12. M. Schauer, Ph.D. Thesis, Colorado State University, 1984. E.R. Bernstein, K. Law and M. Schauer, *J. Chem. Phys.* 80, 207 (1984).
13. The skimmer used in the experiments is a model 1 skimmer purchased from Beam Dynamics, 623 E. 57th Street, Minneapolis, Minnesota 55417.
14. W.C. Reynolds and H.C. Perkins, "Engineering Thermodynamics," (McGraw-Hill Book Co., Inc., New York, 1977); M.J. Zucrow and J.D. Hoffman, "Gas Dynamics," Vol. I (J. Wiley and Sons, Inc., New York, 1976).

15. P.P. Wegener, "Molecular Beams and Low Density Gas Dynamics," (Marcel Dekker, Inc., New York, 1974).
16. A. Amirav, U. Even, J. Jortner, Chem. Phys. 51, 31 (1980).
17. K. Bier and O. Hegena, "Rarefied Gas Dynamics," edited by J.A. Laurmann (Academic Press, New York) Vol. 1, p. 478-496, 1963.
18. U. Bossel, Entropic 30, 11 (1969).
19. A. Kantowitz and J. Grey, Rev. of Scientific Instruments 22, 328 (1957).
20. K. Bier and O. Hegena, "Rarefied Gas Dynamics," edited by J.H. el Leeuw (Academic Press, New York) Vol. II, p. 260-278, 1966.
21. M.G. Liverman, S.M. Beck, D.L. Monts, and R.E. Smalley, "Rarefied Gas Dynamics" edited by R. Campargue (Academic Press, New York) Vol. II, p. 1037-1048, 1979; D.H. Levy, L. Wharton, and R.E. Smalley, "Laser Spectroscopy in Supersonic Jets," in Chemical and Biological Applications of Lasers, Vol. II, edited by C. Bradley Moore (Academic Press, New York) 1977; J.B. Fenn and J. Deckers, "Rarefied Gas Dynamics," edited by J.A. Laurmann (Academic Press, New York) Vol. I, p. 497-515, 1963; J.G. SkoFronick, Review of Scientific Instruments, 38 1628, 1967.

CHAPTER EIGHT

FUTURE EXPERIMENTS AND CONCLUSIONS

This chapter presents the basic ideas and motivations for future experiments which can be conducted using the techniques and experimental set-ups currently available in the Bernstein group laboratory. The proposed studies entail those experiments that will extend or complement the work presented in this dissertation. This chapter also summarizes the conclusions drawn from the work accomplished on the molecules and clusters presented in Chapters 2-7. The conclusions include the most important results obtained from the work. For specific conclusions pertaining to each of the systems studies, the appropriate chapters in the dissertation should be consulted.

Future Experiments.

Effects of Macrocycle Ring Substitution on Solvation - The high temperature supersonic molecular jet techniques utilized to study H_2Pc , $MgPc$, and their respective vdW clusters with small solvents (Chapter 6) also gives us the opportunity to study the effects of ring substitution in the macrocycles on their solvation properties in an ultracold isolated environment. For example in the H_2Pc and $MgPc$ cluster studies, major differences exist between the two cluster solutes in that the H_2Pc clusters exhibit enhanced stabilization in the S_1 state relative to the S_0 state whereas the $MgPc$ clusters exhibit enhanced stabilization in the

S_0 state relative to the S_1 state. This difference appears to be due to the magnesium substitution in the phthalocyano core. Furthermore, the spectra suggest that the intermolecular interactions between MgPc and solvents having lone electron pairs possess major contributions from the central magnesium atom and the solvent electron pairs.

These observations pose several questions pertaining to the physics and chemistry responsible for the solvation properties of the phthalocyanines (Pc's). Questions that can be considered include: 1) are the solvation properties of Pc's dependent upon the specific metal atom present in the phthalocyano core; 2) does the relative stabilization of one electronic state over another depend upon the specific central metal atom; 3) do cluster geometries and solute solvation sites change significantly with different central metal atoms; and 4) are the central metal atoms in the Pc moieties responsible for a major portion of the intermolecular interaction.

To explore the effects of central metal atom substitution in Pc's, initial experiments can be conducted on zinc phthalocyanine (ZnPc). The fluorescence quantum yield for ZnPc is about .3 which is comparable to those for H_2Pc (.7) and MgPc (.6).¹ This quantum yield is large enough to allow for observation of ZnPc and its respective vdW clusters in fluorescence excitation experiments. The experiments could initially entail clustering ZnPc with solvents such as those used in the H_2Pc and MgPc studies. By comparing the ZnPc cluster spectra and calculated cluster geometries with those for the MgPc cluster systems, the effects of the central metal atom on cluster properties can be explored. Subsequent experiments in this area could include spectroscopic and modeling studies on Pc's containing cadmium, sodium, and lithium.

Another set of experiments which can be conducted to study the effects of ring substitution on the Pc solvation properties involves the analysis of a tetrabenzoporphyrin (TBP) solute series clustered with various solvents. Macrocycles which can be initially studied in this class include free base tetrabenzoporphyrin (H_2TBP), magnesium tetrabenzoporphyrin ($MgTBP$), and zinc tetrabenzoporphyrin² ($ZnTBP$). This class of compounds offers the opportunity to study the effects of the solute bridge nitrogens on the solvation properties of the Pc class as H_2TBP , $MgTBP$, and $ZnTBP$ differ from their respective Pc analogues only by replacement of the bridge nitrogens in Pc by methine bridges in TBP. The TBP compounds proposed for study also possess fluorescence quantum yields (.46 for H_2TBP , .55 for $MgTBP$, and .35 for $ZnTBP$)¹ which are favorable for observation in a supersonic molecular jet fluorescence excitation experiment. Through the analysis of the cluster spectral shifts, chromophore vibronic structures, and calculational modeling of the cluster geometries and binding energies, the effects of the bridge nitrogens on the macrocycle solvation properties may be established. Cluster studies using the TBP solutes are interesting and important as they will provide the link between the Pc's and their biologically active analogues, the porphyrins, in regard to cluster geometry, binding energy, preferred solute solvation sites, and major interaction types responsible for solvation.

Aromatic Solute/Aromatic Solvent Clusters - All the aforementioned Pc and TBP solutes can be clustered with a number of small aromatic solvents such as benzene, pyrazine, pyrimidine, and pyridine. Studying these clusters gives us the opportunity to explore cluster

energetics and dynamics from the point of view of both the cluster solute and solvent. Supersonic molecular jet studies can be conducted by probing both the Pc/TBP solute and the benzene/N-heterocycle solvent optical transitions. The studies will yield insight into the importance of the solvent aromatic π cloud and/or nonbonded electron pairs on solvation. For example, clustering MgPc with pyrazine should provide detailed information on the participation of the solvent nonbonded electron pairs with the magnesium central metal atom. If the solvent nonbonded electron pairs are major contributors in cluster formation/stabilization, the $n\pi^*$ transition in pyrazine should not exist or be highly perturbed (blue shifted). The cluster systems are also interesting in the respect that they may allow one to determine if changes in the cluster binding energy upon electronic excitation depend on the specific electronic excitation analyzed. In particular, one could ask the question: will the change in cluster binding energy be different in magnitude if the cluster solvent optical transition is probed rather than the cluster solute optical transition? Furthermore, these studies may yield information on differences in the relative stabilization of the solute and solvent electronic states. Do the spectral shifts observed when probing the solvent optical spectrum differ in sign than those observed when probing the cluster solute spectrum; that is, are the spectral shifts both bathochromic or hypsochromic or is the solvent spectral shift bathochromic and the solute shift hypsochromic (or vice versa)?

Phthalocyanine and Porphyrin Vibronic Structure - Up to this point, we have only considered analyzing the Pc and TBP macrocycles in cluster systems. The vibrational spectroscopy of these molecules is

also important in the understanding of the vibrational structure present in biologically significant systems. In particular, elucidation of the vibrational structure in the Pc and TBP systems may yield valuable information regarding which portions of the macrocycles participate in the various vibrational motions. Supersonic molecular jet studies on isolated Pc and TBP can contribute to the resolution of the excited state energetics present in the systems since the techniques greatly simplify the vibronic spectra and thus facilitate their interpretation. As discussed in Chapter 6, the low frequency motion present in the H_2Pc and $MgPc$ vibronic spectra is characterized using the results of an out-of-plane normal coordinate analysis; and in Chapter 7, the calculations on H_2Pc are compared to infrared data. These studies make it possible for us to determine the detailed nature of the out-of-plane motion occurring in specific regions within the H_2Pc vibrational manifold. In order to obtain a complete understanding of the macrocycles vibrational structure, the in-plane motion should be characterized. The vibronic spectra of the Pc and TBP molecules presented above can be analyzed using the results of both in-plane and out-of-plane normal coordinate analyses. In these studies, the in-plane motion can be modeled using a refined force field determined from normal coordinate analyses on the in-plane motion occurring in porphyrins.³⁻⁷ The combination of calculational modeling and spectroscopic studies on these systems should increase our understanding of the structural changes (nuclear motion) occurring in the various electronic states as well as the extent of interelectronic state mixing (vibronic coupling) between the different electronic states in the macrocycles. These studies will also be useful in the basic understanding of the spectroscopy in more complex systems such as substituted Pc's and porphyrins.

$\pi - \pi$ Solute/Solvent Interaction in Clusters - The $\text{MgPc}(\text{CO}_2)_1$ and $\text{H}_2\text{Pc}(\text{CO}_2)_1$ clusters presented in Chapter 6 exhibit vibronic spectra with distinctive spectral shifts. The $\text{H}_2\text{Pc}(\text{CO}_2)_1$ cluster is the only cluster observed with H_2Pc which possesses a hypsochromic shift upon excitation to the S_1 state. The $\text{MgPc}(\text{CO}_2)_1$ cluster also exhibits a hypsochromic shift comparable to that observed in $\text{H}_2\text{Pc}(\text{CO}_2)_1$. The exact nature of the intermolecular interaction responsible for the spectral shifts is not known; however, based upon cluster experiments with alcohol and hydrocarbon solvents, it is possible to speculate that $\pi-\pi$ solute/solvent interactions may be responsible for the observed spectral shifts. To study this behavior, a series of experiments on single ring solutes such as benzene, pyrazine, and pyrimidine solvated by carbon dioxide, carbon monoxide, and oxygen can be conducted using 2-color TOFMS techniques. The benzene/solvent vibronic spectra will reveal whether the solvents orient perpendicular or parallel to the solute molecular plane through the observation of forbidden cluster chromophore transitions. In these studies, the spectral shifts may be related to particular cluster geometries which may yield information on the major interactions contributing to the intermolecular potentials between the solutes and solvents. The pyrazine and pyrimidine/solvent clusters may tell us about the effects of the ring nitrogens on the cluster geometry, binding energy, and solute solvation. Computer modeling of cluster geometry, binding energy, and intermolecular vibrational structure may also aid in the understanding of the intricacies of the intermolecular interactions present in these systems.

vdW Vibrational Structure in N-Heterocycle Dimers and Solute Solvent Clusters - Calculation of the intermolecular vibrational structure for the N-heterocycle dimers and solute/solvent clusters discussed

in Chapters 4 and 5 can also be conducted. The modeling studies of the N-heterocycle solute/solvent clusters are interesting since they may show the effects of the solute nitrogen atoms on the intermolecular vibrational structure when compared to the analogous benzene solute/solvent clusters. Furthermore, the studies are important as little to no intermolecular vibronic structure is observed in the cluster spectra. In this regard the studies will yield predictions of the frequencies of those vdW modes not observed in the spectra as well as aid in assigning the weak features present in some of the spectra. Intermolecular vibrational structure modeling of the N-heterocycle dimer systems could serve as a major contribution to the understanding of their spectroscopy. The studies may be useful in the determination/confirmation of the dimer geometries responsible for the observed spectra as well as help to elucidate the nature of the intermolecular energetics and dynamics present in the systems. Of particular interest is the elucidation of the vdW torsional structure present in the planar dimers, especially for the vdW torsional coordinate in which the cluster subunits rotate/librate about an axis joining their centers-of-mass. This motion is similar to torsional motion occurring in polyring systems such as biphenyl and biphyridyl. Studying the torsional motion in the clusters may yield information concerning the long-range (π -electron effects) and short-range (hydrogen-hydrogen repulsions) interactions present between the cluster subunits which may be considered precursors to the interactions responsible for the potential well shape in the polyring systems. The studies will also contribute to the understanding of hydrogen bonding interactions in the cluster systems and how it affects cluster geometry and intermolecular energetics.

Conclusions.

Supersonic molecular jet expansion, TOFMS, and FE spectroscopic techniques have been employed to study the gas phase optical spectra of a wide array of weakly bound vdW clusters in an ultracold isolated molecular environment. The techniques have proved useful in studying the vdW clusters of aromatic molecules ranging from benzene and its N-heterocyclic analogues to macrocycles such as H_2Pc and $MgPc$ solvated by small hydrocarbons/fluorocarbons, small alcohols, water, ammonia, argon, and carbon dioxide. The studies reveal detailed information regarding the geometries/symmetries, the intermolecular energetics, and the physical nature of the vdW interactions present in the cluster systems. Spectroscopic observables, such as cluster spectral shifts, forbidden cluster chromophore vibronic transitions, vdW motions, and cluster ionization energies, combined with computer modeling of cluster ground state binding energies, geometries, and intermolecular energetics proves essential in the analysis and understanding of the physics involved in cluster formation, stabilization, and behavior.

The experimental and theoretical studies of the benzene/solvent clusters reveal detailed information regarding cluster geometries, symmetries, and the nature of the intermolecular vibronic motion present in the systems. In these studies, we found that the preferred benzene solvation site is located over the aromatic π cloud where solute/solvent vdW interaction is maximal. Through computer modeling, we have demonstrated the correlation between cluster geometry and spectral features. Specifically, we showed that the calculations yield useful information regarding cluster geometry, binding energy, and intermolecular vibrational structure. These calculated results are consistent with

experiment and can be used to elucidate the details of vdW cluster energetics. By comparing the calculations and the experiments, we are able to assign cluster vibronic transitions to specific cluster geometries and to specific vdW vibrations.

Detailed experimental and theoretical studies of the intermolecular torsional structure in the benzene/solvent clusters show that the clusters are rigid systems with regard to internal rotation of the cluster subunits. In this regard, the clusters possess unique equilibrium geometries for which the intermolecular motion is oscillatory. The motion is not an admixture of vdW bends, stretches, and free internal rotations as would occur if the clusters were internally nonrigid.

The N-heterocycle/solvent cluster studies demonstrate that the solute ring nitrogen atoms influence, to some extent, both the cluster geometry and spectroscopy. In the N-heterocycle/hydrocarbon clusters, we find that the presence of the nitrogen atoms in the aromatic rings has a small but discernible effect on the intermolecular interaction. In particular, the solvent hydrogen atoms preferentially orient towards the solvent nitrogen atoms. The overall behavior of these clusters with regard to geometry, binding energy, and spectroscopy, however, is very similar to that found in the benzene/hydrocarbon clusters.

The N-heterocycle/water and ammonia clusters, on the other hand, clearly demonstrate major interactions between the ring nitrogens and the solvent hydrogens. These studies suggest that hydrogen bonding is present between the ring nitrogens and the solvent hydrogens as evidenced by the hypsochromic spectral shifts present in the cluster spectra.

The single ring/solvent clusters also exhibit spectra and calculated geometries consistent with the notion that the intermolecular potential is primarily composed of solute/solvent π cloud interactions. In this regard, the preferred solvation sites on the cluster solutes are located over the aromatic π clouds. Thus, the cluster geometries are such that the solvents lie over the center of the solutes unless other large intermolecular interactions are present which may alter this behavior. In particular, hydrogen bonding interactions present in the N-heterocycle and benzene/solvent systems appear to cause geometrical changes in the clusters. The changes range from simple reorientation of the solvents to minimize solute ring nitrogen/solvent hydrogen distance or solvent hydrogen/solute π cloud distance to large reorganization of the cluster geometry from a "sitting atop" configuration to planar hydrogen bonded geometries as suggested by pyrimidine/ammonia and N-heterocycle dimer studies.

The spectroscopic studies of phthalocyanines and their respective vdW clusters with small molecules take advantage of the characteristics of the supersonic molecular jet. This technique makes it possible to simplify the complicated phthalocyanine spectra and to control the solvent and environmental effects on the chromophores in a set and controlled manner. The interplay of spectroscopy and an out-of-plane normal coordinate analysis enables us to characterize the low-lying out-of-plane motion present in H_2Pc and $MgPc$. The correlation between the spectra and the calculations is excellent which allows for the elucidation of the motion types observed in the first few hundred wavenumbers of the $H_2Pc/MgPc$ S_1 manifolds. The correlation also makes possible the identification of specific species/geometries responsible for the

cluster vibronic spectra observed in the vicinities of the chromophore Q band origins.

In the cluster studies, we find that the H₂Pc/hydrocarbon cluster experimental and theoretical results parallel those observed for the benzene and N-heterocycle/hydrocarbon clusters. The cluster geometries favor forms for which solvent/solute π cloud overlap is maximal. The spectral shifts are all bathochromic and the magnitudes of the shifts increase with increasing solvent size and polarizability. The H₂Pc and MgPc/water and /alcohol clusters exhibit spectra and calculated geometries which demonstrate that the solvent OH groups are large contributors to the spectral shifts and intermolecular interactions. In all the cluster systems studies, the preferred H₂Pc and MgPc solvation sites are located over the phthalocyano core. As in the benzene/water and benzene/ammonia clusters, the H₂Pc and MgPc clusters exhibit reduced symmetry with respect to the isolated chromophores. This reduction in symmetry is demonstrated by the observation of forbidden chromophore transitions and S₁ state splitting in the clusters.

Overall, computer modeling proved to be an essential component of the studies on both the isolated molecules and the cluster systems. The spectroscopic data obtained are necessary to validate and refine the models used, and the calculations help to assign and understand spectra which are otherwise difficult, if not impossible, to uniquely interpret. In this way, the combination of spectroscopy and computer modeling leads to an increased understanding of the behavior of the molecules and clusters over what could be obtained by either study alone.

REFERENCES

1. Martin Gouterman. Optical Spectra and Electronic Structure of Porphyrins and Related Rings, in "The Porphyrins" edited by David Dolphin (Academic Press, New York) Vol. III, 1978.
2. Uzi Even, Jacob Magen, and Joshua Jortner, J. Chem. Phys. 77, 4384 (1982).
3. S. Sunder and H.J. Bernstein, J. of Raman Spectros. 5, 351 (1976).
4. M. Abe, T. Kitagawa, and Y. Kyogoku, J. Chem. Phys. 69, 4526 (1978).
5. C.A. Melandres and V.A. Maroni, J. of Raman Spectros. 15, 319 (1984).
6. L.L. Gladkov and K.N. Solovyov, Spectrochimica Acta. 41, 1437 (1985); 41, 1443 (1985); 42, 1 (1986).
7. L.L. Gladkov, A.T. Gradyushko, A.M. Shulga, K.N. Solovyov, and A.S. Starukhin, J. of Molecular Structure 47, 463 (1978).

APPENDIX ONE

HYDROGEN BONDED AND NON-HYDROGEN BONDED VAN DER WAALS
CLUSTERS: COMPARISON BETWEEN CLUSTERS OF PYRAZINE, PYRIMIDINE,
AND BENZENE WITH VARIOUS SOLVENTS

Hydrogen bonded and non-hydrogen bonded van der Waals clusters: Comparison between clusters of pyrazine, pyrimidine, and benzene with various solvents^{a)}

J. Wanna, J. A. Menapace, and E. R. Bernstein

Department of Chemistry, Condensed Matter Sciences Laboratory, Colorado State University, Fort Collins, Colorado 80523

(Received 13 December 1985; accepted 1 May 1986)

Solute-solvent clusters of pyrazine, pyrimidine, and benzene (solutes) and C_nH_{2n+2} ($n = 1, 2$), NH_3 , and H_2O (solvents) are studied by the techniques of supersonic molecular jet spectroscopy and two-color time-of-flight mass spectroscopy (two-color TOFMS). Spectral shifts, van der Waals (vdW) modes, dissociation energies, and vdW mode-solute mode vibronic couplings are characterized for most of the observed clusters. Based on these data and previous results for hydrocarbon systems, cluster geometries can be suggested. Lennard-Jones potential (6-12-1) calculations are also performed for these clusters and in all instances for which comparisons can be readily made, calculated and experimentally estimated geometries and binding energies agree completely. Clusters of *N*-heterocyclic solutes and H_2O are not observed experimentally. Systematics and trends among the clusters reported herein and those previously reported are discussed and analyzed.

I. INTRODUCTION

Supersonic molecular jet spectroscopy has made possible the study of a wide variety of weakly bound, solute-solvent van der Waals (vdW) clusters in the gas phase. Cluster investigations have enhanced our understanding of intra- and intermolecular interactions and potentials, vibrational energy dynamics and chemical reactions, structural properties of small aggregates of solute and solvent molecules, and nucleation and growth of small clusters. Clusters can also be considered as model systems for condensed phase behavior. Moreover, these vdW systems can be thought of as an important new state of matter in which the static and dynamic properties of small aggregates of weakly coupled molecules can be studied.

vdW clusters, after being produced in a supersonic jet expansion, can be probed by three distinct techniques: fluorescence excitation (FE), dispersed emission (DE), and two-color time-of-flight mass spectroscopy (two-color TOFMS). The latter technique is employed most often in our studies of clusters because it gives unique cluster identification, brackets the cluster binding energies, and elucidates cluster vibrational energy dynamics and vibrational predissociation.

In the past few years, we have reported several studies of vdW clusters using the three spectroscopic techniques mentioned above.¹⁻⁷ Cluster geometry, binding energy, nucleation and growth dynamics, and limits on the vibrational energy dynamics and vibrational predissociation times have been determined. The vdW solute-solvent clusters investigated initially are for the most part restricted to aromatic hydrocarbon solutes (e.g., benzene and toluene) and small alkane solvents (CH_4 , C_2H_6 , and C_3H_8) in which only one type of interaction, that is one potential form, is found to be

important for the solute-solvent coordination. Expanding on these previous studies we are now exploring solute-solvent clusters with *N*-heterocyclic solutes (e.g., pyrazine and pyrimidine) and alkane solvents and *N*-heterocyclic solutes with hydrogen bonding solvents (e.g., water and ammonia). The initial report of this effort for pyrazine and methane, ethane and propane clusters has already appeared.⁷

In this paper we discuss the two-color TOFMS study of pyrimidine clustered with CH_4 and C_2H_6 , pyrazine and pyrimidine clustered with NH_3 , and benzene clusters with H_2O and NH_3 . The pyrimidine-alkane clusters are presented for comparison with the previously published⁷ pyrazine-alkane data: The effect of the ring nitrogen atoms on the cluster geometry can thereby be evaluated. The pyrazine and pyrimidine ammonia clusters reveal the role of hydrogen bonding interactions in simple clusters. Benzene-water and -ammonia clusters serve as an example of clusters with these more complicated solvent systems (i.e., two possible interaction potentials) interacting with aromatic hydrocarbons. Theoretical and experimental studies of such a series of systems should eventually lead to a fuller understanding of solute-solvent coordination structure, dynamics, and the hydrogen bonding interaction.

Although extensive efforts were made and a wide variety of experimental conditions explored, pyrazine and pyrimidine clusters with water were not observed. Both FE and two-color TOFMS detection techniques were employed. A broad feature (roughly 50 cm^{-1} FWHM) was observed in FE at 580 cm^{-1} to the blue of pyrazine 0_0^0 transition for pyrazine and water expanded with helium. No signal, however, was observed at the pyrazine water mass channel for two-color TOFMS. We must thus conclude that the pyrazine and the pyrimidine water clusters have not been observed. Either the excited $n\pi^*$ state of the cluster is dissociative or internal conversion or intersystem crossing is so rapid for these clusters that the lifetime of the $n\pi^*$ state is greatly reduced (~ 0.1 ps). Pyrimidine-fluorinated alcohol clusters

^{a)} Supported in part by grants from ONR and the Philip Morris Corporation.

also exhibit broad features and reduced lifetimes.⁸

Hydrogen bonding interactions are known to play an important role in intra- and intermolecular interactions important for secondary and tertiary molecular structure, molecular dynamics, and ionic and molecular solvation. Hydrogen bonding interactions have received attention in previous supersonic molecular jet spectroscopic studies: These systems include phenol clustered with various proton accepting molecules,⁹ indole and 2-aminopyridine clustered with various solvents,¹⁰ benzoic acid dimers,¹¹ *s*-tetrazine dimers,¹² 1,4-dihydroxyanthraquinone,¹³ and methylsalicylate.¹⁴ In most instances blue-shifted cluster spectra are found due to the cluster stabilization of the ground state and destabilization of the excited state.¹⁵

In this and our other cluster studies, the experimental data are supplemented by potential energy Lennard-Jones (LJ) atom-atom (6-12-1) calculations of cluster structure, binding energy, and internal motion. The calculations and the potential are discussed thoroughly in our previous studies.⁷ The LJ calculations produce identical geometries but slightly lower binding energies than the exp-6 potential form used in earlier calculations.¹⁻⁶ The LJ hydrogen bonding (LJ-HB) potential form proves to be more versatile than the exp-6 form since many more constants for different types of atom-atom interactions have been independently reported for the LJ potential.¹⁶ None of the potential parameters employed in this work is fit to the cluster data.

As is well known and widely accepted, geometries of isolated molecules and clusters are best obtained through spectroscopic observation of rotational structure. In fact, rotational structure of a number of simple clusters has been observed under molecular jet conditions: *s*-tetrazine and iodine with He and Ar¹⁷ and aniline with Ne and Ar.¹⁸ The resolution available to us at present is 0.08 cm⁻¹; at this resolution only rotational envelopes are observable which do not lend themselves readily to a unique interpretation of cluster structure. We calculate that 0.005 cm⁻¹ resolution would be required to resolve rotational structure for C₄H₄N₂(NH₃), etc., under the restriction of a rigid geometry. We are thus for the present forced to employ less direct methods to obtain cluster geometry. Assignment of the spectra is accomplished through the determination of ionization energies, spectral shifts, relative intensities, (molecular) symmetry forbidden cluster transitions, and potential calculations. The understanding of these more complex systems rests heavily on the previous data obtained for other clusters.¹⁻⁷ For all systems discussed in this paper, complete agreement between spectroscopic data, calculations, and results for previously analyzed solute-solvent clusters is found.

II. EXPERIMENTAL PROCEDURES

The experimental apparatus and procedures are similar to those used previously for the study of vdW clusters. The vacuum system consists of two chambers with a pulsed nozzle and mass detection system in the second chamber. A skimmer separates the pulsed nozzle and the time-of-flight mass spectrometer. The first chamber contains either a pulsed or cw nozzle, the molecular beam from which can be

taken into the second chamber through a skimmer. FE and DE experiments are carried out in the first chamber.

The two independent Nd³⁺/YAG pulsed lasers the doubled output of which pumps two dye lasers. The dye laser output can be mixed with the 1.064 μm Nd³⁺/YAG fundamental, frequency mixed and doubled, or just doubled using various nonlinear KDP crystals. The laser output can be extended from greater than 4.5 to ~0.215 μm. One laser is employed to excite the cluster to its first excited *nπ** or *ππ** electronic state and the second laser then ionizes this cluster starting from the S₁ vibronic manifold. The maximum ionization energy achievable with this second laser is roughly 46 500 cm⁻¹.

The solute or cluster chromophore is typically placed in an in-line trap or filter cup directly behind the pulsed valve. Water is placed in a trap before the valve and solute; the helium carrier gas passes over both materials and into the valve. Gaseous solvents are premixed with the helium carrier gas in a holding tank (~2000 psi) at concentrations varying from 2.0 to 0.1 mol/mol.

The LJ potential function (6-12-1) with the additional HB form is described in detail in a previous publication.⁷ Table I contains a list of the previously unreported constants employed with this potential form. Pyrazine and pyrimidine structures used in the calculations are obtained from Ref. 19.

TABLE I. Parameters for the energy expression in the computer modeling.

$E_q = 1.16 \times 10^2 q_i q_j / 2r_{ij} + A_q / r_{ij}^{12} - C_q / r_{ij}^6 \text{ (LJ)}$		
	$A \left(\frac{\text{cm}^{-1} \text{Å}^{12}}{\text{mol}} \right)$	$C \left(\frac{\text{cm}^{-1} \text{Å}^6}{\text{mol}} \right)$
Amine-aromatic		
N-N	1.312×10^8	1.403×10^5
N-C	1.728×10^8	1.575×10^5
N-H	2.523×10^7	4.527×10^4
H-C	2.749×10^7	5.217×10^4
H-H	3.872×10^6	1.590×10^4
H-N	1.990×10^7	4.527×10^4
Water-aromatic		
O-N	7.548×10^7	1.021×10^5
O-C	9.868×10^7	1.130×10^5
O-H	1.363×10^7	3.162×10^4
H-C	3.160×10^7	5.217×10^4
H-H	4.537×10^6	1.590×10^4
H-N	2.297×10^7	4.527×10^4
$E_q = 1.16 \times 10^2 q_i q_j / 2r_{ij} + A' / r_{ij}^{12} - B' / r_{ij}^{10} \text{ (HB)}$		
	$A' \left(\frac{\text{cm}^{-1} \text{Å}^{12}}{\text{mol}} \right)$	$B' \left(\frac{\text{cm}^{-1} \text{Å}^{10}}{\text{mol}} \right)$
H...N	1.150×10^7	2.882×10^6
q		
NH ₃ :	N	-0.438
	H	+0.146
H ₂ O:	O	-0.34
	H	+0.17
C ₄ H ₄ N ₂ :	N	-0.182
	C	+0.091
	H	0
C ₄ H ₆ :	C	-0.0074
	H	+0.0074

also exhibit broad features and reduced lifetimes.⁸

Hydrogen bonding interactions are known to play an important role in intra- and intermolecular interactions important for secondary and tertiary molecular structure, molecular dynamics, and ionic and molecular solvation. Hydrogen bonding interactions have received attention in previous supersonic molecular jet spectroscopic studies: These systems include phenol clustered with various proton accepting molecules,⁹ indole and 2-aminopyridine clustered with various solvents,¹⁰ benzoic acid dimers,¹¹ *s*-tetrazine dimers,¹² 1,4-dihydroxyanthraquinone,¹³ and methylsalicylate.¹⁴ In most instances blue-shifted cluster spectra are found due to the cluster stabilization of the ground state and destabilization of the excited state.¹⁵

In this and our other cluster studies, the experimental data are supplemented by potential energy Lennard-Jones (LJ) atom-atom (6-12-1) calculations of cluster structure, binding energy, and internal motion. The calculations and the potential are discussed thoroughly in our previous studies.⁷ The LJ calculations produce identical geometries but slightly lower binding energies than the exp-6 potential form used in earlier calculations.¹⁻⁶ The LJ hydrogen bonding (LJ-HB) potential form proves to be more versatile than the exp-6 form since many more constants for different types of atom-atom interactions have been independently reported for the LJ potential.¹⁶ None of the potential parameters employed in this work is fit to the cluster data.

As is well known and widely accepted, geometries of isolated molecules and clusters are best obtained through spectroscopic observation of rotational structure. In fact, rotational structure of a number of simple clusters has been observed under molecular jet conditions: *s*-tetrazine and iodine with He and Ar¹⁷ and aniline with Ne and Ar.¹⁸ The resolution available to us at present is 0.08 cm⁻¹; at this resolution only rotational envelopes are observable which do not lend themselves readily to a unique interpretation of cluster structure. We calculate that 0.005 cm⁻¹ resolution would be required to resolve rotational structure for C₄H₄N₂(NH₃)₁ etc., under the restriction of a rigid geometry. We are thus for the present forced to employ less direct methods to obtain cluster geometry. Assignment of the spectra is accomplished through the determination of ionization energies, spectral shifts, relative intensities, (molecular) symmetry forbidden cluster transitions, and potential calculations. The understanding of these more complex systems rests heavily on the previous data obtained for other clusters.¹⁻⁷ For all systems discussed in this paper, complete agreement between spectroscopic data, calculations, and results for previously analyzed solute-solvent clusters is found.

II. EXPERIMENTAL PROCEDURES

The experimental apparatus and procedures are similar to those used previously for the study of vdW clusters. The vacuum system consists of two chambers with a pulsed nozzle and mass detection system in the second chamber. A skimmer separates the pulsed nozzle and the time-of-flight mass spectrometer. The first chamber contains either a pulsed or cw nozzle, the molecular beam from which can be

taken into the second chamber through a skimmer. FE and DE experiments are carried out in the first chamber.

The two independent lasers used in the two-color TOFMS experiments are Nd³⁺/YAG pulsed lasers the doubled output of which pumps two dye lasers. The dye laser output can be mixed with the 1.064 μm Nd³⁺/YAG fundamental, frequency mixed and doubled, or just doubled using various nonlinear KDP crystals. The laser output can be extended from greater than 4.5 to ~0.215 μm. One laser is employed to excite the cluster to its first excited $n\pi\pi^*$ or $\pi\pi^*$ electronic state and the second laser then ionizes this cluster starting from the *S*₁ vibronic manifold. The maximum ionization energy achievable with this second laser is roughly 46 500 cm⁻¹.

The solute or cluster chromophore is typically placed in an in-line trap or filter cup directly behind the pulsed valve. Water is placed in a trap before the valve and solute; the helium carrier gas passes over both materials and into the valve. Gaseous solvents are premixed with the helium carrier gas in a holding tank (~2000 psi) at concentrations varying from 2.0 to 0.1 mol/mol%.

The LJ potential function (6-12-1) with the additional HB form is described in detail in a previous publication.⁷ Table I contains a list of the previously unreported constants employed with this potential form. Pyrazine and pyrimidine structures used in the calculations are obtained from Ref. 19.

TABLE I. Parameters for the energy expression in the computer modeling.

$E_q = 1.16 \times 10^3 q_i q_j / 2r_{ij} + A_i / r_{ij}^{12} - C_{ij} / r_{ij}^6 \text{ (LJ)}$		
	$A \left(\frac{\text{cm}^{-1} \text{Å}^{12}}{\text{mol}} \right)$	$C \left(\frac{\text{cm}^{-1} \text{Å}^6}{\text{mol}} \right)$
Amine-aromatic		
N-N	1.312 × 10 ⁸	1.403 × 10 ³
N-C	1.728 × 10 ⁸	1.575 × 10 ³
N-H	2.523 × 10 ⁷	4.527 × 10 ²
H-C	2.749 × 10 ⁷	5.217 × 10 ²
H-H	3.872 × 10 ⁶	1.590 × 10 ¹
H-N	1.990 × 10 ⁷	4.527 × 10 ²
Water-aromatic		
O-N	7.548 × 10 ⁷	1.021 × 10 ³
O-C	9.868 × 10 ⁷	1.130 × 10 ³
O-H	1.363 × 10 ⁷	3.162 × 10 ²
H-C	3.160 × 10 ⁷	5.217 × 10 ²
H-H	4.537 × 10 ⁶	1.590 × 10 ¹
H-N	2.297 × 10 ⁷	4.527 × 10 ²
$E_q = 1.16 \times 10^3 q_i q_j / 2r_{ij} + A' / r_{ij}^{12} - B / r_{ij}^{10} \text{ (HB)}$		
	$A' \left(\frac{\text{cm}^{-1} \text{Å}^{12}}{\text{mol}} \right)$	$B \left(\frac{\text{cm}^{-1} \text{Å}^{10}}{\text{mol}} \right)$
H...N	1.150 × 10 ⁷	2.882 × 10 ⁶
q		
NH ₃ :	N	-0.438
	H	+0.146
H ₂ O:	O	-0.34
	H	+0.17
C ₄ H ₄ N ₂ :	N	-0.182
	C	+0.091
	H	0
C ₆ H ₆ :	C	-0.0074
	H	+0.0074

III. RESULTS

This section contains the experimental and calculation results for the various clusters investigated. We first present pyrimidine with methane and ethane for comparison with the previously reported pyrazine clusters.⁷ Pyrimidine and pyrazine ammonia clusters are then discussed and benzene water and ammonia clusters are presented for a comparison with the *N*-heterocyclic systems. Based on previous experience with a number of different clusters,¹⁻⁷ we have not made an extensive experimental study of the binding energies of these clusters. We rely on the calculations which have always fallen within the range bracketed by the experimental two-color TOFMS data. Preliminary checks made on both pyrazine and pyrimidine clusters are in agreement with the calculations. Vibrational vdW modes observed in the spectra will not be assigned in this publication. Future publications will assign them as bends, stretches, torsions, and combinations utilizing a normal coordinate calculational analysis.²⁰

A. Pyrimidine-methane

Figure 1 and Table II present the data for the pyrimidine (CH_4)₁ and (CH_4)₂ complexes taken near the pyrimidine O_0^0 transition ($31\,073.0\text{ cm}^{-1}$). The cluster of pyrimidine (CH_4)₁ has a spectral shift of -56.6 cm^{-1} and a low frequency mode at 4.5 cm^{-1} from this origin. These spectra are obtained by two-color TOFMS. Hints of other vdW modes can also be seen in the trace in Fig. 1 but we are hesitant to report such weak transitions. Pyrimidine (CH_4)₂ spectra clearly show two clusters, similar to previously reported clusters for other aromatic systems.¹⁻⁷ The feature at -112.1 cm^{-1} in Fig. 1 is assigned as the O_0^0 transition of the isotropic (symmetric), additive shift cluster and the feature at -47.2 cm^{-1} is attributed to the O_0^0 transition of the anisotropic (asymmetric) cluster with both methanes on the same side of the aromatic ring. Note that without both mass and energy resolution, the spectra of pyrimidine (CH_4)₁ and (CH_4)₂ would not be resolved and the clusters could not be separated and uniquely identified. A vdW mode at 5.1 cm^{-1} from the isotropic cluster origin is observed.

Potential energy calculations using LJ potentials for these clusters generate geometries and binding energies comparable to those previously reported for other aromatic-al-

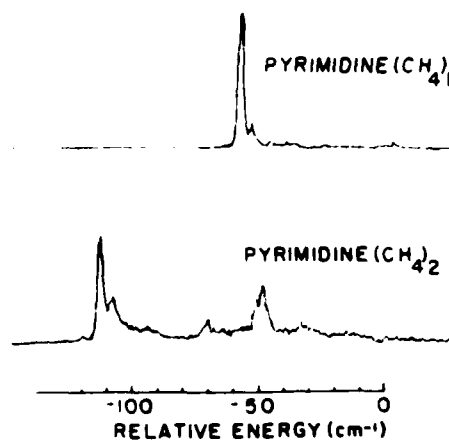


FIG. 1. Two-color time-of-flight mass spectra (two-color TOFMS) of pyrimidine (CH_4)₁ and pyrimidine (CH_4)₂ in the region of the pyrimidine origin ($31\,073.0\text{ cm}^{-1}$).

kane systems and in complete accord with the above experimental findings (see Fig. 2). Calculations for pyrimidine (CH_4)₁ clusters yield only one geometry for which the methane is coordinated with the aromatic π system of the pyrimidine ring. The calculated binding energy for this cluster is 514 cm^{-1} . The methane-carbon atom is above the ring at 3.5 \AA and is shifted $\sim 0.1\text{ \AA}$ from the ring center toward the nitrogen atoms. The three hydrogen atoms of methane that point down toward the ring are equidistant from the ring at 3.1 \AA ; two of these hydrogens point directly at the ring nitrogen atoms. Again in agreement with the main experimental observations for these clusters, the calculations for pyrimidine (CH_4)₂ clusters yield two distinct geometrical arrangements. The isotropic cluster has a calculated binding energy of 1029 cm^{-1} and the anisotropic cluster has a calculated binding energy of 879 cm^{-1} .

B. Pyrimidine-ethane

The pyrimidine (C_2H_6)₁ spectrum is quite complicated, consisting of a number of low intensity features and an intense feature at -60.7 cm^{-1} with respect to the pyrimidine

TABLE II Observed peaks in the spectra of pyrimidine-methane clusters.

Species	Energy (vac cm^{-1})	Energy relative to pyrimidine O_0^0 (cm^{-1})	Energy relative to cluster O_0^0 (cm^{-1})	Assignment ^a
$\text{C}_4\text{H}_6\text{N}_2(\text{CH}_4)_1$	31 016.4	-56.6	0	O_0^0
	31 020.9	-52.1	4.5	
$\text{C}_4\text{H}_6\text{N}_2(\text{CH}_4)_2$	30 960.9	-112.1	0	iso O_0^0
	30 966.0	-107.0	5.1	
	31 025.8	-47.2	0	aniso O_0^0

^a The -112.1 cm^{-1} shift is associated with two methanes added symmetrically above and below the pyrimidine ring (isotropic), as shown in Fig. 2. The -47.2 cm^{-1} shift is associated with the anisotropic configuration, as shown in Fig. 2.

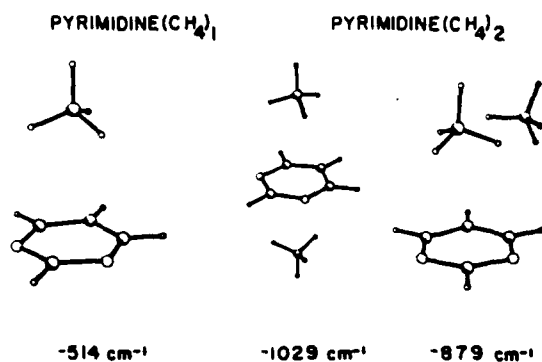


FIG. 2. Minimum energy configurations and binding energies for pyrimidine (C_4H_4), and pyrimidine (C_4H_6), as obtained using the LJ potential calculation described in the text.

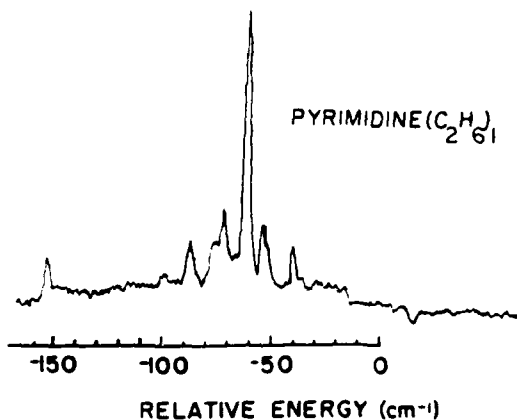


FIG. 3. Two-color TOFMS of pyrimidine (C_2H_6), in the region of the pyrimidine origin.

origin (see Fig. 3). We might expect that little vdW vibronic intensity would be observed, based on pyrazine and other pyrimidine clusters. In order to begin to interpret these features we must consult the vapor phase room temperature pyrimidine monomer spectrum.²¹ In these reports, features at -156 and $+22$ cm^{-1} are assigned as the $16a_1^+$ and $16b_1^+$ sequence bands, respectively. The feature that appears in Fig. 3 at -39.1 cm^{-1} may be assigned as the $16b_1^+$ sequence band of the pyrimidine (C_2H_6)₁ cluster built on the intense -60.7 cm^{-1} cluster origin. If this identification is correct, then the clusters of pyrimidine (C_2H_6)₁ are hot ($T_{\text{rot}} \approx 260$ K) and the features in Fig. 3 and Table II at -153.5 , -99.3 , -86.9 , and -75.4 cm^{-1} may well be hot bands associated with the cluster origins at -71.4 , -60.7 , and -52.7 cm^{-1} . Apparently the cluster formation process for pyrimidine ethane tends to warm the cluster. Table III summarizes these results.

Supersonic expansion of pyrimidine apparently does not produce the expected cooling for vibrational modes $16b_1$ and $16a_1$. Vibrational temperatures for the $16b_1$ mode have been reported to be in excess of 200 K. Ito and co-workers^{21d} have also observed the $16b_1^+$ transition for pyrimidine clustered with argon and nitrogen. In the present work, changes in backing pressure from 10 to 120 psi do not change the rela-

tive band intensities: apparently these modes present a bottleneck for vibrational cooling.

As can be seen in Fig. 4, three different configurations are calculated to be stable for the pyrimidine (C_2H_6)₁ cluster. Configuration I has the long axis of ethane perpendicular to the plane of the pyrimidine ring. Configurations II and III have the ethane molecule long axis more or less parallel to the plane of the ring; for configuration II, the axis of ethane lies between a nitrogen and a carbon and for configuration III this axis lies between two carbon atoms. In each instance a CH_3 group lies more or less over the ring center.

C. Pyrimidine-ammonia

The pyrimidine (NH_3)₁ two-color TOFMS spectrum in the range 300 to 500 cm^{-1} to the blue of the pyrimidine origin is presented in Fig. 5. The three features are associated with the 0_0^0 transitions of the pyrimidine (NH_3)₁ clusters. The lack of significant vdW vibrational mode intensity indicates that the ground and excited state vdW potentials are nearly identical. The large cluster blue shift implies a strong hydrogen bonding interaction between the pyrimidine and the ammonia. The spectrum of Fig. 5 is taken with an ioniza-

TABLE III. Observed peaks in the spectra of pyrimidine-ethane clusters.

Species	Energy	Energy relative to pyrimidine 0_0^0 (cm^{-1})	Energy relative to cluster 0_0^0 (cm^{-1})	Tentative assignment
$\text{C}_4\text{H}_6\text{N}_2(\text{C}_2\text{H}_6)_1$	30 919.5	-153.5		
	30 973.7	-99.3		
	30 986.1	-86.9		
	30 997.6	-75.4		
	31 001.6	-71.4	0	I 0_0^0
	31 012.3	-60.7	0	II 0_0^0
	31 020.3	-52.7	0	III 0_0^0
	31 033.9	-39.1	21.6	II $16b_1^+$

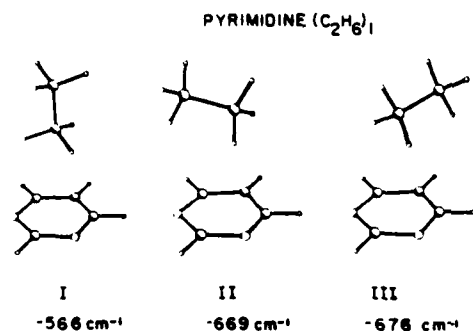


FIG. 4. Minimum energy configurations and binding energies for pyrimidine (C₂H₆)₁, as obtained using a LJ potential calculation.

tion energy of 45 110 cm⁻¹; lowering the ionization energy to ~42 000 cm⁻¹ the two nearly degenerate features at +367 cm⁻¹ decrease in intensity much more rapidly than the feature at +496 cm⁻¹. Table IV gives the energies and assignments for the pyrimidine (NH₃)₁ clusters. Based on the idea that the three features in this spectrum are associated with three different pyrimidine (NH₃)₁ cluster geometries, the two nearly isoenergetic configurations must be quite similar. The feature at +496 cm⁻¹ must correspond to a different (more hydrogen bonded) geometry.

Three different configurations are calculated for the pyrimidine (NH₃)₁ cluster using the LJ-HB potential form (see Table I and Ref. 7). Two of these configurations have the ammonia above the pyrimidine plane and the third configuration has the NH₃ molecule not above the ring. These clusters are presented in Fig. 6 along with the calculated cluster binding energies. Configuration I has the ammonia N-atom 3.2 Å above the pyrimidine ring with the three am-

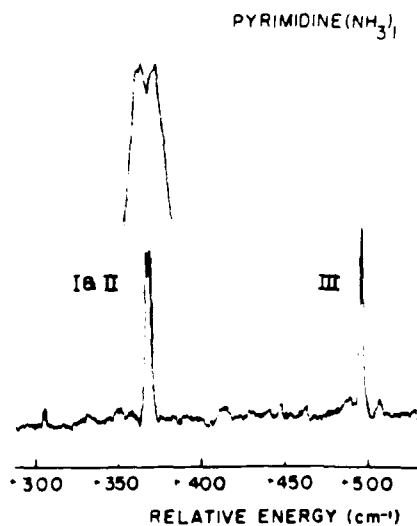


FIG. 5. Two-color TOFMS of pyrimidine (NH₃)₁ in the region 300–500 cm⁻¹ to the blue of the pyrimidine origin. An insert is shown of the first two features with an expanded scale.

monia hydrogen atoms pointing down toward the π cloud. The two closest hydrogen atoms of the ammonia in this configuration are 2.7 Å from the pyrimidine plane. In configuration II, the ammonia nitrogen atom is 3.2 Å above the ring plane and points in the general direction of the ring N atoms. The closest two ammonia hydrogen atoms to the ring are at 2.7 Å. This cluster has a somewhat lower binding energy than cluster I (667 vs 689 cm⁻¹). In the third pyrimidine (NH₃)₁ configuration, the ammonia molecule does not reside over the pyrimidine ring: the NH₃ has a N–H bond in

TABLE IV. Pyrimidine (NH₃)₁.

Energy (vac. cm ⁻¹)	Energy relative to corresponding pyrimidine feature (cm ⁻¹)	Energy relative to corresponding pyrimidine-ammonia feature (cm ⁻¹)	Assignment
31 378.2	305.2	-60.9	
31 439.1	366.1	0	I 0 _g
31 441.0	368.0	0	II 0 _g
31 485.7	412.7	46.6	
31 520.0	447.0	80.9	
31 535.2	462.2	96.1	
31 561.3	488.3	122.2	
31 568.9	495.9	0	III 0 _g
31 579.3	506.3	10.4	
31 610.1	537.1	41.2	
31 685.1	612.1	116.2	
32 044.6	360.6	0	I 6a ₁
32 050.8	366.8	0	II 6a ₁
32 097.2	355.2	0	I 6b ₁
32 108.2			
32 121.5	379.5	0	II 6b ₁
32 162.6			
32 176.1	492.1	0	III 6a ₁
32 224.7	482.7	0	III 6b ₁

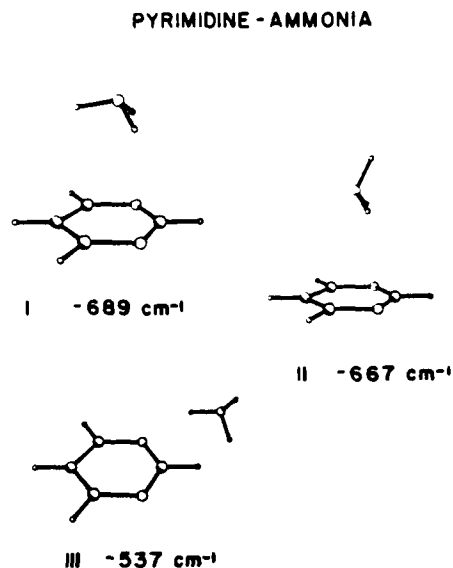


FIG. 6. Minimum energy configurations and binding energies for pyrimidine (NH_3), as obtained using a LJ plus HB potential calculation.

the plane of the pyrimidine ring with the H atom pointing to one of the pyrimidine nitrogens, 2.23 Å from it. The ammonia nitrogen is displaced in the xy plane by 3.3 and 2.8 Å along the x axis and y axis, respectively, as shown in Fig. 6, configuration III. This configuration has a calculated binding energy of 537 cm^{-1} .

D. Pyrazine-ammonia

The pyrazine (NH_3)₁ spectra in the 0_0^0 , $10a_0^1$, and $6a_0^1$ regions are presented in Fig. 7. One first notices the significant difference between these data and those of pyrimidine (NH_3)₁. The spectra all strongly suggest that only one configuration is present for the pyrazine (NH_3)₁ system. The intense feature in the 0_0^0 spectrum is the cluster origin at + 117 cm^{-1} from the pyrazine 0_0^0 transition. The remaining features of this spectrum are vdW vibrational modes of the cluster. They will be analyzed in a future publication.²⁰ Table V gives the energies and the features observed in the spectrum. In this case, the ground and excited state potential surfaces must be significantly different.

The cluster $10a_0^1$ transition is quite different from the cluster 0_0^0 or $6a_0^1$ transitions. From this one concludes that strong vdW-internal mode coupling exists for the $10a_0^1$ out of plane ring mode.²² The vdW overtones and combination bands extend to more than 180 cm^{-1} from the $10a_0^1$ cluster origin feature. This is particularly striking in comparison with the $6a_0^1$ vibronic band.

Only one configuration is calculated for the pyrazine (NH_3)₁ cluster using the LJ plus HB potential function, in agreement with expectations from the spectra. The ammonia molecule hydrogen bonds to the ring nitrogens,

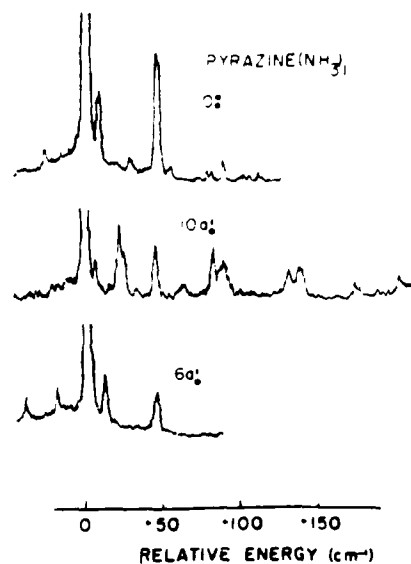


FIG. 7. Two-color TOFMS of pyrazine (NH_3), at the origin, $10a_0^1$, and $6a_0^1$ regions are shown. The cluster origin (0 cm^{-1}) is + 117 cm^{-1} to the blue of the pyrazine origin.

through two ammonia hydrogens. The nitrogen atom of the ammonia molecule is 3.2 Å above the ring plane with all three hydrogens pointing toward the ring. This geometry is depicted in Fig. 8. The calculated binding energy of the cluster is 677 cm^{-1} .

E. Benzene-ammonia

The origin and 6_0^1 transitions of the $\text{C}_6\text{H}_6(\text{NH}_3)_1$ cluster are observed in two-color TOFMS. One can immediately conclude that at least one configuration of this cluster does not retain the benzene threefold axis. The spectra are traced in Fig. 9. The spectra for both transitions are far more complicated than any other cluster previously reported from our laboratory. Regions with similar structure can be found in the 0_0^0 and 6_0^1 spectra; in particular, the regions around + 20, - 20 and - 60 cm^{-1} in each spectra bear some resemblance to one another. Nonetheless, features appearing in one spectrum do not appear in the other, and therefore at least two clusters of different geometry are probably responsible for the 6_0^1 transition. The 0_0^0 transition could arise from one reduced symmetry cluster. Since very little *a priori* spectroscopic analysis seems possible in this situation at the present time, great stock must be placed in the calculations.

Two different configurations are calculated for the $\text{C}_6\text{H}_6(\text{NH}_3)_1$ cluster and both of them have the NH_3 molecule placed over the ring. Configuration I in Fig. 10 preserves the benzene C_3 axis and configuration II does not. The high symmetry cluster has the N atom 3.3 Å from the ring plane and the three H atoms of NH_3 are 2.9 Å above the ring plane. Configuration II has the N atom 3.3 Å above the plane and slightly shifted from the ring center. Two H atoms of the

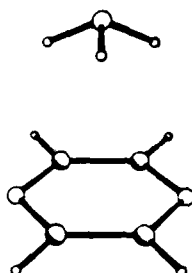
TABLE V. Pyrazine (NH₂)₂.

Energy (vac. cm ⁻¹)	Energy relative to corresponding pyrazine feature (cm ⁻¹)	Energy relative to corresponding pyrazine- ammonia cluster (cm ⁻¹)	Assignment
30 967.3	91.3	-25.7	
30 993.0	117.0	0	0 _g ⁺
31 000.8	124.8	7.8	
31 019.5	143.5	26.5	
31 036.5	160.5	43.5	
31 043.6	167.6	50.6	
31 045.4	169.4	52.4	
31 067.3	191.3	74.3	
31 070.0	194.0	77.0	
31 077.4	201.4	84.4	
31 089.9	213.9	96.9	
31 093.7	217.7	100.7	
31 099.2	223.2	106.2	
31 378.7	119.7	0	10 a _g ⁺
31 384.9	125.9	6.2	
31 400.5	141.5	21.8	
31 403.7	144.7	25.0	
31 424.3	165.3	45.6	
31 441.8	182.8	63.1	
31 461.3	202.3	(82.6) ^a	
31 467.5	208.5	(88.8)	
31 507.5	248.5	128.8	
31 513.7	254.7	135.0	
31 539.5	280.5	160.8	
31 559.7	300.7	181.0	
31 580.2	120.5	0	6 a _g ⁺
31 590.8	131.1	10.6	
31 624.8	165.1	44.6	

^a May be associated with other pyrazine features.

NH₂ point towards C-C bonds and one points away from the ring plane. The NH₂ H-atoms in this configuration are at 2.9 (two of them) and 4.3 Å from the ring. The calculated binding energies of these two configurations are given in Fig. 10. Configuration II alone must generate the 0_g⁺ spectrum in Fig. 9.

PYRAZINE - AMMONIA



-677 cm⁻¹

FIG 8 Minimum energy configuration and binding energy for pyrazine (NH₂)₂, as obtained using a LJ HB form potential calculation.

F. Benzene-water

The C₆H₆(H₂O)₂ cluster 0_g⁺ and 6_g⁺ are presented in Fig. 11. They are strikingly different from those of C₆H₆(NH₂)₂ (Fig. 9) but bear a strong resemblance to the pyrazine (NH₂)₂ spectra displayed in Fig. 7, as well as spectra of other systems studied in our laboratory.¹⁻⁷ In particular, a very clear vibronic progression is present for the 0_g⁺ spectrum and will be analyzed in a future publication.²⁰ Table VI gives

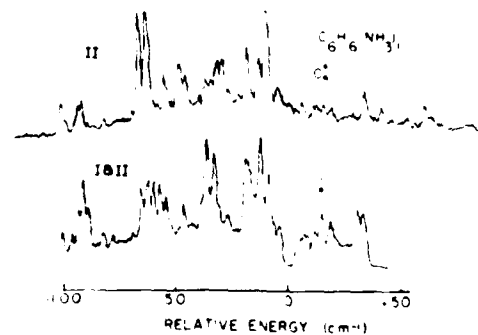


FIG 9 Two-color TOFMS of benzene (NH₂)₂, in the region of the benzene 0_g⁺ and 6_g⁺ transitions.

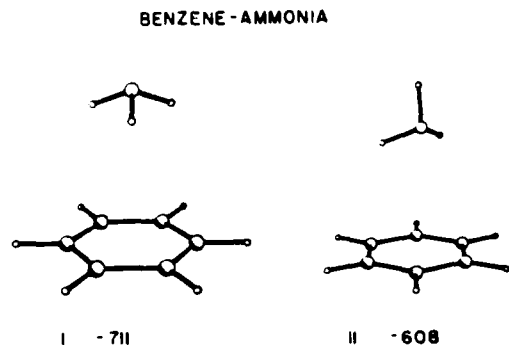


FIG. 10. Minimum energy configurations and binding energies for benzene (NH_3), as obtained using a LJ potential calculation.

these features and their energies. The 6_0^1 spectrum of $\text{C}_6\text{H}_6(\text{H}_2\text{O})_1$ has a different shift ($+50$ vs $+85$ cm^{-1}) and a different general pattern than the 0_0^0 . In addition, the 6_0^1 origin is split by roughly 1 cm^{-1} . Considerable vibronic coupling must occur between the in plane carbon-carbon stretch 6^1 and the vdW modes. The $\text{C}_6\text{H}_6(\text{H}_2\text{O})_1$ cluster two-color TOFMS spectra are observed only at a higher ionization energy than required to observe the 6_0^1 spectrum of bare C_6H_6 . The $\text{C}_6\text{H}_6(\text{H}_2\text{O})_1$ spectra depicted in Fig. 11 are taken with an ionization laser energy of $44\,480$ cm^{-1} compared to $36\,100$ cm^{-1} for the benzene monomer. The ionization energy for the benzene water cluster is 3300 cm^{-1} higher than that of the benzene monomer.

Only one geometry is calculated for the $\text{C}_6\text{H}_6(\text{H}_2\text{O})_1$ cluster employing the LJ potential. The configuration and binding energy are given in Fig. 12. The oxygen atom of water is roughly centered over the ring at 3.2 \AA above it and

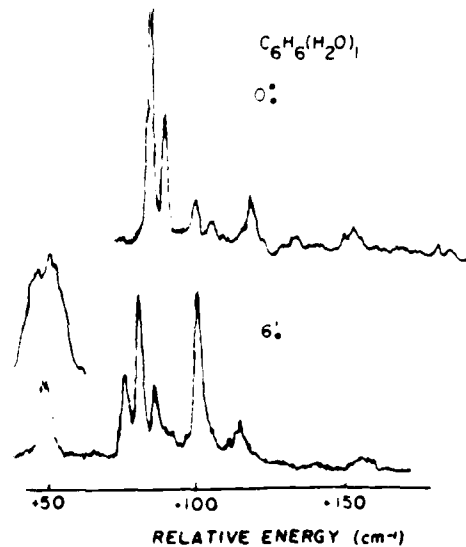


FIG. 11. Two-color TOFMS of benzene (H_2O)₁ in the region of benzene origin 0_0^0 and 6_0^1 . An expanded scale insert is shown of the 6_0^1 origin of the cluster.

the water hydrogen atoms are at 3.0 \AA above the ring. The calculated water benzene binding energy is 505 cm^{-1} .

IV. DISCUSSION

Cluster geometry is determined through analysis of two-color TOFMS data for individual clusters and through calculations of cluster geometry and binding energies using an augmented LJ potential. Calculated binding energies have

TABLE VI Benzene (H_2O)₁.

Energy (vac. cm^{-1})	Energy relative to corresponding benzene feature (cm^{-1})	Energy relative to corresponding benzene- water feature (cm^{-1})	Assignment
			0_0^0
38 168.6	84.6	0	
38 173.9	89.9	5.3	
38 183.5	101.5	16.9	
39 191.0	107.0	22.4	
38 205.3	121.3	36.7	
38 221.6	137.6	53.0	
38 243.5	159.5	74.9	
38 274.9	190.9	106.3	
			6_0^1
			a
38 655.4	48.4	0	
38 656.8	49.8		
38 683.8	76.8	27.7	
38 688.6	81.6	32.5	
38 694.2	87.2	38.1	
38 709.1	102.1	53.0	
38 720.7	113.7	64.6	
38 762.1	155.1	106.0	

^aShift taken with 6_0^1 at 49.1

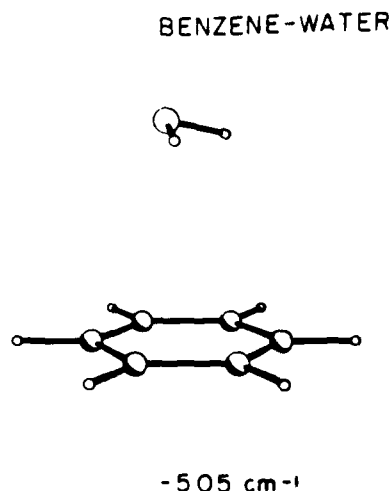


FIG. 12. Minimum energy configuration and binding energy for benzene (H_2O), as obtained using a LJ potential calculation.

always been roughly bracketed by the experimentally observable range defined by two solute molecule vibrations (e.g., 520 to 850 cm^{-1} for the 1:1 complex).¹⁻⁷

Before discussing the details of the clusters observed, some general remarks are in order. First, one should take note of the great apparent differences between the spectra of the various clusters studied: pyrazine and pyrimidine hydrocarbon spectra show little vdW vibronic structure but intense origins; the pyrazine (NH_3)₁ spectrum displays elaborate and well developed vibronic progressions with a +117 cm^{-1} cluster shift for a single cluster; the pyrimidine (NH_3)₁ spectra consist only of intense origins for three large shift (+366, +368, +496 cm^{-1}) configurations with no vdW vibronic development; the benzene (NH_3)₁ spectra are red shifted, and too complex to interpret without further calculations; and the benzene (H_2O)₁ spectra are blue shifted with extensive vdW structure. Second, and perhaps even more astonishing, the LJ-HB (where appropriate) potential calculations parallel and reinforce these differences in all cases. That is, for example, the calculations suggest one hydrogen-bonded configuration for pyrazine (NH_3)₁ but three hydrogen-bonded configurations for pyrimidine (NH_3)₁, in agreement with the straightforward interpretation of the spectra. Third, the binding energies of the clusters seem relatively insensitive to the detailed configuration of the cluster. Fourth, spectral shifts are found to be a sensitive function of the detailed geometry of the cluster. Proximity to the π system is important for cluster red shifts, while hydrogen bonding yields in general cluster blue shifts with respect to the solute monomer origin.

A. Pyrimidine-methane

In the pyrimidine (CH_4)₁ cluster the CH_4 molecule is situated above the pyrimidine ring coordinated to the π cloud of the aromatic ring. The cluster has a simple spectrum with little vdW vibronic intensity following the pyrimidine

vibronic origins. The cluster spectrum is red shifted, indicating that the excited state cluster is more tightly bound than the ground state cluster by roughly 60 cm^{-1} . The overall appearance of the spectrum is similar to that of pyrazine methane.⁷

The additive shift features in the spectrum of pyrimidine (CH_4)₂ are attributed to the isotropic (symmetrical) geometry with a methane molecule on either side of the pyrimidine ring. The feature at -47.2 cm^{-1} in the pyrimidine (CH_4)₂ spectrum is attributed to the anisotropic configuration with both CH_4 molecules on the same side of the ring. In this asymmetric geometry, one methane is more or less above the ring, and responsible for most of the CH_4 - π -cloud interactions, and the other methane molecule is off the ring interacting primarily with the first methane, contributing little to the cluster spectral shift.

The overall behavior of this cluster system with regard to geometry, binding energy, and cluster population in the beam is very similar to that found for benzene, toluene, and pyrazine methane species.¹⁻⁷

B. Pyrimidine-ethane

The pyrimidine (C_2H_6)₁ cluster is similar to the pyrazine (C_2H_6)₁ cluster;⁷ both clusters have three geometrical configurations and each configuration of the two clusters has a similar binding energy. These configurations are also similar to those of the benzene (C_2H_6)₁ cluster with the exception that, in the *N*-heterocyclic systems, two parallel orientations of the C_2H_6 long axis with respect to the ring plane are now possible.

The identification of calculated geometries with the three distinct spectroscopic features is of course tentative but can be pursued in the spirit of the arguments and correlations employed with the benzene and pyrazine systems.¹⁻⁷ Referring to Figs. 3 and 4, the feature at -71.4 cm^{-1} can be associated with configuration I, the intense feature at -60.7 cm^{-1} can be associated with configuration II, and the -52.7 cm^{-1} feature is associated with configuration III. The lack of vdW vibronic structure for these transitions must be due to the similarity between the ground and excited state potentials for the clusters.

C. Pyrimidine-ammonia

The pyrimidine (NH_3)₁ clusters have a unique spectrum which can only be interpreted as due to three distinct configurations with no vdW mode progression intensity following the well defined origins. Calculations, as pointed out previously, gave exactly these conclusions and identification of origins in the spectrum with configurations seems straightforward. Configurations I and II of Fig. 6 are associated with the features at 366 and 368 cm^{-1} in Fig. 5. These two configurations are quite similar and have less hydrogen bonding interaction than the more blue-shifted single feature at 496 cm^{-1} . The large spectral blue shifts of ~365 and ~500 cm^{-1} must arise from the strong hydrogen bonding interactions. While none of these observations seem particularly striking in and of itself, in comparison with the pyrazine (NH_3)₁ and benzene (NH_3)₁ results, they are surprising; these will be discussed below.

D. Pyrazine-ammonia

The pyrazine $(\text{NH}_3)_1$ cluster spectrum is completely different from that of pyrimidine $(\text{NH}_3)_1$. The cluster 0_0^0 is shifted $+117 \text{ cm}^{-1}$ from the pyrazine 0_0^0 , only one cluster geometry is present, and a rather extensive vdW vibronic structure is built upon the origin. The $6a_1^1$ spectrum is quite similar. Two intense vdW vibronic transitions are associated with these cluster transitions. The $10a_1^1$ vibration region of the pyrazine $(\text{NH}_3)_1$ cluster, on the other hand, looks quite different from these other features and vibronic interactions between the out of plane $10a_1^1$ carbon-carbon mode and the vdW modes are quite evident in the overall vibronic intensity pattern in the $10a_1^1$ region.

Calculations predict only one configuration for this cluster system. The fact that the potential energy calculations can accurately parallel the spectral data for pyrimidine and pyrazine ammonia clusters which are clearly so different, gives us a high degree of confidence in the calculational process, the binding energies, and the potential form accuracy.

E. Benzene-ammonia

Assignment of the benzene $(\text{NH}_3)_1$ spectra has not been attempted as yet because the spectra are too complicated. We present them only as part of the general picture indicating what spectra of relatively simple clusters of such systems can be like. The benzene $(\text{NH}_3)_1$ clusters yield much more complicated spectra than either pyrazine or pyrimidine $(\text{NH}_3)_1$ clusters do. In the benzene $(\text{NH}_3)_1$ cluster, strong vdW vibronic interactions must be important for the cluster transition intensity.

Both calculated configurations (Fig. 10) contribute to the 6_1^1 transition but only configuration II generates the 0_0^0 spectrum. Note too, that both configurations most likely generate a red shift.

F. Benzene-water

Any $\text{C}_6\text{H}_6(\text{H}_2\text{O})_1$ cluster will in principle generate a 0_0^0 transition. The 0_0^0 spectrum of $\text{C}_6\text{H}_6(\text{H}_2\text{O})_1$ (Fig. 11) thus strongly suggests that only one cluster geometry is realized for this system. The $\text{C}_6\text{H}_6(\text{H}_2\text{O})_1$ 0_0^0 transition is much like the pyrazine $(\text{NH}_3)_1$ spectrum. Well developed vdW vibronic features are observed. The 6_1^1 spectrum implies strong vibronic mixing between the in plane carbon-carbon deformation 6^1 and the vdW bends and torsions: the cluster shift is different for 6_1^1 , as is the intensity pattern. The cluster shift at the 0_0^0 transition is $+85 \text{ cm}^{-1}$ which indicates that the cluster excited state is destabilized with respect to the ground state. The blue shift may be related to the unique hydrogen bonding capabilities of the H_2O molecule with the π system of benzene. The calculated binding energy is probably $\sim 50 \text{ cm}^{-1}$ low for this cluster because the 6_1^1 transition at 0_0^0 plus 520 cm^{-1} is observed. We have previously noted that the LJ potential binding energy is roughly 50 cm^{-1} low compared to exp-6 and experimental values.⁷

An infrared study of the 1:1 benzene-water complex in an argon matrix has been reported.²³ The work suggests that the water molecule hydrogen bonds to the benzene π system

in a manner nearly identical to that found in the calculations presented in Fig. 12.

V. CONCLUSIONS

The clusters studied in this work fall into two broad categories: a conventional set containing pyrimidine hydrocarbon clusters, the spectra of which are quite similar to those of other aromatic and pyrazine hydrocarbon systems, and benzene, pyrimidine, and pyrazine ammonia and benzene water clusters, the spectra of which are all unique and surprisingly erratic. In the latter grouping, spectral cluster shifts range from -100 to $+500 \text{ cm}^{-1}$, vdW vibronic spectra range from nonexistent to intense, vdW modes can be highly perturbing to the solute vibronic structure and energy, and the number of cluster configurations varies from one to three in an apparently arbitrary fashion. These differences notwithstanding, the Lennard-Jones (6-12-1) potential, augmented appropriately with hydrogen bonding interactions (10-12) as required, always gives geometry and binding energy results that are in complete agreement with the spectra as far as the comparison can be made (i.e., symmetry, numbers of configurations, red and blue shifts with regard to hydrogen bonding, etc). The atom-atom LJ potential form has been chosen for these calculations because a large number of parameters for different types of atoms are available in the literature.

The benzene $(\text{NH}_3)_1$ and $(\text{H}_2\text{O})_1$ spectra are quite different from one another. The shifts for these two clusters and their geometries seem to emphasize the importance of hydrogen bonding in the benzene $(\text{H}_2\text{O})_1$ cluster.

Pyrazine and pyrimidine water clusters are not found in these studies although they have been extensively investigated. These clusters are not observed perhaps because their excited states are dissociative, but more likely because of rapid excited state intersystem crossing and/or internal conversion.

¹M. Schauer and E. R. Bernstein, *J. Chem. Phys.* **82**, 726 (1985).

²M. Schauer, K. S. Law, and E. R. Bernstein, *J. Chem. Phys.* **82**, 716 (1985).

³K. S. Law and E. R. Bernstein, *J. Chem. Phys.* **82**, 2856 (1985).

⁴K. S. Law, M. Schauer, and E. R. Bernstein, *J. Chem. Phys.* **81**, 4871 (1984).

⁵E. R. Bernstein, K. Law, and M. Schauer, *J. Chem. Phys.* **80**, 207 (1984).

⁶M. Schauer, K. Law, and E. R. Bernstein, *J. Chem. Phys.* **81**, 49 (1984).

⁷J. Wanna and E. R. Bernstein, *J. Chem. Phys.* **84**, 927 (1986).

⁸M. M. Carrabba, J. E. Kenny, W. R. Moomaw, J. Cordes, and M. Denton, *J. Phys. Chem.* **89**, 674 (1985).

⁹(a) H. Abe, N. Mikami, and M. Ito, *J. Phys. Chem.* **86**, 1768 (1982); (b)

H. Abe, N. Mikami, M. Ito, and Y. Udagawa, *ibid.* **86**, 2567 (1982); (c)

K. Fuke, H. Yoshiuchi, K. Kaya, Y. Achiba, K. Sato, and K. Kimura,

Chem. Phys. Lett. **100**, 179 (1984); (d) N. Gonohe, H. Abe, N. Mikami,

and M. Ito, *J. Phys. Chem.* **89**, 3642 (1985).

¹⁰(a) J. Hager and S. C. Wallace, *J. Phys. Chem.* **88**, 5513 (1984); (b) **89**

3833 (1985).

¹¹D. E. Poeltl and J. K. McVey, *J. Chem. Phys.* **78**, 4349 (1983).

¹²(a) C. A. Haynam, D. V. Brumbaugh, and D. H. Levy, *J. Chem. Phys.* **79**

1581 (1983); (b) L. Young, C. A. Haynam, and D. H. Levy, *ibid.* **79**, 1592

(1983).

¹³G. Smulevich, A. Amirav, V. Even, and J. Jortner, *Chem. Phys.* **73**, 1

(1982).

¹⁴(a) P. M. Felker, W. R. Lambert, and A. H. Zewail, *J. Chem. Phys.* **77**

1603 (1982); (b) L. A. Heimbrook, J. E. Kenny, B. E. Kohler, and G. W.

Scott, *J. Phys. Chem.* **87**, 280 (1983).

Wanna, Menapace, and Bernstein: Hydrogen bonded clusters

- ¹M. Kasha, *Discuss. Faraday Soc.*, **9**, 14 (1950).
- ²(a) F. A. Momany, L. M. Carruthers, R. F. McGuire, and H. A. Scheraga, *J. Phys. Chem.*, **78**, 1595 (1974); (b) G. Nemethy, M. S. Pottle, and H. A. Scheraga, *ibid.*, **87**, 1883 (1983).
- ³(a) C. A. Haynam, D. V. Brumbaugh, and D. H. Levy, *J. Chem. Phys.*, **80**, 2256 (1984); (b) D. V. Brumbaugh, J. E. Kenny, and D. H. Levy, *ibid.*, **78**, 3415 (1983); (c) K. E. Johnson, W. Sharfin, and D. H. Levy, *ibid.*, **74**, 163 (1981); (d) K. E. Johnson, L. Wharton, and D. H. Levy, *ibid.*, **69**, 2719 (1978).
- ⁴K. Yamanouchi, H. Watanabe, S. Koda, S. Tsuchiya, and K. Kuchitsu, *Chem. Phys. Lett.*, **107**, 290 (1984).
- ⁵(a) P. J. Wheatley, *Acta Crystallogr.*, **10**, 182 (1957); (b) **13**, 80 (1960).
- ⁶J. A. Menapace and E. R. Bernstein, *J. Chem. Phys.* (to be published).
- ⁷(a) A. E. W. Knight, C. M. Lawburgh, and C. S. Parmenter, *J. Chem. Phys.*, **63**, 4336 (1975); (b) I. Knoth, H. J. Neusser, and E. W. Schlag, *J. Phys. Chem.*, **86**, 891 (1982); (c) A. K. Jameson, H. Salgusa, and E. C. Lim, *ibid.*, **87**, 3007 (1983); (d) H. Abe, Y. Ohyanagi, M. Ichijo, N. Mikami, and M. Ito, *ibid.*, **89**, 3512 (1985).
- ⁸M. L. Sage and J. Jortner, *J. Chem. Phys.*, **82**, 5437 (1985).
- ⁹A. Engdahl and B. Nelander, *J. Phys. Chem.*, **89**, 2860 (1985).

APPENDIX TWO

SUPERSONIC MOLECULAR JET STUDIES OF THE PYRAZINE AND
PYRIMIDINE DIMERS

Supersonic molecular jet studies of the pyrazine and pyrimidine dimers^{a)}

J. Wanna, J. A. Menapace, and E. R. Bernstein

Department of Chemistry, Condensed Matter Sciences Laboratory, Colorado State University, Fort Collins, Colorado 80523

(Received 13 December 1985; accepted 8 April 1986)

Mass selected optical spectra for the first excited singlet $n\pi^*$ states of the pyrazine and pyrimidine dimers are presented. The species are created in a pulsed supersonic jet expansion. The spectra are analyzed based on ionization energy, vibronic structure, and relative energy with respect to the isolated monomer (cluster spectroscopic shift). Calculations of binding energy and geometry for these dimers are carried out employing a Lennard-Jones (6-12-1) and hydrogen bonding (10-12-1) potential. In the case of pyrazine, calculations and experiments agree that both parallel planar hydrogen bonded and perpendicular dimers are present in the expansion. The calculations also predict a parallel stacked and 90° rotated pyrazine dimer which is not observed. This latter species most likely forms an excimer in the excited state with a short lifetime and a highly red shifted broad spectrum. In the case of pyrimidine, calculations yield four planar hydrogen bonded species and a parallel stacked and displaced species. The spectra for the pyrimidine dimer are consistent with these configurations, in agreement with the calculations. No perpendicular configuration is calculated for the pyrimidine dimer and no spectroscopic features require postulating the existence of such a configuration. To explore further the agreement between calculated and experimental results for aromatic dimers, calculations are also presented for the tetrazine dimer. Three calculated geometries are obtained for the tetrazine dimer: a parallel stacked and 90° rotated species, a planar hydrogen bonded species, and a perpendicular species. Experimental spectra and calculations are in basic agreement for all dimers studied and, in general, support one another.

I. INTRODUCTION

Molecular dimers are of interest for a number of reasons. They can serve as model systems for condensed phase structure, dynamics, and nucleation and growth. Vibrational dynamics and reactions can be studied in clusters through the observation of vibrational dephasing or intramolecular vibrational redistribution (IVR) and vibrational predissociation (VP). Dimers also provide a model for higher order (i.e., secondary, tertiary, etc.) structure of more complex, flexible molecules. Finally, these small clusters can be treated as a new, weakly coupled state of matter appropriate in its own right for investigation and focused attention.

Small clusters or dimers are best studied by molecular jet techniques,¹⁻⁶ as the species are thereby isolated and free of extraneous perturbations. Of the molecular supersonic jet spectroscopy techniques available, the most useful is two-color time of flight mass spectroscopy¹ (2-color TOFMS) because many different clusters [e.g., dimers, trimers, dimers (He)_n, etc.] are simultaneously produced in the expansion process. Two-color TOFMS selects a cluster of particular mass, does not allow fragmentation of clusters to take place, thus maintaining mass integrity of the clusters, and yields a plot of cluster ion intensity in the chosen mass channel as a function of the cluster absorption spectrum.

Dimers of benzene, toluene, and benzene-toluene have been studied in our laboratory using the 2-color TOFMS technique.¹ Coupled with the experimental findings, a potential energy calculation of the structure and binding ener-

gy of these dimers based on an exponential-six (exp-6) function has also been reported.² Spectroscopic data and potential energy calculations have been analyzed to arrive at a set of consistent geometries for these dimers. The benzene dimer is suggested to have a parallel displaced structure and the toluene and toluene-benzene dimers are suggested to have both parallel displaced and perpendicular geometries. The benzene dimer characterization rests on isotopic substitution, absence of resolved splittings at the cluster 0_0^0 , observation of only one feature, respectively, for (C₆H₆)₂, (C₆D₆)₂, and C₆H₆C₆D₆ at the cluster 0_0^0 , and calculations employing the observed molecular quadrupole moment of C₆H₆ to set partial and atomic charges and multipolar terms. In all instances, the experiments and calculations appear to arrive at self-consistent and independent conclusions which are in agreement with one another.

Molecular jet studies of other isolated dimers have also been reported. Rotationally resolved fluorescence excitation and dispersed emission spectra of tetrazine,³ phenyltetrazine,⁴ and dimethyltetrazine⁵ dimers have been reported. Hydrogen bonded benzoic acid⁶ and benzoic acid-*p*-toluic acid⁷ dimers have also been studied.

In this paper we report rotationally resolved 2-color TOFMS of pyrazine and pyrimidine isolated molecules at a resolution of 0.08 cm⁻¹. Unfortunately, this is insufficient resolution to obtain rotationally resolved 2-color TOFMS of the pyrazine and pyrimidine dimers. Computer simulations, based on a reasonable symmetric top algorithm, predict a resolution of at least 0.005 cm⁻¹ (150 MHz) is needed to observe rotational structure for the dimers, assuming they are rigid.

^{a)} Supported in part by grants from ONR and the Philip Morris Corporation.

In addition to the experimental spectroscopic methods used to study these dimers, potential energy calculations utilizing a Lennard-Jones (LJ; 6-12-1) potential are performed to yield minimum energy geometries and binding energies. This potential form is replaced with a LJ-hydrogen bonding (HB; 10-12-1) form for the appropriate set of atoms. The calculation and parameters employed are discussed and presented in an earlier publication.³ These potentials, with literature parameter values, give the same results as the exp-6 with dipole-dipole, dipole-quadrupole, and quadrupole-quadrupole terms for the benzene, toluene, and benzene-toluene (and pyrazine and pyrimidine) dimers. The major advantage of the LJ form presently used in our studies is that more atomic parameters are available in the literature³ and experimental multipole moments are not required for each system.

Dimer geometry is determined through analysis of experimental (e.g., shifts, ionization energies, origin identification, vibronic analyses, etc.) and calculational results.

II. EXPERIMENTAL PROCEDURES

A pulsed valve supersonic molecular jet system is used to generate the dimers. The pulsed valve is mounted in the mass spectroscopy chamber of a two chambered vacuum system. Since the duty cycle of the valve is roughly 10^{-3} , the 10 in. diffusion pump on the chamber and the 6 in. diffusion pump on the TOFMS flight tube adequately handle the gas load and maintain the chamber pressure below 2×10^{-6} Torr. The system is described in previous publications.^{1,8} The beam passes through a skimmer and then into the ionization region of a TOFMS. Two separately tunable lasers provide the photons for the $S_0 \rightarrow S_1$ transition and the $S_1 \rightarrow$ cluster ion transition.

Rotationally resolved 2-color TOFMS are obtained through pressure tuning of the grating box of the pump ($S_0 \rightarrow S_1$) dye laser oscillator cavity. The output of this laser is narrowed by an etalon placed between the dye cell and the grating in the oscillator cavity. The doubled output from this dye laser is 0.08 cm^{-1} in width. The laser can be scanned over roughly 20 cm^{-1} for a N_2 pressure variation of 10 to 1500 Torr.

Pyrazine and pyrimidine are obtained from Aldrich Chemical Company and used without purification. The sample is placed in a trap behind the pulsed valve through which He flows at 120 psig.

The LJ potential energy function and calculational procedure have previously been described.⁸ The additional constants needed for this work are the (aromatic) N...H hydrogen bonding values: $B = 8.244 \times 10^2 \text{ kcal } \text{Å}^{10}/\text{mol}$ and $A' = 3.2897 \times 10^6 \text{ kcal } \text{Å}^{12}/\text{mol}$. In order to check the LJ potential form, in particular for the pyrimidine dimer, LJ plus multipolar (i.e., dipole-dipole, dipole-quadrupole, and quadrupole-quadrupole) potential calculations are also performed.² The pyrimidine dipole and quadrupole moments¹⁰ are taken to be $-2.97 \times 10^{-18} \text{ esu cm}$ and $-1.91 \times 10^{-26} \text{ esu cm}^2$, respectively.

Calculations are also reported which simulate the rotational structure of pyrazine and pyrimidine monomers and dimers. A symmetric top model is employed for this fit be-

cause it is simple, reasonably accurate, and in general is well suited to the purpose of roughly predicting the unresolved dimer structure. Both molecules are nearly symmetric tops ($\kappa \approx 0.9$). The form of the equations and methods employed are given by Herzberg.¹¹ The rotational temperature achieved in our system is $\sim 2 \text{ K}$. The rotational constants used in the dimer rotational spectra calculations are found from the calculated LJ geometries. The molecular geometries can be found in Ref. 12 for pyrazine and Ref. 13 for pyrimidine.

III. RESULTS

A. Pyrazine dimer

The spectrum of the pyrazine dimer at the O_0^0 transition is presented in Fig. 1 at two ionization energies, both of which are lower than the minimum ionization (second photon) energy of $44\,000 \text{ cm}^{-1}$ required to observe the 2-color TOFMS of the pyrazine monomer. Lowering the ionization energy from $43\,182$ to $42\,185 \text{ cm}^{-1}$ causes three of the dimer related peaks to disappear: these features are found at -11.0 , 12.0 , and 26.2 cm^{-1} on the scale of Fig. 1. From the nature and appearance of these features, the $+12$ and $+26 \text{ cm}^{-1}$ peaks are quite likely vibrations built on the -11 cm^{-1} origin of a given configuration cluster. The intense features that remain at the lower ionization energy are found at -26.3 , -5.8 , $+34.1$, and 50.7 cm^{-1} . From this variation of ionization energy one can determine that at least two configurations of the pyrazine dimer are present in the su-

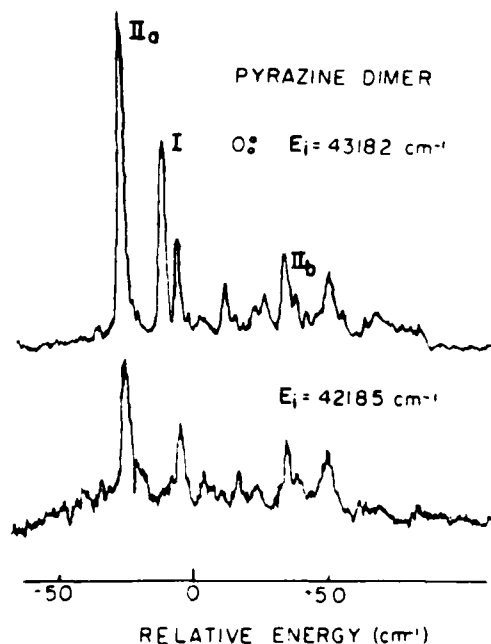


FIG. 1. Two-color TOFMS of the pyrazine dimer in the region of the pyrazine origin at two different ionization energies, top trace at an ionization energy of $43\,182 \text{ cm}^{-1}$ and the lower trace at an ionization energy of $42\,185 \text{ cm}^{-1}$. The pyrazine origin at $30\,876 \text{ cm}^{-1}$ lies at 0 cm^{-1} on the scale of the figure.

personic jet expansion. The pyrazine- d_4 dimer 0_0^0 spectrum at two different ionization energies is presented in Fig. 2: the similarity between the pyrazine- h_4 and - d_4 dimer spectra is quite striking and reinforces our identification of origins and vdW vibronic features. The features that vanish at lower ionization energy are found at -11.5 , 11.5 , 25.5 , and 64.1 cm^{-1} with respect to the pyrazine- d_4 0_0^0 transition ($31\,030.4$ cm^{-1}). These should be compared with the numbers in Table I. The features that remain with lower ionization energy are located at -26.9 , -6.5 , 31.0 , and 45.9 cm^{-1} .

The spectra of the pyrazine dimer at other pyrazine vibronic origins are presented, along with the 0_0^0 spectrum for comparison, in Fig. 3. The feature at roughly $+61$ cm^{-1} in this figure ($+34.1$ cm^{-1} in Fig. 1) is clearly an additional origin. The energy values and shifts for these features are presented in Table I. Since the pyrazine dimer is still observed at $10a_0^0$, its binding energy is greater than 800 cm^{-1} . No other features, appearing in the dimer mass channel, are found within -400 cm^{-1} of the pyrazine 0_0^0 transition. The spectra of the pyrazine- d_4 dimer at these other vibronic monomer origins are again very similar to those of the pyrazine- h_4 dimer. We concluded from these spectra (not presented) that the third origin for the deuterated dimer lies at 31.0 cm^{-1} from the 0_0^0 of the deuterated monomer.

Utilizing a Lennard-Jones potential function with a hydrogen bonding form, three configurations for the pyrazine dimer are calculated. Two of these configurations, a planar hydrogen bonded form and a perpendicular form, are displayed in Fig. 4. A parallel, stacked and 90° rotated structure

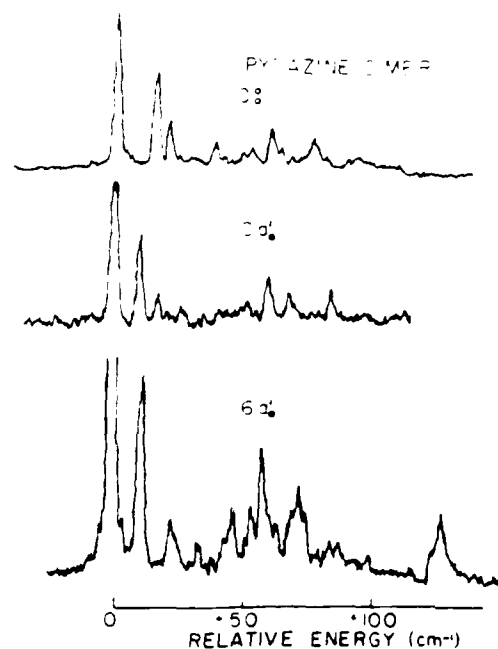


FIG. 3. Two-color TOFMS of the pyrazine dimer in the 0_0^0 , $10a_0^0$, and $6a_0^0$ regions. These spectra are taken at high ($\sim 43\,200$ cm^{-1}) ionization energy.

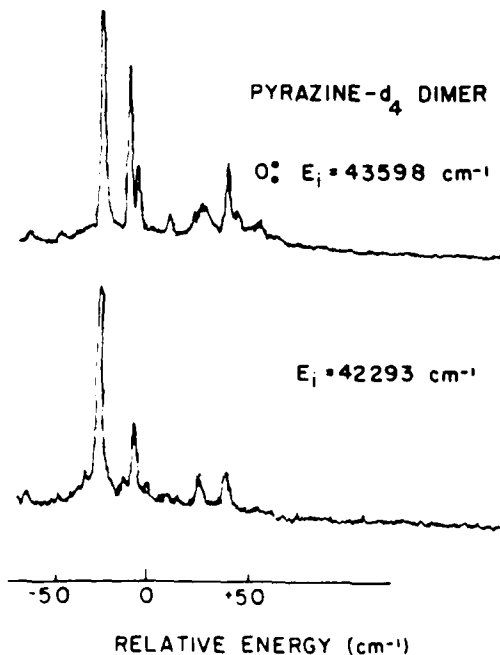


FIG. 2. Two-color TOFMS of the pyrazine- d_4 dimer in the region of the pyrazine- d_4 origin. Two different ionization energies are presented. The pyrazine- d_4 monomer origin lies at 0 cm^{-1} on the scale of the figure. Compare to Fig. 1 for the pyrazine- h_4 dimer.

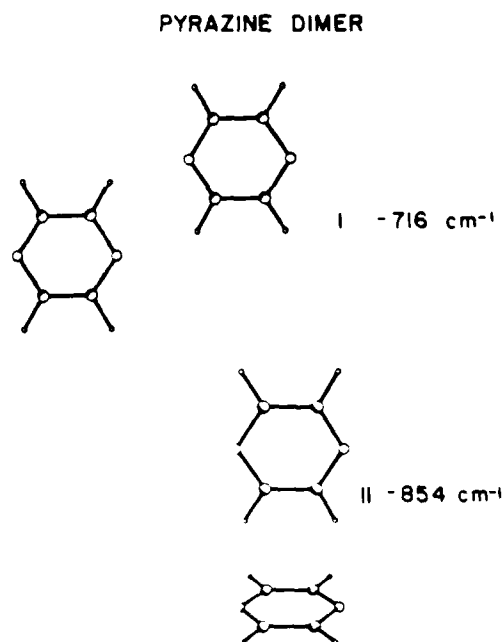


FIG. 4. Minimum energy configurations and binding energies of pyrazine dimer as obtained with a LJ plus HB potential calculation.

is also found. The binding energies for the former two configurations are presented in the figure. In the planar geometry the ring centers are at 5.6 Å from each other and the suggested C-H...N hydrogen bonds are 2.3 Å long. The pyrazine at the stem of the perpendicular configuration is situated in a symmetric position above the base pyrazine, with two of its hydrogens pointing to the base pyrazine nitrogens and equidistant from them. This perpendicular configuration has a 4.6 Å pyrazine center to center separation and apparent 2.6 Å H...N bond lengths.

B. Pyrimidine dimer

Three segments of the pyrimidine dimer 2-color TOFMS spectrum in the O_0^+ region are displayed in Fig. 5 for two different ionization energies. Based only on the position and appearance of these segments we suggest that the features at -168 and $+296$ cm^{-1} are each associated with different geometries. The grouping of features in the $+170$ cm^{-1} region must be associated with more than one dimer configuration, as these eight sharp, relatively intense features are clearly not vdW vibronic progressions built on a single O_0^+ origin. The minimum ionization energy for the pyrimidine monomer is near $44\,090$ cm^{-1} above the $^1B_1(\pi\pi^*)$ excited state at $31\,073$ cm^{-1} . As can be seen from Fig. 5, features in two of the three regions displayed disappear as the ionization energy is lowered from $44\,363$ to $42\,320$ cm^{-1} .

Calculations using a LJ-HB potential function yield four planar configurations, a parallel stacked head-to-tail displaced configuration, and a parallel stacked undisplaced configuration with the two pyrimidine molecules rotated 90° with respect to each other. The latter configuration most likely does not contribute to the observed dimer spectrum since it will probably form an excimer. No perpendicular geometry is calculated even with the LJ-HB potential augmented with multipolar terms. Figures 6 and 7 give those calculated geometries for the pyrimidine dimer which can produce the observed spectral features. The parallel displaced geometry shown in Fig. 6 is head-to-tail displaced by

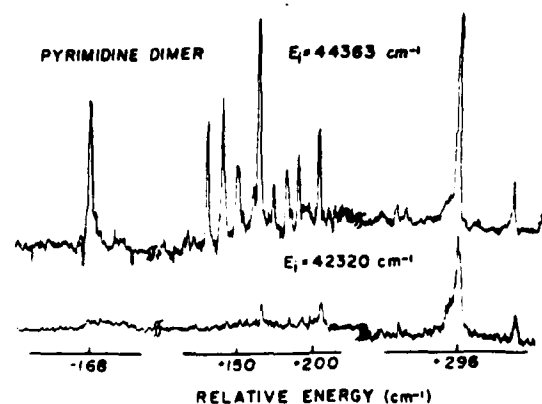
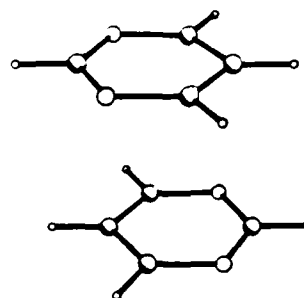


FIG. 5. Three segments of the 2-color TOFMS spectra of the pyrimidine dimer at two ionization energies, top trace at an ionization energy of $44\,363$ cm^{-1} and the lower trace at an ionization energy of $42\,320$ cm^{-1} . The energy scale is relative to the pyrimidine monomer O_0^+ .

PYRIMIDINE DIMER



-1478 cm^{-1}

FIG. 6. Minimum energy configuration and binding energy for the stacked pyrimidine dimer as obtained with a LJ plus HB potential calculation.

0.6 Å along the CH-CH line from the molecular center; the interplane separation is 3.3 Å. The calculated binding energy for this dimer is 1478 cm^{-1} .

The planar configurations are displayed in Fig. 7. Configuration I has a center to center distance of 5.5 Å, two N-H hydrogen bonds (2.3 Å separation), and a calculated binding energy of 709 cm^{-1} . Configurations II, III, and IV also display some hydrogen bonding but to a lesser extent than that displayed in configuration I. In these latter three cases, the less "acidic" hydrogens, not between the two N atoms, are involved in the "hydrogen bonds": the pyrimidine molecule center to center distance is ~ 6.0 Å and the calculated binding energies range from 400 to 430 cm^{-1} , substantially less than the binding energy for configuration I. Configuration II has two N-H hydrogen bonds each of 2.9 Å. Configurations III and IV have a nitrogen atom of one pyrimidine equidistant from two hydrogens of the other pyrimidine with an apparent hydrogen bond distance of 2.9 Å. Planar configurations in which two nitrogens are facing each other are not stable.

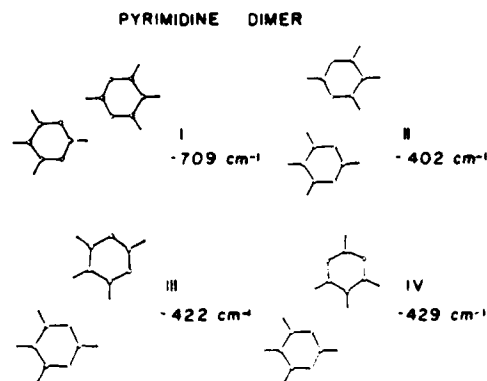


FIG. 7. Minimum energy configurations and binding energies for the planar pyrimidine dimers as obtained with a LJ plus HB potential calculation.

C. Rotational structure

Rotationally resolved 2-color TOFMS data can be obtained for the pyrazine and pyrimidine monomers using the resolution presently available in our laboratory ($\Delta\nu \sim 0.08 \text{ cm}^{-1}$). The spectra are presented in Fig. 8. These well resolved spectra evidence a central *Q* branch with well developed *R* and *P* branches to the high and low energy sides, respectively. The calculated rotational structures for these transitions are presented in Fig. 9. In order to make the fit look reasonable, a 0.1 cm^{-1} Gaussian linewidth was incorporated in the calculated spectrum.

Considering that a symmetric top equation is used for the fit, the agreement between the calculated and experimental results is excellent. The purpose of this exercise is to observe and calculate the rotational spectrum of a dimer. One can see from Fig. 10 (top) that the rotational structure of the pyrazine dimer is not evident at this laser linewidth. Similar conclusions arise from the spectra of the benzene dimer (see Fig. 11). Computer simulations of the pyrazine dimer spectrum (based on the symmetric top calculations), show that a $\sim 0.005 \text{ cm}^{-1}$ laser linewidth is required to resolve rotational transitions for the aromatic dimers (Fig. 10 bottom). An attempt to fit the rotational contours to parallel or perpendicular transitions of parallel or perpendicular dimers demonstrates that no convincing conclusions concerning dimer geometry can be reached in this manner. In fact, the spectra of the parallel and perpendicular pyrazine dimer origins do not appear different at this resolution. The calculated contours are found using transition moments for the perpendicular dimer and $A'' = 0.0611$, $B'' = 0.0157$, and $C'' = 0.0141 \text{ cm}^{-1}$ for the perpendicular dimer and $A'' = 0.0381$, $B'' = 0.0153$, and $C'' = 0.0112 \text{ cm}^{-1}$ for the parallel planar dimer.

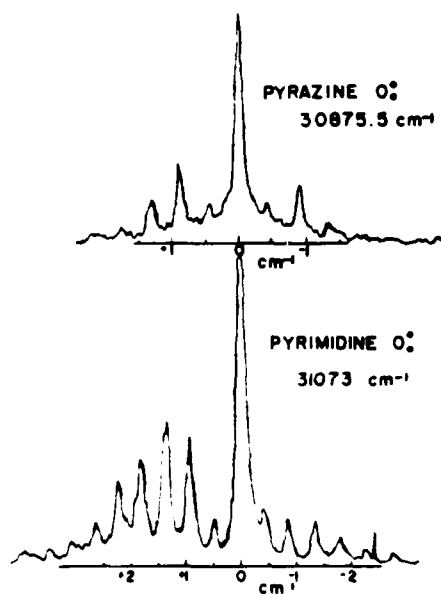


FIG. 8. Two-color TOFMS rotational spectra of the origins of pyrazine (top) and pyrimidine (bottom) monomers.

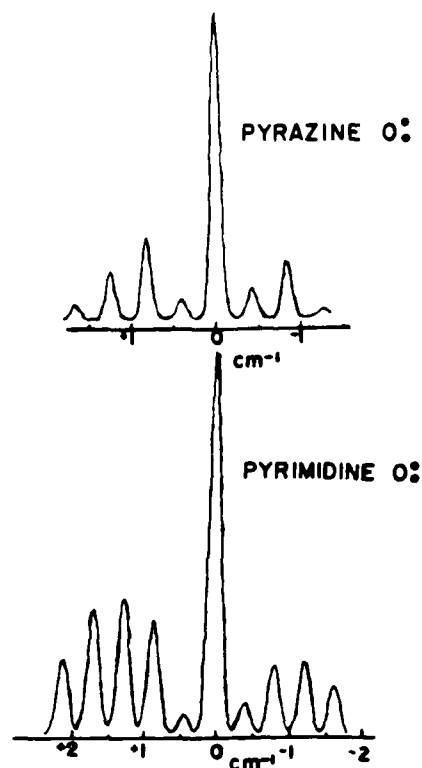


FIG. 9. Simulated rotational spectra of the pyrazine and pyrimidine origins.

IV. DISCUSSION

A. Pyrazine dimer

In the following paragraphs, only the pyrazine- h_s dimer results will be discussed in detail. The similarity between the pyrazine- h_s and - d_s dimer results obviates the need for discussion of these data separately.

One of the most important experimental observations concerning the pyrazine dimer is the change in the spectrum as a function of ionization laser or second photon energy. Lowering the ionization laser energy by 1000 cm^{-1} to 42185 cm^{-1} causes three features to disappear: two of these are assigned as vibrations built on a single origin (see Table I and Fig. 1). Further reduction of the ionization energy to 41721 cm^{-1} results in no observed TOFMS spectrum for the pyrazine dimer. At least two different geometries of the pyrazine dimer are therefore present in the beam. The dimer with the higher ionization energy is probably a symmetrical dimer with two symmetry equivalent molecules because only one origin is associated with the high ionization energy spectrum.

Different geometries will possess different ionization energies depending on the involvement of the π clouds in the overall dimer interaction. For example, a poor ioner hydrogen bonded dimer would probably have a poor ioner "solvation" or stabilization and might therefore have a higher ionization energy. This geometry would in addition have only one spec-

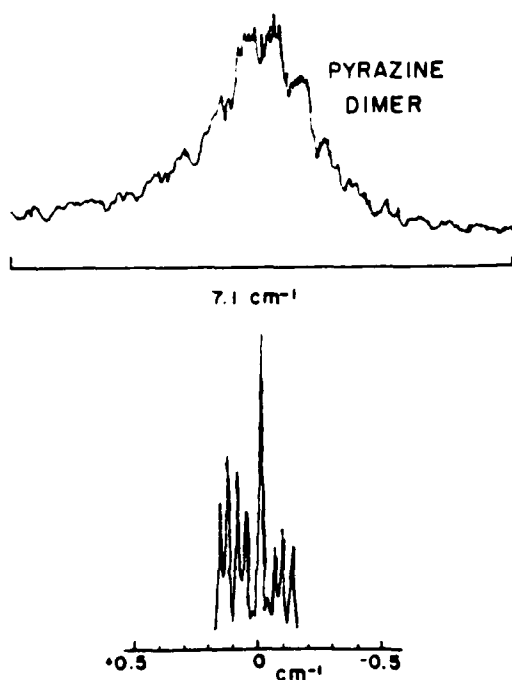


FIG. 10. Two-color TOFMS rotational spectrum of the pyrazine dimer origin (top) and computer simulated rotational spectra of the pyrazine dimer origin (bottom). The origin is at $30\,849.5\text{ cm}^{-1}$ (-26.5 cm^{-1} origin in Fig. 1). The FWHM is roughly 2 cm^{-1} . The $30\,865.0\text{ cm}^{-1}$ origin looks nearly identical to this one at the experimental resolution.

troscopic origin. A perpendicular geometry dimer would, on the other hand, probably evidence two features and a lower ionization energy due to the π -cloud involvement of the "horizontal" pyrazine in the stabilization of the ion.

The calculations give three general geometries for the pyrazine dimer: a parallel planar, a perpendicular, and a parallel stacked on 90° rotated geometry. The latter geometry is not discussed in this work because it likely is not important for any of the spectroscopic observations presented earlier. The remaining two configurations give rise to three separate spectra: one for the parallel planar geometry (I) and two for the perpendicular geometry (base IIa and stem IIb).

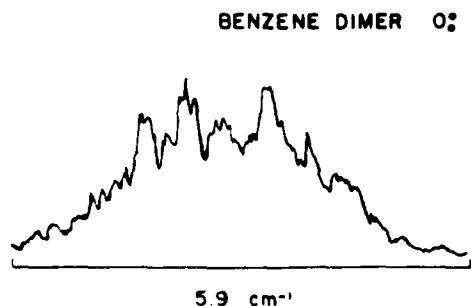


FIG. 11. Two-color TOFMS of the benzene dimer O_2^+ transition at 0.08 cm^{-1} resolution. Most of the "features" in this trace are noise and are not reproducible.

TABLE I. Pyrazine dimer.

Energy (vac. cm^{-1})	Energy relative to corresponding pyrazine feature (cm^{-1})	Energy relative to corresponding pyrazine dimer feature (cm^{-1})	Assignments ^a
30 849.5	-26.5	0	II base O_2^+
30 865.0	-11.0	0	I O_2^+
30 870.2	-5.8	20.7	
30 879.1	3.1	29.6	
30 888.0	12.0	23.0	
30 891.4	15.4	41.9	
30 898.7	22.7	49.2	
30 902.3	26.3	37.3	
39 910.1	34.1	0	II stem O_2^+
30 914.0	38.0	3.9	
30 918.2	42.2	8.1	
30 926.7	50.7	16.6	
31 228.5	-30.5	0	II base $10a_1'$
31 238.5	-20.5	0	I $10a_1'$
31 245.4	-13.6		
31 254.8	-4.2		
31 289.4	30.4	0	II stem $10a_1'$
31 297.6	38.6		
31 314.4	55.4		
31 433.3	-26.4	0	II base $6a_1'$
31 445.1	-14.6	0	I $6a_1'$
31 456.8	-2.9		
31 467.8	8.1		
31 481.7	22.0		
31 488.9	29.2		
31 493.2	33.5	0	II stem $6a_1'$
31 507.9	48.2		
31 565.7	106.0		
31 677.9	-21.1	0	II base $10a_2'$
31 686.1	-12.9	0	I $10a_2'$

^a See Fig. 4.

Table I gives the assignment of the dimer spectra. The planar geometry (I) is assigned to the origin at -11 cm^{-1} (Fig. 1) since this single origin feature is associated with the higher ionization energy. The other two origins at -26.5 and $+34.1\text{ cm}^{-1}$ (Fig. 1) with respect to the pyrazine monomer origin are assigned to the perpendicular dimer because they both show the same low ionization energy. The base (IIa) is associated with the red shifted origin and the stem (IIb) is associated with the blue shifted origin. This latter correlation between spectra and calculated structures is based on the argument presented in previous publications^{1,2} relating solvent cluster shifts and π -cloud involvement in the solute-solvent interaction: the larger the red shift, the more direct is the interaction between the system and the solvent. Thus the base molecule should be expected to have a larger red shift than the stem molecule.

The pyrazine $6a_1'$ (in-plane C-C stretch) and $10a_1'$ (out-of-plane C-C bend) vibrational modes show strong interaction with the van der Waals modes (Fig. 3).

B. Pyrimidine dimer

The ionization energy for the pyrimidine dimer system is again an important piece of information used to help determine the number of different configurations responsible for

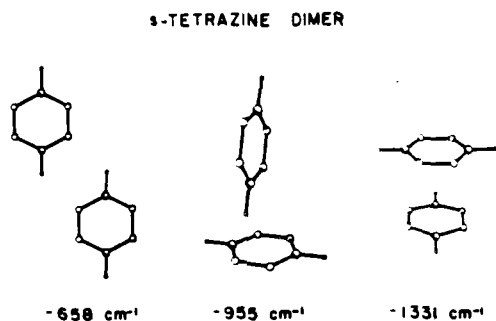


FIG. 12. Minimum energy configurations and binding energies for the tetrazine dimer as obtained with a LJ plus HB potential calculation.

the observed spectra and, perhaps, their geometry. Lowering the ionization by $2\,043\text{ cm}^{-1}$ to $42\,320\text{ cm}^{-1}$ causes the feature at -168 cm^{-1} to disappear, the features at $\sim +175\text{ cm}^{-1}$ nearly to disappear, and the feature at $+296\text{ cm}^{-1}$ to reduce in intensity. In addition, dimer spectral shifts can also be employed to associate calculated geometries with spectroscopic features: red shifted origins can be assigned to parallel stacked geometries, and blue shifted origins to planar hydrogen bonded forms. Perpendicular geometries can be responsible for both red and blue shifts depending on which molecule of the dimer is involved.¹

LJ-HB potential calculations suggest one parallel stacked head-to-tail displaced, one parallel stacked rotated, and four parallel planar configurations for the pyrimidine dimer. No perpendicular geometry can be calculated using LJ-HB or a multipolar form.^{1,2} All calculations give nearly identical geometries and binding energies for the parallel planar and stacked configurations.

The features at -168 cm^{-1} is suggested to be due to the parallel stacked and displaced head-to-tail geometry. One would expect this structure to have only one spectroscopically observed Q_0^0 transition and a substantial red shift. The remaining features in the spectra, due to their significant blue shifts, must be attributed to planar hydrogen bonded dimers. The feature at $+296\text{ cm}^{-1}$ is suggested to be due to configuration I shown in Fig. 7. This configuration of the pyrimidine dimer forms two hydrogen bonds both of which involve the hydrogen atoms between the two ring nitrogen atoms on each pyrimidine: these hydrogens are the most electropositive (acidic) hydrogens on the ring. This configuration also has the monomers closest to each other (5.5 \AA compared to 6.0 \AA in the others). These factors suggest that configuration I gives rise to the most blue shifted feature in the spectra. The remaining three configurations II, III, and IV must generate the features in the $+175\text{ cm}^{-1}$ region. Configuration II is a symmetrical dimer and will account for one feature while configurations III and IV each will account for two features since the pyrimidines in these last two configurations are not symmetry equivalent. Assigning these features to configurations II, III, and IV is a difficult task without further information: five of the eight major features in this region can, however, be associated with origins of configurations II, III, and IV.

The parallel planar hydrogen bonded configuration I is assigned to the large blue shift, low ionization energy feature, and the parallel stacked displaced geometry is assigned to the large red shifted, high ionization energy feature. On the other hand, the parallel planar pyrazine dimer is assigned to the feature with the higher ionization energy (and also a small red shift). Clearly the two dimers have a very different electronic structure and the component monomers must interact in a different manner. A possible explanation for these apparent differences is that the N-C-N moiety of the pyrimidine system becomes the positive end of the molecular ion which is in turn well solvated in the parallel planar dimer thus lowering the ionization energy, and that the loss of electron density in the N-C-N region in the $n\pi^*$ excited state reduces the hydrogen bond energy thus increasing the energy of the excited S_1 state and causing a dimer blue shift. Similar arguments can be rendered to rationalize a negligible shift for the pyrazine system. We caution, however, that all such qualitative reasoning is subject to verification by more rigorous quantum mechanical calculations.

To ensure that our LJ-HB potential can produce other perpendicular dimer configurations, we have calculated the geometries expected for the tetrazine system. The tetrazine dimer has been studied by Levy and co-workers,³ who have reported two geometries: a parallel planar configuration and a perpendicular configuration. These experiments involve rotationally resolved fluorescence excitation spectra. Our calculations generate three geometries for this dimer: a parallel planar configuration, a parallel, stacked and 90° rotated configuration, and a perpendicular configuration, as shown in Fig. 12. The calculated perpendicular configuration has one hydrogen of the stem tetrazine pointing towards an N-N

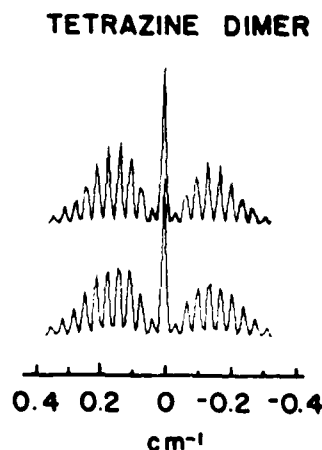


FIG. 13. Calculated rotational contours of the parallel polarized transition of the perpendicular tetrazine dimer centered at $18\,272.0\text{ cm}^{-1}$ (0 cm^{-1} in the figure). The upper trace is calculated using the rotational constants obtained from the perpendicular configuration reported in Ref. 3(a). The lower trace is calculated using the rotational constants obtained from the perpendicular configuration reported in this work. A symmetric top model is assumed for both calculations and the intensities used are those of Ref. 3(a). The rotational constants employed are given in the text, in the symmetric top approximation $\bar{B}^* = (B^* + C^*)/2$.

bond of the base tetrazine. In this configuration the plane of the stem tetrazine bisects the two N-N bonds of the base tetrazine. Levy's published perpendicular configuration^{11(a)} has one hydrogen of the two C-H bonds of the stem tetrazine pointing toward one C-H bond of the base tetrazine and the plane of the stem tetrazine passing through the two C-H bonds of the base tetrazine. Rotational constants reported by Levy and obtained from a rotational analysis of the perpendicular configuration for parallel polarization are $A'' = 0.07287 \text{ cm}^{-1}$, $B'' = 0.01722 \text{ cm}^{-1}$, and $C'' = 0.01649 \text{ cm}^{-1}$. Rotational constants obtained from our calculated perpendicular configuration are $A'' = 0.06458 \text{ cm}^{-1}$, $B'' = 0.01644 \text{ cm}^{-1}$, and $C'' = 0.018466$. These two sets of rotational constants render reasonably similar spectra, as can be seen in Fig. 13.

V. CONCLUSION

The analysis of the structure and properties of the pyrazine and pyrimidine dimers is based on an interpretation of ionization energy dependence, van der Waals vibronic structure, dimer spectral shifts, and potential energy calculations with LJ-HB and multipolar forms.

Variation of the ionizing laser energy allows different configuration dimers of a particular species to be identified. The pyrazine (h_4 and d_4) dimer has two identified geometries based on ionization energy dependence and vibronic analysis. Given the dimer spectral shifts and calculations, these have been associated with a planar parallel hydrogen bonded configuration and a perpendicular configuration. A third geometry, planar stacked and rotated 90° , is calculated but not observed probably due to excimer formation.

The pyrimidine dimers absorb in three spectral regions. The lowest energy feature is thought to be the calculated head-to-tail parallel stacked displaced geometry, the highest energy feature is assigned as a parallel planar strongly hydrogen bonded form in which the most electropositive H atoms are involved in the hydrogen bonding. The features at $+175 \text{ cm}^{-1}$ are attributed to different planar configurations which are only weakly hydrogen bonded through the less acidic hydrogens on the rings.

Dimer spectral shifts are expected to follow the rules determined previously for solute-solvent clusters: the major red shift mechanism is π -system coordination or overlap between the two molecules and the major blue shift mechanism is hydrogen bonding. Ionization energies can be rationalized in accordance with the general notions of ion solvation by either the π system in the case of pyrazine or the N-C-N hydrogen bonding region in the case of pyrimidine.

Calculations are also presented for the tetrazine dimers to compare parallel planar and perpendicular spectroscopically assigned geometries and our calculations. Calculations predict, and experiments suggest, perpendicular geometries for toluene, benzene-toluene, pyrazine, and tetrazine but not for benzene. Moreover, calculations predict, and experiments are consistent with, the absence of perpendicular geometries for the pyrimidine dimer. Perhaps one of the most remarkable results of this study is the rather large number of different, roughly equal binding energy configurations found for the N-heterocyclic aromatic dimers in general.

¹K. S. Law, M. Schauer, and E. R. Bernstein, *J. Chem. Phys.* **81**, 4871 (1984).

²M. Schauer and E. R. Bernstein, *J. Chem. Phys.* **82**, 3722 (1985).

³(a) C. A. Haynam, D. V. Brumbaugh, and D. H. Levy, *J. Chem. Phys.* **79**, 1581 (1983); (b) L. Young, C. A. Haynam, and D. H. Levy, *ibid.* **79**, 1592 (1983).

⁴Y. D. Park and D. H. Levy, *J. Chem. Phys.* **81**, 5527 (1984).

⁵D. V. Brumbaugh, C. A. Haynam, and D. H. Levy, *J. Chem. Phys.* **73**, 5380 (1980).

⁶D. E. Poeltl and J. K. McVey, *J. Chem. Phys.* **78**, 4349 (1983).

⁷Y. Tomioka, H. Abe, N. Mikami, and M. Ito, *J. Phys. Chem.* **88**, 5186 (1984).

⁸J. Wanna and E. R. Bernstein, *J. Chem. Phys.* **84**, 927 (1986).

⁹(a) F. A. Momany, L. M. Carruthers, R. F. McGuire, and H. A. Scheraga, *J. Phys. Chem.* **78**, 1595 (1974); (b) G. Nemethy, M. S. Pottle, and H. A. Scheraga, *ibid.* **87**, 1883 (1983).

¹⁰F. Mulder, G. Van Dijk, and C. Huuszoon, *Mol. Phys.* **38**, 577 (1979).

¹¹G. Herzberg, *Molecular Spectra and Molecular Structure. II. Infrared and Raman Spectra of Polyatomic Molecules* (Van Nostrand Reinhold, New York, 1945), Chaps. I and IV.

¹²P. J. Wheatley, *Acta Crystallogr.* **10**, 182 (1957).

¹³P. J. Wheatley, *Acta Crystallogr.* **13**, 80 (1960).

APPENDIX THREE

"ECCEMP2"

```

10 | .....
20 | Program name: ECCEMP2
30 |
40 | This program calculates cluster binding energy and geometry using an empiri
50 | cal atom-atom Lennard-Jones potential. The potential includes 6-12 general
60 | non-bonding, 10-12 general hydrogen bonding, and 1 monopole charge terms.
70 | The program will perform calculations on clusters composed of up to three
80 | molecules (subunits).
90 |
100 | Geometry and binding energy optimization is accomplished by analyzing the
110 | forces and torques on the cluster subunits which result from the intermole
120 | cular potential between the cluster subunits. The molecules are translated
130 | in three dimensions and rotated about the their centers-of-mass in three
140 | dimensions in response to the forces and torques. Binding energy and
150 | geometry optimization is achieved by simultaneously manipulating the six
160 | degrees of freedom until the forces and torques are zero; that is, until
170 | minimum energy and optimal geometry are obtained.
180 |
190 | This program also calculates the intermolecular force field for van der
200 | Waals vibrational mode modeling which can be conducted using the VDWNCA
210 | program. The ECCEMP2 program will determine the intermolecular force
220 | field for clusters containing up to 25 atoms total (solute+solvent).
230 | .....
240 |
250 | OPTION BASE 1
260 | PRINTER IS 1
270 | OUTPUT 2;CHR$(255)&"K";
280 | DEG
290 |
300 | .....
310 | Coordinate matrices for atoms composing cluster subunits.
320 |
330 | Co(*)=Carbon coordinates.
340 | Hh(*)=Hydrogen coordinates.
350 | Nn(*)=Nitrogen coordinates.
360 | Oo(*)=Oxygen coordinates.
370 | Zn(*)=User defined coordinates.
380 | (*)=(subunit,atom #,atom type,coordinates and charges and hydrogen
390 | bonding flags).
400 | .....
410 |
420 | DIM Co(3,44,5,5),Hh(3,44,5,5),Nn(3,12,5,5),Oo(3,12,5,5),Zn(3,12,5,5)
430 |
440 | .....
450 | N(*)=Number of atoms in cluster subunit. (*)=(subunit,atom,atom type).
460 | Ljpar(*)=non-bonding parameter matrix. (*)=(atom,atom type,polarizabilities
470 | and electrons and intermolecular distances).
480 | Fdir(*)=Force matrix. (*)=(subunit,component,force and direction
490 | indicator and last move direction indicator).
500 | Mdir(*)=Moment (torque) matrix. (*)=(subunit,component,moment and direction
510 | indicator and last direction indicator).
520 | Tx(*),Ty(*),Tz(*)=Translation matrices. (*)=(subunit).

```

```

530 | Rx(*) , Ry(*) , Rz(*) = Rotation matrices. (*) = (subunit).
540 | Cg(*) = Center-of-mass matrix. (*) = (subunit, coordinates).
550 | Rstep(*) = Rotation step matrix. (*) = (subunit, direction).
560 | Tstep(*) = Translation step matrix. (*) = (subunit, direction).
570 | T1(*) = Temporary translation step matrix. (*) = (subunit, direction).
580 | R1(*) = Temporary rotation step matrix. (*) = (subunit, direction).
590 |
600 |
610 DIM N(3,5,5), Ljpar(5,5,3)
620 DIM Fdir(3,3,3), Mdir(3,3,3)
630 DIM Tx(3), Ty(3), Tz(3), Rx(3), Ry(3), Rz(3)
640 DIM Cg(3,3), Rstep(3,3), Tstep(3,3), T1(3,3), R1(3,3)
650 GCLEAR
660 Look=7 | Default graphics display limits set at 7 angstroms.
670 Sol=1 | Default flag which draws solute and solvents.
680 Do=2 | Effective dielectric constant for monopole charge interaction.
690 BEEP
700 QS="Q"
710 INPUT "Do you want expanded graphics?", QS
720 IF QS="Y" THEN DUMP DEVICE IS 710, EXPANDED
730 IF QS="N" THEN DUMP DEVICE IS 710
740 IF QS<>"Y" AND QS<>"N" THEN 700
750 PRINT "....."
760 PRINT "*"
770 PRINT "      Empirical vdW Cluster"
780 PRINT "      Configuration Energy"
790 PRINT "      Minimization Program (ECCEMP)"
800 PRINT "*"
810 PRINT "*"
820 PRINT "      Version ECCEMP/2"
830 PRINT "      by"
840 PRINT "      Joseph A. Menapace"
850 PRINT "      5 October 1986"
860 PRINT "*"
870 PRINT "*"
880 PRINT "      Developed from ECEPP/2"
890 PRINT "      G. Nemethy, M.S. Pottle, and H.A. Scheraga"
900 PRINT "      J. Phys. Chem. 87, 1883 (1983)"
910 PRINT "*"
920 PRINT "....."
930 |
940 |
950 | Main Menu:
960 |
970 | In Coef - Inputs non-bonding parameters from disc storage file LJPARAM or
980 | a file created by the user. Subroutine used - Inputcf.
990 |
1000| In Coord - Inputs a cluster coordinate file from disc storage or from
1010| the keyboard. Subroutine used - Inputco.
1020|
1030| Energy - Calculates the cluster binding energy at any geometry. Subroutine
1040| used - Energy.
1050|
1060| Minimize - Performs cluster geometry and binding energy optimization.
1070| Subroutine used - Minimize.
1080|
1090| Move - Translates and rotates cluster subunits in three dimensions.

```

```

1100 | Subroutine used - Hand.
1110 |
1120 | Draw - Draws the cluster geometry in four perspectives. Subroutine
1130 | used - Draw.
1140 |
1150 | NCA - Generates the intermolecular force field for the intermolecular
1160 | normal coordinate analysis performed by VDWNCA. Subroutine used - Eigen.
1170 |
1180 | Quit - Stops the subroutines and returns execution to the Main Menu.
1190 | Subroutine used - Quit.
1200 |
1210 | Stor Con - Stores the cluster coordinates in user defined storage files.
1220 | Subroutine used - File.
1230 |
1240 |
1250 ON KEY 0 LABEL "In Coef",3 GOSUB Inputcf
1260 ON KEY 1 LABEL "In Coord",3 GOSUB Inputco
1270 ON KEY 2 LABEL "Energy",3 GOSUB Energy
1280 ON KEY 3 LABEL "Minimize",3 GOTO Minimize
1290 ON KEY 4 LABEL "Move",3 GOSUB Hand
1300 ON KEY 5 LABEL "Draw",3 GOSUB Draw
1310 ON KEY 6 LABEL "NCA",3 GOSUB Eigen
1320 ON KEY 9 LABEL "Quit",3 GOTO Quit
1330 ON KEY 7 LABEL "Stor Con",3 GOSUB File
1340 BEEP
1350 GOTO 1350
1360 |
1370 |
1380 | Subroutine: Inputcf
1390 |
1400 | Inputs non-bonding parameter data file from disc storage or from
1410 | keyboard. Parameters are stored in Ljper(*). Parameters include polariza-
1420 | bilities, number of electrons, and intermolecular distances for the atoms
1430 | in question.
1440 |
1450 |
1460 Inputcf: PRINTER IS 1 |
1470 OUTPUT 2;CHR$(255)&"K";
1480 GOTO 1500
1490 CAT
1500 QS="Q"
1510 INPUT "Do you want to start another COEFICIENT data file?",QS
1520 IF QS="N" THEN 1830
1530 IF QS<>"Y" THEN 1500
1540 ON ERROR GOTO 1490
1550 |
1560 |
1570 | This routine allows the user to enter and update data from the keyboard.
1580 |
1590 |
1600 INPUT "What is your N E W COEFICIENT file name?",Coef$
1610 CREATE BDAT Coef$&":INTERNAL",75,8
1620 OFF ERROR
1630 GOSUB Atommenu
1640 INPUT "Select the atom.",AtomI$
1650 GOSUB Attpmenu
1660 INPUT "Select the atom type.",AttpI$

```



```

2220 INPUT "Do you want to make changes or additions?",Q$
2230 IF Q$="N" THEN 2250
2240 IF Q$<>"Y" THEN 2210
2250 GOTO 1630
2260 BEEP
2270 OUTPUT 2;CHR$(255)&"K";
2290 RETURN
2290 !
2300 !!!!!!!!!!!!!!!!!!!!!!!!!!!!!!!!!!!!!!!!!!!!!!!!!!!!!!!!!!!!!!!!!!!!!!!!!!!!!!!
2310 ! Subroutine: Inputco
2320 !
2330 ! Inputs cluster coordinates, atomic charges, and hydrogen bonding flags
2340 ! into coordinate matrices from disc storage or from the keyboard.
2350 !!!!!!!!!!!!!!!!!!!!!!!!!!!!!!!!!!!!!!!!!!!!!!!!!!!!!!!!!!!!!!!!!!!!!!!!!!!!!!!
2360 !
2370 Inputco: !
2380 OUTPUT 2;CHR$(255)&"K";
2390 GOTO 2410
2400 CAT
2410 Q$="Q"
2420 INPUT "Do you want to start another COORDINATE file name?",Q$
2430 IF Q$="N" THEN 3890
2440 IF Q$<>"Y" THEN 2410
2450 ON ERROR GOTO 2400
2460 !
2470 !!!!!!!!!!!!!!!!!!!!!!!!!!!!!!!!!!!!!!!!!!!!!!!!!!!!!!!!!!!!!!!!!!!!!!!!!!!!!!!
2480 ! This routine allows the user to enter the coordinates, charges, and
2490 ! hydrogen bonding flags from the keyboard.
2500 !!!!!!!!!!!!!!!!!!!!!!!!!!!!!!!!!!!!!!!!!!!!!!!!!!!!!!!!!!!!!!!!!!!!!!!!!!!!!!!
2510 !
2520 INPUT "What is your N E W COORDINATE file name?",Coord$
2530 CREATE BDAT Coord$&":INTERNAL",9400,8
2540 OFF ERROR
2550 INPUT "Enter the total number of molecules.",L
2560 IF L<1 OR L>3 THEN 2550
2570 INPUT "What ligand are you working on (1 for solute)?",K
2580 IF K<1 OR K>3 THEN 2570
2590 INPUT "Center of mass X coordinate?",Cq(K,1)
2600 INPUT "Center of mass Y coordinate?",Cq(K,2)
2610 INPUT "Center of mass Z coordinate?",Cq(K,3)
2620 GOSUB Atommenu
2630 INPUT "What atom coords are you inputting?",Atom1$
2640 GOSUB Attpmenu
2650 INPUT "What is the atom type?",Attp1$
2660 GOSUB Atomnumbers
2670 IF Atom1=0 OR Attp1=0 THEN DISP "BAD SELECTION !!!!!"
2680 IF Atom1=0 OR Attp1=0 THEN WAIT 2
2690 IF Atom1=0 OR Attp1=0 THEN 2620
2700 INPUT "How many?",N(K,Atom1,Attp1)
2710 FOR J=1 TO N(K,Atom1,Attp1)
2720 OUTPUT 2;CHR$(255)&"K";
2730 GOSUB Atomnames
2740 PRINT Attp1$;" ";Atom1$;" Number";J
2750 PRINT
2760 !
2770 !!!!!!!!!!!!!!!!!!!!!!!!!!!!!!!!!!!!!!!!!!!!!!!!!!!!!!!!!!!!!!!!!!!!!!!!!!!!!!!
2780 ! Inputs carbon coordinates, charges, and hydrogen bonding flags from the

```

```

2790 | keyboard.
2800 |
2810 |
2820 IF Atom1=1 THEN INPUT "Enter X coordinate.",Co(K,J,Attpl,1)
2830 IF Atom1=1 THEN PRINT "X Coordinate":Co(K,J,Attpl,1)
2840 IF Atom1=1 THEN INPUT "Enter Y coordinate.",Co(K,J,Attpl,2)
2850 IF Atom1=1 THEN PRINT "Y Coordinate":Co(K,J,Attpl,2)
2860 IF Atom1=1 THEN INPUT "Enter Z coordinate.",Co(K,J,Attpl,3)
2870 IF Atom1=1 THEN PRINT "Z Coordinate":Co(K,J,Attpl,3)
2880 IF Atom1=1 THEN INPUT "Enter atom charge.",Co(K,J,Attpl,4)
2890 IF Atom1=1 THEN PRINT "Atom Charge":Co(K,J,Attpl,4)
2900 QS="Q"
2910 IF Atom1=1 THEN INPUT "Is the atom a hydrogen bonder?",QS
2920 IF Atom1=1 AND QS="N" THEN Co(K,J,Attpl,5)=0
2930 IF Atom1=1 AND QS="Y" THEN Co(K,J,Attpl,5)=1
2940 IF Atom1=1 AND QS<>"Y" AND QS<>"N" THEN 2900
2950 IF Atom1=1 THEN PRINT "Hydrogen Bonding":Co(K,J,Attpl,5)
2960 |
2970 |
2980 | Inputs hydrogen coordinates, charges, and hydrogen bonding flags from the
2990 | keyboard.
3000 |
3010 |
3020 IF Atom1=2 THEN INPUT "Enter X coordinate.",Hh(K,J,Attpl,1)
3030 IF Atom1=2 THEN PRINT "X Coordinate":Hh(K,J,Attpl,1)
3040 IF Atom1=2 THEN INPUT "Enter Y coordinate.",Hh(K,J,Attpl,2)
3050 IF Atom1=2 THEN PRINT "Y Coordinate":Hh(K,J,Attpl,2)
3060 IF Atom1=2 THEN INPUT "Enter Z coordinate.",Hh(K,J,Attpl,3)
3070 IF Atom1=2 THEN PRINT "Z Coordinate":Hh(K,J,Attpl,3)
3080 IF Atom1=2 THEN INPUT "Enter atom charge.",Hh(K,J,Attpl,4)
3090 IF Atom1=2 THEN PRINT "Atom Charge":Hh(K,J,Attpl,4)
3100 QS="Q"
3110 IF Atom1=2 THEN INPUT "Is the atom a hydrogen bonder?",QS
3120 IF Atom1=2 AND QS="N" THEN Hh(K,J,Attpl,5)=0
3130 IF Atom1=2 AND QS="Y" THEN Hh(K,J,Attpl,5)=1
3140 IF Atom1=2 AND QS<>"Y" AND QS<>"N" THEN 3100
3150 IF Atom1=2 THEN PRINT "Hydrogen Bonding":Hh(K,J,Attpl,5)
3160 |
3170 |
3180 | Inputs nitrogen coordinates, charges, and hydrogen bonding flags from the
3190 | keyboard.
3200 |
3210 |
3220 IF Atom1=3 THEN INPUT "Enter X coordinate.",Nn(K,J,Attpl,1)
3230 IF Atom1=3 THEN PRINT "X Coordinate":Nn(K,J,Attpl,1)
3240 IF Atom1=3 THEN INPUT "Enter Y coordinate.",Nn(K,J,Attpl,2)
3250 IF Atom1=3 THEN PRINT "Y Coordinate":Nn(K,J,Attpl,2)
3260 IF Atom1=3 THEN INPUT "Enter Z coordinate.",Nn(K,J,Attpl,3)
3270 IF Atom1=3 THEN PRINT "Z Coordinate":Nn(K,J,Attpl,3)
3280 IF Atom1=3 THEN INPUT "Enter atom charge.",Nn(K,J,Attpl,4)
3290 IF Atom1=3 THEN PRINT "Atom Charge":Nn(K,J,Attpl,4)
3300 QS="Q"
3310 IF Atom1=3 THEN INPUT "Is the atom a hydrogen bonder?",QS
3320 IF Atom1=3 AND QS="N" THEN Nn(K,J,Attpl,5)=0
3330 IF Atom1=3 AND QS="Y" THEN Nn(K,J,Attpl,5)=1
3340 IF Atom1=3 AND QS<>"Y" AND QS<>"N" THEN 3300
3350 IF Atom1=3 THEN PRINT "Hydrogen Bonding":Nn(K,J,Attpl,5)

```

```

3360 |
3370 |
3380 | Inputs oxygen coordinates, charges, and hydrogen bonding flags from the
3390 | keyboard.
3400 |
3410 |
3420 IF Atom1=4 THEN INPUT "Enter X coordinate.",Oo(K,J,Attp1,1)
3430 IF Atom1=4 THEN PRINT "X Coordinate";Oo(K,J,Attp1,1)
3440 IF Atom1=4 THEN INPUT "Enter Y coordinate.",Oo(K,J,Attp1,2)
3450 IF Atom1=4 THEN PRINT "Y Coordinate";Oo(K,J,Attp1,2)
3460 IF Atom1=4 THEN INPUT "Enter Z coordinate.",Oo(K,J,Attp1,3)
3470 IF Atom1=4 THEN PRINT "Z Coordinate";Oo(K,J,Attp1,3)
3480 IF Atom1=4 THEN INPUT "Enter atom charge.",Oo(K,J,Attp1,4)
3490 IF Atom1=4 THEN PRINT "Atom Charge";Oo(K,J,Attp1,4)
3500 Q$="Q"
3510 IF Atom1=4 THEN INPUT "Is the atom a hydrogen bonder?",Q$
3520 IF Atom1=4 AND Q$="N" THEN Oo(K,J,Attp1,5)=0
3530 IF Atom1=4 AND Q$="Y" THEN Oo(K,J,Attp1,5)=1
3540 IF Atom1=4 AND Q$<>"Y" AND Q$<>"N" THEN 3500
3550 IF Atom1=4 THEN PRINT "Hydrogen Bonding";Oo(K,J,Attp1,5)
3560 |
3570 |
3580 | Inputs user defined coordinates, charges, and hydrogen bonding flags from
3590 | the keyboard.
3600 |
3610 |
3620 IF Atom1=5 THEN INPUT "Enter X coordinate.",Zn(K,J,Attp1,1)
3630 IF Atom1=5 THEN PRINT "X Coordinate";Zn(K,J,Attp1,1)
3640 IF Atom1=5 THEN INPUT "Enter Y coordinate.",Zn(K,J,Attp1,2)
3650 IF Atom1=5 THEN PRINT "Y Coordinate";Zn(K,J,Attp1,2)
3660 IF Atom1=5 THEN INPUT "Enter Z coordinate.",Zn(K,J,Attp1,3)
3670 IF Atom1=5 THEN PRINT "Z Coordinate";Zn(K,J,Attp1,3)
3680 IF Atom1=5 THEN INPUT "Enter atom charge.",Zn(K,J,Attp1,4)
3690 IF Atom1=5 THEN PRINT "Atom Charge";Zn(K,J,Attp1,4)
3700 Q$="Q"
3710 IF Atom1=5 THEN INPUT "Is the atom a hydrogen bonder?",Q$
3720 IF Atom1=5 AND Q$="N" THEN Zn(K,J,Attp1,5)=0
3730 IF Atom1=5 AND Q$="Y" THEN Zn(K,J,Attp1,5)=1
3740 IF Atom1=5 AND Q$<>"Y" AND Q$<>"N" THEN 3700
3750 IF Atom1=5 THEN PRINT "Hydrogen Bonding";Zn(K,J,Attp1,5)
3760 NEXT J
3770 Q$="Q"
3780 INPUT "Are you done with this molecule?",Q$
3790 IF Q$="N" THEN 2620
3800 IF Q$<>"Y" THEN 3770
3810 Q$="Q"
3820 INPUT "Are you done inputting?",Q$
3830 IF Q$="N" THEN 2570
3840 IF Q$<>"Y" THEN 3810
3850 ASSIGN @Coord TO Coord$
3860 OUTPUT @Coord;L,Cq(*),N(*),Co(*),Hh(*),Nn(*),Oo(*),Zn(*)
3870 ASSIGN @Coord TO *
3880 GOTO 3970
3890 ON ERROR GOTO 2400
3900 |
3910 |
3920 | This routine inputs a user defined cluster coordinate file from

```

```

3930 ! disc storage and displays it on the screen.
3940 ! .....
3950 !
3960 INPUT "What is your COORDINATE data file name?",Coord$
3970 OUTPUT 2;CHR$(255)&"K":
3980 PRINT "Your COORDINATE data file name is",Coord$
3990 ASSIGN @Coord TO Coord$
4000 ENTER @Coord:L,Cq(*),N(*),Co(*),Hh(*),Nn(*),Oo(*),Zn(*)
4010 ASSIGN @Coord TO *
4020 OFF ERROR
4030 FOR K=1 TO L
4040 PRINT
4050 IF K=1 THEN PRINT "Solute"
4060 IF K>1 THEN PRINT "Ligand ";K-1
4070 PRINT
4080 PRINT "Center of mass",Cq(K,1);Cq(K,2);Cq(K,3)
4090 PRINT
4100 FOR Atom1=1 TO 5
4110 FOR Attp1=1 TO 5
4120 FOR J=1 TO N(K,Atom1,Attp1)
4130 GOSUB Atomnames
4140 IF Atom1=1 THEN PRINT Attp1$;" ";Atom1$;J;Co(K,J,Attp1,1);Co(K,J,Attp1,2);C
o(K,J,Attp1,3);
4150 IF Atom1=1 THEN PRINT Co(K,J,Attp1,4);Co(K,J,Attp1,5)
4160 IF Atom1=2 THEN PRINT Attp1$;" ";Atom1$;J;Hh(K,J,Attp1,1);Hh(K,J,Attp1,2);H
h(K,J,Attp1,3);
4170 IF Atom1=2 THEN PRINT Hh(K,J,Attp1,4);Hh(K,J,Attp1,5)
4180 IF Atom1=3 THEN PRINT Attp1$;" ";Atom1$;J;Nn(K,J,Attp1,1);Nn(K,J,Attp1,2);N
n(K,J,Attp1,3);
4190 IF Atom1=3 THEN PRINT Nn(K,J,Attp1,4);Nn(K,J,Attp1,5)
4200 IF Atom1=4 THEN PRINT Attp1$;" ";Atom1$;J;Oo(K,J,Attp1,1);Oo(K,J,Attp1,2);O
o(K,J,Attp1,3);
4210 IF Atom1=4 THEN PRINT Oo(K,J,Attp1,4);Oo(K,J,Attp1,5)
4220 IF Atom1=5 THEN PRINT Attp1$;" ";Atom1$;J;Zn(K,J,Attp1,1);Zn(K,J,Attp1,2);Z
n(K,J,Attp1,3);
4230 IF Atom1=5 THEN PRINT Zn(K,J,Attp1,4);Zn(K,J,Attp1,5)
4240 NEXT J
4250 NEXT Attp1
4260 NEXT Atom1
4270 NEXT K
4280 DISP "Here are your coordinates."
4290 WAIT 1
4300 QS="Q"
4310 !
4320 ! .....
4330 ! This routine allows for coordinate, charge, and hydrogen bonding flag
4340 ! changes and/or additions.
4350 ! .....
4360 !
4370 INPUT "Do you want to make changes or additions?",QS
4380 IF QS="N" THEN 5390
4390 IF QS<>"Y" THEN 4300
4400 QS="Q"
4410 INPUT "Do you want to add or change ENTIRE ligands?",QS
4420 IF QS="N" THEN 4450
4430 IF QS="Y" THEN 4400
4440 GOTO 2450

```

```

4450 INPUT "Enter molecule number (1 for solute).",K
4460 IF K<1 OR K>3 THEN 4450
4470 QS="Q"
4480 INPUT "Do you want to change the center of mass?",QS
4490 IF QS="N" THEN 4550
4500 IF QS<>"Y" THEN 4470
4510 INPUT "Center of mass X coordinate?",Cq(K,1)
4520 INPUT "Center of mass Y coordinate?",Cq(K,2)
4530 INPUT "Center of mass Z coordinate?",Cq(K,3)
4540 GOTO 4300
4550 GOSUB Atommenu
4560 INPUT "What atom coordinates?",Atom1$
4570 GOSUB Attpmenu
4580 INPUT "What is the atom type?",Attp1$
4590 INPUT "What number is the atom chosen?",J
4600 GOSUB Atomnumbers
4610 IF Atom1=0 OR Attp1=0 THEN DISP "BAD SELECTION !!!!!"
4620 IF Atom1=0 OR Attp1=0 THEN WAIT 2
4630 IF Atom1=0 OR Attp1=0 THEN 4550
4640 OUTPUT 2;CHR$(255)&"K";
4650 GOSUB Atomnames
4660 PRINT Attp1$;" ";Atom1$;" Number";J
4670 QS="Q"
4680 INPUT "Do you want to change the charge?",QS
4690 IF QS="N" THEN 4810
4700 IF QS<>"Y" THEN 4670
4710 IF Atom1=1 THEN INPUT "Enter atom charge.",Co(K,J,Attp1,4)
4720 IF Atom1=1 THEN PRINT "Atom Charge";Co(K,J,Attp1,4)
4730 IF Atom1=2 THEN INPUT "Enter atom charge.",Hh(K,J,Attp1,4)
4740 IF Atom1=2 THEN PRINT "Atom Charge";Hh(K,J,Attp1,4)
4750 IF Atom1=3 THEN INPUT "Enter atom charge.",Nn(K,J,Attp1,4)
4760 IF Atom1=3 THEN PRINT "Atom Charge";Nn(K,J,Attp1,4)
4770 IF Atom1=4 THEN INPUT "Enter atom charge.",Oo(K,J,Attp1,4)
4780 IF Atom1=4 THEN PRINT "Atom Charge";Oo(K,J,Attp1,4)
4790 IF Atom1=5 THEN INPUT "Enter atom charge.",Zn(K,J,Attp1,4)
4800 IF Atom1=5 THEN PRINT "Atom Charge";Zn(K,J,Attp1,4)
4810 QS="Q"
4820 INPUT "Do you want to change hydrogen bonding capability?",QS
4830 IF QS="N" THEN 4990
4840 IF QS<>"Y" THEN 4810
4850 QS="Q"
4860 INPUT "Is the atom a hydrogen bonder?",QS
4870 IF QS="Y" AND Atom1=1 THEN Co(K,J,Attp1,5)=1
4880 IF QS="Y" AND Atom1=2 THEN Hh(K,J,Attp1,5)=1
4890 IF QS="Y" AND Atom1=3 THEN Nn(K,J,Attp1,5)=1
4900 IF QS="Y" AND Atom1=4 THEN Oo(K,J,Attp1,5)=1
4910 IF QS="Y" AND Atom1=5 THEN Zn(K,J,Attp1,5)=1
4920 IF QS="Y" THEN 4990
4930 IF QS<>"N" THEN 4850
4940 IF Atom1=1 THEN Co(K,J,Attp1,5)=0
4950 IF Atom1=2 THEN Hh(K,J,Attp1,5)=0
4960 IF Atom1=3 THEN Nn(K,J,Attp1,5)=0
4970 IF Atom1=4 THEN Oo(K,J,Attp1,5)=0
4980 IF Atom1=5 THEN Zn(K,J,Attp1,5)=0
4990 IF Atom1=1 THEN PRINT "Hydrogen Bonding";Co(K,J,Attp1,5)
5000 IF Atom1=2 THEN PRINT "Hydrogen Bonding";Hh(K,J,Attp1,5)
5010 IF Atom1=3 THEN PRINT "Hydrogen Bonding";Nn(K,J,Attp1,5)

```



```

5590 PRINT
5600 IF Bcc=1 AND Bhb=1 THEN PRINT "Potential=Lennard-Jones+Charges+Hydrogen Bonding"
5610 IF Bcc=1 AND Bhb=0 THEN PRINT "Potential=Lennard-Jones+Charges"
5620 IF Bcc=0 AND Bhb=1 THEN PRINT "Potential=Lennard-Jones+Hydrogen Bonding"
5630 IF Bcc=0 AND Bhb=0 THEN PRINT "Potential=Lennard-Jones"
5640 PRINT
5650 FOR K=1 TO L
5660 IF K=1 THEN PRINT "Solute"
5670 IF K>1 THEN PRINT "Ligand";K-1
5680 PRINT
5690 PRINT "Center of Mass=";Cq(K,1);Cq(K,2);Cq(K,3)
5700 PRINT
5710 FOR Atoml=1 TO 5
5720 FOR Attpl=1 TO 5
5730 FOR J=1 TO N(K,Atoml,Attpl)
5740 GOSUB Atomnames
5750 PRINT Attpl$;" ";Atoml$;
5760 IF Atoml=1 THEN PRINT Co(K,J,Attpl,1);Co(K,J,Attpl,2);Co(K,J,Attpl,3);
5770 IF Atoml=1 THEN PRINT Co(K,J,Attpl,4);Co(K,J,Attpl,5)
5780 IF Atoml=2 THEN PRINT Hh(K,J,Attpl,1);Hh(K,J,Attpl,2);Hh(K,J,Attpl,3);
5790 IF Atoml=2 THEN PRINT Hh(K,J,Attpl,4);Hh(K,J,Attpl,5)
5800 IF Atoml=3 THEN PRINT Nn(K,J,Attpl,1);Nn(K,J,Attpl,2);Nn(K,J,Attpl,3);
5810 IF Atoml=3 THEN PRINT Nn(K,J,Attpl,4);Nn(K,J,Attpl,5)
5820 IF Atoml=4 THEN PRINT Oo(K,J,Attpl,1);Oo(K,J,Attpl,2);Oo(K,J,Attpl,3);
5830 IF Atoml=4 THEN PRINT Oo(K,J,Attpl,4);Oo(K,J,Attpl,5)
5840 IF Atoml=5 THEN PRINT Zn(K,J,Attpl,1);Zn(K,J,Attpl,2);Zn(K,J,Attpl,3);
5850 IF Atoml=5 THEN PRINT Zn(K,J,Attpl,4);Zn(K,J,Attpl,5)
5860 NEXT J
5870 NEXT Attpl
5880 NEXT Atoml
5890 PRINT
5900 NEXT K
5910 PRINT "Minimum Energy=";E
5920 PRINT
5930 FOR J=1 TO L
5940 IF J=1 THEN PRINT "Solute Forces "; "Fx=";Fdir(J,1,1); "Fy=";Fdir(J,2,1); "Fz=";
Fdir(J,3,1)
5950 IF J>1 THEN PRINT "Ligand";J-1; "Forces "; "Fx=";Fdir(J,1,1); "Fy=";Fdir(J,2,1);
"Fz=";Fdir(J,3,1)
5960 IF J=1 THEN PRINT "Solute Moments "; "Mx=";Mdir(J,1,1); "My=";Mdir(J,2,1); "Mz=";
Mdir(J,3,1)
5970 IF J>1 THEN PRINT "Ligand";J-1; "Moments "; "Mx=";Mdir(J,1,1); "My=";Fdir(J,2,1);
"Mz=";Mdir(J,3,1)
5980 PRINT
5990 NEXT J
6000 PRINT "Potential Curvature "; "Kxx=";Cvx; "Kyy=";Cvy; "Kzz=";Cvz
6010 PRINT
6020 PRINT
6030 PRINTER IS 1
6040 RETURN
6050 |
6060 |
6070 | Subroutine: Energy
6080 |
6090 | Calculates the cluster binding energy, forces, and torques for a specific
6100 | cluster geometry. Also calculates the intermolecular force field

```

```

6110 ! for UDWNCA.
6120 !!!!!!!!!!!!!!!!!!!!!!!!!!!!!!!!!!!!!!!!!!!!!!!!!!!!!!!!!!!!!!!!!!!!!!!!!!!!!!!!!!!!!!!!!!!!!!!!!!!!!!!!!!!!!!!!!!!!!
6130 !
6140 Energy: !
6150 !
6160 !!!!!!!!!!!!!!!!!!!!!!!!!!!!!!!!!!!!!!!!!!!!!!!!!!!!!!!!!!!!!!!!!!!!!!!!!!!!!!!!!!!!!!!!!!!!!!!!!!!!!!!!!!!!!!!!!!!!!
6170 ! Initialization of variables to start routine.
6180 !!!!!!!!!!!!!!!!!!!!!!!!!!!!!!!!!!!!!!!!!!!!!!!!!!!!!!!!!!!!!!!!!!!!!!!!!!!!!!!!!!!!!!!!!!!!!!!!!!!!!!!!!!!!!!!!!!!!!
6190 !
6200 E=0 ! Cluster binding energy.
6210 Eij=0 ! non-bonding term energy.
6220 Eqq=0 ! Monopole charge term energy.
6230 Ehb=0 ! Hydrogen bonding term energy.
6240 Cvx=0 ! Curvature x-x direction.
6250 Cvy=0 ! Curvature y-y direction.
6260 Cvz=0 ! Curvature z-z direction.
6270 FOR J=1 TO L
6280 FOR Dir1=1 TO 3
6290 Fdir(J,Dir1,1)=0
6300 Mdir(J,Dir1,1)=0
6310 NEXT Dir1
6320 NEXT J
6330 Row=1 ! Control variables for intermolecular force field disc storage.
6340 Fg=75 ! routine. Force field is stored in file: H2OE16.
6350 !
6360 !!!!!!!!!!!!!!!!!!!!!!!!!!!!!!!!!!!!!!!!!!!!!!!!!!!!!!!!!!!!!!!!!!!!!!!!!!!!!!!!!!!!!!!!!!!!!!!!!!!!!!!!!!!!!!!!!!!!!
6370 ! Summation over all atom-atom interactions between solute and solvents for
6380 ! intermolecular potential calculation.
6390 !!!!!!!!!!!!!!!!!!!!!!!!!!!!!!!!!!!!!!!!!!!!!!!!!!!!!!!!!!!!!!!!!!!!!!!!!!!!!!!!!!!!!!!!!!!!!!!!!!!!!!!!!!!!!!!!!!!!!
6400 !
6410 FOR K1=1 TO L
6420 FOR C1=1 TO 5
6430 FOR A1=1 TO N(K1,C1,A1)
6440 FOR J1=1 TO N(K1,C1,A1)
6450 FOR K2=2 TO L
6460 FOR C2=1 TO 5
6470 FOR A2=1 TO N(K2,C2,A2)
6480 FOR J2=1 TO N(K2,C2,A2)
6490 IF K2<=K1 THEN 11630
6500 D=0 ! Intermolecular distance initialization for atoms in question.
6510 !
6520 !!!!!!!!!!!!!!!!!!!!!!!!!!!!!!!!!!!!!!!!!!!!!!!!!!!!!!!!!!!!!!!!!!!!!!!!!!!!!!!!!!!!!!!!!!!!!!!!!!!!!!!!!!!!!!!!!!!!!
6530 ! Determines coordinates, charges, and hydrogen bonding flags for atoms
6540 ! involved in atom-atom potential terms.
6550 !!!!!!!!!!!!!!!!!!!!!!!!!!!!!!!!!!!!!!!!!!!!!!!!!!!!!!!!!!!!!!!!!!!!!!!!!!!!!!!!!!!!!!!!!!!!!!!!!!!!!!!!!!!!!!!!!!!!!
6560 !
6570 !!!!!!!!!!!!!!!!!!!!!!!!!!!!!!!!!!!!!!!!!!!!!!!!!!!!!!!!!!!!!!!!!!!!!!!!!!!!!!!!!!!!!!!!!!!!!!!!!!!!!!!!!!!!!!!!!!!!!
6580 ! Carbon coordinates, charges, and hydrogen bonding flags.
6590 !!!!!!!!!!!!!!!!!!!!!!!!!!!!!!!!!!!!!!!!!!!!!!!!!!!!!!!!!!!!!!!!!!!!!!!!!!!!!!!!!!!!!!!!!!!!!!!!!!!!!!!!!!!!!!!!!!!!!
6600 !
6610 IF C1=1 THEN Coord11=Co(K1,J1,A1,1)
6620 IF C1=1 THEN Coord12=Co(K1,J1,A1,2)
6630 IF C1=1 THEN Coord13=Co(K1,J1,A1,3)
6640 IF C1=1 THEN Coord14=Co(K1,J1,A1,4)
6650 IF C1=1 THEN Coord15=Co(K1,J1,A1,5)
6660 IF C2=1 THEN Coord21=Co(K2,J2,A2,1)
6670 IF C2=1 THEN Coord22=Co(K2,J2,A2,2)

```



```
6680 IF C2=1 THEN Coord23=Co(K2,J2,A2,3)
6690 IF C2=1 THEN Coord24=Co(K2,J2,A2,4)
6700 IF C2=1 THEN Coord25=Co(K2,J2,A2,5)
6710 !
6720 !!!!!!!!!!!!!!!!!!!!!!!!!!!!!!!!!!!!!!!!!!!!!!!!!!!!!!!!!!!!!!!!!!!!!!!!!!!!!!!
6730 ! Hydrogen coordinates, charges, and hydrogen bonding flags.
6740 !!!!!!!!!!!!!!!!!!!!!!!!!!!!!!!!!!!!!!!!!!!!!!!!!!!!!!!!!!!!!!!!!!!!!!!!!!!!!!!
6750 !
6760 IF C1=2 THEN Coord11=Hh(K1,J1,A1,1)
6770 IF C1=2 THEN Coord12=Hh(K1,J1,A1,2)
6780 IF C1=2 THEN Coord13=Hh(K1,J1,A1,3)
6790 IF C1=2 THEN Coord14=Hh(K1,J1,A1,4)
6800 IF C1=2 THEN Coord15=Hh(K1,J1,A1,5)
6810 IF C2=2 THEN Coord21=Hh(K2,J2,A2,1)
6820 IF C2=2 THEN Coord22=Hh(K2,J2,A2,2)
6830 IF C2=2 THEN Coord23=Hh(K2,J2,A2,3)
6840 IF C2=2 THEN Coord24=Hh(K2,J2,A2,4)
6850 IF C2=2 THEN Coord25=Hh(K2,J2,A2,5)
6860 !
6870 !!!!!!!!!!!!!!!!!!!!!!!!!!!!!!!!!!!!!!!!!!!!!!!!!!!!!!!!!!!!!!!!!!!!!!!!!!!!!!!
6880 ! Nitrogen coordinates, charges, and hydrogen bonding flags.
6890 !!!!!!!!!!!!!!!!!!!!!!!!!!!!!!!!!!!!!!!!!!!!!!!!!!!!!!!!!!!!!!!!!!!!!!!!!!!!!!!
6900 !
6910 IF C1=3 THEN Coord11=Nn(K1,J1,A1,1)
6920 IF C1=3 THEN Coord12=Nn(K1,J1,A1,2)
6930 IF C1=3 THEN Coord13=Nn(K1,J1,A1,3)
6940 IF C1=3 THEN Coord14=Nn(K1,J1,A1,4)
6950 IF C1=3 THEN Coord15=Nn(K1,J1,A1,5)
6960 IF C2=3 THEN Coord21=Nn(K2,J2,A2,1)
6970 IF C2=3 THEN Coord22=Nn(K2,J2,A2,2)
6980 IF C2=3 THEN Coord23=Nn(K2,J2,A2,3)
6990 IF C2=3 THEN Coord24=Nn(K2,J2,A2,4)
7000 IF C2=3 THEN Coord25=Nn(K2,J2,A2,5)
7010 !
7020 !!!!!!!!!!!!!!!!!!!!!!!!!!!!!!!!!!!!!!!!!!!!!!!!!!!!!!!!!!!!!!!!!!!!!!!!!!!!!!!
7030 ! Oxygen coordinates, charges, and hydrogen bonding flags.
7040 !!!!!!!!!!!!!!!!!!!!!!!!!!!!!!!!!!!!!!!!!!!!!!!!!!!!!!!!!!!!!!!!!!!!!!!!!!!!!!!
7050 !
7060 IF C1=4 THEN Coord11=Oo(K1,J1,A1,1)
7070 IF C1=4 THEN Coord12=Oo(K1,J1,A1,2)
7080 IF C1=4 THEN Coord13=Oo(K1,J1,A1,3)
7090 IF C1=4 THEN Coord14=Oo(K1,J1,A1,4)
7100 IF C1=4 THEN Coord15=Oo(K1,J1,A1,5)
7110 IF C2=4 THEN Coord21=Oo(K2,J2,A2,1)
7120 IF C2=4 THEN Coord22=Oo(K2,J2,A2,2)
7130 IF C2=4 THEN Coord23=Oo(K2,J2,A2,3)
7140 IF C2=4 THEN Coord24=Oo(K2,J2,A2,4)
7150 IF C2=4 THEN Coord25=Oo(K2,J2,A2,5)
7160 !
7170 !!!!!!!!!!!!!!!!!!!!!!!!!!!!!!!!!!!!!!!!!!!!!!!!!!!!!!!!!!!!!!!!!!!!!!!!!!!!!!!
7180 ! User defined atom coordinates, charges, and hydrogen bonding flags.
7190 !!!!!!!!!!!!!!!!!!!!!!!!!!!!!!!!!!!!!!!!!!!!!!!!!!!!!!!!!!!!!!!!!!!!!!!!!!!!!!!
7200 !
7210 IF C1=5 THEN Coord11=Zn(K1,J1,A1,1)
7220 IF C1=5 THEN Coord12=Zn(K1,J1,A1,2)
7230 IF C1=5 THEN Coord13=Zn(K1,J1,A1,3)
7240 IF C1=5 THEN Coord14=Zn(K1,J1,A1,4)
```

```

7250 IF C1=5 THEN Coord15=Zn(K1,J1,A1,5)
7250 IF C2=5 THEN Coord21=Zn(K2,J2,A2,1)
7270 IF C2=5 THEN Coord22=Zn(K2,J2,A2,2)
7280 IF C2=5 THEN Coord23=Zn(K2,J2,A2,3)
7290 IF C2=5 THEN Coord24=Zn(K2,J2,A2,4)
7300 IF C2=5 THEN Coord25=Zn(K2,J2,A2,5)
7310 !
7320 !
7330 ! Calculates atom-atom distances for atoms in question.
7340 !
7350 !
7360 D=(Coord21-Coord11)^2+(Coord22-Coord12)^2+(Coord23-Coord13)^2
7370 Dr=D^.5
7380 IF Dr=0 THEN 11600
7390 !
7400 !
7410 ! Calculates unit position vectors in each cartesian direction.
7420 !
7430 !
7440 Dx=(Coord21-Coord11)/Dr
7450 Dy=(Coord22-Coord12)/Dr
7460 Dz=(Coord23-Coord13)/Dr
7470 !
7480 !
7490 ! Calculates moment arm components in each cartesian direction. Moment arms
7500 ! are calculated relative to the cluster subunit center-of-mass.
7510 !
7520 !
7530 Dmx2=Coord21-Cq(K2,1)
7540 Dmy2=Coord22-Cq(K2,2)
7550 Dmz2=Coord23-Cq(K2,3)
7560 Dmx1=Coord11-Cq(K1,1)
7570 Dmy1=Coord12-Cq(K1,2)
7580 Dmz1=Coord13-Cq(K1,3)
7590 !
7600 !
7610 ! Initialization of variables for routine looping.
7620 !
7630 !
7640 Ehb=0
7650 Fhb=0 ! Force of hydrogen bonding interaction.
7660 Chb=0 ! Curvature of hydrogen bonding interaction.
7670 Elj=0
7680 Flj=0 ! Force of non-bonding interaction.
7690 Clj=0 ! Curvature of non-bonding interaction.
7700 Eqq=0
7710 Fqq=0 ! Force of monopole charge interaction.
7720 Cqqv=0 ! Curvature of monopole charge interaction.
7730 Ha=0 ! Hydrogen bonding repulsive parameter.
7740 Hb=0 ! Hydrogen bonding attractive parameter.
7750 Aa=0 ! Non-bonding repulsive parameter.
7760 Cc=0 ! Non-bonding attractive parameter.
7770 !
7780 !
7790 ! Calculates atom-atom non-bonding parameters using the Slater-Kirkwood
7800 ! approximation.
7810 !

```

```

7830 |
7830 | IF Ljpar(C1,A1,2)=0 OR Ljpar(C2,A2,2)=0 THEN 7900
7840 | Ljdenom=(Ljpar(C1,A1,1)*1.E-24/Ljpar(C1,A1,2)**1.5+Ljpar(C2,A2,1)*1.E-24/Lj
7840 | par(C2,A2,2))**.5
7850 | Ljnum=Ljpar(C1,A1,1)*1.E-24+Ljpar(C2,A2,1)*1.E-24
7860 | Ljconst=3/2*4.803242E-12*1.054887E-27/(9.109534E-29)**1.5*1.40681610E+10*1.E-
48*349.64
7870 | Cc=Ljconst*Ljnum/Ljdenom
7880 | Ljrad=(Ljpar(C1,A1,3)+Ljpar(C2,A2,3))/2
7890 | Aa=Cc/2*(Ljrad)**6
7900 | IF Coord15=0 OR Coord25=0 THEN 8550
7910 | Ha=0
7920 | Hb=0
7930 |
7940 |
7950 | Selects hydrogen bonding parameters to use in calculations.
7960 |
7970 |
7980 |
7990 | Amin hydrogen/amin nitrogen hydrogen bonding parameters.
8000 |
8010 |
8020 | IF C1=2 AND A1=2 AND C2=3 AND A2=1 THEN Hb=8244*349.64
8030 | IF C1=2 AND A1=2 AND C2=3 AND A2=1 THEN Ha=3.2897E+4*349.64
8040 | IF C1=3 AND A1=1 AND C2=2 AND A2=2 THEN Hb=8244*349.64
8050 | IF C1=3 AND A1=1 AND C2=2 AND A2=2 THEN Ha=3.2897E+4*349.64
8060 |
8070 |
8080 | Carb hydrogen/amin nitrogen hydrogen bonding parameters.
8090 |
8100 |
8110 | IF C1=2 AND A1=4 AND C2=3 AND A2=1 THEN Hb=8244*349.64
8120 | IF C1=2 AND A1=4 AND C2=3 AND A2=1 THEN Ha=3.2897E+4*349.64
8130 | IF C1=3 AND A1=1 AND C2=2 AND A2=4 THEN Hb=8244*349.64
8140 | IF C1=3 AND A1=1 AND C2=2 AND A2=4 THEN Ha=3.2897E+4*349.64
8150 |
8160 |
8170 | Amin hydrogen/carb oxygen hydrogen bonding parameters.
8180 |
8190 |
8200 | IF C1=2 AND A1=2 AND C2=4 AND A2=1 THEN Hb=4014*349.64
8210 | IF C1=2 AND A1=2 AND C2=4 AND A2=1 THEN Ha=1.2040E+4*349.64
8220 | IF C1=4 AND A1=1 AND C2=2 AND A2=2 THEN Hb=4014*349.64
8230 | IF C1=4 AND A1=1 AND C2=2 AND A2=2 THEN Ha=1.2040E+4*349.64
8240 |
8250 |
8260 | Hydr hydrogen/carb oxygen hydrogen bonding parameters.
8270 |
8280 |
8290 | IF C1=2 AND A1=4 AND C2=4 AND A2=1 THEN Hb=5783*349.64
8300 | IF C1=2 AND A1=4 AND C2=4 AND A2=1 THEN Ha=1.3344E+4*349.64
8310 | IF C1=4 AND A1=1 AND C2=2 AND A2=4 THEN Hb=5783*349.64
8320 | IF C1=4 AND A1=1 AND C2=2 AND A2=4 THEN Ha=1.3344E+4*349.64
8330 |
8340 |
8350 | Amin hydrogen/hydr oxygen hydrogen bonding parameters.
8360 |

```

```

8370 |
8380 IF C1=2 AND A1=2 AND C2=4 AND A2=2 THEN Hb=2524*349.64
8390 IF C1=2 AND A1=2 AND C2=4 AND A2=2 THEN Ha=5.690E+3*349.64
8400 IF C1=4 AND A1=2 AND C2=2 AND A2=2 THEN Hb=2524*349.64
8410 IF C1=4 AND A1=2 AND C2=2 AND A2=2 THEN Ha=5.890E+3*349.64
8420 |
8430 |
8440 | Hydr hydrogen/hydr oxygen hydrogen bonding parameters.
8450 |
8460 |
8470 IF C1=2 AND A1=4 AND C2=4 AND A2=2 THEN Hb=4610*349.64
8480 IF C1=2 AND A1=4 AND C2=4 AND A2=2 THEN Ha=1.122E+4*349.64
8490 IF C1=4 AND A1=2 AND C2=2 AND A2=4 THEN Hb=4610*349.64
8500 IF C1=4 AND A1=2 AND C2=2 AND A2=4 THEN Ha=1.122E+4*349.64
8510 |
8520 |
8530 | Calculates hydrogen bonding interaction between atoms in question.
8540 |
8550 |
8560 Ehb=8hb*(Ha/Dr^12-Hb/Dr^10)
8570 Fhb=8hb*(12*Ha/Dr^13-10*Hb/Dr^11)
8580 Chb=8hb*(12*13*Ha/Dr^14-10*11*Hb/Dr^12)
8590 IF Ehb<>0 THEN 8730
8600 |
8610 |
8620 | Calculates non-bonding interaction between atoms in question.
8630 |
8640 |
8650 E1j=Aa/Dr^12-Cc/Dr^6
8660 F1j=12*Aa/Dr^13-6*Cc/Dr^7
8670 C1j=12*13*Aa/Dr^14-6*7*Cc/Dr^8
8680 |
8690 |
8700 | Calculates monopole charge interaction between atoms in question.
8710 |
8720 |
8730 Eqq=8cc*Coord14*Coord24/Do/Dr*332*349.64
8740 Fqq=8cc*Coord14*Coord24/Do/Dr^2*332*349.64
8750 Cqqv=8cc*Coord14*Coord24*2/Do/Dr^3*332*349.64
8760 IF E1j=0 AND Ehb=0 THEN DISP "NO PARAMETER IN THE POTENTIAL"
8770 IF E1j=0 AND Ehb=0 THEN WAIT 2
8780 IF E1j=0 AND Ehb=0 THEN GOTO Quit
8790 |
8800 |
8810 | Determines total interaction energy, force, and curvature.
8820 |
8830 |
8840 E=E+E1j+Eqq+Ehb
8850 Force=F1j+Fqq+Fhb
8860 IF Cutoff=0 THEN 8900
8870 IF C1j<0 THEN C1j=0
8880 IF Cqqv<0 THEN Cqqv=0
8890 IF Chb<0 THEN Chb=0
8900 Curve=C1j+Cqqv+Chb
8910 IF Eigen=0 THEN 11360
8920 |
8930 |

```

```

8940 | Generates intermolecular force field for VDWCA and stores the field in
8950 | file H2OEIG. The force field is calculated using the central force
8960 | approximation. The calculations are conducted in the cartesian coordinate
8970 | system.
8980 |
8990 | Matel=Force constant matrix element in file H2OEIG.
9000 | Forcon=Intermolecular force constant for atom in question.
9010 | .....
9020 |
9030 | .....
9040 | Force constant in x-x direction.
9050 | .....
9060 |
9070 ASSIGN @Dest TO "H2OEIG"
9080 CONTROL @Dest,S;(Column-1)*Fg+Column
9090 ENTER @Dest;Matel
9100 CONTROL @Dest,S;(Column-1)*Fg+Column
9110 Forcon=Curve*(Dx^2)
9120 OUTPUT @Dest;Forcon+Matel
9130 CONTROL @Dest,S;(Row-1)*Fg+Column
9140 ENTER @Dest;Matel
9150 CONTROL @Dest,S;(Row-1)*Fg+Column
9160 Forcon=-Curve*(Dx^2)
9170 OUTPUT @Dest;Forcon+Matel
9180 CONTROL @Dest,S;(Column-1)*Fg+Row
9190 ENTER @Dest;Matel
9200 CONTROL @Dest,S;(Column-1)*Fg+Row
9210 Forcon=-Curve*(Dx)^2
9220 OUTPUT @Dest;Forcon+Matel
9230 CONTROL @Dest,S;(Row-1)*Fg+Row
9240 ENTER @Dest;Matel
9250 CONTROL @Dest,S;(Row-1)*Fg+Row
9260 Forcon=Curve*(Dx^2)
9270 |
9280 | .....
9290 | Force constant in x-y direction.
9300 | .....
9310 |
9320 OUTPUT @Dest;Forcon+Matel
9330 CONTROL @Dest,S;(Column-1)*Fg+Column+1
9340 ENTER @Dest;Matel
9350 CONTROL @Dest,S;(Column-1)*Fg+Column+1
9360 Forcon=Curve*(Dx*Dy)
9370 OUTPUT @Dest;Forcon+Matel
9380 CONTROL @Dest,S;(Column-1)*Fg+Row+1
9390 ENTER @Dest;Matel
9400 CONTROL @Dest,S;(Column-1)*Fg+Row+1
9410 Forcon=-Curve*(Dx*Dy)
9420 OUTPUT @Dest;Forcon+Matel
9430 CONTROL @Dest,S;(Row-1)*Fg+Column+1
9440 ENTER @Dest;Matel
9450 CONTROL @Dest,S;(Row-1)*Fg+Column+1
9460 Forcon=-Curve*(Dx*Dy)
9470 OUTPUT @Dest;Forcon+Matel
9480 CONTROL @Dest,S;(Row-1)*Fg+Row+1
9490 ENTER @Dest;Matel
9500 CONTROL @Dest,S;(Row-1)*Fg+Row+1

```

```

9510 Forcon=Curve*(Dx*Dy)
9520 |
9530 |
9540 | Force constant in x-z direction.
9550 |
9560 |
9570 OUTPUT @Dest:Forcon+Matel
9580 CONTROL @Dest,S:(Column-1)*Fg+Column+2
9590 ENTER @Dest:Matel
9600 CONTROL @Dest,S:(Column-1)*Fg+Column+2
9610 Forcon=Curve*(Dx*Dz)
9620 OUTPUT @Dest:Forcon+Matel
9630 CONTROL @Dest,S:(Column-1)*Fg+Row+2
9640 ENTER @Dest:Matel
9650 CONTROL @Dest,S:(Column-1)*Fg+Row+2
9660 Forcon=-Curve*(Dx*Dz)
9670 OUTPUT @Dest:Forcon+Matel
9680 CONTROL @Dest,S:(Row-1)*Fg+Column+2
9690 ENTER @Dest:Matel
9700 CONTROL @Dest,S:(Row-1)*Fg+Column+2
9710 Forcon=-Curve*(Dx*Dz)
9720 OUTPUT @Dest:Forcon+Matel
9730 CONTROL @Dest,S:(Row-1)*Fg+Row+2
9740 ENTER @Dest:Matel
9750 CONTROL @Dest,S:(Row-1)*Fg+Row+2
9760 Forcon=Curve*(Dx*Dz)
9770 |
9780 |
9790 | Force constant in y-x direction.
9800 |
9810 |
9820 OUTPUT @Dest:Forcon+Matel
9830 CONTROL @Dest,S:(Column+1-1)*Fg+Column
9840 ENTER @Dest:Matel
9850 CONTROL @Dest,S:(Column+1-1)*Fg+Column
9860 Forcon=Curve*(Dy*Dx)
9870 OUTPUT @Dest:Forcon+Matel
9880 CONTROL @Dest,S:(Column+1-1)*Fg+Row
9890 ENTER @Dest:Matel
9900 CONTROL @Dest,S:(Column+1-1)*Fg+Row
9910 Forcon=-Curve*(Dy*Dx)
9920 OUTPUT @Dest:Forcon+Matel
9930 CONTROL @Dest,S:(Row+1-1)*Fg+Column
9940 ENTER @Dest:Matel
9950 CONTROL @Dest,S:(Row+1-1)*Fg+Column
9960 Forcon=-Curve*(Dy*Dx)
9970 OUTPUT @Dest:Forcon+Matel
9980 CONTROL @Dest,S:(Row+1-1)*Fg+Row
9990 ENTER @Dest:Matel
10000 CONTROL @Dest,S:(Row+1-1)*Fg+Row
10010 Forcon=Curve*(Dy*Dx)
10020 |
10030 |
10040 | Force constant in y-y direction.
10050 |
10060 |
10070 OUTPUT @Dest:Forcon+Matel

```

```

10080 CONTROL @Dest,S1(Column+1-1)*Fg+Column+1
10090 ENTER @Dest:Matel
10100 CONTROL @Dest,S1(Column+1-1)*Fg+Column+1
10110 Forcon=Curve*(Dy^2)
10120 OUTPUT @Dest;Forcon+Matel
10130 CONTROL @Dest,S1(Column+1-1)*Fg+Row+1
10140 ENTER @Dest:Matel
10150 CONTROL @Dest,S1(Column+1-1)*Fg+Row+1
10160 Forcon=-Curve*(Dy^2)
10170 OUTPUT @Dest;Forcon+Matel
10180 CONTROL @Dest,S1(Row+1-1)*Fg+Column+1
10190 ENTER @Dest:Matel
10200 CONTROL @Dest,S1(Row+1-1)*Fg+Column+1
10210 Forcon=-Curve*(Dy^2)
10220 OUTPUT @Dest;Forcon+Matel
10230 CONTROL @Dest,S1(Row+1-1)*Fg+Row+1
10240 ENTER @Dest:Matel
10250 CONTROL @Dest,S1(Row+1-1)*Fg+Row+1
10260 Forcon=Curve*(Dy^2)
10270 !
10280 !!!!!!!!!!!!!!!!!!!!!!!!!!!!!!!!!!!!!!!!!!!!!!!!!!!!!!!!!!!!!!!!!!!!!!!!!!!!!!!
10290 ! Force constant in y-z direction.
10300 !!!!!!!!!!!!!!!!!!!!!!!!!!!!!!!!!!!!!!!!!!!!!!!!!!!!!!!!!!!!!!!!!!!!!!!!!!!!!!!
10310 !
10320 OUTPUT @Dest;Forcon+Matel
10330 CONTROL @Dest,S1(Column+1-1)*Fg+Column+2
10340 ENTER @Dest:Matel
10350 CONTROL @Dest,S1(Column+1-1)*Fg+Column+2
10360 Forcon=Curve*(Dy*Dz)
10370 OUTPUT @Dest;Forcon+Matel
10380 CONTROL @Dest,S1(Column+1-1)*Fg+Row+2
10390 ENTER @Dest:Matel
10400 CONTROL @Dest,S1(Column+1-1)*Fg+Row+2
10410 Forcon=-Curve*(Dy*Dz)
10420 OUTPUT @Dest;Forcon+Matel
10430 CONTROL @Dest,S1(Row+1-1)*Fg+Column+2
10440 ENTER @Dest:Matel
10450 CONTROL @Dest,S1(Row+1-1)*Fg+Column+2
10460 Forcon=-Curve*(Dy*Dz)
10470 OUTPUT @Dest;Forcon+Matel
10480 CONTROL @Dest,S1(Row+1-1)*Fg+Row+2
10490 ENTER @Dest:Matel
10500 CONTROL @Dest,S1(Row+1-1)*Fg+Row+2
10510 Forcon=Curve*(Dy*Dz)
10520 !
10530 !!!!!!!!!!!!!!!!!!!!!!!!!!!!!!!!!!!!!!!!!!!!!!!!!!!!!!!!!!!!!!!!!!!!!!!!!!!!!!!
10540 ! Force constant in z-x direction.
10550 !!!!!!!!!!!!!!!!!!!!!!!!!!!!!!!!!!!!!!!!!!!!!!!!!!!!!!!!!!!!!!!!!!!!!!!!!!!!!!!
10560 !
10570 OUTPUT @Dest;Forcon+Matel
10580 CONTROL @Dest,S1(Column+2-1)*Fg+Column
10590 ENTER @Dest:Matel
10600 CONTROL @Dest,S1(Column+2-1)*Fg+Column
10610 Forcon=Curve*(Dz*Dx)
10620 OUTPUT @Dest;Forcon+Matel
10630 CONTROL @Dest,S1(Column+2-1)*Fg+Row
10640 ENTER @Dest:Matel

```

```

10650 CONTROL @Dest,S;(Column+2-1)*Fg+Row
10660 Forcon=-Curve*(Dz*Dx)
10670 OUTPUT @Dest;Forcon+Matel
10680 CONTROL @Dest,S;(Row+2-1)*Fg+Column
10690 ENTER @Dest;Matel
10700 CONTROL @Dest,S;(Row+2-1)*Fg+Column
10710 Forcon=-Curve*(Dz*Dx)
10720 OUTPUT @Dest;Forcon+Matel
10730 CONTROL @Dest,S;(Row+2-1)*Fg+Row
10740 ENTER @Dest;Matel
10750 CONTROL @Dest,S;(Row+2-1)*Fg+Row
10760 Forcon=Curve*(Dz*Dx)
10770 !
10780 !!!!!!!!!!!!!!!!!!!!!!!!!!!!!!!!!!!!!!!!!!!!!!!!!!!!!!!!!!!!!!!!!!!!!!!!!!!!!!!
10790 ! Force constant in x-y direction.
10800 !!!!!!!!!!!!!!!!!!!!!!!!!!!!!!!!!!!!!!!!!!!!!!!!!!!!!!!!!!!!!!!!!!!!!!!!!!!!!!!
10810 !
10820 OUTPUT @Dest;Forcon+Matel
10830 CONTROL @Dest,S;(Column+2-1)*Fg+Column+1
10840 ENTER @Dest;Matel
10850 CONTROL @Dest,S;(Column+2-1)*Fg+Column+1
10860 Forcon=Curve*(Dz*Dy)
10870 OUTPUT @Dest;Forcon+Matel
10880 CONTROL @Dest,S;(Column+2-1)*Fg+Row+1
10890 ENTER @Dest;Matel
10900 CONTROL @Dest,S;(Column+2-1)*Fg+Row+1
10910 Forcon=-Curve*(Dz*Dy)
10920 OUTPUT @Dest;Forcon+Matel
10930 CONTROL @Dest,S;(Row+2-1)*Fg+Column+1
10940 ENTER @Dest;Matel
10950 CONTROL @Dest,S;(Row+2-1)*Fg+Column+1
10960 Forcon=-Curve*(Dz*Dy)
10970 OUTPUT @Dest;Forcon+Matel
10980 CONTROL @Dest,S;(Row+2-1)*Fg+Row+1
10990 ENTER @Dest;Matel
11000 CONTROL @Dest,S;(Row+2-1)*Fg+Row+1
11010 Forcon=Curve*(Dz*Dy)
11020 !
11030 !!!!!!!!!!!!!!!!!!!!!!!!!!!!!!!!!!!!!!!!!!!!!!!!!!!!!!!!!!!!!!!!!!!!!!!!!!!!!!!
11040 ! Force constant in z-z direction.
11050 !!!!!!!!!!!!!!!!!!!!!!!!!!!!!!!!!!!!!!!!!!!!!!!!!!!!!!!!!!!!!!!!!!!!!!!!!!!!!!!
11060 !
11070 OUTPUT @Dest;Forcon+Matel
11080 CONTROL @Dest,S;(Column+2-1)*Fg+Column+2
11090 ENTER @Dest;Matel
11100 CONTROL @Dest,S;(Column+2-1)*Fg+Column+2
11110 Forcon=Curve*(Dz^2)
11120 OUTPUT @Dest;Forcon+Matel
11130 CONTROL @Dest,S;(Row+2-1)*Fg+Column+2
11140 ENTER @Dest;Matel
11150 CONTROL @Dest,S;(Row+2-1)*Fg+Column+2
11160 Forcon=-Curve*(Dz^2)
11170 OUTPUT @Dest;Forcon+Matel
11180 CONTROL @Dest,S;(Column+2-1)*Fg+Row+2
11190 ENTER @Dest;Matel
11200 CONTROL @Dest,S;(Column+2-1)*Fg+Row+2
11210 Forcon=-Curve*(Dz)^2

```



```

11220 OUTPUT @Dest:Forcon+Matel
11230 CONTROL @Dest,S:(Row+2-1)*Fg+Row+2
11240 ENTER @Dest:Matel
11250 CONTROL @Dest,S:(Row+2-1)*Fg+Row+2
11260 Forcon=Curve*(Dz^2)
11270 OUTPUT @Dest:Forcon+Matel
11280 Column=Column+3
11290 IF Column=Last THEN Column=Begin
11300 !
11310 !
11320 ! Calculates force and curvature components in the three cartesian
11330 ! directions.
11340 !
11350 !
11360 Fdir(K2,1,1)=Fdir(K2,1,1)+Force*Dx
11370 Fdir(K2,2,1)=Fdir(K2,2,1)+Force*Dy
11380 Fdir(K2,3,1)=Fdir(K2,3,1)+Force*Dz
11390 Cvx=Cvx+Curve*Dx^2
11400 Cvy=Cvy+Curve*Dy^2
11410 Cvz=Cvz+Curve*Dz^2
11420 IF K1<>1 THEN Cvx=Cvx+Curve*Dx^2
11430 IF K1<>1 THEN Cvy=Cvy+Curve*Dy^2
11440 IF K1<>1 THEN Cvz=Cvz+Curve*Dz^2
11450 IF K1<>1 THEN Fdir(K1,1,1)=Fdir(K1,1,1)-Force*Dx
11460 IF K1<>1 THEN Fdir(K1,2,1)=Fdir(K1,2,1)-Force*Dy
11470 IF K1<>1 THEN Fdir(K1,3,1)=Fdir(K1,3,1)-Force*Dz
11480 !
11490 !
11500 ! Calculates the moments (torques) about the cartesian axes. Moments are
11510 ! determined relative to the cluster subunit center-of-mass.
11520 !
11530 !
11540 Mdir(K2,1,1)=Mdir(K2,1,1)+(Dmy2*Force*Dz-Dmz2*Force*Dy)
11550 Mdir(K2,2,1)=Mdir(K2,2,1)+(Dmz2*Force*Dx-Dmx2*Force*Dz)
11560 Mdir(K2,3,1)=Mdir(K2,3,1)+(Dmx2*Force*Dy-Dmy2*Force*Dx)
11570 IF K1<>1 THEN Mdir(K1,1,1)=Mdir(K1,1,1)+(Dmy1*(-Force)*Dz-Dmz1*(-Force)*Dy)
)
11580 IF K1<>1 THEN Mdir(K1,2,1)=Mdir(K1,2,1)+(Dmz1*(-Force)*Dx-Dmx1*(-Force)*Dz)
)
11590 IF K1<>1 THEN Mdir(K1,3,1)=Mdir(K1,3,1)+(Dmx1*(-Force)*Dy-Dmy1*(-Force)*Dx)
)
11600 NEXT J2
11610 NEXT A2
11620 NEXT C2
11630 NEXT K2
11640 Row=Row+3
11650 NEXT J1
11660 NEXT A1
11670 NEXT C1
11680 NEXT K1
11690 ASSIGN @Dest TO *
11700 IF Eigen=1 THEN RETURN
11710 IF Done=1 THEN RETURN
11720 IF Handl=0 THEN OUTPUT 2:CHR$(255)&"K";
11730 !
11740 !
11750 ! Prints the binding energy, forces, moments, and curvature on the screen.

```

```

11750 | .....
11760 |
11780 PRINT "Energy      :E"
11790 PRINT
11800 FOR J=2 TO L
11810 PRINT "Forces on Ligand ";J-1;" (X,Y,Z)"
11820 PRINT Fdir(J,1,1);Fdir(J,2,1);Fdir(J,3,1)
11830 PRINT
11840 PRINT "Moments on Ligand ";J-1;" (X,Y,Z)"
11850 PRINT Mdir(J,1,1);Mdir(J,2,1);Mdir(J,3,1)
11860 PRINT
11870 NEXT J
11880 PRINT "Potential Curvature (X,Y,Z)"
11890 PRINT Cvx;Cvy;Cvz
11900 PRINT
11910 RETURN
11920 |
11930 | .....
11940 | Subroutine: Minimize
11950 |
11960 | Performs binding energy and geometry optimization by analyzing the
11970 | forces and moments on cluster subunits.
11980 | .....
11990 |
12000 Minimize: PRINTER IS 1 |
12010 Eskip=1
12020 Passes=0 | Initialize number of iterations.
12030 Flag2=1
12040 OUTPUT 2;CHR$(255)&"K";
12050 GRAPHICS OFF
12060 OFF KEY
12070 |
12080 | .....
12090 | Optimization Graphics Menu:
12100 |
12110 | Sketch Y - Activates cluster geometry drawing routine during
12120 | optimization. Subroutine used - Sketchy.
12130 |
12140 | Sketch N - Deactivates cluster geometry drawing routine during
12150 | optimization. Subroutine used - Sketchn.
12160 |
12170 | Gclear - Clears the graphics display. Subroutine used - Wipe.
12180 |
12190 | Solute Y - Draws solute and solvent during optimization. Subroutine
12200 | used - Solutey.
12210 |
12220 | Solute N - Draws solvent only during optimization. Subroutine
12230 | used - Soluten.
12240 |
12250 | Quit - Stops optimization and returns program to Main Menu. Subroutine
12260 | used - Quit.
12270 |
12280 | Inc Pic - Decreases graphics display limits by 1 angstrom. Subroutine
12290 | used - Incpic.
12300 |
12310 | Dec Pic - Increases graphics display limits by 1 angstrom. Subroutine

```

```

12320 ! used - Decpic.
12330 !!!!!!!!!!!!!!!!!!!!!!!!!!!!!!!!!!!!!!!!!!!!!!!!!!!!!!!!!!!!!!!!!!!!!!!!!!!!!!!
12340 !
12350 ON KEY 0 LABEL "Sketch Y",3 GOSUB Sketchy
12360 ON KEY 5 LABEL "Sketch N",3 GOSUB Sketchn
12370 ON KEY 2 LABEL "Gclear",3 GOSUB Wipe
12380 ON KEY 3 LABEL "Solute Y",3 GOSUB Solutey
12390 ON KEY 8 LABEL "Solute N",3 GOSUB Soluten
12400 ON KEY 9 LABEL "Quit",3 GOTO Quit
12410 ON KEY 1 LABEL "Inc Pic",3 GOSUB Incpic
12420 ON KEY 6 LABEL "Dec Pic",3 GOSUB Decpic
12430 !
12440 !!!!!!!!!!!!!!!!!!!!!!!!!!!!!!!!!!!!!!!!!!!!!!!!!!!!!!!!!!!!!!!!!!!!!!!!!!!!!!!
12450 ! Initialization of variables before optimization.
12460 !!!!!!!!!!!!!!!!!!!!!!!!!!!!!!!!!!!!!!!!!!!!!!!!!!!!!!!!!!!!!!!!!!!!!!!!!!!!!!!
12470 !
12480 FOR J=1 TO L
12490 Tx(J)=0
12500 Ty(J)=0
12510 Tz(J)=0
12520 Rx(J)=0
12530 Ry(J)=0
12540 Rz(J)=0
12550 FOR Dir1=1 TO 3
12560 FOR Dir2=1 TO 3
12570 Fdir(J,Dir1,Dir2)=0
12580 Mdir(J,Dir1,Dir2)=0
12590 NEXT Dir2
12600 NEXT Dir1
12610 NEXT J
12620 FOR J=1 TO L
12630 FOR Dir1=1 TO 3
12640 T1(J,Dir1)=1
12650 R1(J,Dir1)=1
12660 Tstep(J,Dir1)=0
12670 Rstep(J,Dir1)=0
12680 NEXT Dir1
12690 NEXT J
12700 Cutoff=0
12710 Bcc=0
12720 Bhb=0
12730 Q$="Q"
12740 INPUT "Do you want to include charges?",Q$
12750 IF Q$="Y" THEN Bcc=1
12760 IF Q$="Y" THEN 12780
12770 IF Q$<>"N" THEN 12730
12780 Q$="Q"
12790 INPUT "Do you want to include hydrogen bonding?",Q$
12800 IF Q$="Y" THEN Bhb=1
12810 IF Q$="Y" THEN 12830
12820 IF Q$<>"N" THEN 12780
12830 Q$="Q"
12840 INPUT "Do you want to cut off the negative curvature?",Q$
12850 IF Q$="Y" THEN Cutoff=1
12860 IF Q$="Y" THEN 12880
12870 IF Q$<>"N" THEN 12830
12880 SET TIME 0

```

```

12990 GOSUB Energy
12900 !
12910 !
12920 ! Determines force and moment direction change between current move
12930 ! and last move to calculate translation and rotation step sizes for
12940 ! cluster subunits.
12950 !
12960 !
12970 FOR J=2 TO L
12980 FOR Dir1=1 TO 3
12990 IF Fdir(J,Dir1,2)=0 THEN 13020
13000 IF ABS(Fdir(J,Dir1,2)-Fdir(J,Dir1,3))=2 THEN T1(J,Dir1)=T1(J,Dir1)+.2
13010 IF ABS(Fdir(J,Dir1,2)-Fdir(J,Dir1,3))>2 THEN T1(J,Dir1)=T1(J,Dir1)-.05
13020 IF Mdir(J,Dir1,2)=0 THEN 13110
13030 IF ABS(Mdir(J,Dir1,2)-Mdir(J,Dir1,3))=2 THEN R1(J,Dir1)=R1(J,Dir1)+.2
13040 IF ABS(Mdir(J,Dir1,2)-Mdir(J,Dir1,3))>2 THEN R1(J,Dir1)=R1(J,Dir1)-.05
13050 !
13060 !
13070 ! Determines translation and rotation step sizes. Maximum translation step
13080 ! size is .1 angstroms. Maximum rotation step size is 10 degrees.
13090 !
13100 !
13110 IF T1(J,Dir1)<1 THEN T1(J,Dir1)=1
13120 IF R1(J,Dir1)<1 THEN R1(J,Dir1)=1
13130 Tstep(J,Dir1)=1/1000*10^(-.5*T1(J,Dir1)+2.5)
13140 Rstep(J,Dir1)=1/10*10^(-.5*R1(J,Dir1)+2.5)
13150 Fdir(J,Dir1,3)=Fdir(J,Dir1,2)
13160 Mdir(J,Dir1,3)=Mdir(J,Dir1,2)
13170 NEXT Dir1
13180 NEXT J
13190 FOR S=2 TO L
13200 GOSUB Trans
13210 NEXT S
13220 GOSUB Energy
13230 Min=0
13240 Passes=Passes+1
13250 FOR J=2 TO L
13260 FOR Dir1=1 TO 3
13270 !
13280 !
13290 ! Determines current force and moment directions and determines which
13300 ! degrees of freedom are optimized. Optimization is accomplished when
13310 ! forces and torques are less that or equal to +/- .01.
13320 !
13330 !
13340 IF Fdir(J,Dir1,1)>0 THEN Fdir(J,Dir1,2)=1
13350 IF Fdir(J,Dir1,1)<0 THEN Fdir(J,Dir1,2)=-1
13360 IF ABS(Fdir(J,Dir1,1))<=.01 THEN Fdir(J,Dir1,2)=0
13370 IF Fdir(J,Dir1,2)=0 THEN Min=Min+1
13380 IF Mdir(J,Dir1,1)>0 THEN Mdir(J,Dir1,2)=1
13390 IF Mdir(J,Dir1,1)<0 THEN Mdir(J,Dir1,2)=-1
13400 IF ABS(Mdir(J,Dir1,1))<=.01 THEN Mdir(J,Dir1,2)=0
13410 IF Mdir(J,Dir1,2)=0 THEN Min=Min+1
13420 NEXT Dir1
13430 NEXT J
13440 !
13450 !

```

```

13460 ! Determines if all degrees of freedom are optimized and if so terminates
13470 ! the routine.
13480 !!!!!!!!!!!!!!!!!!!!!!!!!!!!!!!!!!!!!!!!!!!!!!!!!!!!!!!!!!!!!!!!!!!!!!!!!!!!!
13490 !
13500 IF Min=6*L-6 THEN 13520
13510 IF Sk=1 THEN GOSUB Draw
13520 IF Min=6*L-6 THEN GOSUB Draw
13530 IF Min=6*L-6 THEN 13550
13540 GOTO 12970
13550 BEEP
13560 DISP "Done !!!! "
13570 Tim=(TIMEDATE MOD 86400)/60
13580 Done=1
13590 Eck=E
13600 Iter=1
13610 Handl=1
13620 !
13630 !!!!!!!!!!!!!!!!!!!!!!!!!!!!!!!!!!!!!!!!!!!!!!!!!!!!!!!!!!!!!!!!!!!!!!!!!!!!!
13640 ! Checks final geometry for minimum energy by translating and rotating
13650 ! about the minimum energy cluster configuration.
13660 !!!!!!!!!!!!!!!!!!!!!!!!!!!!!!!!!!!!!!!!!!!!!!!!!!!!!!!!!!!!!!!!!!!!!!!!!!!!!
13670 !
13680 FOR S=2 TO L
13690 FOR Xxx=1 TO 3
13700 Tstep(S,Xxx)=.001
13710 GOSUB 22000
13720 !
13730 !!!!!!!!!!!!!!!!!!!!!!!!!!!!!!!!!!!!!!!!!!!!!!!!!!!!!!!!!!!!!!!!!!!!!!!!!!!!!
13740 ! Translation checks in three directions.
13750 !!!!!!!!!!!!!!!!!!!!!!!!!!!!!!!!!!!!!!!!!!!!!!!!!!!!!!!!!!!!!!!!!!!!!!!!!!!!!
13760 !
13770 IF Xxx=1 AND E>Eck THEN PRINT " +X Minimum"
13780 IF Xxx=1 AND E<Eck THEN PRINT " +X Not Min"
13790 IF Xxx=2 AND E>Eck THEN PRINT " +Y Minimum"
13800 IF Xxx=2 AND E<Eck THEN PRINT " +Y Not Min"
13810 IF Xxx=3 AND E>Eck THEN PRINT " +Z Minimum"
13820 IF Xxx=3 AND E<Eck THEN PRINT " +Z Not Min"
13830 Tstep(S,Xxx)=-.002
13840 GOSUB 22000
13850 IF Xxx=1 AND E>Eck THEN PRINT " -X Minimum"
13860 IF Xxx=1 AND E<Eck THEN PRINT " -X Not Min"
13870 IF Xxx=2 AND E>Eck THEN PRINT " -Y Minimum"
13880 IF Xxx=2 AND E<Eck THEN PRINT " -Y Not Min"
13890 IF Xxx=3 AND E>Eck THEN PRINT " -Z Minimum"
13900 IF Xxx=3 AND E<Eck THEN PRINT " -Z Not Min"
13910 Tstep(S,Xxx)=.001
13920 GOSUB 22000
13930 Rstep(S,Xxx)=.001
13940 GOSUB 22380
13950 !
13960 !!!!!!!!!!!!!!!!!!!!!!!!!!!!!!!!!!!!!!!!!!!!!!!!!!!!!!!!!!!!!!!!!!!!!!!!!!!!!
13970 ! Rotation checks in three directions.
13980 !!!!!!!!!!!!!!!!!!!!!!!!!!!!!!!!!!!!!!!!!!!!!!!!!!!!!!!!!!!!!!!!!!!!!!!!!!!!!
13990 !
14000 IF Xxx=1 AND E<Eck THEN PRINT " +Rx Minimum"
14010 IF Xxx=1 AND E>Eck THEN PRINT " +Rx Not Min"
14020 IF Xxx=2 AND E<Eck THEN PRINT " +Ry Minimum"

```



```

14590 !
14600 ! Translates and rotates the cluster subunits in three dimensions.
14610 !
14620 !
14630 Trans: !
14640 !
14650 !
14660 ! Determines the force and moment magnitudes.
14670 !
14680 !
14690 Fmag=(Fdir(S,1,1)^2+Fdir(S,2,1)^2+Fdir(S,3,1)^2)^.5
14700 Mmag=(Mdir(S,1,1)^2+Mdir(S,2,1)^2+Mdir(S,3,1)^2)^.5
14710 IF Fmag=0 THEN 14800
14720 !
14730 !
14740 ! Translates the cluster subunit screen parameters.
14750 !
14760 !
14770 Tx(S)=Tx(S)+Fdir(S,1,2)*Tstep(S,1)*ABS(Fdir(S,1,1)/Fmag)
14780 Ty(S)=Ty(S)+Fdir(S,2,2)*Tstep(S,2)*ABS(Fdir(S,2,1)/Fmag)
14790 Tz(S)=Tz(S)+Fdir(S,3,2)*Tstep(S,3)*ABS(Fdir(S,3,1)/Fmag)
14800 IF Mmag=0 THEN 14890
14810 !
14820 !
14830 ! Rotates the cluster subunit screen parameters.
14840 !
14850 !
14860 Rx(S)=Rx(S)+Mdir(S,1,2)*Rstep(S,1)*ABS(Mdir(S,1,1)/Mmag)
14870 Ry(S)=Ry(S)+Mdir(S,2,2)*Rstep(S,2)*ABS(Mdir(S,2,1)/Mmag)
14880 Rz(S)=Rz(S)+Mdir(S,3,2)*Rstep(S,3)*ABS(Mdir(S,3,1)/Mmag)
14890 IF Rx(S)>=360 THEN Rx(S)=Rx(S)-360
14900 IF Rx(S)<=-360 THEN Rx(S)=Rx(S)+360
14910 IF Ry(S)>=360 THEN Ry(S)=Ry(S)-360
14920 IF Ry(S)<=-360 THEN Ry(S)=Ry(S)+360
14930 IF Rz(S)>=360 THEN Rz(S)=Rz(S)-360
14940 IF Rz(S)<=-360 THEN Rz(S)=Rz(S)+360
14950 IF Done=1 THEN 15080
14960 IF Hand=1 THEN OUTPUT 2;CHR$(255)&"K";
14970 !
14980 !
14990 ! Prints the translation and rotation of the cluster subunits on the
15000 ! screen display.
15010 !
15020 !
15030 PRINT "Translation of Ligand";S-1
15040 PRINT USING "S3D.4D";Tx(S);Ty(S);Tz(S)
15050 PRINT "Rotation of Ligand";S-1
15060 PRINT USING "S3D.4D";Rx(S);Ry(S);Rz(S)
15070 PRINT
15080 IF Fmag=0 THEN 15600
15090 !
15100 !
15110 ! Translates the cluster subunit coordinates.
15120 !
15130 !
15140 FOR C=1 TO S
15150 FOR A=1 TO S

```

```

15160 FOR J=1 TO N(S,C,A)
15170 FOR X=1 TO 3
15180 |
15190 |
15200 | Translates carbon atoms.
15210 |
15220 |
15230 IF C=1 THEN Co(S,J,A,X)=Co(S,J,A,X)+Fdir(S,X,2)*Tstep(S,X)*ABS(Fdir(S,X,1)
/Fmag)
15240 |
15250 |
15260 | Translates hydrogen atoms.
15270 |
15280 |
15290 IF C=2 THEN Hh(S,J,A,X)=Hh(S,J,A,X)+Fdir(S,X,2)*Tstep(S,X)*ABS(Fdir(S,X,1)
/Fmag)
15300 |
15310 |
15320 | Translates nitrogen atoms.
15330 |
15340 |
15350 IF C=3 THEN Nn(S,J,A,X)=Nn(S,J,A,X)+Fdir(S,X,2)*Tstep(S,X)*ABS(Fdir(S,X,1)
/Fmag)
15360 |
15370 |
15380 | Translates oxygen atoms.
15390 |
15400 |
15410 IF C=4 THEN Oo(S,J,A,X)=Oo(S,J,A,X)+Fdir(S,X,2)*Tstep(S,X)*ABS(Fdir(S,X,1)
/Fmag)
15420 |
15430 |
15440 | Translates user defined atoms.
15450 |
15460 |
15470 IF C=5 THEN Zn(S,J,A,X)=Zn(S,J,A,X)+Fdir(S,X,2)*Tstep(S,X)*ABS(Fdir(S,X,1)
/Fmag)
15480 NEXT X
15490 NEXT J
15500 NEXT A
15510 NEXT C
15520 |
15530 |
15540 | Translates the cluster subunit center-of-mass.
15550 |
15560 |
15570 FOR X=1 TO 3
15580 Cq(S,X)=Cq(S,X)+Fdir(S,X,2)*Tstep(S,X)*ABS(Fdir(S,X,1)/Fmag)
15590 NEXT X
15600 IF Mmag=0 THEN 16990
15610 Munitx=ABS(Mdir(S,1,1)/Mmag)
15620 Munity=ABS(Mdir(S,2,1)/Mmag)
15630 Munitz=ABS(Mdir(S,3,1)/Mmag)
15640 |
15650 |
15660 | Rotates the cluster subunits about their centers-of-mass.
15670 |

```



```

15630 |
15630 FOR C=1 TO 5
15700 FOR A=1 TO 5
15710 FOR J=1 TO N(S,C,A)
15720 IF C=1 THEN 15820
15730 IF C=2 THEN 16060
15740 IF C=3 THEN 16300
15750 IF C=4 THEN 16780
15760 IF C=5 THEN 16540
15770 |
15780 |
15790 | Rotates carbon atoms about molecular center-of-mass.
15800 |
15810 |
15820 Co1=Co(S,J,A,2)-Cq(S,2)
15830 Co2=Co(S,J,A,3)-Cq(S,3)
15840 Co(S,J,A,2)=Co1*COS(Mdir(S,1,2)*Rstep(S,1)*Munitx)-Co2*SIN(Mdir(S,1,2)*Rst
ep(S,1)*Munitx)
15850 Co(S,J,A,3)=Co1*SIN(Mdir(S,1,2)*Rstep(S,1)*Munitx)+Co2*COS(Mdir(S,1,2)*Rst
ep(S,1)*Munitx)
15860 Co(S,J,A,2)=Co(S,J,A,2)+Cq(S,2)
15870 Co(S,J,A,3)=Co(S,J,A,3)+Cq(S,3)
15880 Co1=Co(S,J,A,3)-Cq(S,3)
15890 Co2=Co(S,J,A,1)-Cq(S,1)
15900 Co(S,J,A,3)=Co1*COS(Mdir(S,2,2)*Rstep(S,2)*Munity)-Co2*SIN(Mdir(S,2,2)*Rst
ep(S,2)*Munity)
15910 Co(S,J,A,1)=Co1*SIN(Mdir(S,2,2)*Rstep(S,2)*Munity)+Co2*COS(Mdir(S,2,2)*Rst
ep(S,2)*Munity)
15920 Co(S,J,A,3)=Co(S,J,A,3)+Cq(S,3)
15930 Co(S,J,A,1)=Co(S,J,A,1)+Cq(S,1)
15940 Co1=Co(S,J,A,1)-Cq(S,1)
15950 Co2=Co(S,J,A,2)-Cq(S,2)
15960 Co(S,J,A,1)=Co1*COS(Mdir(S,3,2)*Rstep(S,3)*Munitz)-Co2*SIN(Mdir(S,3,2)*Rst
ep(S,3)*Munitz)
15970 Co(S,J,A,2)=Co1*SIN(Mdir(S,3,2)*Rstep(S,3)*Munitz)+Co2*COS(Mdir(S,3,2)*Rst
ep(S,3)*Munitz)
15980 Co(S,J,A,1)=Co(S,J,A,1)+Cq(S,1)
15990 Co(S,J,A,2)=Co(S,J,A,2)+Cq(S,2)
16000 GOTO 16960
16010 |
16020 |
16030 | Rotates hydrogen atoms about molecular center-of-mass.
16040 |
16050 |
16060 Co1=Hh(S,J,A,2)-Cq(S,2)
16070 Co2=Hh(S,J,A,3)-Cq(S,3)
16080 Hh(S,J,A,2)=Co1*COS(Mdir(S,1,2)*Rstep(S,1)*Munitx)-Co2*SIN(Mdir(S,1,2)*Rst
ep(S,1)*Munitx)
16090 Hh(S,J,A,3)=Co1*SIN(Mdir(S,1,2)*Rstep(S,1)*Munitx)+Co2*COS(Mdir(S,1,2)*Rst
ep(S,1)*Munitx)
16100 Hh(S,J,A,2)=Hh(S,J,A,2)+Cq(S,2)
16110 Hh(S,J,A,3)=Hh(S,J,A,3)+Cq(S,3)
16120 Co1=Hh(S,J,A,3)-Cq(S,3)
16130 Co2=Hh(S,J,A,1)-Cq(S,1)
16140 Hh(S,J,A,3)=Co1*COS(Mdir(S,2,2)*Rstep(S,2)*Munity)-Co2*SIN(Mdir(S,2,2)*Rst
ep(S,2)*Munity)
16150 Hh(S,J,A,1)=Co1*SIN(Mdir(S,2,2)*Rstep(S,2)*Munity)+Co2*COS(Mdir(S,2,2)*Rst

```

```

ep(S,2)*Munity)
16160 Hn(S,J,A,3)=Hn(S,J,A,3)+Cq(S,3)
16170 Hn(S,J,A,1)=Hn(S,J,A,1)+Cq(S,1)
16180 Co1=Hn(S,J,A,1)-Cq(S,1)
16190 Co2=Hn(S,J,A,2)-Cq(S,2)
16200 Hn(S,J,A,1)=Co1*cos(Mdir(S,3,2)*Rstep(S,3)*Munitz)-Co2*sin(Mdir(S,3,2)*Rst
ep(S,3)*Munitz)
16210 Hn(S,J,A,2)=Co1*sin(Mdir(S,3,2)*Rstep(S,3)*Munitz)+Co2*cos(Mdir(S,3,2)*Rst
ep(S,3)*Munitz)
16220 Hn(S,J,A,1)=Hn(S,J,A,1)+Cq(S,1)
16230 Hn(S,J,A,2)=Hn(S,J,A,2)+Cq(S,2)
16240 GOTO 16960
16250 |
16260 |
16270 | Rotates nitrogen atoms about molecular center-of-mass.
16280 |
16290 |
16300 Co1=Nn(S,J,A,2)-Cq(S,2)
16310 Co2=Nn(S,J,A,3)-Cq(S,3)
16320 Nn(S,J,A,2)=Co1*cos(Mdir(S,1,2)*Rstep(S,1)*Munitx)-Co2*sin(Mdir(S,1,2)*Rst
ep(S,1)*Munitx)
16330 Nn(S,J,A,3)=Co1*sin(Mdir(S,1,2)*Rstep(S,1)*Munitx)+Co2*cos(Mdir(S,1,2)*Rst
ep(S,1)*Munitx)
16340 Nn(S,J,A,2)=Nn(S,J,A,2)+Cq(S,2)
16350 Nn(S,J,A,3)=Nn(S,J,A,3)+Cq(S,3)
16360 Co1=Nn(S,J,A,3)-Cq(S,3)
16370 Co2=Nn(S,J,A,1)-Cq(S,1)
16380 Nn(S,J,A,3)=Co1*cos(Mdir(S,2,2)*Rstep(S,2)*Munity)-Co2*sin(Mdir(S,2,2)*Rst
ep(S,2)*Munity)
16390 Nn(S,J,A,1)=Co1*sin(Mdir(S,2,2)*Rstep(S,2)*Munity)+Co2*cos(Mdir(S,2,2)*Rst
ep(S,2)*Munity)
16400 Nn(S,J,A,3)=Nn(S,J,A,3)+Cq(S,3)
16410 Nn(S,J,A,1)=Nn(S,J,A,1)+Cq(S,1)
16420 Co1=Nn(S,J,A,1)-Cq(S,1)
16430 Co2=Nn(S,J,A,2)-Cq(S,2)
16440 Nn(S,J,A,1)=Co1*cos(Mdir(S,3,2)*Rstep(S,3)*Munitz)-Co2*sin(Mdir(S,3,2)*Rst
ep(S,3)*Munitz)
16450 Nn(S,J,A,2)=Co1*sin(Mdir(S,3,2)*Rstep(S,3)*Munitz)+Co2*cos(Mdir(S,3,2)*Rst
ep(S,3)*Munitz)
16460 Nn(S,J,A,1)=Nn(S,J,A,1)+Cq(S,1)
16470 Nn(S,J,A,2)=Nn(S,J,A,2)+Cq(S,2)
16480 GOTO 16960
16490 |
16500 |
16510 | Rotates user defined atoms about molecular center-of-mass.
16520 |
16530 |
16540 Co1=Zn(S,J,A,2)-Cq(S,2)
16550 Co2=Zn(S,J,A,3)-Cq(S,3)
16560 Zn(S,J,A,2)=Co1*cos(Mdir(S,1,2)*Rstep(S,1)*Munitx)-Co2*sin(Mdir(S,1,2)*Rst
ep(S,1)*Munitx)
16570 Zn(S,J,A,3)=Co1*sin(Mdir(S,1,2)*Rstep(S,1)*Munitx)+Co2*cos(Mdir(S,1,2)*Rst
ep(S,1)*Munitx)
16580 Zn(S,J,A,2)=Zn(S,J,A,2)+Cq(S,2)
16590 Zn(S,J,A,3)=Zn(S,J,A,3)+Cq(S,3)
16600 Co1=Zn(S,J,A,3)-Cq(S,3)
16610 Co2=Zn(S,J,A,1)-Cq(S,1)

```



```

17090 IF Flag2=1 THEN 17400
17100 OFF KEY
17110 |
17120 | .....
17130 | Drawing Menu:
17140 |
17150 | Gclear - Clears the graphics display. Subroutine used - Wipe.
17160 |
17170 | Solute Y - Draws the solute and solvent. Subroutine used - Solutey.
17180 |
17190 | Solute N - Draws the solvent only. Subroutine used - Soluten.
17200 |
17210 | Inc Pic - Decreases the graphics display limits by 1 angstrom.
17220 | Subroutine used - Incpic.
17230 |
17240 | Dec Pic - Increases the graphics display limits by 1 angstrom.
17250 | Subroutine used - Decpic.
17260 |
17270 | Draw - Draws the cluster geometries.
17280 |
17290 | No Draw - Stops drawing at any time.
17300 | .....
17310 |
17320 ON KEY 0 LABEL "Gclear",9 GOSUB Wipe
17330 ON KEY 1 LABEL "Solute Y",9 GOSUB Solutey
17340 ON KEY 6 LABEL "Solute N",9 GOSUB Soluten
17350 ON KEY 2 LABEL "Inc Pic",9 GOSUB Incpic
17360 ON KEY 7 LABEL "Dec Pic",9 GOSUB Decpic
17370 ON KEY 5 LABEL "Draw ",9 GOTO 17400
17380 ON KEY 9 LABEL "No Draw",9 GOTO 19240
17390 GOTO 17390
17400 GRAPHICS ON
17410 ALPHA OFF
17420 IF Min=L*6-6 THEN GINIT
17430 IF Min=L*6-6 THEN Sol=1
17440 FOR Pic=1 TO 4
17450 |
17460 | .....
17470 | 3 dimensional perspective.
17480 | .....
17490 |
17500 IF Pic=1 THEN VIEWPORT 0,66,0,50
17510 IF Pic=1 THEN Dwx=-10
17520 IF Pic=1 THEN Dwz=15
17530 |
17540 | .....
17550 | Top view perspective.
17560 | .....
17570 |
17580 IF Pic=2 THEN VIEWPORT 66,133,0,50
17590 IF Pic=2 THEN Dwx=0
17600 IF Pic=2 THEN Dwz=90
17610 |
17620 | .....
17630 | End view perspective.
17640 | .....
17650 |

```

```

17660 IF Pic=3 THEN VIEWPORT 0,66,50,100
17670 IF Pic=3 THEN Dwx=-90
17680 IF Pic=3 THEN Dwz=0
17690 !
17700 !!!!!!!!!!!!!!!!!!!!!!!!!!!!!!!!!!!!!!!!!!!!!!!!!!!!!!!!!!!!!!!!!!!!!!!!!!!!!!!
17710 ! Side view perspective.
17720 !!!!!!!!!!!!!!!!!!!!!!!!!!!!!!!!!!!!!!!!!!!!!!!!!!!!!!!!!!!!!!!!!!!!!!!!!!!!!!!
17730 !
17740 IF Pic=4 THEN VIEWPORT 66,133,50,100
17750 IF Pic=4 THEN Dwx=0
17760 IF Pic=4 THEN Dwz=0
17770 SHOW -Look,Look,-Look,Look
17780 FRAME
17790 !
17800 !!!!!!!!!!!!!!!!!!!!!!!!!!!!!!!!!!!!!!!!!!!!!!!!!!!!!!!!!!!!!!!!!!!!!!!!!!!!!!!
17810 ! Draws cartesian axes on graphics display.
17820 !!!!!!!!!!!!!!!!!!!!!!!!!!!!!!!!!!!!!!!!!!!!!!!!!!!!!!!!!!!!!!!!!!!!!!!!!!!!!!!
17830 !
17840 LINE TYPE 3
17850 Cf1(1)=-S*Look*COS(Dwx)
17860 Ce1(2)=-S*Look*SIN(Dwx)
17870 Cf2(1)=S*Look*COS(Dwx)
17880 Ce2(2)=S*Look*SIN(Dwx)
17890 Cf1(3)=Ce1(2)*SIN(Dwz)
17900 Cf2(3)=Ce2(2)*SIN(Dwz)
17910 MOVE Cf1(1),Cf1(3)
17920 DRAW Cf2(1),Cf2(3)
17930 Cf1(1)=S*Look*SIN(Dwx)
17940 Ce1(2)=-S*Look*COS(Dwx)
17950 Cf2(1)=-S*Look*SIN(Dwx)
17960 Ce2(2)=S*Look*COS(Dwx)
17970 Cf1(3)=Ce1(2)*SIN(Dwz)
17980 Cf2(3)=Ce2(2)*SIN(Dwz)
17990 MOVE Cf1(1),Cf1(3)
18000 DRAW Cf2(1),Cf2(3)
18010 Cf1(1)=0
18020 Ce1(2)=0
18030 Cf2(1)=0
18040 Ce2(2)=0
18050 Cf1(3)=-S*Look*COS(Dwz)
18060 Cf2(3)=S*Look*COS(Dwz)
18070 MOVE Cf1(1),Cf1(3)
18080 DRAW Cf2(1),Cf2(3)
18090 LINE TYPE 1
18100 !
18110 !!!!!!!!!!!!!!!!!!!!!!!!!!!!!!!!!!!!!!!!!!!!!!!!!!!!!!!!!!!!!!!!!!!!!!!!!!!!!!!
18120 ! Draws cluster geometry using balls and sticks.
18130 !!!!!!!!!!!!!!!!!!!!!!!!!!!!!!!!!!!!!!!!!!!!!!!!!!!!!!!!!!!!!!!!!!!!!!!!!!!!!!!
18140 !
18150 FOR K=So1 TO L
18160 FOR C1=1 TO 5
18170 FOR A1=1 TO 5
18180 FOR J1=1 TO N(K,C1,A1)
18190 FOR C2=1 TO 5
18200 FOR A2=1 TO 5
18210 FOR J2=1 TO N(K,C2,A2)
18220 D=0

```

```
18230 |
18240 | .....
18250 | Determines atoms to be connected by bonds.
18260 | .....
18270 |
18280 | .....
18290 |
18300 | Carbon atom coordinates.
18310 | .....
18320 | IF C1=1 THEN Coord11=Co(K,J1,A1,1)
18330 | IF C1=1 THEN Coord12=Co(K,J1,A1,2)
18340 | IF C1=1 THEN Coord13=Co(K,J1,A1,3)
18350 | IF C2=1 THEN Coord21=Co(K,J2,A2,1)
18360 | IF C2=1 THEN Coord22=Co(K,J2,A2,2)
18370 | IF C2=1 THEN Coord23=Co(K,J2,A2,3)
18380 |
18390 | .....
18400 | Hydrogen atom coordinates.
18410 | .....
18420 |
18430 | IF C1=2 THEN Coord11=Hh(K,J1,A1,1)
18440 | IF C1=2 THEN Coord12=Hh(K,J1,A1,2)
18450 | IF C1=2 THEN Coord13=Hh(K,J1,A1,3)
18460 | IF C2=2 THEN Coord21=Hh(K,J2,A2,1)
18470 | IF C2=2 THEN Coord22=Hh(K,J2,A2,2)
18480 | IF C2=2 THEN Coord23=Hh(K,J2,A2,3)
18490 |
18500 | .....
18510 | Nitrogen atom coordinates.
18520 | .....
18530 |
18540 | IF C1=3 THEN Coord11=Nn(K,J1,A1,1)
18550 | IF C1=3 THEN Coord12=Nn(K,J1,A1,2)
18560 | IF C1=3 THEN Coord13=Nn(K,J1,A1,3)
18570 | IF C2=3 THEN Coord21=Nn(K,J2,A2,1)
18580 | IF C2=3 THEN Coord22=Nn(K,J2,A2,2)
18590 | IF C2=3 THEN Coord23=Nn(K,J2,A2,3)
18600 |
18610 | .....
18620 | Oxygen atom coordinates.
18630 | .....
18640 |
18650 | IF C1=4 THEN Coord11=Oo(K,J1,A1,1)
18660 | IF C1=4 THEN Coord12=Oo(K,J1,A1,2)
18670 | IF C1=4 THEN Coord13=Oo(K,J1,A1,3)
18680 | IF C2=4 THEN Coord21=Oo(K,J2,A2,1)
18690 | IF C2=4 THEN Coord22=Oo(K,J2,A2,2)
18700 | IF C2=4 THEN Coord23=Oo(K,J2,A2,3)
18710 |
18720 | .....
18730 | User defined atom coordinates.
18740 | .....
18750 |
18760 | IF C1=5 THEN Coord11=Zn(K,J1,A1,1)
18770 | IF C1=5 THEN Coord12=Zn(K,J1,A1,2)
18780 | IF C1=5 THEN Coord13=Zn(K,J1,A1,3)
18790 | IF C2=5 THEN Coord21=Zn(K,J2,A2,1)
```

```

18800 IF C2=5 THEN Coord22=Zn(K,J2,A2,2)
18810 IF C2=5 THEN Coord23=Zn(K,J2,A2,3)
18820 !
18830 !!!!!!!!!!!!!!!!!!!!!!!!!!!!!!!!!!!!!!!!!!!!!!!!!!!!!!!!!!!!!!!!!!!!!!!!!!!!!!!
18840 ! Determines ball sizes for specific atoms.
18850 !!!!!!!!!!!!!!!!!!!!!!!!!!!!!!!!!!!!!!!!!!!!!!!!!!!!!!!!!!!!!!!!!!!!!!!!!!!!!!!
18860 !
18870 IF C2=1 THEN Siz=.3
18880 IF C2=2 THEN Siz=.18
18890 IF C2=3 THEN Siz=.24
18900 IF C2=4 THEN Siz=.28
18910 IF C2=5 THEN Siz=.32
18920 D=(Coord21-Coord11)^2+(Coord22-Coord12)^2+(Coord23-Coord13)^2
18930 Dr=D^.5
18940 !
18950 !!!!!!!!!!!!!!!!!!!!!!!!!!!!!!!!!!!!!!!!!!!!!!!!!!!!!!!!!!!!!!!!!!!!!!!!!!!!!!!
18960 ! Determines 2 dimensional projections for drawing 3 dimensional
18970 ! representations of clusters.
18980 !!!!!!!!!!!!!!!!!!!!!!!!!!!!!!!!!!!!!!!!!!!!!!!!!!!!!!!!!!!!!!!!!!!!!!!!!!!!!!!
18990 !
19000 IF C1=2 THEN GOTO 19190
19010 Cf1(1)=Coord11*COS(Dwx)-Coord12*SIN(Dwx)
19020 Ce1(2)=Coord11*SIN(Dwx)+Coord12*COS(Dwx)
19030 Cf2(1)=Coord21*COS(Dwx)-Coord22*SIN(Dwx)
19040 Ce2(2)=Coord21*SIN(Dwx)+Coord22*COS(Dwx)
19050 Cf1(3)=Ce1(2)*SIN(Dwz)+Coord13*COS(Dwz)
19060 Cf2(3)=Ce2(2)*SIN(Dwz)+Coord23*COS(Dwz)
19070 MOVE Cf1(1),Cf1(3)
19080 IF Dr>1.7 THEN 19140
19090 DRAW Cf2(1),Cf2(3)
19100 FOR Cir=0 TO 360 STEP 30
19110 IF Cir=0 THEN MOVE Cf2(1)+Siz*SIN(Cir),Cf2(3)+Siz*COS(Cir)
19120 DRAW Cf2(1)+Siz*SIN(Cir),Cf2(3)+Siz*COS(Cir)
19130 NEXT Cir
19140 NEXT J2
19150 NEXT A2
19160 NEXT C2
19170 NEXT J1
19180 NEXT A1
19190 NEXT C1
19200 NEXT K
19210 NEXT Pic
19220 GRAPHICS OFF
19230 ALPHA ON
19240 IF Flag2=1 THEN 19410
19250 OFF KEY
19260 !
19270 !!!!!!!!!!!!!!!!!!!!!!!!!!!!!!!!!!!!!!!!!!!!!!!!!!!!!!!!!!!!!!!!!!!!!!!!!!!!!!!
19280 ! Sets up Main Menu for use after geometry and binding energy optimization
19290 ! is complete.
19300 !!!!!!!!!!!!!!!!!!!!!!!!!!!!!!!!!!!!!!!!!!!!!!!!!!!!!!!!!!!!!!!!!!!!!!!!!!!!!!!
19310 !
19320 ON KEY 0 LABEL "In Coef",3 GOSUB Inputcf
19330 ON KEY 1 LABEL "In Coord",3 GOSUB Inputco
19340 ON KEY 2 LABEL "Energy",3 GOSUB Energy
19350 ON KEY 3 LABEL "Minimize",3 GOTO Minimize
19360 ON KEY 4 LABEL "Move",3 GOSUB Hand

```

```

19370 ON KEY 5 LABEL "Draw",3 GOSUB Draw
19380 ON KEY 6 LABEL "NCA",3 GOSUB Eigen
19390 ON KEY 9 LABEL "Quit",3 GOTO Quit
19400 ON KEY 7 LABEL "Stor Con",3 GOSUB File
19410 RETURN
19420 !
19430 !!!!!!!!!!!!!!!!!!!!!!!!!!!!!!!!!!!!!!!!!!!!!!!!!!!!!!!!!!!!!!!!!!!!!!!!!!!!!!!
19440 ! Subroutine: Atomnames
19450 !
19460 ! Assigns atomic symbols and atom types to the atoms composing the
19470 ! clusters. Used in paper print and screen display routines.
19480 !!!!!!!!!!!!!!!!!!!!!!!!!!!!!!!!!!!!!!!!!!!!!!!!!!!!!!!!!!!!!!!!!!!!!!!!!!!!!!!
19490 !
19500 Atomnames: !
19510 !
19520 !!!!!!!!!!!!!!!!!!!!!!!!!!!!!!!!!!!!!!!!!!!!!!!!!!!!!!!!!!!!!!!!!!!!!!!!!!!!!!!
19530 ! Assigns atomic symbols.
19540 !!!!!!!!!!!!!!!!!!!!!!!!!!!!!!!!!!!!!!!!!!!!!!!!!!!!!!!!!!!!!!!!!!!!!!!!!!!!!!!
19550 !
19560 IF Atom1=1 THEN Atom1$=" C"
19570 IF Atom1=2 THEN Atom1$=" H"
19580 IF Atom1=3 THEN Atom1$=" N"
19590 IF Atom1=4 THEN Atom1$=" O"
19600 IF Atom1=5 THEN Atom1$=" Zn"
19610 IF Atom1=1 THEN 19720
19620 IF Atom1=2 THEN 19780
19630 IF Atom1=3 THEN 19840
19640 IF Atom1=4 THEN 19900
19650 IF Atom1=5 THEN 19960
19660 RETURN
19670 !
19680 !!!!!!!!!!!!!!!!!!!!!!!!!!!!!!!!!!!!!!!!!!!!!!!!!!!!!!!!!!!!!!!!!!!!!!!!!!!!!!!
19690 ! Assigns atom types.
19700 !!!!!!!!!!!!!!!!!!!!!!!!!!!!!!!!!!!!!!!!!!!!!!!!!!!!!!!!!!!!!!!!!!!!!!!!!!!!!!!
19710 !
19720 IF Attp1=1 THEN Attp1$=" Alip"
19730 IF Attp1=2 THEN Attp1$=" Carb"
19740 IF Attp1=3 THEN Attp1$=" Arom"
19750 IF Attp1=4 THEN Attp1$=" YYYY"
19760 IF Attp1=5 THEN Attp1$=" ZZZZ"
19770 RETURN
19780 IF Attp1=1 THEN Attp1$=" Alip"
19790 IF Attp1=2 THEN Attp1$=" Amin"
19800 IF Attp1=3 THEN Attp1$=" Arom"
19810 IF Attp1=4 THEN Attp1$=" Carb"
19820 IF Attp1=5 THEN Attp1$=" ZZZZ"
19830 RETURN
19840 IF Attp1=1 THEN Attp1$=" Amin"
19850 IF Attp1=2 THEN Attp1$=" WWWW"
19860 IF Attp1=3 THEN Attp1$=" XXXX"
19870 IF Attp1=4 THEN Attp1$=" YYYY"
19880 IF Attp1=5 THEN Attp1$=" ZZZZ"
19890 RETURN
19900 IF Attp1=1 THEN Attp1$=" Carb"
19910 IF Attp1=2 THEN Attp1$=" Hydr"
19920 IF Attp1=3 THEN Attp1$=" XXXX"
19930 IF Attp1=4 THEN Attp1$=" YYYY"

```



```
19940 IF Attp1=5 THEN Attp1$=" ZZZZ"
19950 RETURN
19960 IF Attp1=1 THEN Attp1$=" Alip"
19970 IF Attp1=2 THEN Attp1$=" WWWW"
19980 IF Attp1=3 THEN Attp1$=" XXXX"
19990 IF Attp1=4 THEN Attp1$=" YYYY"
20000 IF Attp1=5 THEN Attp1$=" ZZZZ"
20010 RETURN
20020 !
20030 !
20040 ! Subroutine: Atomnumbers
20050 !
20060 ! Assigns atoms and atom types to numbers for array element
20070 ! identification.
20080 !
20090 !
20100 Atomnumbers: !
20110 Atom1=0
20120 Attp1=0
20130 !
20140 !
20150 ! Assign numbers to atoms.
20160 !
20170 !
20180 IF Atom1$="C" THEN Atom1=1
20190 IF Atom1$="H" THEN Atom1=2
20200 IF Atom1$="N" THEN Atom1=3
20210 IF Atom1$="O" THEN Atom1=4
20220 IF Atom1$="Z" THEN Atom1=5
20230 IF Atom1$="C" THEN 20340
20240 IF Atom1$="H" THEN 20400
20250 IF Atom1$="N" THEN 20460
20260 IF Atom1$="O" THEN 20520
20270 IF Atom1$="Z" THEN 20580
20280 RETURN
20290 !
20300 !
20310 ! Assign numbers to atom types.
20320 !
20330 !
20340 IF Attp1$="ALIP" THEN Attp1=1
20350 IF Attp1$="CARB" THEN Attp1=2
20360 IF Attp1$="AROM" THEN Attp1=3
20370 IF Attp1$="YYYY" THEN Attp1=4
20380 IF Attp1$="ZZZZ" THEN Attp1=5
20390 RETURN
20400 IF Attp1$="ALIP" THEN Attp1=1
20410 IF Attp1$="AMIN" THEN Attp1=2
20420 IF Attp1$="AROM" THEN Attp1=3
20430 IF Attp1$="CARB" THEN Attp1=4
20440 IF Attp1$="ZZZZ" THEN Attp1=5
20450 RETURN
20460 IF Attp1$="AMIN" THEN Attp1=1
20470 IF Attp1$="WWWW" THEN Attp1=2
20480 IF Attp1$="XXXX" THEN Attp1=3
20490 IF Attp1$="YYYY" THEN Attp1=4
20500 IF Attp1$="ZZZZ" THEN Attp1=5
```



```
21090 PRINT
21090 PRINT "YYYY - YYYY"
21100 PRINT
21110 PRINT "ZZZZ - ZZZZ"
21120 RETURN
21130 PRINT "          Hydrogen Atom Types"
21140 PRINT "-----"
21150 PRINT
21160 PRINT "ALIP - Aliphatic"
21170 PRINT
21180 PRINT "AMIN - Amine or 1(2) Degree Amide"
21190 PRINT
21200 PRINT "AROM - Aromatic or Sulfhydryl"
21210 PRINT
21220 PRINT "CARB - Hydroxyl or Carboxylic Acid"
21230 PRINT
21240 PRINT "ZZZZ - ZZZZ"
21250 RETURN
21260 PRINT "          Nitrogen Atom Types"
21270 PRINT "-----"
21280 PRINT
21290 PRINT "AMIN - Amine or Amide"
21300 PRINT
21310 PRINT "WWW - WWW"
21320 PRINT
21330 PRINT "XXXX - XXXX"
21340 PRINT
21350 PRINT "YYYY - YYYY"
21360 PRINT
21370 PRINT "ZZZZ - ZZZZ"
21380 RETURN
21390 PRINT "          Oxygen Atom Types"
21400 PRINT "-----"
21410 PRINT
21420 PRINT "CARB - Carbonyl or Carboxylic Acid"
21430 PRINT
21440 PRINT "HYDR - Hydroxyl, Carboxylic Acid, or Ester"
21450 PRINT
21460 PRINT "XXXX - XXXX"
21470 PRINT
21480 PRINT "YYYY - YYYY"
21490 PRINT
21500 PRINT "ZZZZ - ZZZZ"
21510 RETURN
21520 PRINT "          Zinc/Other Atom Types"
21530 PRINT "-----"
21540 PRINT
21550 PRINT "ALIP - Aliphatic"
21560 PRINT
21570 PRINT "WWW - WWW"
21580 PRINT
21590 PRINT "XXXX - XXXX"
21600 PRINT
21610 PRINT "YYYY - YYYY"
21620 PRINT
21630 PRINT "ZZZZ - ZZZZ"
21640 RETURN
```

```

21650 !
21660 ! .....
21670 ! Subroutine: Hand
21680 !
21690 ! Allows user to translate and rotate cluster subunits.
21700 ! .....
21710 !
21720 Hand: !
21730 ON ERROR GOTO 21750
21740 OUTPUT 2;CHR$(255)&"K";
21750 INPUT "What molecule are you working on (1 for solute)?",S
21760 INPUT "Do you want to rotate or translate?",Rt$
21770 HandI=1
21780 IF Rt$="R" THEN 22250
21790 IF Rt$="T" THEN 21860
21800 IF Rt$<>"T" AND Rt$<>"R" THEN 21760
21810 !
21820 ! .....
21830 ! Cluster subunit translation routine.
21840 ! .....
21850 !
21860 INPUT "What direction for translation?",Dt$
21870 IF Dt$="X" THEN Xxx=1
21880 IF Dt$="Y" THEN Xxx=2
21890 IF Dt$="Z" THEN Xxx=3
21900 IF Dt$<>"X" AND Dt$<>"Y" AND Dt$<>"Z" THEN 21860
21910 INPUT "What interval?",Tstep(S,Xxx)
21920 INPUT "How many iterations?",Iter
21930 Eskip=0
21940 Q$="Q"
21950 INPUT "Do you want to calculate the energy?",Q$
21960 IF Q$="Y" THEN Eskip=1
21970 IF Q$="Y" THEN 21990
21980 IF Q$<>"N" THEN 21940
21990 OFF ERROR
22000 FOR G=1 TO Iter
22010 Fmag=1
22020 Mmag=1
22030 FOR J=1 TO L
22040 FOR Xx=1 TO 3
22050 FOR Y=1 TO 3
22060 Fdir(J,Xx,Y)=0
22070 Mdir(J,Xx,Y)=0
22080 NEXT Y
22090 NEXT Xx
22100 NEXT J
22110 Fdir(S,Xxx,1)=1
22120 Fdir(S,Xxx,2)=1
22130 GOSUB 14710
22140 IF Eskip=0 THEN 22160
22150 GOSUB Energy
22160 IF Done=1 THEN 22190
22170 GOSUB Draw
22180 NEXT G
22190 GOTO 22570
22200 !
22210 ! .....

```



```

22770 INPUT "What matrix row does solvent begin?",Begin
22780 Column=Begin
22790 INPUT "What matrix row does solvent end?",Lastm
22800 Last=Lastm+1
22810 Q$="Q"
22820 INPUT "Do you want charges?",Q$
22830 IF Q$="Y" THEN Bcc=1
22840 IF Q$<>"Y" AND Q$<"N" THEN 22810
22850 Q$="Q"
22860 INPUT "Do you want hydrogen bonding?",Q$
22870 IF Q$="Y" THEN Bhb=1
22880 IF Q$<>"Y" AND Q$<"N" THEN 22850
22890 GOSUB Energy
22900 Eigen=0
22910 RETURN
22920 !
22930 !!!!!!!!!!!!!!!!!!!!!!!!!!!!!!!!!!!!!!!!!!!!!!!!!!!!!!!!!!!!!!!!!!!!!!!!!!!!!!!
22940 ! Subroutine: File
22950 !
22960 ! Stores the coordinates of a specific cluster geometry in a disc file.
22970 !!!!!!!!!!!!!!!!!!!!!!!!!!!!!!!!!!!!!!!!!!!!!!!!!!!!!!!!!!!!!!!!!!!!!!!!!!!!!!!
22980 !
22990 File: !
23000 Q$="Q"
23010 ON ERROR GOTO 23000
23020 INPUT "Do you want to start another COORDINATE file?",Q$
23030 IF Q$="N" THEN 23070
23040 IF Q$<>"Y" THEN 23020
23050 INPUT "Enter your N E W COORDINATE file name.",Coord$
23060 CREATE BDAT Coord$&"":INTERNAL",9400,8
23070 GOSUB 5390
23080 OFF ERROR
23090 RETURN
23100 !
23110 !!!!!!!!!!!!!!!!!!!!!!!!!!!!!!!!!!!!!!!!!!!!!!!!!!!!!!!!!!!!!!!!!!!!!!!!!!!!!!!
23120 ! Subroutine: Quit
23130 !
23140 ! Stops subroutine execution and returns program to Main Menu.
23150 !!!!!!!!!!!!!!!!!!!!!!!!!!!!!!!!!!!!!!!!!!!!!!!!!!!!!!!!!!!!!!!!!!!!!!!!!!!!!!!
23160 !
23170 Quit: !
23180 OFF KEY
23190 Flag2=0
23200 GOTO 1250
23210 !
23220 !!!!!!!!!!!!!!!!!!!!!!!!!!!!!!!!!!!!!!!!!!!!!!!!!!!!!!!!!!!!!!!!!!!!!!!!!!!!!!!
23230 ! Subroutine: Sketchy
23240 !
23250 ! Activated the graphics display during geometry and binding energy
23260 ! optimization.
23270 !!!!!!!!!!!!!!!!!!!!!!!!!!!!!!!!!!!!!!!!!!!!!!!!!!!!!!!!!!!!!!!!!!!!!!!!!!!!!!!
23280 !
23290 Sketchy: !
23300 S$=1
23310 DISP "Graphics activated."
23320 RETURN
23330 !

```

```
23340 | .....  
23350 | Subroutine: Sketchn  
23360 |  
23370 | Deactivates the graphics display during geometry and binding energy  
23380 | optimization.  
23390 | .....  
23400 |  
23410 Sketchn: |  
23420 Sk=0  
23430 DISP "Graphics deactivated."  
23440 RETURN  
23450 |  
23460 | .....  
23470 | Subroutine: Wipe  
23480 |  
23490 | Clears the graphics display.  
23500 | .....  
23510 |  
23520 Wipe: |  
23530 GINIT  
23540 DISP "Clear screen."  
23550 RETURN  
23560 |  
23570 | .....  
23580 | Subroutine: Solutey  
23590 |  
23600 | Allows he user to draw the cluster solute and solvent.  
23610 | .....  
23620 |  
23630 Solutey: |  
23640 Sol=1  
23650 DISP "Draw solvent and solute."  
23660 RETURN  
23670 |  
23680 | .....  
23690 | Subroutine: Soluten  
23700 |  
23710 | Allows the user to draw the solvent only.  
23720 | .....  
23730 |  
23740 Soluten: |  
23750 Sol=2  
23760 DISP "Draw solvent only."  
23770 RETURN  
23780 |  
23790 | .....  
23800 | Subroutine: Incpic  
23810 |  
23820 | Decreases the graphics display limits by 1 angstrom.  
23830 | .....  
23840 |  
23850 Incpic: |  
23860 Look=Look-1  
23870 IF Look < 1 THEN Look=1  
23880 ALPHA ON  
23890 DISP "Graphics limits are ";Look;" angstroms."  
23900 RETURN
```

```
23910 |
23920 | .....
23930 | Subroutine: Decpic
23940 |
23950 | Increases the graphics display limits by 1 angstrom.
23960 | .....
23970 |
23980 Decpic: |
23990 Look=Look+1
24000 ALPHA ON
24010 DISP "Graphics limits are ";Look;" angstroms."
24020 RETURN
24030 END
```


APPENDIX FOUR

"VDWNCA"

```

10 | .....
20 | Program name: VDWNCA
30 |
40 | This program calculates van der Waals cluster intermolecular vibrational
50 | modes using a normal coordinate analysis (NCA). The NCA is conducted using
60 | the FG matrix method. The clusters are treated as "giant molecules" in the
70 | NCA for which the intra- and intermolecular motions are treated
80 | simultaneously. The intermolecular force field used in the calculations is
90 | generated using ECCEMP2 and is stored on disc as H2OEIG. The intramolecular
100 | force fields are taken as those of each cluster subunit. Both the intra-
110 | and intermolecular force fields are treated using the central force and
120 | harmonic oscillator approximations.
130 |
140 |
150 |
160 | NOTICE: This program will not run with documentation contained in program
170 | if not more than 256 Kbyte RAM is available.
180 | .....
190 |
200 | OPTION BASE 1
210 | PRINTER IS 1
220 |
230 | .....
240 | Matrices used:
250 |
260 | A(*)=Energy (FG) matrix.
270 | Evr(*)=Real eigenvalue matrix.
280 | Evi(*)=Imaginary eigenvalue matrix.
290 | Vecr(*)=Real eigenvector matrix.
300 | Veci(*)=Imaginary eigenvector matrix.
310 | Indic(*)= Matrix diagonalization indicator matrix.
320 | Mol(*)=Cluster coordinates matrix.
330 | .....
340 |
350 | DIM A(75,75),Evr(75),Evi(75),Vecr(75,75),Veci(75,75),Indic(75),Mol(75,4)
360 | DEG
370 | VIEWPORT 0,134,0,100
380 | LORG 5
390 | Paper=1
400 | Look=6 | Default graphics display limits set at 6 angstroms.
410 | Dwx=-45 | Default X axis orientation for graphics display.
420 | Dwz=20 | Default Z axis orientation for graphics display.
430 | Dwx=1 | Default top view for force field graphics display.
440 |
450 | .....
460 | Main Menu:
470 |
480 | LJ MAT - Inputs intermolecular force field into matrix A(*) from disc
490 | storage file H2OEIG. Subroutine used - Implj.
500 |
510 | OWN VAL - Allows the user to input F matrix elements from keyboard.
520 | Subroutine used - Inpown.

```



```

1090 | Subroutine: Inpdat
1100 |
1110 | Inputs the intramolecular force fields from data statements. These force
1120 | fields are added to the intermolecular force field placed in A(x,y,z).
1130 | .....
1140 |
1150 Inpdat: |
1160 WINDOW -Look,Look,-Look,Look
1170 GCLEAR
1180 RESTORE
1190 INPUT "ENTER MATRIX DIMENSION",Mdim
1200 READ Numberdat
1210 FOR Y=1 TO Numberdat
1220 |
1230 | .....
1240 | Reads coordinates and force constants from data statements.
1250 | .....
1260 |
1270 READ X1,Y1,Z1
1280 READ X2,Y2,Z2
1290 READ Forc
1300 |
1310 | .....
1320 | Converts force constants from dynes/cm to wavenumbers/square angstrom.
1330 | .....
1340 |
1350 Forc=Forc/3.E+10/6.626E-27/1.E+16
1360 |
1370 | .....
1380 | Reads matrix row and column from data statements.
1390 | .....
1400 |
1410 READ Row
1420 READ Col
1430 |
1440 | .....
1450 | Calculates unit position vectors.
1460 | .....
1470 |
1480 D=((X2-X1)^2+(Y2-Y1)^2+(Z2-Z1)^2)^.5
1490 Dx=(X2-X1)/D
1500 Dy=(Y2-Y1)/D
1510 Dz=(Z2-Z1)/D
1520 PRINT X1;Y1;Z1
1530 PRINT X2;Y2;Z2
1540 PRINT Dx;Dy;Dz
1550 PRINT Forc,D
1560 PRINT Row,Col
1570 |
1580 | .....
1590 | Draws the intramolecular force field.
1600 | .....
1610 |
1620 GRAPHICS ON
1630 IF Dwx=1 THEN MOVE X1,Y1
1640 IF Dwy=1 THEN DRAW X2,Y2
1650 IF Dwx=0 THEN MOVE X1,Z1

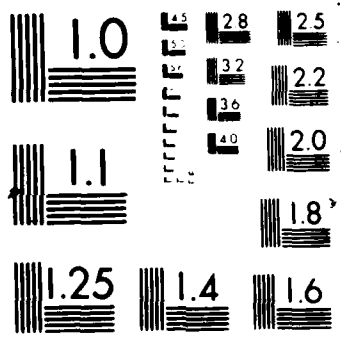
```



```

2230 | Force constant in z-x direction.
2240 |
2250 |
2260 A(Col+2,Col)=Force*(Dz*Dx)+A(Col+2,Col)
2270 A(Col+2,Row)=-Force*(Dz*Dx)+A(Col+2,Row)
2280 A(Row+2,Col)=-Force*(Dz*Dx)+A(Row+2,Col)
2290 A(Row+2,Row)=Force*(Dz*Dx)+A(Row+2,Row)
2300 |
2310 |
2320 | Force constant in z-y direction.
2330 |
2340 |
2350 A(Col+2,Col+1)=Force*(Dz*Dy)+A(Col+2,Col+1)
2360 A(Col+2,Row+1)=-Force*(Dz*Dy)+A(Col+2,Row+1)
2370 A(Row+2,Col+1)=-Force*(Dz*Dy)+A(Row+2,Col+1)
2380 A(Row+2,Row+1)=Force*(Dz*Dy)+A(Row+2,Row+1)
2390 |
2400 |
2410 | Force constant in z-z direction.
2420 |
2430 |
2440 A(Col+2,Col+2)=Force*(Dz^2)+A(Col+2,Col+2)
2450 A(Col+2,Row+2)=-Force*(Dz^2)+A(Col+2,Row+2)
2460 A(Row+2,Col+2)=-Force*(Dz^2)+A(Row+2,Col+2)
2470 A(Row+2,Row+2)=Force*(Dz^2)+A(Row+2,Row+2)
2480 NEXT Y
2490 BEEP
2500 RETURN
2510 |
2520 |
2530 | Subroutine: Eigen
2540 |
2550 | Diagonalizes the EB matrix.
2560 |
2570 |
2580 Eigen
2590 |
2600 |
2610 | Inputs: A matrix and half sizes of the matrix.
2620 |
2630 |
2640 |
2650 |
2660 |
2670 |
2680 |
2690 |
2700 |
2710 |
2720 |
2730 |
2740 |
2750 |
2760 |
2770 |
2780 |
2790 |
2800 |
2810 |
2820 |
2830 |
2840 |
2850 |
2860 |
2870 |
2880 |
2890 |
2900 |
2910 |
2920 |
2930 |
2940 |
2950 |
2960 |
2970 |
2980 |
2990 |

```


```

3370 | Subroutine used - Decx.
3380 |
3390 | INC Z - Increases the z axis orientation by 1 degree.
3400 | Subroutine used - Incz.
3410 |
3420 | DEC Z - Decreases the z axis orientation by 1 degree.
3430 | Subroutine used - Decz.
3440 |
3450 | DONE - Stops drawing the clusters. Subroutine used - Flag.
3460 |
3470 |
3480 OFF KEY
3490 ON KEY 0 LABEL "INC X",5 GOSUB Incx
3500 ON KEY 5 LABEL "DEC X",5 GOSUB Decx
3510 ON KEY 1 LABEL "INC Z",5 GOSUB Incz
3520 ON KEY 6 LABEL "DEC Z",5 GOSUB Decz
3530 ON KEY 9 LABEL "DONE",5 GOSUB Flag
3540 |
3550 |
3560 | Reads cluster subunit coordinates from data statements.
3570 |
3580 |
3590 FOR N=1 TO Mdim/3
3600 FOR M=1 TO 4
3610 READ Mol(N,M)
3620 NEXT M
3630 NEXT N
3640 Q$="Q"
3650 INPUT "OUTPUT TO PRINTER",Q$
3660 IF Q$="Y" THEN Paper=710
3670 IF Q$="Y" THEN 3700
3680 Paper=1
3690 IF Q$<>"N" THEN 3650
3700 PRINTER IS Paper
3710 |
3720 |
3730 | Prints eigenvalues.
3740 |
3750 |
3760 PRINT
3770 PRINT "----- EIGENVALUES (cm-1) -----"
3780 PRINT
3790 FOR N=1 TO Mdim STEP 3
3800 IMAGE K,A,X,MZ.9DE,3X,K,A,X,MZ.9DE,3X,K,A,X,MZ.9DE
3810 IF Paper=710 THEN PRINT USING 3800;N,".",Evr(N),N+1,".",Evr(N+1),N+2,".",E.
r(N+2)
3820 IF Paper=1 THEN PRINT USING 3830;Evr(N);Evr(N+1);Evr(N+2)
3830 IMAGE MZ.9DE,MZ.9DE,MZ.9DE
3840 NEXT N
3850 PRINT
3860 Q$="Q"
3870 INPUT "DO YOU WANT EIGENVECTORS",Q$
3880 IF Q$="N" THEN 5080
3890 IF Q$<>"Y" THEN 3870
3900 INPUT "WHAT EIGENVECTOR DO YOU WANT",M
3910 IF M=0 OR M Mdim THEN 3900

```

```

3920 !
3930 !!!!!!!!!!!!!!!!!!!!!!!!!!!!!!!!!!!!!!!!!!!!!!!!!!!!!!!!!!!!!!!!!!!!!!!!!!!!!!!
3940 ! Prints eigenvector for selected eigenvalue.
3950 !!!!!!!!!!!!!!!!!!!!!!!!!!!!!!!!!!!!!!!!!!!!!!!!!!!!!!!!!!!!!!!!!!!!!!!!!!!!!!!
3960 !
3970 PRINT "----- EIGENVECTORS (A) -----"
-----"
3980 PRINT
3990 PRINT "EIGENVECTOR FOR EIGENVALUE":M;Evr(M)
4000 PRINT
4010 FOR N=1 TO Mdim STEP 3
4020 IF Paper=710 THEN PRINT USING 3800;N,".",Vecr(N,M),N+1,".",Vecr(N+1,M),N+2,
".",Vecr(N+2,M)
4030 IF Paper=1 THEN PRINT USING 3830;Vecr(N,M);Vecr(N+1,M);Vecr(N+2,M)
4040 NEXT N
4050 PRINT
4060 IF Paper=710 THEN 3870
4070 GCLEAR
4080 Flag=0
4090 !
4100 !!!!!!!!!!!!!!!!!!!!!!!!!!!!!!!!!!!!!!!!!!!!!!!!!!!!!!!!!!!!!!!!!!!!!!!!!!!!!!!
4110 ! Draws cluster geometry and eigenvector displacement vectors using a stick
4120 ! model.
4130 !!!!!!!!!!!!!!!!!!!!!!!!!!!!!!!!!!!!!!!!!!!!!!!!!!!!!!!!!!!!!!!!!!!!!!!!!!!!!!!
4140 !
4150 GRAPHICS ON
4160 ALPHA OFF
4170 GCLEAR
4180 VIEWPORT 0,123,0,100
4190 LORG 1
4200 SHOW -Look,Look,-Look,Look
4210 MOVE -Look,Look-1
4220 LABEL Dwx;Dwz;M;Evr(M)
4230 LORG 5
4240 LINE TYPE 3
4250 !
4260 !!!!!!!!!!!!!!!!!!!!!!!!!!!!!!!!!!!!!!!!!!!!!!!!!!!!!!!!!!!!!!!!!!!!!!!!!!!!!!!
4270 ! Draws cartesian axes on graphics display.
4280 !!!!!!!!!!!!!!!!!!!!!!!!!!!!!!!!!!!!!!!!!!!!!!!!!!!!!!!!!!!!!!!!!!!!!!!!!!!!!!!
4290 !
4300 Cf1(1)=-5*Look*COS(Dwx)
4310 Ce1(2)=-5*Look*SIN(Dwx)
4320 Cf2(1)=5*Look*COS(Dwx)
4330 Ce2(2)=5*Look*SIN(Dwx)
4340 Cf1(3)=Ce1(2)*SIN(Dwz)
4350 Cf2(3)=Ce2(2)*SIN(Dwz)
4360 MOVE Cf1(1),Cf1(3)
4370 DRAW Cf2(1),Cf2(3)
4380 Cf1(1)=5*Look*SIN(Dwx)
4390 Ce1(2)=-5*Look*COS(Dwx)
4400 Cf2(1)=-5*Look*SIN(Dwx)
4410 Ce2(2)=5*Look*COS(Dwx)
4420 Cf1(3)=Ce1(2)*SIN(Dwz)
4430 Cf2(3)=Ce2(2)*SIN(Dwz)
4440 MOVE Cf1(1),Cf1(3)
4450 DRAW Cf2(1),Cf2(3)
4460 Cf1(1)=0

```



```

5610 |
5615 |
5620 Incz: |
5625 Dwz=Dwz+1
5630 RETURN
5635 |
5640 |
5645 | Subroutine: Decz
5650 |
5655 | Decreases z axis orientation by 1 degree.
5660 |
5665 |
5670 Decz: |
5675 Dwz=Dwz-1
5680 RETURN
5685 |
5690 |
5695 | Subroutine: Flag
5700 |
5705 | Stops drawing cluster geometry and displacement vectors.
5710 |
5715 |
5720 Flag: |
5725 Flag=1
5730 RETURN
5735 |
5740 |
5745 | Intramolecular force fields for cluster subunits.
5750 |
5755 | The force fields are generated using the central force approximation and
5760 | expressed as force constants in a cartesian coordinate system. The
5765 | following data statements are for the intramolecular force fields in
5770 | Benzene-(Methane)1. They are included to give an example on how the
5775 | force fields are generated. Since the benzene subunit is planar, the
5780 | central force field constants must be modified to incorporate
5785 | out-of-plane motion. This is accomplished by setting the atoms composing
5790 | benzene slightly out-of-plane. One angstrom provides sufficient
5795 | out-of-plane displacement to account for the out-of-plane force field.
5800 |
5805 | The force fields are entered as force constants between adjacent atoms
5810 | and between atoms displaced by one intervening atom. The atoms in
5815 | each cluster subunit are numbered in the same order as used in the
5820 | ECCEMP2 calculation. The force constants used are those corresponding to
5825 | general functional group stretches and bends.
5830 |
5835 |
5840 | Order of data entries:
5845 |
5850 | DATA X-Coord,Y-Coord,Z-Coord for atom 1.
5855 | DATA X-Coord,Y-Coord,Z-Coord for atom j.
5860 | DATA Force Constant,Atom 1 X-Coord Matrix Location,Atom j X-Coord Matrix
5865 | Location.
5870 |
5875 |
5880 DATA 52 | Number of force constants used in fields.
5885 |
5890 |

```

```
5895 | Benzene C-C force constant.
5900 | .....
5905 |
5910 DATA -1.395,0,0
5915 DATA -.6975,1.208,0
5920 DATA 6.94E5,1,4
5925 |
5930 | .....
5935 | Benzene C-C force constant.
5940 | .....
5945 |
5950 DATA -1.395,0,0
5955 DATA .6975,1.208,0
5960 DATA 1.054E5,1,7
5965 |
5970 | .....
5975 | Benzene C-C force constant.
5980 | .....
5985 |
5990 DATA -.6975,1.208,0
5995 DATA .6975,1.208,0
6000 DATA 6.94E5,4,7
6005 |
6010 | .....
6015 | Benzene C-C force constant.
6020 | .....
6025 |
6030 DATA -.6975,1.208,0
6035 DATA 1.395,0,0
6040 DATA 1.054E5,4,10
6045 |
6050 | .....
6055 | Benzene C-C force constant.
6060 | .....
6065 |
6070 DATA .6975,1.208,0
6075 DATA 1.395,0,0
6080 DATA 6.94E5,7,10
6085 |
6090 | .....
6095 | Benzene C-C force constant.
6100 | .....
6105 |
6110 DATA .6975,1.208,0
6115 DATA .6975,-1.208,0
6120 DATA 1.054E5,7,13
6125 |
6130 | .....
6135 | Benzene C-C force constant.
6140 | .....
6145 |
6150 DATA 1.395,0,0
6155 DATA .6975,-1.208,0
6160 DATA 6.94E5,10,13
6165 |
6170 | .....
6175 | Benzene C-C force constant.
```

```
5190 | .....
6185 |
5190 DATA 1.395,0,0
5195 DATA -.6975,-1.208,0
6200 DATA 1.054E5,10,16
6205 |
6210 | .....
6215 | Benzene C-C force constant.
6220 | .....
6225 |
6230 DATA .6975,-1.208,0
6235 DATA -.6975,-1.208,0
6240 DATA 6.94E5,13,16
6245 |
6250 | .....
6255 | Benzene C-C force constant.
6260 | .....
6265 |
6270 DATA .6975,-1.208,0
6275 DATA -1.395,0,0
6280 DATA 1.054E5,13,1
6285 |
6290 | .....
6295 | Benzene C-C force constant.
6300 | .....
6305 |
6310 DATA -.6975,-1.208,0
6315 DATA -1.395,0,0
6320 DATA 6.94E5,16,1
6325 |
6330 | .....
6335 | Benzene C-C force constant.
6340 | .....
6345 |
6350 DATA -.6975,-1.208,0
6355 DATA -.6975,1.208,0
6360 DATA 1.054E5,16,4
6365 |
6370 | .....
6375 | Benzene C-H force constant.
6380 | .....
6385 |
6390 DATA -2.479,0,0
6395 DATA -1.395,0,0
6400 DATA 5.508E5,19,1
6405 |
6410 | .....
6415 | Benzene C-H force constant.
6420 | .....
6425 |
6430 DATA -2.479,0,0
6435 DATA -.6975,1.208,0
6440 DATA 1.093E5,19,4
6445 |
6450 | .....
6455 | Benzene C-H force constant.
6460 | .....
```



```
6465 |
6470 DATA -2.479,0,0
6475 DATA -.6375,-1.208,0
6480 DATA 1.093E5,19,16
6485 |
6490 |.....
6495 | Benzene C-H force constant.
6500 |.....
6505 |
6510 DATA -1.24,2.147,0
6515 DATA -.6975,1.208,0
6520 DATA 5.508E5,22,4
6525 |
6530 |.....
6535 | Benzene C-H force constant.
6540 |.....
6545 |
6550 DATA -1.24,2.147,0
6555 DATA .6975,1.208,0
6560 DATA 1.093E5,22,7
6565 |
6570 |.....
6575 | Benzene C-H force constant.
6580 |.....
6585 |
6590 DATA -1.24,2.147,0
6595 DATA -1.395,0,0
6600 DATA 1.093E5,22,1
6605 |
6610 |.....
6615 | Benzene C-H force constant.
6620 |.....
6625 |
6630 DATA 1.24,2.147,0
6635 DATA .6975,1.208,0
6640 DATA 5.508E5,25,7
6645 |
6650 |.....
6655 | Benzene C-H force constant.
6660 |.....
6665 |
6670 DATA 1.24,2.147,0
6675 DATA 1.395,0,0
6680 DATA 1.093E5,25,10
6685 |
6690 |.....
6695 | Benzene C-H force constant.
6700 |.....
6705 |
6710 DATA 1.24,2.147,0
6715 DATA -.6975,1.208,0
6720 DATA 1.093E5,25,4
6725 |
6730 |.....
6735 | Benzene C-H force constant.
6740 |.....
6745 |
```

```
6750 DATA 2.479,0,0
6755 DATA 1.395,0,0
6760 DATA 5.503E5,29,10
6765 |
6770 | .....
6775 | Benzene C-H force constant.
6780 | .....
6785 |
6790 DATA 2.479,0,0
6795 DATA .6975,1.208,0
6800 DATA 1.093E5,29,7
6805 |
6810 | .....
6815 | Benzene C-H force constant.
6820 | .....
6825 |
6830 DATA 2.479,0,0
6835 DATA .6975,-1.208,0
6840 DATA 1.093E5,28,13
6845 |
6850 | .....
6855 | Benzene C-H force constant.
6860 | .....
6865 |
6870 DATA 1.24,-2.147,0
6875 DATA .6975,-1.208,0
6880 DATA 5.508E5,31,13
6885 |
6890 | .....
6895 | Benzene C-H force constant.
6900 | .....
6905 |
6910 DATA 1.24,-2.147,0
6915 DATA 1.395,0,0
6920 DATA 1.093E5,31,10
6925 |
6930 | .....
6935 | Benzene C-H force constant.
6940 | .....
6945 |
6950 DATA 1.24,-2.147,0
6955 DATA -.6975,-1.208,0
6960 DATA 1.093E5,31,16
6965 |
6970 | .....
6975 | Benzene C-H force constant.
6980 | .....
6985 |
6990 DATA -1.24,-2.147,0
6995 DATA -.6975,-1.208,0
7000 DATA 5.508E5,34,16
7005 |
7010 | .....
7015 | Benzene C-H force constant.
7020 | .....
7025 |
7030 DATA -1.24,-2.147,0
```

```
7035 DATA .6975,-1.208,0
7040 DATA 1.093E5,34,13
7045 |
7050 |
7055 | Benzene C-H force constant.
7060 |
7065 |
7070 DATA -1.24,-2.147,0
7075 DATA -1.395,0,0
7080 DATA 1.093E5,34,1
7085 |
7090 |
7095 | Benzene C-C out-of-plane force constant.
7100 |
7105 |
7110 DATA -1.395,0,1
7115 DATA -.6975,1.208,0
7120 DATA 1E5,1,4
7125 |
7130 |
7135 | Benzene C-C out-of-plane force constant.
7140 |
7145 |
7150 DATA -.6975,1.208,1
7155 DATA .6975,1.208,0
7160 DATA 1E5,4,7
7165 |
7170 |
7175 | Benzene C-C out-of-plane force constant.
7180 |
7185 |
7190 DATA .6975,1.208,1
7195 DATA 1.395,0,0
7200 DATA 1E5,7,10
7205 |
7210 |
7215 | Benzene C-C out-of-plane force constant.
7220 |
7225 |
7230 DATA 1.395,0,1
7235 DATA .6975,-1.208,0
7240 DATA 1E5,10,13
7245 |
7250 |
7255 | Benzene C-C out-of-plane force constant.
7260 |
7265 |
7270 DATA .6975,-1.208,1
7275 DATA -.6975,-1.208,0
7280 DATA 1E5,13,16
7285 |
7290 |
7295 | Benzene C-C out-of-plane force constant.
7300 |
7305 |
7310 DATA -.6975,-1.208,1
7315 DATA -1.395,0,0
```

```

7375 Benzene C-H out-of-plane force constant.
7380
7385
7390
7395
7400 DATA 1.24,2.147,1
7405 DATA 1.6975,1.208,0
7410 DATA 1E5,22,4
7415
7420
7425
7430 DATA 1.24,2.147,1
7435 DATA 1.6975,1.208,0
7440 DATA 1E5,25,7
7445
7450
7455 Benzene C-H out-of-plane force constant.
7460
7465
7470 DATA 2.479,0,1
7475 DATA 1.395,0,0
7480 DATA 1E5,28,10
7485
7490
7495 Benzene C-H out-of-plane force constant.
7500
7505
7510 DATA 1.24,-2.147,1
7515 DATA 1.6975,-1.208,0
7520 DATA 1E5,31,13
7525
7530
7535 Benzene C-H out-of-plane force constant.
7540
7545
7550 DATA -1.24,-2.147,1
7555 DATA -1.6975,-1.208,0
7560 DATA 1E5,34,16
7565
7570
7575 Methane C-H force constant.
7580
7585
7590 DATA 0,7.79346319179E-5,3.46941045213
7595 DATA -1.8999,-1.518921585724,3.10438237398
7600 DATA 4.73E5,37,40

```

7505 |
7510 |
7515 | Methane C-H force constant.
7520 |
7525 |
7530 DATA 0,7.78346319178E-5,3.46941045213
7535 DATA .8989,-.518821585724,3.10438237398
7540 DATA 4.79E5,37,43
7545 |
7550 |
7555 | Methane C-H force constant.
7560 |
7565 |
7570 DATA 0,7.78346319178E-5,3.46941045213
7575 DATA 0,1.03987841578,3.1043966958
7580 DATA 4.79E5,37,46
7585 |
7590 |
7595 | Methane C-H force constant.
7700 |
7705 |
7710 DATA 0,7.78346319178E-5,3.46941045213
7715 DATA 6.77616018046E-21,.000106109702385,4.56937173828
7720 DATA 4.79E5,37,49
7725 |
7730 |
7735 | Methane H-H force constant.
7740 |
7745 |
7750 DATA -.8989,-.518821585724,3.10438237398
7755 DATA .8989,-.518821585724,3.10438237398
7760 DATA 1.85E5,40,43
7765 |
7770 |
7775 | Methane H-H force constant.
7780 |
7785 |
7790 DATA .8989,-.518821585724,3.10438237398
7795 DATA 0,1.03987841578,3.1043966958
7800 DATA 1.85E5,43,46
7805 |
7810 |
7815 | Methane H-H force constant.
7820 |
7825 |
7830 DATA 0,1.03987841578,3.1043966958
7835 DATA -.8989,-.518821585724,3.10438237398
7840 DATA 1.85E5,46,40
7845 |
7850 |
7855 | Methane H-H force constant.
7860 |
7865 |
7870 DATA 0,1.03987841578,3.1043966958
7875 DATA 6.77616018046E-21,.000106109702385,4.56937173828
7880 DATA 1.85E5,46,49
7885 |

```

7330 | .....
7335 | Methane H-H force constant.
7340 | .....
7345 |
7350 DATA 6.77616018046E-21,.000106109702395,4.56937173828
7355 DATA -.8989,-.518821585724,3.10438237398
7360 DATA 1.85E5,49,43
7365 |
7370 | .....
7375 | Methane H-H force constant.
7380 | .....
7385 |
7390 DATA 6.77616018046E-21,.000106109702395,4.56937173828
7395 DATA -.8989,-.518821585724,3.10438237398
7400 DATA 1.85E5,49,40
7405 |
7410 | .....
7415 | Data statements containing cluster subunit coordinates.
7420 | The data is used to draw the cluster geometry and vdW mode displacement
7425 | vectors. The coordinates are entered as they are numbered in ECCEMP2.
7430 |
7435 |
7440 | Order of data entries:
7445 |
7450 | DATA X-Coord,Y-Coord,Z-Coord,Atom #.
7455 |
7460 | Atom #:
7465 |     1 - Carbon.
7470 |     2 - Hydrogen.
7475 |     3 - Nitrogen.
7480 |     4 - Oxygen.
7485 |     5 - User defined atom.
7490 | .....
7495 |
7500 DATA -1.395,0,0,1
7505 DATA -.6975,1.208,0,1
7510 DATA .6975,1.208,0,1
7515 DATA 1.395,0,0,1
7520 DATA .6975,-1.208,0,1
7525 DATA -.6975,-1.208,0,1
7530 DATA -2.479,0,0,2
7535 DATA -1.24,2.147,0,2
7540 DATA 1.24,2.147,0,2
7545 DATA 2.479,0,0,2
7550 DATA 1.24,-2.147,0,2
7555 DATA -1.24,-2.147,0,2
7560 DATA 0,0,3.4694,1
7565 DATA -.8989,-.5188,3.10438,2
7570 DATA .8989,-.5188,3.10438,2
7575 DATA 0,1.0398,3.10439,2
7580 DATA 0,.000106,4.56937,2
7585 END
7590 |
7595 |
7600 |
7605 |
7610 |

```

```

3175 |
3180 |
3185 |
3190 |
3195 |
3200 |
3205 |
3210 | .....
3215 | Subprogram: Eigen
3220 |
3225 | This subprogram determines all the eigenvalues and eigenvectors of a real
3230 | general matrix. The eigenvalues are computed by the QR double-step method
3235 | and the eigenvectors by inverse iteration.
3240 |
3245 |
3250 | This subprogram was taken from HP 98821A BASIC Numerical Analysis Library
3255 | which is designed to be executed using HP series 200 computers.
3260 | .....
3265 |
3270 |
3275 |
3280 |
3285 |
3290 |
3295 |
3300 |
9860 SUB Eigen(N,A(*),Evr(*),Evi(*),Vecr(*),Veci(*),Indic(*))
9870   Baddta=(N<=0)
9880   IF Baddta=0 THEN 9930
9890   PRINT FNLine(2);"ERROR IN SUBPROGRAM Eigen."
9900   PRINT "N=";N;FNLine(2)
9910   PAUSE
9920   GOTO 9870
9930   OPTION BASE 1
9940   ALLOCATE INTEGER Local(N)
9950   ALLOCATE Prfact(N),Subdia(N),Work(N)
9960   IF N<>1 THEN 10030
9970   Evr(1)=A(1,1)
9980   Evi(1)=0
9990   Vecr(1,1)=1
10000  Veci(1,1)=0
10010  Indic(1)=2
10020  GOTO 11200
10030  CALL Scale(N,A(*),Veci(*),Prfact(*),Enorm)
10040  Ex=EXP(-39*LOG(2))
10050  CALL Hesqr(N,A(*),Veci(*),Evr(*),Evi(*),Subdia(*),Indic(*),Eps,Ex)
10060  J=N
10070  I=1
10080  Local(I)=1
10090  IF J=1 THEN 10160
10100  IF ABS(Subdia(J-1)) Eps THEN 10130
10110  I=I+1
10120  Local(I)=0
10130  J=J-1
10140  Local(I)=Local(I)+1
10150  IF J=1 THEN 10100
10160  N=1

```

```

10170 Kon=0
10180 L=Local(1)
10190 M=N
10200 FOR I=1 TO N
10210   Ivec=N-I+1
10220   IF I<=L THEN 10260
10230   K=K+1
10240   M=N-L
10250   L=L+Local(K)
10260   IF Indic(Ivec)=0 THEN 10420
10270   IF Evi(Ivec)<>0 THEN 10370
10280   FOR K1=1 TO M
10290     FOR L1=K1 TO M
10300       A(K1,L1)=Veci(K1,L1)
10310     NEXT L1
10320     IF K1=1 THEN 10340
10330     A(K1,K1-1)=Subdia(K1-1)
10340   NEXT K1
10350   CALL Realve(N,M,Ivec,A(*),Vecr(*),Evr(*),Evi(*),Work(*),Indic(*),Eps,Ex)
10360   GOTO 10420
10370   IF Kon<>0 THEN 10410
10380   Kon=1
10390   CALL Compve(N,M,Ivec,A(*),Vecr(*),Veci(*),Evr(*),Evi(*),Indic(*),Subdia
(*),Work(*),Eps,Ex)
10400   GOTO 10420
10410   Kon=0
10420 NEXT I
10430 FOR I=1 TO N
10440   FOR J=1 TO N
10450     A(I,J)=0
10460   NEXT J
10470   A(I,I)=1
10480 NEXT I
10490 IF N<=2 THEN 10640
10500 M=N-2
10510 FOR K=1 TO M
10520   L=K+1
10530   FOR J=2 TO N
10540     D1=0
10550     FOR I=L TO N
10560       D2=Veci(I,K)
10570       D1=D1+D2*A(J,I)
10580     NEXT I
10590     FOR I=L TO N
10600       A(J,I)=A(J,I)-Veci(I,K)*D1
10610     NEXT I
10620   NEXT J
10630 NEXT K
10640 Kon=1
10650 FOR I=1 TO N
10660   L=0
10670   IF Evi(I)=0 THEN 10720
10680   L=1
10690   IF Kon=0 THEN 10720
10700   Kon=0
10710   GOTO 11190

```



```

10720   FOR J=1 TO N
10730     D1=0
10740     D2=0
10750     FOR K=1 TO N
10760       D3=A(J,K)
10770       D1=D1+D3*Vecr(K,I)
10780       IF L=0 THEN 10800
10790       D2=D2+D3*Vecr(K,I-1)
10800     NEXT K
10810     Work(J)=D1/Prfact(J)
10820     IF L=0 THEN 10840
10830     Subdia(J)=D2/Prfact(J)
10840   NEXT J
10850   IF L=1 THEN 10970
10860   D1=0
10870   FOR M=1 TO N
10880     D1=D1+Work(M)^2
10890   NEXT M
10900   D1=SQR(D1)
10910   FOR M=1 TO N
10920     Vec1(M,I)=0
10930     Vecr(M,I)=Work(M)/D1
10940   NEXT M
10950   Evr(I)=Evr(I)*Enorm
10960   GOTO 11190
10970   Kon=1
10980   Evr(I)=Evr(I)*Enorm
10990   Evr(I-1)=Evr(I)
11000   Evi(I)=Evi(I)*Enorm
11010   Evi(I-1)=-Evi(I)
11020   R=0
11030   FOR J=1 TO N
11040     R1=Work(J)^2+Subdia(J)^2
11050     IF R>R1 THEN 11080
11060     R=R1
11070     L=J
11080   NEXT J
11090   D3=Work(L)
11100   R1=Subdia(L)
11110   FOR J=1 TO N
11120     D1=Work(J)
11130     D2=Subdia(J)
11140     Vecr(J,I)=(D1*D3+D2*R1)/R
11150     Vec1(J,I)=(D2*D3-D1*R1)/R
11160     Vecr(J,I-1)=Vecr(J,I)
11170     Vec1(J,I-1)=-Vec1(J,I)
11180   NEXT J
11190 NEXT I
11200 SUBEXIT
11210 SUBEND!

11220 SUB Scale(N,A(*),H(*),Prfact(*),Enorm)
11230 OPTION BASE 1
11240 INTEGER I,J,Iter,Ncount
11250 FOR I=1 TO N
11260   FOR J=1 TO N
11270     H(I,J)=A(I,J)

```

```

11280     NEXT J
11290     Prfact(I)=1
11300 NEXT I
11310 Bound1=.75
11320 Bound2=1.33
11330 Iter=0
11340 Ncount=0
11350 FOR I=1 TO N
11360     Column=0
11370     Row=0
11380     FOR J=1 TO N
11390         IF I=J THEN 11420
11400         Column=Column+ABS(A(J,I))
11410         Row=Row+ABS(A(I,J))
11420     NEXT J
11430     IF Column=0 THEN 11480
11440     IF Row=0 THEN 11480
11450     Q=Column/Row
11460     IF Q<Bound1 THEN 11500
11470     IF Q>Bound2 THEN 11500
11480     Ncount=Ncount+1
11490     GOTO 11570
11500     Factor=SQR(Q)
11510     FOR J=1 TO N
11520         IF I=J THEN 11550
11530         A(I,J)=A(I,J)*Factor
11540         A(J,I)=A(J,I)/Factor
11550     NEXT J
11560     Prfact(I)=Prfact(I)*Factor
11570 NEXT I
11580 Iter=Iter+1
11590 IF Iter>30 THEN 11760
11600 IF Ncount<N THEN 11340
11610 Fnorm=0
11620 FOR I=1 TO N
11630     FOR J=1 TO N
11640         Q=A(I,J)
11650         Fnorm=Fnorm+Q*Q
11660     NEXT J
11670 NEXT I
11680 Fnorm=SQR(Fnorm)
11690 FOR I=1 TO N
11700     FOR J=1 TO N
11710         A(I,J)=A(I,J)/Fnorm
11720     NEXT J
11730 NEXT I
11740 Enorm=Fnorm
11750 GOTO 11830
11760 FOR I=1 TO N
11770     Prfact(I)=1
11780     FOR J=1 TO N
11790         A(I,J)=H(I,J)
11800     NEXT J
11810 NEXT I
11820 Enorm=1
11830 SUBEXIT
11840 SUBEND

```

```

11850 SUB Hesqr(N,A(*),H(*),Evr(*),Evl(*),Subdia(*),Indic(*),Eps,Ex)
11860 OPTION BASE 1
11870 INTEGER I,J,K,L,M,Maxst,M1,Ns
11880 IF N-2<0 THEN 12460
11890 IF N-2>0 THEN 11920
11900 Subdia(1)=A(2,1)
11910 GOTO 12460
11920 M=N-2
11930 FOR K=1 TO M
11940   L=K+1
11950   S=0
11960   FOR I=L TO N
11970     H(I,K)=A(I,K)
11980     S=S+ABS(A(I,K))
11990   NEXT I
12000   IF S<>ABS(A(K+1,K)) THEN 12040
12010   Subdia(K)=A(K+1,K)
12020   H(K+1,K)=0
12030   GOTO 12410
12040   Sr2=0
12050   FOR I=L TO N
12060     Sr=A(I,K)
12070     Sr=Sr/S
12080     A(I,K)=Sr
12090     Sr2=Sr2+Sr*Sr
12100   NEXT I
12110   Sr=SQR(Sr2)
12120   IF A(L,K)<0 THEN 12140
12130   Sr=-Sr
12140   Sr2=Sr2-Sr*A(L,K)
12150   A(L,K)=A(L,K)-Sr
12160   H(L,K)=H(L,K)-Sr*S
12170   Subdia(K)=Sr*S
12180   X=S*SQR(Sr2)
12190   FOR I=L TO N
12200     H(I,K)=H(I,K)/X
12210     Subdia(I)=A(I,K)/Sr2
12220   NEXT I
12230   FOR J=L TO N
12240     Sr=0
12250     FOR I=L TO N
12260       Sr=Sr+A(I,K)*A(I,J)
12270     NEXT I
12280     FOR I=L TO N
12290       A(I,J)=A(I,J)-Subdia(I)*Sr
12300     NEXT I
12310   NEXT J
12320   FOR J=1 TO N
12330     Sr=0
12340     FOR I=L TO N
12350       Sr=Sr+A(J,I)*A(I,K)
12360     NEXT I
12370     FOR I=L TO N
12380       A(J,I)=A(J,I)-Subdia(I)*Sr
12390     NEXT I
12400   NEXT J

```

```

12410 NEXT K
12420 FOR K=1 TO M
12430   A(K+1,K)=Subdia(K)
12440 NEXT K
12450 Subdia(N-1)=A(N,N-1)
12460 Eps=0
12470 FOR K=1 TO N
12480   Indic(K)=0
12490   IF K<>N THEN Eps=Eps+Subdia(K)^2
12500   FOR I=K TO N
12510     H(K,I)=A(K,I)
12520     Eps=Eps+A(K,I)^2
12530   NEXT I
12540 NEXT K
12550 Eps=Exp*SQR(Eps)
12560 Shift=A(N,N-1)
12570 IF N<=2 THEN Shift=0
12580 IF A(N,N)<>0 THEN Shift=0
12590 IF A(N-1,N)<>0 THEN Shift=0
12600 IF A(N-1,N-1)<>0 THEN Shift=0
12610 M=N
12620 Ns=0
12630 Maxst=N+10
12640 FOR I=2 TO N
12650   FOR K=I TO N
12660     IF A(I-1,K)<>0 THEN 12750
12670   NEXT K
12680 NEXT I
12690 FOR I=1 TO N
12700   Indic(I)=1
12710   Evr(I)=A(I,I)
12720   Evi(I)=0
12730 NEXT I
12740 GOTO 13780
12750 K=M-1
12760 M1=K
12770 I=K
12780 IF K<0 THEN 13780
12790 IF K=0 THEN 13530
12800 IF ABS(A(M,K))<=Eps THEN 13530
12810 IF M-2=0 THEN 13580
12820 I=I-1
12830 IF ABS(A(K,I))<=Eps THEN 12860
12840 K=I
12850 IF K>1 THEN 12820
12860 IF K=M1 THEN 13580
12870 S=A(M,M)+A(M1,M1)+Shift
12880 Sp=A(M,M)+A(M1,M1)-A(M,M1)+A(M1,M)+.25*Shift^2
12890 A(K+2,K)=0
12900 X=A(K,K)+A(K,K)-S+A(K,K+1)+A(K+1,K)+Sp
12910 Y=A(K+1,K)+A(K,K+1)+A(K+1,K+1)-S
12920 R=ABS(X)+ABS(Y)
12930 IF R=0 THEN Shift=A(M,M-1)
12940 IF R=0 THEN 12860
12950 Z=A(K+2,K+1)+A(K+1,K+1)
12960 Shift=0
12970 Ns=Ns+1

```

```

12980 FOR I=K TO M1
12990 IF I=K THEN 13050
13000 X=A(I,I-1)
13010 Y=A(I+1,I-1)
13020 Z=0
13030 IF I+2>M THEN 13050
13040 Z=A(I+2,I-1)
13050 Sr2=ABS(X)+ABS(Y)+ABS(Z)
13060 IF Sr2=0 THEN 13100
13070 X=X/Sr2
13080 Y=Y/Sr2
13090 Z=Z/Sr2
13100 S=SQR(X*X+Y*Y+Z*Z)
13110 IF X<0 THEN 13130
13120 S=-S
13130 IF I=K THEN 13150
13140 A(I,I-1)=S*Sr2
13150 IF Sr2<>0 THEN 13180
13160 IF I+3>M THEN 13500
13170 GOTO 13470
13180 Sr=1-X/S
13190 S=X-S
13200 X=Y/S
13210 Y=Z/S
13220 FOR J=I TO M
13230 S=A(I,J)+A(I+1,J)*X
13240 IF I+2>M THEN 13260
13250 S=S+A(I+2,J)*Y
13260 S=S*Sr
13270 A(I,J)=A(I,J)-S
13280 A(I+1,J)=A(I+1,J)-S*X
13290 IF I+2>M THEN 13310
13300 A(I+2,J)=A(I+2,J)-S*Y
13310 NEXT J
13320 L=I+2
13330 IF I<M1 THEN 13350
13340 L=M
13350 FOR J=K TO L
13360 S=A(J,I)+A(J,I+1)*X
13370 IF I+2>M THEN 13390
13380 S=S+A(J,I+2)*Y
13390 S=S*Sr
13400 A(J,I)=A(J,I)-S
13410 A(J,I+1)=A(J,I+1)-S*X
13420 IF I+2>M THEN 13440
13430 A(J,I+2)=A(J,I+2)-S*Y
13440 NEXT J
13450 IF I+3>M THEN 13500
13460 S=-A(I+3,I+2)*Y*Sr
13470 A(I+3,I)=S
13480 A(I+3,I+1)=S*X
13490 A(I+3,I+2)=S*Y+A(I+3,I+2)
13500 NEXT I
13510 IF Ns Ma-st THEN 13780
13520 GOTO 10750
13530 Evr(M)=A(M,M)
13540 Evi(M)=0

```

```

13550 Indic(M)=1
13560 M=K
13570 GOTO 12750
13580 R=.5*(A(K,K)+A(M,M))
13590 S=.5*(A(M,M)-A(K,K))
13600 S=S+A(K,M)*A(M,K)
13610 Indic(K)=1
13620 Indic(M)=1
13630 IF S<0 THEN 13710
13640 T=SQR(S)
13650 Evr(K)=R-T
13660 Evr(M)=R+T
13670 Evi(K)=0
13680 Evi(M)=0
13690 M=M-2
13700 GOTO 12750
13710 T=SQR(-S)
13720 Evr(K)=R
13730 Evi(K)=T
13740 Evr(M)=R
13750 Evi(M)=-T
13760 M=M-2
13770 GOTO 12750
13780 SUBEXIT
13790 SUBEND!

13800 SUB Realve(N,M,Ivec,A(*),Vecr(*),Evr(*),Evi(*),Work(*),Indic(*),Eps,Ex)
13810 Baddta=(N<=0) OR (M<=0) OR (Ivec<=0)
13820 IF Baddta=0 THEN 13860
13830 PRINT FNLine(2);"ERROR IN SUBPROGRAM Realve."
13840 PRINT "N=";N,"M=";M,"Ivec=";Ivec;FNLine(2)
13850 PAUSE
13860 OPTION BASE 1
13870 ALLOCATE INTEGER Iwork(N)
13880 INTEGER I,Iter,J,K,L,Ns
13890 Vecr(1,Ivec)=1
13900 IF M=1 THEN 14850
13910 Evalue=Evr(Ivec)
13920 IF Ivec=M THEN 14010
13930 K=Ivec+1
13940 R=0
13950 FOR I=K TO M
13960   IF Evalue<>Evr(I) THEN 13990
13970   IF Evi(I)<>0 THEN 13990
13980   R=R+3
13990 NEXT I
14000 Evalue=Evalue+R*Ex
14010 FOR K=1 TO M
14020   A(K,K)=A(K,K)-Evalue
14030 NEXT K
14040 M=M-1
14050 FOR I=1 TO K
14060   L=I+1
14070   Iwork(L)=0
14080   IF A(I+1,I) < 0 THEN 14120
14090   IF A(I,I) < 0 THEN 14040
14100   A(I,I)=Eps

```

```

14110 GOTO 14240
14120 IF ABS(A(I,I))>=ABS(A(I+1,I)) THEN 14190
14130 Iwork(I)=1
14140 FOR J=I TO M
14150 R=A(I,J)
14160 A(I,J)=A(I+1,J)
14170 A(I+1,J)=R
14180 NEXT J
14190 R=-A(I+1,I)/A(I,I)
14200 A(I+1,I)=R
14210 FOR J=L TO M
14220 A(I+1,J)=A(I+1,J)+R*A(I,J)
14230 NEXT J
14240 NEXT I
14250 IF A(M,M)<>0 THEN 14270
14260 A(M,M)=Eps
14270 FOR I=1 TO N
14280 IF I>M THEN 14310
14290 Work(I)=1
14300 GOTO 14320
14310 Work(I)=0
14320 NEXT I
14330 Bound=.01/(Ex*N)
14340 Ns=0
14350 Iter=1
14360 R=0
14370 FOR I=1 TO M
14380 J=M-I+1
14390 S=Work(J)
14400 IF J=M THEN 14460
14410 L=J+1
14420 FOR K=L TO M
14430 Sr=Work(K)
14440 S=S-Sr*A(J,K)
14450 NEXT K
14460 Work(J)=S/A(J,J)
14470 T=ABS(Work(J))
14480 IF R>=T THEN 14500
14490 R=T
14500 NEXT I
14510 FOR I=1 TO M
14520 Work(I)=Work(I)/R
14530 NEXT I
14540 R1=0
14550 FOR I=1 TO M
14560 T=0
14570 FOR J=I TO M
14580 T=T+A(I,J)*Work(J)
14590 NEXT J
14600 T=ABS T
14610 IF R1<=T THEN 14630
14620 R1=T
14630 NEXT I
14640 IF Iter=1 THEN 14660
14650 IF Fprev =R1 THEN 14650
14660 FOR I=1 TO M
14670 Vecn(I,Vec)=Work(I)

```

```

14680 NEXT I
14690 PRevis=R1
14700 IF Ns=1 THEN 14850
14710 IF Iter>6 THEN 14860
14720 Iter=Iter+1
14730 IF R<Bound THEN 14750
14740 Ns=1
14750 k=M-1
14760 FOR I=1 TO K
14770   R=Work(I+1)
14780   IF Iwork(I)=0 THEN 14820
14790   Work(I+1)=Work(I)+Work(I+1)*A(I+1,I)
14800   Work(I)=R
14810   GOTO 14830
14820   Work(I+1)=Work(I)*A(I+1,I)+Work(I+1)
14830 NEXT I
14840 GOTO 14360
14850 Indic(Ivec)=2
14860 IF M=N THEN 14910
14870 J=M+1
14880 FOR I=J TO N
14890   Vecr(I,Ivec)=0
14900 NEXT I
14910 SUBEXIT
14920 SUBEND

14930 SUB Compve(N,M,Ivec,A(*),Vecr(*),H(*),Evr(*),Evi(*),Indic(*),Subdia(*),Work(*),Eps,Ex)
14940 Baddta=(N<=0) OR (M<=0) OR (Ivec<=0)
14950 IF Baddta=0 THEN 14990
14960 PRINT FNLine(2);"ERROR IN SUBPROGRAM Compve."
14970 PRINT "N=";N,"M=";M,"Ivec=";Ivec;FNLine(2)
14980 PAUSE
14990 OPTION BASE 1
15000 ALLOCATE INTEGER Iwork(N)
15010 ALLOCATE Work1(N),Work2(N)
15020 INTEGER I,I1,I2,Iter,J,K,L,Ns
15030 Fks1=Evr(Ivec)
15040 Eta=Evi(Ivec)
15050 IF Ivec=M THEN 15160
15060 K=Ivec+1
15070 R=0
15080 FOR I=K TO M
15090   IF Fks1<>Evr(I) THEN 15120
15100   IF ABS(Eta)<>ABS(Evi(I)) THEN 15120
15110   R=R+3
15120 NEXT I
15130 R=R+E.
15140 Fks1=Fks1+R
15150 Eta=Eta+R
15160 R=Fks1+Fks1+Eta+Eta
15170 E=2+E.
15180 L=M-1
15190 FOR I=1 TO M
15200   FOR J=1 TO M
15210     E=0
15220     A(J,I)=0

```



```

15230     FOR K=I TO J
15240         D=D+H(I,K)*H(K,J)
15250     NEXT K
15260     A(I,J)=D-S+H(I,J)
15270     NEXT J
15280     A(I,I)=A(I,I)+R
15290     NEXT I
15300     FOR I=1 TO L
15310         R=Subdia(I)
15320         A(I+1,I)=-S+R
15330         I1=I+1
15340         FOR J=1 TO I1
15350             A(J,I)=A(J,I)+R*H(J,I+1)
15360         NEXT J
15370         IF I=1 THEN 15390
15380         A(I+1,I-1)=R+Subdia(I-1)
15390         FOR J=I TO M
15400             A(I+1,J)=A(I+1,J)+R*H(I,J)
15410         NEXT J
15420     NEXT I
15430     Y=M-1
15440     FOR I=1 TO K
15450         I1=I+1
15460         I2=I+2
15470         Iwork(I)=0
15480         IF I=K THEN 15500
15490         IF A(I+2,I)<>0 THEN 15540
15500         IF A(I+1,I)<>0 THEN 15540
15510         IF A(I,I)<>0 THEN 15770
15520         A(I,I)=Eps
15530         GOTO 15770
15540         IF I=K THEN 15600
15550         IF ABS(A(I+1,I))>=ABS(A(I+2,I)) THEN 15600
15560         IF ABS(A(I,I))>=ABS(A(I+2,I)) THEN 15700
15570         L=I+2
15580         Iwork(I)=2
15590         GOTO 15630
15600         IF ABS(A(I,I))>=ABS(A(I+1,I)) THEN 15680
15610         L=I+1
15620         Iwork(I)=1
15630         FOR J=I TO M
15640             R=A(I,J)
15650             A(I,J)=A(L,J)
15660             A(L,J)=R
15670         NEXT J
15680         IF I<>K THEN 15700
15690         I2=I1
15700         FOR L=I1 TO I2
15710             R=-A(L,I)/A(I,I)
15720             A(L,I)=R
15730             FOR J=I1 TO M
15740                 A(L,J)=A(L,J)+R*A(I,J)
15750             NEXT J
15760         NEXT L
15770     NEXT I
15780     IF A(M,M)=0 THEN 15800
15790     A(M,M)=Eps

```

```

15800 FOR I=1 TO N
15810   IF I>M THEN 15850
15820   Vecr(I,Ivec)=1
15830   Vecr(I,Ivec-1)=1
15840   GOTO 15870
15850   Vecr(I,Ivec)=0
15860   Vecr(I,Ivec-1)=0
15870 NEXT I
15880 Bound=.01/(E.*N)
15890 Ns=0
15900 Iter=1
15910 FOR I=1 TO M
15920   Work(I)=H(I,I)-Fks1
15930 NEXT I
15940 FOR I=1 TO M
15950   D=Work(I)*Vecr(I,Ivec)
15960   IF I=1 THEN 15980
15970   D=D+Subdia(I-1)*Vecr(I-1,Ivec)
15980   L=I+1
15990   IF L>M THEN 16030
16000   FOR K=L TO M
16010     D=D+H(I,K)*Vecr(K,Ivec)
16020   NEXT K
16030   Vecr(I,Ivec-1)=D-Eta*Vecr(I,Ivec-1)
16040 NEXT I
16050 K=M-1
16060 FOR I=1 TO K
16070   L=I+Iwork(I)
16080   R=Vecr(L,Ivec-1)
16090   Vecr(L,Ivec-1)=Vecr(I,Ivec-1)
16100   Vecr(I,Ivec-1)=R
16110   Vecr(I+1,Ivec-1)=Vecr(I+1,Ivec-1)+A(I+1,I)*R
16120   IF I=K THEN 16140
16130   Vecr(I+2,Ivec-1)=Vecr(I+2,Ivec-1)+A(I+2,I)*R
16140 NEXT I
16150 FOR I=1 TO M
16160   J=M-I+1
16170   D=Vecr(J,Ivec-1)
16180   IF J=M THEN 16240
16190   L=J+1
16200   FOR K=L TO M
16210     D1=A(J,K)
16220     D=D-D1*Vecr(K,Ivec-1)
16230   NEXT K
16240   Vecr(J,Ivec-1)=D/A(J,J)
16250 NEXT I
16260 FOR I=1 TO M
16270   D=Work(I)*Vecr(I,Ivec-1)
16280   IF I=1 THEN 16300
16290   D=D+Subdia(I-1)*Vecr(I-1,Ivec-1)
16300   L=I+1
16310   IF L>M THEN 16350
16320   FOR K=L TO M
16330     D=D+H(I,K)*Vecr(K,Ivec-1)
16340   NEXT K
16350   Vecr(I,Ivec)=Vecr(I,Ivec-1)+D/Eta
16360 NEXT I

```

```

16370 L=1
16380 S=0
16390 FOR I=1 TO M
16400   R=Vecr(I,Ivec)^2+Vecr(I,Ivec-1)^2
16410   IF R=S THEN 16440
16420   S=R
16430   L=I
16440 NEXT I
16450 U=Vecr(L,Ivec-1)
16460 V=Vecr(L,Ivec)
16470 FOR I=1 TO M
16480   B=Vecr(I,Ivec)
16490   R=Vecr(I,Ivec-1)
16500   Vecr(I,Ivec)=(R*U+B*V)/S
16510   Vecr(I,Ivec-1)=(B*U-R*V)/S
16520 NEXT I
16530 B=0
16540 FOR I=1 TO M
16550   R=Work(I)*Vecr(I,Ivec-1)-Eta*Vecr(I,Ivec)
16560   U=Work(I)*Vecr(I,Ivec)+Eta*Vecr(I,Ivec-1)
16570   IF I=1 THEN 16600
16580   R=R+Subdia(I-1)*Vecr(I-1,Ivec-1)
16590   U=U+Subdia(I-1)*Vecr(I-1,Ivec)
16600   L=I+1
16610   IF L>M THEN 16660
16620   FOR J=L TO M
16630     R=R+H(I,J)*Vecr(J,Ivec-1)
16640     U=U+H(I,J)*Vecr(J,Ivec)
16650   NEXT J
16660   U=R*R+U*U
16670   IF B>=U THEN 16690
16680   B=U
16690 NEXT I
16700 IF Iter=1 THEN 16720
16710 IF Previs<=B THEN 16830
16720 FOR I=1 TO N
16730   Work1(I)=Vecr(I,Ivec)
16740   Work2(I)=Vecr(I,Ivec-1)
16750 NEXT I
16760 Previs=B
16770 IF Ns=1 THEN 16870
16780 IF Iter>6 THEN 16890
16790 Iter=Iter+1
16800 IF Bound>SQR(S) THEN 15940
16810 Ns=1
16820 GOTO 15940
16830 FOR I=1 TO N
16840   Vecr(I,Ivec)=Work1(I)
16850   Vecr(I,Ivec-1)=Work2(I)
16860 NEXT I
16870 Indic(Ivec-1)=2
16880 Indic(Ivec)=2
16890 SUBEND

16900 DEF FNIns(X1)
16910 X=INT(X1+.5)
16920 IF X=0 THEN RETURN CHR$(13)

```

```
16930 Eol$=CHR$(13)&CHR$(10)
16940 IF X=0 THEN Eol$=CHR$(10)
16950 ALLOCATE RS(X*LEN(Eol$))
16960 RS=""
16970 FOR I=1 TO X
16980   RS=RS&Eol$
16990 NEXT I
17000 RETURN RS
17010 FNEND'
```

APPENDIX FIVE

"H₂PCNCA"


```

520 Y9=0
530 Y10=0
540 |
550 | .....
560 | Reads in force field into F matrix from data statements.
570 |
580 | R=Row.
590 | C=Column.
600 | Sd=Flag - 0 to add, 1 to subtract.
610 | Fel1=Force constant 1.
620 | Fel2=Force constant 2.
630 | .....
640 |
650 READ R
660 IF R=9999 THEN 870
670 READ C,Sd,Fel1,Fel2
680 IF Sd=0 THEN Fel=Fel1+Fel2
690 IF Sd=1 THEN Fel=Fel1-Fel2
700 |
710 | .....
720 | Deletes rows and columns in F matrix which are not needed.
730 | .....
740 |
750 IF Y1=R OR Y1=C THEN Fel=0
760 IF Y2=R OR Y2=C THEN Fel=0
770 IF Y3=R OR Y3=C THEN Fel=0
780 IF Y4=R OR Y4=C THEN Fel=0
790 IF Y5=R OR Y5=C THEN Fel=0
800 IF Y6=R OR Y6=C THEN Fel=0
810 IF Y7=R OR Y7=C THEN Fel=0
820 IF Y8=R OR Y8=C THEN Fel=0
830 IF Y9=R OR Y9=C THEN Fel=0
840 IF Y10=R OR Y10=C THEN Fel=0
850 F(R,C)=Fel
860 GOTO 650
870 READ Fin6
880 PRINT Fin6
890 PRINT
900 |
910 | .....
920 | Reads in G matrix elements from data statements.
930 |
940 | R=Row.
950 | C=Column.
960 | Sd=Flag - 0 to add, 1 to subtract.
970 | Gel1=G matrix element 1.
980 | Gel2=G matrix element 2.
990 | .....
1000|
1010 READ R
1020 IF R=9999 THEN 1030
1030 READ C,Sd,Gel1,Gel2
1040 IF Sd=0 THEN Gel=Gel1+Gel2
1050 IF Sd=1 THEN Gel=Gel1-Gel2
1060 |
1070 | .....
1080 | Deletes row and columns in G matrix which are not needed.

```



```

1660 NEXT Z
1670 N=N-1
1680 GOTO 1430
1690 NEXT C
1700 |
1710 | .....
1720 | Multiplies the F and G matrices to yield the FG matrix for
1730 | diagonalization.
1740 | .....
1750 |
1760 FOR R=1 TO N
1770 FOR C=1 TO N
1780 Sum=0
1790 FOR E1=1 TO N
1800 Sum=G(R,E1)*F(E1,C)+Sum
1810 NEXT E1
1820 A(R,C)=Sum
1830 NEXT C
1840 NEXT R
1850 |
1860 | .....
1870 | Call subprogram Eigen to diagonalize the FG matrix.
1880 | .....
1890 |
1900 CALL Eigen(N,A(*),Evr(*),Evl(*),Vecr(*),Veci(*),Indic(*))
1910 BEEP
1920 |
1930 | .....
1940 | Shell sorts the eigenvalues and eigenvectors.
1950 | Sorted in increasing order with respect to eigenvalue.
1960 | .....
1970 |
1980 Pass=N
1990 Pass=INT(Pass/2)
2000 IF Pass=0 THEN 2220
2010 FOR St=1 TO Pass
2020 I1=St
2030 Jj=St+Pass
2040 Sw=0
2050 IF Evr(I1)<=Evr(Jj) THEN 2150
2060 Sw=1
2070 Avr=Evr(I1)
2080 Evr(I1)=Evr(Jj)
2090 Evr(Jj)=Avr
2100 FOR R=1 TO N
2110 Avc=Vecr(R,I1)
2120 Vecr(R,I1)=Vecr(R,Jj)
2130 Vecr(R,Jj)=Avc
2140 NEXT R
2150 I1=Jj
2160 Jj=Jj+Pass
2170 IF Jj>N+1 THEN 2050
2180 IF Sw=0 THEN 2200
2190 GOTO 2020
2200 NEXT St
2210 GOTO 1990
2220 IF Pertflg=1 THEN 4490

```

```

2230 |
2240 | .....
2250 | Prints the NCA results on the screen or on a paper printer.
2260 | .....
2270 |
2280 PRINTER IS Dev
2290 PRINT
2300 PRINT
2310 PRINT "Au Vibrational Modes for Free Base Phthalocyanine"
2320 PRINT
2330 PRINT
2340 |
2350 | .....
2360 | Prints the F matrix.
2370 | .....
2380 |
2390 PRINT "----- F Matrix -----"
2400 PRINT
2410 PRINT
2420 L=INT(N/8)+1
2430 E=8
2440 Z=1
2450 FOR B=1 TO L
2460 IF B=L THEN E=N
2470 FOR C=Z TO E
2480 PRINT USING 2490;C
2490 IMAGE XX,DDD,XXXXX,*
2500 NEXT C
2510 PRINT
2520 FOR R=1 TO N
2530 J=Z
2540 FOR C=Z TO E
2550 IF J>=E THEN PRINT USING 2560;F(R,C)
2560 IMAGE DD.DDDDD
2570 IF J>=E THEN 2600
2580 PRINT USING 2590;F(R,C)
2590 IMAGE DD.DDDDD,XX,*
2600 J=J+1
2610 IF J>E THEN J=Z
2620 NEXT C
2630 NEXT R
2640 PRINT
2650 PRINT
2660 Z=Z+8
2670 E=E+8
2680 NEXT B
2690 PRINT
2700 PRINT
2710 |
2720 | .....
2730 | Prints the G matrix.
2740 | .....
2750 |
2760 PRINT "----- G Matrix -----"
2770 PRINT

```



```

3900 ! a eigenvalue fit is obtained.
3910 ! .....
3920 !
3930 ! .....
3940 ! Prints the eigenvalues to be selected in the fitting routine.
3950 ! .....
3960 !
3970 PRINT "Vibrational Eigenvalues: Numbers 1 to";N;"in cm-1"
3980 PRINT
3990 FOR R=1 TO N
4000 PRINT USING 4010;R,Vib(R)
4010 IMAGE ODDD,".",1X,ODDDD.ODD
4020 NEXT R
4030 PRINT
4040 R=0
4050 !
4060 ! .....
4070 ! Selects the eigenvalues to be used in fit and inputs the values which
4080 ! are to be fit to.
4090 ! .....
4100 !
4110 INPUT "Eigenvalue Number(s) to be Fit: [CONT] to End",R
4120 IF R=0 THEN 4210
4130 IF R>N THEN 4040
4140 Fpert(R,2)=1
4150 PRINT "Eigenvalue";R;" is to be fit"
4160 INPUT "Enter the NEW Eigenvalue",Fpert(R,1)
4170 PRINT "New:";Fpert(R,1);" Old:";Vib(R)
4180 IF Fpert(R,1)>=0 THEN Fpert(R,1)=(Fpert(R,1)*2*PI*3.E+10)^2/6.02E+23/1.E+8*
1000
4190 IF Fpert(R,1)<0 THEN Fpert(R,1)=-((ABS(Fpert(R,1))*2*PI*3.E+10)^2/6.02E+23/1
.E+8*1000
4200 GOTO 4040
4210 PRINT
4220 FOR P=1 TO N
4230 IF Fpert(P,2)=0 THEN 4350
4240 !
4250 ! .....
4260 ! Refines force constants using eigenvectors.
4270 ! .....
4280 !
4290 FOR R=1 TO N
4300 FOR C=1 TO N
4310 IF R<>C THEN 4330
4320 F(R,C)=F(R,C)+(Fpert(P,1)-Evr(P))*Vecr(R,P)*Vecr(C,P)*Amp
4330 NEXT C
4340 NEXT R
4350 NEXT P
4360 Pertflg=1
4370 !
4380 ! .....
4390 ! Returns execution to part of program where F and G matrices are
4400 ! multiplied and the FG matrix is diagonalized.
4410 ! .....
4420 !
4430 GOTO 1760
4440 !

```



```

5000 1 6 matrix elements.
5010 .....
5200 .....
5230 ..... Row/Column A .....
5240 DATA 1,1,0,.566893424036,0
5250 DATA 1,2,0,-.320683347477,-.320683347477
5260 DATA 1,3,0,.160341673739,.160341673739
5270 DATA 1,4,0,-.113378684807,0
5280 DATA 1,15,1,.333006762504,-.333006762504
5290 DATA 1,16,1,-.183860876595,.183860876595
5100 DATA 1,20,1,.0347149906857,-.0347149906857
5110 ..... Row/Column B .....
5120 DATA 2,2,0,.566893424036,.226757369615
5130 DATA 2,3,0,-.453514739229,-.113378684807
5140 DATA 2,4,0,.320683347478,0
5150 DATA 2,5,0,.0805797038531,.0510728876983
5160 DATA 2,6,0,-.0494507276469,0
5170 DATA 2,15,1,-.470942679895,.26001854527
5180 DATA 2,16,1,.470942679895,-.0490944106454
5190 DATA 2,20,1,-.226146200577,.0367387608396
5200 DATA 2,21,1,.0389677051594,0
5210 ..... Row/Column C .....
5220 DATA 3,3,0,.566893424036,.226757369615
5230 DATA 3,4,0,-.641366694954,0
5240 DATA 3,5,0,-.212232295405,-.18272547925
5250 DATA 3,6,0,.0989014552938,.0494507276469
5260 DATA 3,15,1,.26001854527,-.0490944106454
5270 DATA 3,16,1,-.470942679895,.0490944106454
5280 DATA 3,20,1,.390842340703,-.201434900966
5290 DATA 3,21,1,-.0779354103188,.0389677051594
5300 ..... Row/Column D .....
5310 DATA 4,4,0,.566893424036,0
5320 DATA 4,5,0,.186184880494,.186184880494
5330 DATA 4,6,0,-.0699338897075,-.0699338897075
5340 DATA 4,15,1,-.0347149906857,.0347149906857
5350 DATA 4,16,1,.183860876595,-.183860876595
5360 DATA 4,20,1,-.267630505722,.267630505722
5370 DATA 4,21,1,.055108657131,-.055108657131
5380 ..... Row/Column E .....
5390 DATA 5,5,0,.32337728364,.10262392793
5400 DATA 5,6,0,-.262922216048,.103016745283
5410 DATA 5,7,0,-.254211554548,.0510773809802
5420 DATA 5,8,0,.0914781725126,0
5430 DATA 5,16,1,.0697840705662,-.0442304181914
5440 DATA 5,20,1,-.276334047244,.167501525476
5450 DATA 5,21,1,.28849914471,.000594132862558
5460 ..... Row/Column F .....
5470 DATA 6,6,0,.33321393988,-.273298586424
5480 DATA 6,7,0,.290995674509,-.214876283361
5490 DATA 6,8,0,-.093065914028,.0587868211474
5500 DATA 6,16,1,-.0428255863778,0
5510 DATA 6,20,1,.174036720164,.00737992993753
5520 DATA 6,21,1,-.29377409633,-.185808381849
5530 ..... Row/Column G .....
5540 DATA 7,7,0,.754497398141,-.0612867429647
5550 DATA 7,8,0,-.539541002456,0
5560 DATA 7,13,0,0,.0914781725126 ..... 1 AND 4

```



```

10  !!!!!!!!!!!!!!!!!!!!!!!!!!!!!!!!!!!!!!!!!!!!!!!!!!!!!!!!!!!!!!!!!!!!!!!!!!!!!!!
20  ! F and G matrix elements for free base phthalocyanine used to
30  ! calculate Blu vibrations in program H2PCNCA.
40  !!!!!!!!!!!!!!!!!!!!!!!!!!!!!!!!!!!!!!!!!!!!!!!!!!!!!!!!!!!!!!!!!!!!!!!!!!!!!!!
50  !
60  !!!!!!!!!!!!!!!!!!!!!!!!!!!!!!!!!!!!!!!!!!!!!!!!!!!!!!!!!!!!!!!!!!!!!!!!!!!!!!!
70  ! F matrix elements.
80  !!!!!!!!!!!!!!!!!!!!!!!!!!!!!!!!!!!!!!!!!!!!!!!!!!!!!!!!!!!!!!!!!!!!!!!!!!!!!!!
90  !
100 DATA 1,1,0,.119,0 ! Row/Column A.
110 DATA 2,2,0,.119,0 ! Row/Column B.
120 DATA 3,3,0,.119,0 ! Row/Column C.
130 DATA 4,4,0,.119,0 ! Row/Column D.
140 DATA 5,5,0,.119,0 ! Row/Column E.
150 DATA 6,6,0,.119,0 ! Row/Column F.
160 DATA 7,7,0,.119,0 ! Row/Column G.
170 DATA 8,8,0,.119,0 ! Row/Column H.
180 DATA 9,9,0,.119,0 ! Row/Column I.
190 DATA 10,10,0,.119,0 ! Row/Column J.
200 DATA 11,11,0,.119,0 ! Row/Column K.
210 DATA 12,12,0,.119,0 ! Row/Column L.
220 DATA 13,13,0,.119,0 ! Row/Column M.
230 DATA 14,14,0,.119,0 ! Row/Column N.
240 DATA 15,15,0,.3237,0 ! Row/Column P.
250 DATA 16,16,0,.3237,0 ! Row/Column Q.
260 DATA 17,17,0,.3237,0 ! Row/Column R.
270 DATA 18,18,0,.3237,0 ! Row/Column S.
280 DATA 19,19,0,.3237,0 ! Row/Column T.
290 DATA 20,20,0,.3237,0 ! Row/Column U.
300 DATA 21,21,0,.3237,0 ! Row/Column V.
310 DATA 22,22,0,.3237,0 ! Row/Column W.
320 DATA 23,23,0,.3237,0 !
330 DATA 9999
340 DATA F Matrix Loaded
350 !
360 !!!!!!!!!!!!!!!!!!!!!!!!!!!!!!!!!!!!!!!!!!!!!!!!!!!!!!!!!!!!!!!!!!!!!!!!!!!!!!!
370 ! G matrix elements.
380 !!!!!!!!!!!!!!!!!!!!!!!!!!!!!!!!!!!!!!!!!!!!!!!!!!!!!!!!!!!!!!!!!!!!!!!!!!!!!!!
390 !
400 !!!!!!!!!!!!!!! Row/Column A !!!!!!!!!!!!!!!!!!!!!!!!!!!!!!!!!!!!!!!!!!!!!!!
410 DATA 1,1,0,.566893424036,0
420 DATA 1,2,0,-.320683347477,-.320683347477
430 DATA 1,3,0,.160341673739,.160341673739
440 DATA 1,4,0,-.113378684807,0
450 DATA 1,15,1,.333006762504,-.333006762504
460 DATA 1,16,1,-.183860876595,.183860876595
470 DATA 1,20,1,.0347149906857,-.0347149906857
480 !!!!!!!!!!!!!!! Row/Column B !!!!!!!!!!!!!!!!!!!!!!!!!!!!!!!!!!!!!!!!!!!!!!!
490 DATA 2,2,1,.566893424036,.226757369615
500 DATA 2,3,1,-.453514739229,-.113378684807
510 DATA 2,4,1,.320683347478,0
520 DATA 2,5,1,.0805797038531,.0510728676963

```



```

1100 DATA 9,9,1,.566893424036,0
1110 DATA 9,10,1,-.320683347477,-.320683347477
1120 DATA 9,11,1,.160341673739,.160341673739
1130 DATA 9,12,1,-.113378684807,0
1140 DATA 9,17,0,.333006762504,-.333006762504
1150 DATA 9,18,0,-.183860876595,.183860876595
1160 DATA 9,22,0,.0347149906857,-.0347149906857
1170 !!!!!!!!!!!!! Row/Column J !!!!!!!!!!!!!!!!!!!!!!!!!!!!!!!!!!!!!!!!!!!!!
1180 DATA 10,10,1,.566893424036,.226757369615
1190 DATA 10,11,1,-.453514739229,-.113378684807
1200 DATA 10,12,1,.320683347478,0
1210 DATA 10,13,1,.0805797038531,.0510728876983
1220 DATA 10,14,1,-.0494507276469,0
1230 DATA 10,17,0,-.470942679895,-.26001854527
1240 DATA 10,18,0,.470942679895,-.0490944106454
1250 DATA 10,22,0,-.226146200577,.0367387608396
1260 DATA 10,23,0,.0389677051594,0
1270 !!!!!!!!!!!!! Row/Column K !!!!!!!!!!!!!!!!!!!!!!!!!!!!!!!!!!!!!!!!!!!!!
1280 DATA 11,11,1,.566893424036,.226757369615
1290 DATA 11,12,1,-.641366694954,0
1300 DATA 11,13,1,-.212232295405,-.18272547925
1310 DATA 11,14,1,.0989014552938,.0494507276469
1320 DATA 11,17,0,.26001854527,-.0490944106454
1330 DATA 11,18,0,-.470942679895,.0490944106454
1340 DATA 11,22,0,.390842340703,-.201434900966
1350 DATA 11,23,0,-.0779354103188,.0389677051594
1360 !!!!!!!!!!!!! Row/Column L !!!!!!!!!!!!!!!!!!!!!!!!!!!!!!!!!!!!!!!!!!!!!
1370 DATA 12,12,1,.566893424036,0
1380 DATA 12,13,1,.186184880494,.186184880494
1390 DATA 12,14,1,-.0699338897075,-.0699338897075
1400 DATA 12,17,0,-.0347149906857,.0347149906857
1410 DATA 12,18,0,.183860876595,-.183860876595
1420 DATA 12,22,0,-.267630505722,.267630505722
1430 DATA 12,23,0,.055108657131,-.0551086571318
1440 !!!!!!!!!!!!! Row/Column M !!!!!!!!!!!!!!!!!!!!!!!!!!!!!!!!!!!!!!!!!!!!!
1450 DATA 13,13,1,.32337728364,.10262392793
1460 DATA 13,14,1,-.262922216048,.103016745283
1470 DATA 13,18,0,.0697840705662,-.0442304181914
1480 DATA 13,19,0,-.269084916899,0
1490 DATA 13,22,0,-.276334047244,.167501525476
1500 DATA 13,23,0,.28849914471,.000594132862558
1510 !!!!!!!!!!!!! Row/Column N !!!!!!!!!!!!!!!!!!!!!!!!!!!!!!!!!!!!!!!!!!!!!
1520 DATA 14,14,1,.333321393988,-.273298586424
1530 DATA 14,18,0,-.0428255863778,0
1540 DATA 14,19,0,.445083571317,0
1550 DATA 14,22,0,.174036720164,.00737992993753
1560 DATA 14,23,0,-.29377409633,-.185808381849
1570 !!!!!!!!!!!!! Row/Column O !!!!!!!!!!!!!!!!!!!!!!!!!!!!!!!!!!!!!!!!!!!!!
1580 DATA 15,15,0,1.4043443166,-.280297304107
1590 DATA 15,16,0,-.280297304107,.0425170068027
1600 DATA 15,20,0,.0425170068027,0
1610 !!!!!!!!!!!!! Row/Column P !!!!!!!!!!!!!!!!!!!!!!!!!!!!!!!!!!!!!!!!!!!!!
1620 DATA 16,16,0,1.4043443166,0
1630 DATA 16,20,0,-.250962993117,.0318167001907
1640 DATA 16,21,0,.0337470225952,0
1650 !!!!!!!!!!!!! Row/Column Q !!!!!!!!!!!!!!!!!!!!!!!!!!!!!!!!!!!!!!!!!!!!!
1660 DATA 17,17,0,1.4043443166,-.280297304107

```



```

10      | F and G matrix elements for free base phthalocyanine used to calculate
20      | 83g vibrations in program H2PCNCA.
30      |
40      |
50      |
60      |
70      | F matrix elements.
80      |
90      |
100     DATA 1,1,0,.119,0 | Row/Column A.
110     DATA 2,2,0,.119,0 | Row/Column B.
120     DATA 3,3,0,.119,0 | Row/Column C.
130     DATA 4,4,0,.119,0 | Row/Column D.
140     DATA 5,5,0,.119,0 | Row/Column E.
150     DATA 6,6,0,.119,0 | Row/Column F.
160     DATA 7,7,0,.119,0 | Row/Column G.
170     DATA 8,8,0,.119,0 | Row/Column H.
180     DATA 9,9,0,.119,0 | Row/Column I.
190     DATA 10,10,0,.119,0 | Row/Column J.
200     DATA 11,11,0,.119,0 | Row/Column K.
210     DATA 12,12,0,.119,0 | Row/Column L.
220     DATA 13,13,0,.119,0 | Row/Column M.
230     DATA 14,14,0,.119,0 | Row/Column N.
240     DATA 15,15,0,.3237,0 | Row/Column O.
250     DATA 16,16,0,.3237,0 | Row/Column P.
260     DATA 17,17,0,.3237,0 | Row/Column Q.
270     DATA 18,18,0,.3237,0 | Row/Column R.
280     DATA 19,19,0,.3237,0 | Row/Column S.
290     DATA 20,20,0,.3237,0 | Row/Column T.
300     DATA 21,21,0,.3237,0 | Row/Column U.
310     DATA 22,22,0,.3237,0 | Row/Column V.
320     DATA 23,23,0,.3237,0 | Row/Column W.
330     DATA 9999
340     DATA F Matrix Loaded
350     |
360     |
370     | G matrix elements.
380     |
390     |
400     |!!!!!! Row/Column A !!!!!!!
410     DATA 1,1,1,.566893424036,0
420     DATA 1,2,0,-.320683347477,-.320683347477
430     DATA 1,3,0,.160341673739,.160341673739
440     DATA 1,4,1,-.113378684807,0
450     DATA 1,15,1,.333006762504,-.333006762504
460     DATA 1,16,1,-.183860876595,.183860876595
470     DATA 1,20,1,.0347149906857,-.0347149906857
480     |!!!!!! Row/Column B !!!!!!!
490     DATA 2,2,0,.566893424036,.226757369615
500     DATA 2,3,0,-.453514739229,-.113378684807
510     DATA 2,4,1,.320683347478,0
520     DATA 2,5,0,.0805797038531,.0510728876983

```

530 DATA 2,6,0,-.0494507276469,0
540 DATA 2,15,1,-.470942679895,.26001854527
550 DATA 2,16,1,-.470942679895,-.0490944106454
560 DATA 2,20,1,-.226146200577,.0367387608236
570 DATA 2,21,1,.0389677051594,0
580 Row/Column C
590 DATA 3,3,0,.566893424036,.226757369615
600 DATA 3,4,1,-.641366694954,0
610 DATA 3,5,0,-.212232295405,-.18272547925
620 DATA 3,6,0,.0989014552938,.0494507276469
630 DATA 3,15,1,.26001854527,-.0490944106454
640 DATA 3,16,1,-.470942679895,.0490944106454
650 DATA 3,20,1,.390842340703,-.201434900966
660 DATA 3,21,1,-.0779354103188,.0389677051594
670 Row/Column D
680 DATA 4,4,1,.566893424036,0
690 DATA 4,5,0,.186184880494,.186184880494
700 DATA 4,6,0,-.0699338897075,-.0699338897075
710 DATA 4,15,1,-.0347149906857,.0347149906857
720 DATA 4,16,1,.183860876595,-.183860876595
730 DATA 4,20,1,-.267630505722,.267630505722
740 DATA 4,21,1,.055108657131,-.055108657131
750 Row/Column E
760 DATA 5,5,0,.32337728364,.10262392793
770 DATA 5,6,0,-.262922216048,.103016745283
780 DATA 5,7,0,-.254211554548,.0510773809802
790 DATA 5,8,0,.0914781725126,0
800 DATA 5,15,1,.0697840705662,-.0442304181914
810 DATA 5,20,1,-.276334047244,.167501525476
820 DATA 5,21,1,.28849914471,.000594132862558
830 Row/Column F
840 DATA 6,6,0,.333321393988,-.273298586424
850 DATA 6,7,0,.290995674509,-.214876283361
860 DATA 6,8,0,-.093065914028,.0587868211474
870 DATA 6,16,1,-.0428255863778,0
880 DATA 6,20,1,.174036720164,.00737992993753
890 DATA 6,21,1,-.29377409633,-.185808381849
900 Row/Column G
910 DATA 7,7,0,.764497398141,-.0612867429647
920 DATA 7,8,0,-.599541002456,0
930 DATA 7,13,0,0,.0914781725126 1 AND 4
940 DATA 7,14,0,-.0587868211474,-.0930659514028 3 AND 4
950 DATA 7,19,1,0,.0676832193445
960 DATA 7,20,1,.103635317135,0
970 DATA 7,21,1,-.485418546828,-.0428370961158
980 DATA 7,22,1,0,.0466704801694 1 AND 4
990 DATA 7,23,1,0,-.259293054322 1 AND 4
1000 Row/Column H
1010 DATA 8,8,1,.764497398141,-.0612867429647 1 AND 4
1020 DATA 8,13,0,-.0510773809802,-.254211554548 3 AND 4
1030 DATA 8,14,0,.214876283361,.290995674509 3 AND 4
1040 DATA 8,19,1,0,-.366404054596
1050 DATA 8,20,1,-.0466704801694,0
1060 DATA 8,21,1,-.259293054322,0
1070 DATA 8,22,1,0,-.103635317135 1 AND 4
1080 DATA 8,23,1,-.0428370961158,.485418546828 3 AND 4
1090 Row/Column I

```

1100 DATA 9,9,0,.566893424036,0
1110 DATA 9,10,0,-.3206933247477,-.3206833247477
1120 DATA 9,11,0,.160341673739,.160341673739
1130 DATA 9,12,0,-.113378684807,0
1140 DATA 9,17,1,.333006762504,-.333006762504
1150 DATA 9,18,1,-.183860876595,.183860876595
1160 DATA 9,22,1,.0347149906857,-.0347149906857
1170 Row/Column J
1180 DATA 10,10,1,.566893424036,.226757369615
1190 DATA 10,11,1,-.453514739229,-.113378684807
1200 DATA 10,13,1,.0805797038531,.0510728876983
1210 DATA 10,14,1,-.0494507276469,0
1220 DATA 10,17,0,-.470942679895,.26001854527
1230 DATA 10,18,0,.470942679895,-.0490944106454
1240 DATA 10,22,0,-.226146200577,.0367387608396
1250 DATA 10,23,0,.0389677051594,0
1260 Row/Column K
1270 DATA 11,11,1,.566893424036,.226757369615
1280 DATA 11,13,1,-.212232295405,-.18272547925
1290 DATA 11,14,1,.0989014552938,.0494507276469
1300 DATA 11,17,0,.26001854527,-.0490944106454
1310 DATA 11,18,0,-.470942679895,.0490944106454
1320 DATA 11,22,0,.390842340703,-.201434900966
1330 DATA 11,23,0,-.0779354103188,.0389677051594
1340 Row/Column L
1350 DATA 12,12,0,.566893426036,0
1360 DATA 12,13,0,.186184880494,.186184880494
1370 DATA 12,14,0,-.0699338897075,-.0699338897075
1380 DATA 12,17,1,-.0347149906857,.0347149906857
1390 DATA 12,18,1,.183860876595,-.183860876595
1400 DATA 12,22,1,-.267630505722,.267630505722
1410 DATA 12,23,1,.055108657131,-.055108657131
1420 Row/Column M
1430 DATA 13,13,1,.32337728364,.10262392793
1440 DATA 13,14,1,-.262922216048,.103016745283
1450 DATA 13,18,0,.0697840705662,-.0442304181914
1460 DATA 13,19,1,-.269084916899,0
1470 DATA 13,22,0,-.276334047244,.167501525476
1480 DATA 13,23,0,.28849914471,.000594132862558
1490 Row/Column N
1500 DATA 14,14,1,.333321393988,-.273298586424
1510 DATA 14,18,0,-.0428255863778,0
1520 DATA 14,19,1,.445083571317,0
1530 DATA 14,22,0,.174036720164,.00737992993753
1540 DATA 14,23,0,-.29377409633,-.185808381849
1550 Row/Column O
1560 DATA 15,15,1,1.4043443166,-.280297304107
1570 DATA 15,16,1,-.280297304107,.0425170068027
1580 DATA 15,20,1,.0425170068027,0
1590 Row/Column P
1600 DATA 16,16,1,1.4043443166,0
1610 DATA 16,20,1,-.250962993117,.0318167001907
1620 DATA 16,21,1,.0337470225952,0
1630 Row/Column Q
1640 DATA 17,17,0,1.4043443166,-.280297304107
1650 DATA 17,18,0,-.280297304107,.0425170068027
1660 DATA 17,22,0,.0425170068027,0

```



```

1670  Row/Column R
1680  DATA 18,19,0,1.4043443166,0
1690  DATA 18,20,0,-.250962993117,.0318167001907
1700  DATA 18,23,0,.0337470225952,0
1710  Row/Column S
1720  DATA 19,19,1,1.55488461455,0
1730  DATA 19,22,0,.022697123287,.022697123287
1740  DATA 19,23,0,-.148555354853,-.148555354853
1750  Row/Column T
1760  DATA 20,20,1,.386448961524,-.16585112319
1770  DATA 20,21,1,-.188670742999,.0252538685337
1780  Row/Column U
1790  DATA 21,21,1,.421776560109,.0299414965597
1800  DATA 21,23,1,0,.0409943591762 1 AND 4
1810  Row/Column V
1820  DATA 22,22,0,.386448961524,-.16585112319
1830  DATA 22,23,0,-.188670742999,.0252538685337
1840  Row/Column W
1850  DATA 23,23,0,.421776560109,.0299414965597
1860  DATA 9999
1870  DATA 6 Matrix Loaded
1880  END

```



```

1100 DATA 9,9,1,.566893424036,0
1110 DATA 9,10,0,-.320683347477,-.320683347477
1120 DATA 9,11,0,.150341673739,.150341673739
1130 DATA 9,12,1,-.113378694807,0
1140 DATA 9,17,1,.333006762504,-.333006762504
1150 DATA 9,18,1,-.183860876595,.183860876595
1160 DATA 9,22,1,.0347149906857,-.0347149906857
1170 !!!!!!!!!!!!! Row/Column J !!!!!!!!!!!!!!!!!!!!!!!!!!!!!!!!!!!!!!!!!!!!!
1180 DATA 10,10,0,.566893424036,.226757369615
1190 DATA 10,11,0,-.453514739229,-.113378684807
1200 DATA 10,12,1,.320683347478,0
1210 DATA 10,13,0,.0805797038531,.0510729876983
1220 DATA 10,14,0,-.0494507276469,0
1230 DATA 10,17,1,-.470942679895,.26001854527
1240 DATA 10,18,1,.470942679895,-.0490944106454
1250 DATA 10,22,1,-.226146200577,.0367387608396
1260 DATA 10,23,1,.0389677051594,0
1270 !!!!!!!!!!!!! Row/Column K !!!!!!!!!!!!!!!!!!!!!!!!!!!!!!!!!!!!!!!!!!!!!
1280 DATA 11,11,0,.566893424036,.226757369615
1290 DATA 11,12,1,-.641366694954,0
1300 DATA 11,13,0,-.212232295405,-.18272547925
1310 DATA 11,14,0,.0989014552938,.0494507276469
1320 DATA 11,17,1,.26001854527,-.0490944106454
1330 DATA 11,18,1,-.470942679895,-.0490944106454
1340 DATA 11,22,1,.390842340703,-.201434900966
1350 DATA 11,23,1,-.0779354103188,.0389677051594
1360 !!!!!!!!!!!!! Row/Column L !!!!!!!!!!!!!!!!!!!!!!!!!!!!!!!!!!!!!!!!!!!!!
1370 DATA 12,12,1,.566833426036,0
1380 DATA 12,13,0,.186184880494,.186184880494
1390 DATA 12,14,0,-.0699338897075,-.0699338897075
1400 DATA 12,17,1,-.0347149906857,.0347149906857
1410 DATA 12,18,1,.183860876595,-.183860876595
1420 DATA 12,22,1,-.267630505722,.267630505722
1430 DATA 12,23,1,.055108657131,-.055108657131
1440 !!!!!!!!!!!!! Row/Column M !!!!!!!!!!!!!!!!!!!!!!!!!!!!!!!!!!!!!!!!!!!!!
1450 DATA 13,13,0,.32337728364,.10262392793
1460 DATA 13,14,0,-.262922216048,.103016745283
1470 DATA 13,18,1,.0697840705662,-.0442304181914
1480 DATA 13,19,1,-.269084916899,0
1490 DATA 13,22,1,-.276334047244,.167501525476
1500 DATA 13,23,1,.28849914471,.000594132862558
1510 !!!!!!!!!!!!! Row/Column N !!!!!!!!!!!!!!!!!!!!!!!!!!!!!!!!!!!!!!!!!!!!!
1520 DATA 14,14,0,.333321393988,-.273298586424
1530 DATA 14,18,1,-.0428255863778,0
1540 DATA 14,19,1,.445083571317,0
1550 DATA 14,22,1,.174036720164,.00737992993753
1560 DATA 14,23,1,-.29377409533,-.185808381849
1570 !!!!!!!!!!!!! Row/Column O !!!!!!!!!!!!!!!!!!!!!!!!!!!!!!!!!!!!!!!!!!!!!
1580 DATA 15,15,0,1.4043443166,-.280297304107
1590 DATA 15,16,0,-.280297304107,.0425170068027
1600 DATA 15,20,0,.0425170068027,0
1610 !!!!!!!!!!!!! Row/Column P !!!!!!!!!!!!!!!!!!!!!!!!!!!!!!!!!!!!!!!!!!!!!
1620 DATA 16,16,0,1.4043443166,0
1630 DATA 16,20,0,-.250962993117,.0318167001907
1640 DATA 16,21,0,.0337470225952,0
1650 !!!!!!!!!!!!! Row/Column Q !!!!!!!!!!!!!!!!!!!!!!!!!!!!!!!!!!!!!!!!!!!!!
1660 DATA 17,17,1,1.4043443166,-.280297304107

```

```
1670 DATA 17,13,1,-.280297304107,.0425170068027
1680 DATA 17,22,1,.0425170068027,0
1690 ***** Row/Column R *****
1700 DATA 18,13,1,1.4043443166,0
1710 DATA 18,22,1,-.250962993117,.0318167001907
1720 DATA 18,23,1,.0337470225952,0
1730 ***** Row/Column S *****
1740 DATA 19,19,0,1.55488461455,0
1750 DATA 19,22,0,.022697123287,.022697123287
1760 DATA 19,23,0,-.148555354853,-.148555354853
1770 ***** Row/Column T *****
1780 DATA 20,20,0,.386448961524,-.16585112319
1790 DATA 20,21,0,-.188670742999,.0252538685337
1800 ***** Row/Column U *****
1810 DATA 21,21,0,.421776560109,.0299414965597
1820 DATA 21,23,0,0,.0409943591762 ***** 1 AND 4
1830 ***** Row/Column V *****
1840 DATA 22,22,1,.386448961524,-.16585112319
1850 DATA 22,23,1,-.188670742999,.0252538685337
1860 ***** Row/Column W *****
1870 DATA 23,23,1,.421776560109,.0299414965597
1880 DATA 9999
1890 DATA G Matrix Loaded
1900 END
```

APPENDIX SIX

"3DHRRA"

```

10 | C -----
20 | C Program: 3DHRRR
30 | C
40 | C This program calculates vdW torsional modes for benzene(methane)1 type
50 | C clusters. The torsional modes are calculated for a specified
60 | C torsional barrier height and torsional potential form. The
70 | C torsional modes are treated using rigid rotor
80 | C symmetric top wavefunctions as a basis set. Under free rotation, these
90 | C wavefunctions are solutions to the spherical top Schrodinger equation.
100 | C Upon application of the torsional potential, the torsional mode
110 | C eigenvalues are obtained by diagonalizing the energy matrix
120 | C which describes the hindered rotational/librational motion.
130 | C -----
140 | C
150 | C   PROGRAM 3DHRRR
160 | C
170 | C -----
180 | C A(*)=Energy matrix to be diagonalized.
190 | C D(*)=Diagonal elements of tridiagonal matrix, or eigenvalues of
200 | C diagonalized matrix.
210 | C E(*)=Subdiagonal elements of tridiagonal matrix.
220 | C ZAP(*)=Orthogonal transformation matrix to tridiagonalize A(*).
230 | C -----
240 | C
250 | C   DIMENSION A(680,680),D(680),E(680),ZAP(680)
260 | C
270 | C -----
280 | C Identifies external functions for integrations subroutine.
290 | C -----
300 | C
310 | C   EXTERNAL THINT,XINT,PHINT
320 | C
330 | C -----
340 | C Sets up common blocks.
350 | C -----
360 | C
370 | C   COMMON /B1A/A/B2ZAP/ZAP/B3D/D/B4E/E/B5F/RJ,RK,RM,CJ,CK,CM
380 | C   * ,ZA,ZB,ZC,ZD,ZE,ZF,ZG,ZH,FLG1
390 | C
400 | C -----
410 | C Declares integers.
420 | C -----
430 | C
440 | C   INTEGER RE,CE,ROWTOT,ORDER,EJ,EIGULE,SJ,Z,FLG1
450 | C
460 | C -----
470 | C Determines the order of the energy matrix in terms of J quantum number.
480 | C SJ=Starting J level.
490 | C EJ Ending J level.
500 | C -----
510 | C
520 | C   SJ=0

```

```

530 |     EJ=7
540 |     ORDER=0
550 |     DO 19 Z=0,EJ
560 |     ORDER=ORDER+(2*Z+1)**2
570 |     19 CONTINUE
580 |     C
590 |     C-----
600 |     C  Initializes the energy matrix.
610 |     C-----
620 |     C
630 |     DO 85 I=1,ORDER
640 |     DO 86 J=1,I
650 |     A(I,J)=0.0
660 |     86 CONTINUE
670 |     85 CONTINUE
680 |     C
690 |     C-----
700 |     C  Maximum size of energy matrix.
710 |     C-----
720 |     C
730 |     ROWTOT=680
740 |     C
750 |     C-----
760 |     C  Torsional barrier height in wavenumbers.
770 |     C-----
780 |     C
790 |     VPERT=500
800 |     C
810 |     C-----
820 |     C  Effective internal rotational constant for cluster in wavenumbers.
830 |     C-----
840 |     C
850 |     ROTCA=2.6025
860 |     PI=3.1415927
870 |     C
880 |     C-----
890 |     C  Determines matrix row element in question.
900 |     C-----
910 |     C
920 |     DO 1 RJ=SJ,EJ
930 |     DO 2 RM=-RJ,RJ
940 |     DO 3 RK=-RJ,RJ
950 |     RE=0
960 |     DO 4 Z=0,RJ
970 |     RE=RE+(2*(Z-1)+1)**2
980 |     4 CONTINUE
990 |     RE=RE+RK+RJ+(2*RJ+1)*(RM+RJ)
1000 |     C
1010 |     C-----
1020 |     C  Determines matrix column element in question.
1030 |     C-----
1040 |     C
1050 |     DO 5 CJ=SJ,EJ
1060 |     DO 6 CM=-CJ,CJ
1070 |     DO 7 CK=-CJ,CJ
1080 |     CE=0
1090 |     DO 8 Z=0,CJ
1100 |     CE=CE+(2*(Z-1)+1)**2
1110 |     8 CONTINUE
1120 |     CE=CE+CK+CJ+(2*CJ+1)*(CM+CJ)

```



```

1130! C
1140! C -----
1150! C Inputs diagonal matrix elements into A(*).
1160! C -----
1170! C
1180!     IF (RE.EQ.CE) A(RE,CE)=ROTCA*RJ*(RJ+1.)+VPERT/2.
1190!     IF (CE.GT.RE) GO TO 7
1200! C
1210! C -----
1220! C Selects possible nonzero off-diagonal matrix elements in A(*).
1230! C -----
1240! C
1250!     IF (ABS(RJ-CJ).LE.2.AND.ABS(RK-CK).EQ.2.AND.ABS(RM-CM).EQ.
1260!     * 1) GO TO 18
1270!     GO TO 7
1280! C
1290! C -----
1300! C Calculates normalization constants for matrix elements.
1310! C -----
1320! C
1330!     18 ZA=(2*RJ+1)/8/PI/PI
1340!     DO 9 Z=RJ+RM,2,-1
1350!     ZA=ZA*Z
1360!     9 CONTINUE
1370!     ZA=SQRT(ZA)
1380!     ZB=1
1390!     DO 10 Z=RJ-RM,2,-1
1400!     ZB=ZB*Z
1410!     10 CONTINUE
1420!     ZB=SQRT(ZB)
1430!     ZC=1
1440!     DO 11 Z=RJ+RK,2,-1
1450!     ZC=ZC*Z
1460!     11 CONTINUE
1470!     ZC=SQRT(ZC)
1480!     ZD=1
1490!     DO 12 Z=RJ-RK,2,-1
1500!     ZD=ZD*Z
1510!     12 CONTINUE
1520!     ZD=SQRT(ZD)
1530!     ZE=(2*CJ+1)/8/PI/PI
1540!     DO 13 Z=CJ+CM,2,-1
1550!     ZE=ZE*Z
1560!     13 CONTINUE
1570!     ZE=SQRT(ZE)
1580!     ZF=1
1590!     DO 14 Z=CJ-CM,2,-1
1600!     ZF=ZF*Z
1610!     14 CONTINUE
1620!     ZF=SQRT(ZF)
1630!     ZG=1
1640!     DO 15 Z=CJ+CK,2,-1
1650!     ZG=ZG*Z
1660!     15 CONTINUE
1670!     ZG=SQRT(ZG)
1680!     ZH=1
1690!     DO 16 Z=CJ-CK,2,-1
1700!     ZH=ZH*Z
1710!     16 CONTINUE
1720!     ZH=SQRT(ZH)

```

```

1730 | C
1740 | C-----
1750 | C Integrates over theta, phi, and chi coordinates.
1760 | C-----
1770 | C
1780 |     DO 17 FLG1=0,0
1790 | C
1800 | C-----
1810 | C Integration over theta coordinate between 0 and pi.
1820 | C-----
1830 | C
1840 |     P=0
1850 |     B=PI
1860 |     EPSABS=1.E-6
1870 |     EPSREL=1.E-6
1880 | C
1890 | C-----
1900 | C Subroutine: STIT
1910 | C
1920 | C This subroutine calculates an approximation result to a given definite
1930 | C integral. The function to be integrated is named THINT.
1940 | C The subroutine is from QUADPACK, a FORTRAN subroutine package for the
1950 | C numerical computation of definite 1 dimensional integrals.
1960 | C Authors: Robert Piessens and Elise de Doncker, Appl. Math. and Progr.
1970 | C Div. - K.U. Leuven.
1980 | C The subroutine name in QUADPACK is QNG.
1990 | C-----
2000 | C
2010 |     CALL STIT(THINT,P,B,EPSABS,EPSREL,RESULT,ABSERR,NEVAL,IER)
2020 |     CADRE1=RESULT
2030 |     IF (CADRE1.EQ.0) GO TO 20
2040 | C
2050 | C-----
2060 | C Integration over chi coordinate between 0 and 2*pi.
2070 | C-----
2080 | C
2090 |     P=0
2100 |     B=PI*2
2110 |     EPSABS=1.E-6
2120 |     EPSREL=1.E-6
2130 | C
2140 | C-----
2150 | C Call subroutine STIT to integrate over the function XINT.
2160 | C-----
2170 | C
2180 |     CALL STIT(XINT,P,B,EPSABS,EPSREL,RESULT,ABSERR,NEVAL,IER)
2190 |     CADRE2=RESULT
2200 |     IF (CADRE2.EQ.0) GO TO 20
2210 | C
2220 | C-----
2230 | C Integration over phi coordinate between 0 and 2*pi.
2240 | C-----
2250 |     P=0
2260 |     B=PI*2
2270 |     EPSABS=1.E-6
2280 |     EPSREL=1.E-6
2290 | C
2300 | C-----
2310 | C Call subroutine STIT to integrate over the function PHINT.
2320 | C-----

```

```

2330 | C
2340 | CALL STIT(PHINT,P,B,EP5ABS,EP5REL,RESULT,ABSERR,NEVAL,IER)
2350 | CADPE3=RESULT
2360 | C0 CADRE=CADRE1+CADRE2+CADRE3
2370 | IF (ABS(CADRE).LT.1.E-5) CADRE=0
2380 | IF (A(RE,CE).NE.0) A(RE,CE)=A(RE,CE)-CADRE*VPERT/2.
2390 | IF (A(RE,CE).EQ.0) A(RE,CE)=CADRE*(-1.)*VPERT/2.
2400 | 17 CONTINUE
2410 | 7 CONTINUE
2420 | 6 CONTINUE
2430 | 5 CONTINUE
2440 | 3 CONTINUE
2450 | 2 CONTINUE
2460 | 1 CONTINUE
2470 | EIGVLE=ORDER
2480 | C IF (ORDER.GT.200) EIGVLE=200
2490 | C
2500 | C-----
2510 | C Subroutine: TDIAG
2520 | C
2530 | C This subroutine reduces a real symmetric matrix to a symmetric
2540 | C tridiagonal matrix using and accumulating orthogonal similarity
2550 | C transformations.
2560 | C The subroutine is from EISPACK, a collection of FORTRAN subroutines
2570 | C for eigenanalysis of matrices.
2580 | C The program is called TRED2 in EISPACK.
2590 | C Authors: Martin, Reinsch, and Wilkinson, Num. Math. 11, 181-195(1968).
2600 | C-----
2610 | C
2620 | CALL TDIAG(ROWTOT,ORDER)
2630 | C
2640 | C-----
2650 | C Subroutine: DIAGIT
2660 | C
2670 | C This subroutine finds the eigenvalues of a symmetric tridiagonal
2680 | C matrix by the implicit QL method.
2690 | C This subroutine is from EISPACK.
2700 | C The subroutine is named INTQL1 in EISPACK.
2710 | C Authors: Martin and Wilkinson, Num. Math. 12, 377-383(1968). Modified
2720 | C by DuBrille, Num. Math. 15, 450(1970).
2730 | C-----
2740 | C
2750 | CALL DIAGIT(ORDER,IERR)
2760 | C
2770 | C-----
2780 | C Prints the results of the diagonalization.
2790 | C-----
2800 | C
2810 | PRINT 90,ORDER,VPERT,ROTCA
2820 | 90 FORMAT(///,IX,'MATRIX ORDER = ',I5,10X,' POTENTIAL = ',F10.5,
2830 | * 10X,'ROTATIONAL CONSTANT = ',F10.4,/)
2840 | PRINT 91,EIGVLE
2850 | 91 FORMAT(IX,'FIRST ',I5,' EIGENVALUES:',/)
2860 | PRINT 80,(D(I),I=1,EIGVLE)
2870 | 80 FORMAT (10(1X,F10.4))
2880 | PRINT 96,EIGVLE
2890 | 96 FORMAT (///,IX,'FIRST ',I5,' EIGENVALUES RELATIVE TO Z.P.:',/)
2900 | DIFF=D(1)
2910 | PRINT 97,(D(I)-DIFF,I=1,EIGVLE)
2920 | 97 FORMAT (10(1X,F10.4))

```

```

2930 |      STOP
2940 |      END
2950 | C
2960 | C-----
2970 | C Function: THINT
2980 | C
2990 | C Part of the symmetric top wavefunction that depends on theta.
3000 | C Also contains the theta component of the torsional potential.
3010 | C This function is integrated between the range of 0 and pi by STIT.
3020 | C-----
3030 | C
3040 |      FUNCTION THINT(X)
3050 |      COMMON/BSF/RJ,RK,RM,CJ,CK,CM,ZA,ZB,ZC,ZD,ZE,ZF,ZG,ZH,FLG1
3060 |      INTEGER FIRSTR,FINR,S,Z,FIRSTC,FINC
3070 | C
3080 | C-----
3090 | C Theta component of the symmetric top wavefunction.
3100 | C-----
3110 | C
3120 |      FR=0
3130 |      FIRSTR=0
3140 |      IF(-1*(RK+RM).GT.FIRSTR) FIRSTR=-1*(RK+RM)
3150 |      FINR=RJ-RM
3160 |      IF(RJ-RK.LT.FINR) FINR=RJ-RK
3170 |      DO 1 S=FIRSTR,FINR
3180 |      S1=RJ-RM-S
3190 |      S2=RM+RK+2*S
3200 |      S3=2*RJ-RM-RK-2*S
3210 |      F1=-1
3220 |      IF(INT(S1/2).EQ.S1/2) F1=1
3230 |      F2=COS(.5*X)
3240 |      IF(ABS(F2).LT.1.E-9) F2=0
3250 |      IF(F2.EQ.0.AND.S2.EQ.0.) F2=1
3260 |      IF(F2.EQ.0.AND.S2.EQ.0.) GO TO 2
3270 |      F2=F2**S2
3280 | 2  F3=SIN(.5*X)
3290 |      IF(ABS(F3).LT.1.E-9) F3=0
3300 |      IF(F3.EQ.0.AND.S3.EQ.0) F3=1
3310 |      IF(F3.EQ.0.AND.S3.EQ.0) GO TO 3
3320 |      F3=F3**S3
3330 | 3  ZZ=F1*F2*F3
3340 |      ZZR=ZA
3350 |      DO 4 Z=S,2,-1
3360 |      ZZR=ZZR/Z
3370 | 4  CONTINUE
3380 |      ZZR=ZZR*ZB
3390 |      DO 5 Z=RJ-RM-S,2,-1
3400 |      ZZR=ZZR/Z
3410 | 5  CONTINUE
3420 |      ZZR=ZZR*ZC
3430 |      DO 6 Z=RM+RK+S,2,-1
3440 |      ZZR=ZZR/Z
3450 | 6  CONTINUE
3460 |      ZZR=ZZR*ZD
3470 |      DO 7 Z=RJ-RK-S,2,-1
3480 |      ZZR=ZZR/Z
3490 | 7  CONTINUE
3500 |      FR=FR+ZZR*ZZ
3510 | 1  CONTINUE
3520 |      FC=0

```

```

3530 | FIRSTC=0
3540 | IF(-1*(CK+CM.GT.FIRSTC) FIRSTC=-1*(CK+CM)
3550 | FINC=CJ-CM
3560 | IF(CJ-CK.LT.FINC) FINC=CJ-CK
3570 | DO 8 S=FIRSTC,FINC
3580 | S1=CJ-CM-S
3590 | S2=CM+CK+2*S
3600 | S3=2*CJ-CM-CK-2*S
3610 | F1=-1
3620 | IF(INT(S1/2).EQ.S1/2) F1=1
3630 | F2=COS(.S*X)
3640 | IF(ABS(F2).LT.1.E-9) F2=0
3650 | IF(F2.EQ.0.AND.S2.EQ.0) F2=1
3660 | IF(F2.EQ.0.AND.S2.EQ.0) GO TO 9
3670 | F2=F2**S2
3680 | 9 F3=SIN(.S*X)
3690 | IF(ABS(F3).LT.1.E-9) F3=0
3700 | IF(F3.EQ.0.AND.S3.EQ.0) F3=1
3710 | IF(F3.EQ.0.AND.S3.EQ.0) GO TO 10
3720 | F3=F3**S3
3730 | 10 ZZ=F1*F2*F3
3740 | ZZR=ZE
3750 | DO 11 Z=S,2,-1
3760 | ZZR=ZZR/Z
3770 | 11 CONTINUE
3780 | ZZR=ZZR*ZF
3790 | DO 12 Z=CJ-CM-S,2,-1
3800 | ZZR=ZZR/Z
3810 | 12 CONTINUE
3820 | ZZR=ZZR*ZG
3830 | DO 13 Z=CM+CK+S,2,-1
3840 | ZZR=ZZR/Z
3850 | 13 CONTINUE
3860 | ZZR=ZZR*ZH
3870 | DO 14 Z=CJ-CK-S,2,-1
3880 | ZZR=ZZR/Z
3890 | 14 CONTINUE
3900 | FC=FC+ZZR*ZZ
3910 | 8 CONTINUE
3920 | C
3930 | C-----
3940 | C Theta component of the torsional potential.
3950 | C-----
3960 | C
3970 | IF(FL61.EQ.0) THINT=FR*FC*SIN(X)*COS(2*X)
3980 | IF(FL61.EQ.1) THINT=FR*FC*SIN(X)*SIN(2*X)
3990 | IF(FL61.EQ.2) THINT=FR*FC*SIN(X)*SIN(2*X)
4000 | IF(FL61.EQ.3) THINT=-1.*FR*FC*SIN(X)*COS(2*X)
4010 | RETURN
4020 | END
4030 | C
4040 | C-----
4050 | C Function: XINT
4060 | C
4070 | C Part of the symmetric top wavefunction that depends on chi.
4080 | C Also contains the chi component of the torsional potential.
4090 | C This function is integrated between the range 0 and 2*pi by STIT.
4100 | C-----
4110 | C
4120 | FUNCTION XINT(X)

```

```

4130 |      COMMON/BSF/RJ ,RK ,RM ,CJ ,CK ,CM ,ZA ,ZB ,ZC ,ZD ,ZE ,ZF ,ZG ,ZH ,FLG1
4140 | C -----
4150 | C
4160 | C Chi component of the symmetric top wavefunction.
4170 | C -----
4180 | C
4190 |      XINT=COS(RK*X)*COS(CK*X)+SIN(RK*X)*SIN(CK*X)
4200 | C
4210 | C -----
4220 | C Chi component of the torsional potential.
4230 | C -----
4240 | C
4250 |      IF (FLG1.EQ.0) XINT=XINT*COS(2*X)
4260 |      IF (FLG1.EQ.1) XINT=XINT*SIN(2*X)
4270 |      IF (FLG1.EQ.2) XINT=XINT*COS(2*X)
4280 |      IF (FLG1.EQ.3) XINT=XINT*SIN(2*X)
4290 |      RETURN
4300 |      END
4310 | C
4320 | C -----
4330 | C Function: PHINT
4340 | C
4350 | C Part of the symmetric top wavefunction that depends on phi.
4360 | C Also contains the phi component of the torsional potential.
4370 | C This function is integrated between the range of 0 and 2*pi by STIT.
4380 | C -----
4390 | C
4400 |      FUNCTION PHINT(X)
4410 |      COMMON/BSF/RJ ,RK ,RM ,CJ ,CK ,CM ,ZA ,ZB ,ZC ,ZD ,ZE ,ZF ,ZG ,ZH ,FLG1
4420 | C
4430 | C -----
4440 | C Phi component of symmetric top wavefunction.
4450 | C -----
4460 | C
4470 |      PHINT=COS(RM*X)*COS(CM*X)+SIN(RM*X)*SIN(CM*X)
4480 | C
4490 | C -----
4500 | C Phi component of the torsional potential.
4510 | C -----
4520 | C
4530 |      IF (FLG1.EQ.0) PHINT=PHINT*COS(X)
4540 |      IF (FLG1.EQ.1) PHINT=PHINT*COS(X)
4550 |      IF (FLG1.EQ.2) PHINT=PHINT*SIN(X)
4560 |      IF (FLG1.EQ.3) PHINT=PHINT*SIN(X)
4570 |      RETURN
4580 |      END
4590 | C
4600 | C -----
4610 | C Subroutines STIT, TDIAG, and DIAGIT are attached at this point
4620 | C in the program.
4630 | C -----

```

END

12-87

DTIC